TECHNICAL AND ECONOMIC EVALUATION OF THE UTILISATION OF WIND ENERGY AT THE SANAE IV BASE IN ANTARCTICA

Heiko Walter Teetz

Thesis presented in partial fulfillment of the requirements for the degree of MSc. in Mechanical Engineering at the University of Stellenbosch

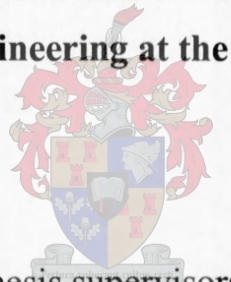

Thesis supervisors:
Doctor T.M.Harms
Department of Mechanical Engineering
Professor T.W. von Backström
Department of Mechanical Engineering

DECEMBER 2002

DECLARATION

I, the undersigned, hereby declare that the work contained in this thesis is my own original work and that I have not previously, in its entirety or in part, submitted it at any university for a degree.

Signature: _____ Date: _____

(H. Teetz)

ABSTRACT

The cost of powering Antarctic research stations by conventional diesel electric generator systems is high (Steel, 1993). In order to reduce these costs and airborne pollution due to the combustion of fossil fuels, an investigation into renewable energy sources has been conducted, with the focus on wind turbine energy generation. The aim was to see whether a wind turbine is feasible, both technically and economically, for partial energy production at the SANAE IV base. The existing diesel electrical generators will still be used for the base demand, when there is not enough wind or when the energy demand is more than can be produced by the wind turbine.

The work accomplished for this study explains and motivates a MSc. (Eng.) thesis on the feasibility of installing wind electricity generators at Antarctica. This evaluation was done for the South African research station SANAE IV in Antarctica. It provides information on the literature consulted to date, the theoretical and practical work covered, the theoretical investigations, the results obtained and future implementations. Also included in this work was a trip to Antarctica, so that all the relevant data, like wind speeds and wind direction could be measured. Another reason for having done the trip was to do an energy audit for SANAE IV, so that the energy demand for the base could be established. The energy demand of the base varies among other factors, for summer and winter conditions, for day and night conditions, and for population variations. With the information obtained during the trip, the theoretical evaluation of a possible wind turbine system was performed.

With the aid of the data from the 6 m wind mast, wind profiles have been established, from which Weibull distributions were obtained, and the energy output from 5 different wind turbines, in the range between 10 kW and 100 kW, were calculated. The annual energy production of the 100 kW wind turbine is 430 MWh with a capacity factor of 49 %. The annual energy demand of the base amounts to 1153 MWh, thus the wind turbine could contribute up to 30 % of the power needed at the base taking losses, such as availability and maintenance losses, into account.

From the automatic weather station of the South African Weather Services, positioned at SANAE IV, wind speed and direction data for the year 2001 was obtained and this data was analyzed. The results show that the winds at SANAE IV are highly directional, coming mostly from an eastern and southeastern direction. This highly directional wind pattern is well suited for wind turbine application. The average wind speed, being measured at 10 m height, is 10.8 m/s and the hourly averaged maximum wind speed for the year 2001 is 38.9 m/s.

From the wind analysis, site survey, cold weather issues and connection to the electricity grid of the base, it becomes evident that the North Wind NW100/19 100 kW wind turbine is the best-suited wind turbine for installation at SANAE IV. One of the major advantages of the NW100/19 is that it features a tilt-up tower erecting system that enables the wind turbine to be installed without the use of a crane. The NW100/19 is the only turbine rated at 100 kW, with this feature.

From the economic analysis it is evident that a wind turbine, with the complete installation, operation and maintenance costs, features a breakeven period of 10 years, when installed at SANAE IV. This relatively short breakeven period, considering that the life of the turbine is 30 years, originates from the fact that the average wind speed at the base is about 11 m/s, which is relatively high and yields enormous power productions. This wind turbine operates for approximately 80 % during a year, which is very high, making this renewable energy source very attractive as a power-generating source for SANAE IV. The cost per kWh produced by the wind-diesel system is R1.63/kWh, while the cost per kWh produced by the current diesel generators, satisfying the power demand of the base, is R1.94/kWh. Thus the hybrid system can reduce the cost of power produced by almost 20 %, which again demonstrates the attractiveness of using wind power at SANAE IV.

From an environmental point of view, the use of wind power at SANAE IV is favorable, since a wind turbine has minimal effects on the environment at Antarctica. The cost of emissions and fuel spills were calculated for SANAE IV. The fuel saving, resulting from the operation of a wind turbine at SANAE IV, converts to a saving in externalities of about

R500 000.00 per year, using an evaluation method that was applied to remote Alaskan villages.

It can therefore be concluded that the aims of the project have been fully accomplished and that the use of wind power at SANAE IV is indeed a very attractive option, regarding all the criteria mentioned above. When it is being decided that a budget will be provided for a wind turbine installation, the economic analysis has to be refined, due to the uncertainty of the market value of the South African currency.

OPSOMMING

Die koste verbonde aan krag voorsiening vir Antarktiese navorsingstasies deur middel van konvensionele diesel elektriese kragopwekkers is baie hoog (Steel, 1993). Om hierdie kostes en lugbesoedeling weens die verbranding van fossielbrandstowwe te verminder, is 'n ondersoek na hernubare energiebronne gedoen, met die fokus op windturbiene energie opwekking. Die doelwit van die studie was om te sien of 'n windturbiene aanwending vir kragopwekking vir die SANAE IV stasie lewensvatbaar is, gebaseer op tegniese en ekonomiese uitgangspunte. Die bestaande diesel elektriese kragopwekkers sal nog altyd gebruik word vir kragopwekking, as daar nie genoeg wind is nie, of as die energievraag hoër is as wat kan verskaf word deur die wind turbine.

Die werk wat vir hierdie studie voltooi is belig en motiveer 'n MSc(Ing) tesis oor die lewensvatbaarheid vir installering van 'n windelektriese kragopwekker op Antarktika. Hierdie evaluasie is gedoen vir die Suid Afrikanse navorsingstasie, SANAE IV, op Antarktika. Dit behels informasie oor die literatuur verwerk tot dusver, die teoretiese en praktiese werk gedoen, die teoretiese ondersoeke, die resultate verkry en toekomstige verwesenlikings. Werk ook ingesluit was 'n expedisie na Antarktika toe, sodat al die relevante data, soos wind spoed en rigtings gemeet kon word. Nog 'n rede om die expedisie te doen was om energie data van SANAE IV te meet, sodat die energieverbruik van die basis bevestig kon word. Die energieverbruik van die basis varieer ten opsigte van somer en winter kondisies, van dag en nag variasies en inwonergetalle. Met die informasie verkry gedurende die expedisie kon 'n evaluasie gedoen word vir 'n moontlike windturbiene stelsel op Antarktika.

Met die hulp van 'n 6m wind toring kon wind profiele gekry word, waarvandaan Weibull verdelings bereken is en die kragopwekking van 5 verskillende windturbienes bereken is, wat wissel van 10 kW tot 100 kW. Die jaarlikse energieopwekking vir die 100 kW wind turbine is 430 MWh met 'n kapasiteitsfaktoor van 49 %. Die jaarlikse energieaanvraag van die stasie is 1153 MWh. Dus kan die wind turbine ongeveer 30 % van die jaarlikse

energieaanvraag dek, as verliese soos beskikbaarheids- en instandhoudingsverliese in berekening gebring word.

Wind spoed en rigting data vir die jaar 2001 is verkry van die outomatiese weerstasie van die Suid Afrikaanse Weer Diens, wat geposisioneer is by die SANAE IV stasie, en hierdie data is geanaliseer. Die resultate verkry bewys die direksionele stabiliteit van die winde by SANAE IV, waarvandaan die meeste winde uit die oostlike en suidoostlike rigting kom. Hierdie hoogs gekosentreede winde is baie goed geskik vir windturbiene aanwending. Die gemiddelde wind spoed, wat gemeet is op 'n hoogte van 10 m is 10.8 m/s en die uurlike gemiddelde maksimum wind spoed vir die jaar 2001 is 38.9 m/s.

Van die wind analise, terrein analise, koue weer informasie en koppeling van die wind turbine by die bestaande elektrisiteits netwerk word bevestig dat die North Wind NW100/19 100 kW windturbiene die geskikste windturbiene vir installasie en werking by SANAE IV is. Een van die grootste voordele van die NW100/19 windturbiene is dat dit 'n selfoprigdende meganisme het, wat sonder die hulp van 'n kraan werk. Die NW100/19 is die enigste windturbiene in sy klas, wat so 'n funksie het.

Van die ekonomiese analise kan afgelei word, dat 'n wind turbine met volledige installasie, werking en diens kostes, 'n kapitale terugbetalings periode van 10 jaar het, as dit by SANAE IV geinstalleer word. Hierdie tydperk is relatief kort, as gekyk word na die ontwerp leeftyd van 30 jaar van die NW100/19 wind turbine. Die rede vir die kort terugbetalings periode is afkomstig van die hoe gemiddelde wind spoed by SANAE IV, wat enorme kragopwekking tot gevolgtrekking het. Dit kan ook gesien word aan die hoë werkingsure van die turbine wat 6942 uur per jaar is. Dus wek die turbine vir omtrent 80 % van die jaar krag op, wat beinvloed dat 'n wind turbine opsie vir SANAE IV baie aantreklik is. Die koste per kWh krag opgewek vir die wind-diesel sisteem is R1.63/kWh, terwyl die koste per kWh krag opgewek vir die huidige diesel generator opstelling R1.94/kWh is. Dus kan 'n kostebesparing van tot 20% van die energie onkostes verkry word, wat weer eens beklemtoon, dat die wind-diesel sisteem baie aantreklik vir kragopwekking by SANAE IV is.

Vanaf 'n omgewingsoogpunt gesien het die gebruik van 'n wind turbine stelsel by die SANAE IV stasie net weglaatbaar klein invloede op die omgewing in vergelyking met die lugbesoedeling van die diesel kragopwekkers. As die koste verbonde aan lugbesoedeling en brandstof lekkasie besoedeling bereken word kan die wind turbine stelsel omtrent R500000.00 per jaar aan besoedeling onkostes spaar. Die getalle vir besoedelings onkostes is gebaseer op die evaluasie van besoedeling vir afgeleë Amerikanse dorpies (Isherwood et al., 1999).

Dit kan dus afgelei word vanaf die bogenoemde bevindings, dat die doelwitte van die tesis bereik is en dat wind krag opwekking by SANAE IV inderdaad 'n baie aantreklike moontlikheid is. Wanneer 'n begroting beskikbaar gestel word vir 'n windturbiene stelsel vir SANAE IV, moet die ekonomiese analise geoptimeer word weens die onsekerheid van die markwaaarde van die Suid Afrikaanse Rand.

ACKNOWLEDGEMENTS

I would like to thank the following people and institutions for their assistance and contributions during the course of this study:

- Dr T. M. Harms, as a supervisor and lecturer, for his valuable advice, support and patience during this project.
- The Department of Environmental Affairs and Tourism for the funding of this project and for giving me a chance to do my experimental work during the takeover period 2001/2002 at SANAE IV, Antarctica.
- Meiring Beyers for his valuable advice and support.
- Mike Strutters for supplying the wind data logging equipment.
- Prof. T. W. von Backström for his valuable advice and contributions.
- My family and friends for their continuous support and understanding.

TABLE OF CONTENTS

LIST OF FIGURES

LIST OF TABLES

LIST OF SYMBOLS

ENGINEERING SYMBOLS:

A	= Area	[m^2]
a	= Rotational area	[m^2]
B	= 5.0 Turbulent wall-law intercept constant	
CF	= Correction factor	
c	= Weibull scale parameter	[m/s]
c_1	= Constant	
c_p	= Capacity factor	
D	= Diameter	[m]
D_1, D_2	= Differences	[%]
d	= number of days	[d]
E_v	= Energy corresponding to particular wind speed	[m/s]
e	= Total error	[%]
e_1, e_2, e_3	= Errors	[%]
F	= Force	[N]
FC	= Fuel cost	[R/l]
F(v)	=Weibull cumulative distribution function	
f(v)	=Weibull probability density function	
$f(v_{i)}$	= Weibull probability function at wind speed v_i	
g	= Acceleration due to gravity	[m/s^2]
h	= Number of hours	[h]
k	= Weibull shape parameter	
k	= Effective roughness height (section 8.1.2)	[m]
LHV	= Lower heating value of fuel	[kWh/L]
M	= Mass flow	[kg/s]
OP	= Operating percentage	[%]
OT	= Operating time	[h]
P	= Power	[kW]
P	= Pressure (equation 9.1)	[kPa]

P_0	= Power of undisturbed wind, wind not passing wind turbine	[kW]
$P_{average}$	= Average power demand	[kW]
P_D	= Power density	[kW]
P_{Dt}	= Power density for complete period	[kWh]
P_i	= Power at each wind speed interval	[kW]
$P_{turbine}$	= Power that can be extracted by wind turbine	[kW]
P_{wind}	= Theoretical power in the wind	[kW]
R	= 0.2870 Gas constant for air	[kJ/kg K]
R^2	= Regression coefficient	
SAB	= Special Antarctic blend diesel fuel	
SAWS	= South African Weather Services	
s^+	= Saltation roughness parameter, dimensionless	
T	= Temperature of air (equation 9.1)	[K]
T	= Time period	[h]
u	= Wind speed, one dimensional	[m/s]
u_{10}	= Wind speed at 10 m height	[m/s]
u^*	= Shear velocity	[m/s]
V_{Emax}	= Wind speed carrying maximum energy	[m/s]
V_{Fmax}	= Most frequent wind speed	[m/s]
v	= Wind speed	[m/s]
$\bar{v}$	= Mean wind speed	[m/s]
$\overline{v^n}$	= Mean wind speed, to the power of n	$[m^n/s^n]$
v_1	= Wind speed in front of wind turbine	[m/s]
v_2	= Wind speed behind wind turbine	[m/s]
v_{ave}	= Calculated average wind speed	[m/s]
$v_{avemeas}$	= Measured average wind speed	[m/s]
$v_{average}$	= Average wind speed	[m/s]
v_{ci}	= Cut-in wind speed of wind turbine	[m/s]
v_{co}	= Cut-out wind speed of wind turbine	[m/s]
v_{hand}	= Wind speed measured by analog handheld anemometer	[m/s]

v_i	= Wind speed at each step i	[m/s]
v_{mast}	= Wind speed measured by 6 m wind mast	[m/s]
v_{median}	= Median wind speed	[m/s]
v_{mode}	= Mode wind speed	[m/s]
v_r	= Rated wind speed of wind turbine	[m/s]
z	= Height above surface level	[m]
z_0	= Roughness height	[m]

Greek Symbols:

κ	= 0.41 von Karman constant	
ρ	= Density	[kg/m^3]
σ	= Standard deviation	[m/s]
σ^2	= Variance	[m^2/s^2]
ν	= Kinematic viscosity	[m^2/s]
$\Gamma(x)$	= Gamma function	

ECONOMIC SYMBOLS:

AS	= Net annual savings	[Rand]
BCR	= Benefit/cost ratio	
C_{cap}	= Capital investment	[Rand]
C_{cum}	= Cumulative costs	[Rand]
C_{fuel}	= Fuel costs	[Rand]
C_{labor}	= Labor costs	[Rand]
C_{maint}	= Maintenance costs	[Rand]
CO	= Carbon monoxide	
CO_2	= Carbon dioxide	
CP	= Cost per kWh energy produced	[Rand/kWh]
C_{pw}	= Present worth capital investment	[Rand]
CSCC	= Cumulative system cost comparison	[Rand]
d	= General inflation rate	[%]
ES	= Externality cost saved	[Rand]

F_{pw}	= Present worth annual fuel costs	[Rand]
FS	= Fuel savings	[Rand]
i_{cap}	= Interest on capital invested	[%
i_{fuel}	= Fuel escalation rate	[%]
i_{labor}	= Labor escalation rate	[%]
i_{maint}	= Maintenance escalation rate	[%]
IRR	= Internal rate of return	[%]
IOC	= Interest on capital	[Rand]
LCC	= Life cycle cost	[Rand]
LMS	= Labor, maintenance and operation costs saved	
L_{pw}	= Present worth annual labor costs	[Rand]]
M_{pw}	= Present worth annual maintenance costs	[Rand]
NO_x	= Oxides of nitrogen	
NPV	= Net present value	[Rand]
N	= Design life of wind turbine	[years]
O&M	= Operating and maintenance cost	[Rand]
PBP	= Payback period	[years]
PBP_d	= Discounted payback period	[years]
PBP_s	= Simple payback period	[years]
P_{gr}	= Annual reduction of energy production by generators	[kWh]
PM	= Particulate matter	
PWF	= Present worth factor including inflation	
PW_s	= Single present worth factor	
P_{wt}	= Annual energy produced by wind turbine	[kWh]
PW_u	= Uniform present worth factor	
SO_2	= Sulphur dioxide	
VOC	= Volatile organic compounds	
X_{pw}	= Present worth annual externality costs	[Rand]

Greek Symbols:

θ	= Year of breakeven	[year]

1 INTRODUCTION

Antarctica is a continent rich in geological history and abundant in biological resources along its extensive coastline and surrounding waters. Antarctica also plays a critical and important role in the earth's climate system, influencing both the ocean and the atmosphere. As a result of these and other factors, many countries are active in this region conducting a multitude of scientific programs. These include:

- Climate related studies of the atmosphere, oceans, ice and glacier fields;
- Biological studies of the ecosystems;
- Cosmic ray studies relating to the dynamics of the upper and outer atmosphere, ionosphere and magnetosphere; and
- Geological studies including plate tectonics and paleontology.

In order to support these programs, permanent and semi-permanent stations, or bases have been established throughout the continent and surrounding oceans. The South African research base, SANAE IV, situated at Våsleskarvet, is one of these bases (71°40'S 2°50'W). An aerial photograph of the Våsleskarvet, before the base was built on the southern buttress can be seen in figure 1-1. Conditions at these bases can be very difficult and harsh. Expeditioners must contend with potentially life threatening low temperatures and strong winds, as well as isolation and separation from family and friends. To provide protection from these elements, the bases have been provided with plentiful and reliable electrical and thermal energy.

Until a few years back, the only practical method to provide this energy on a regular and dependable basis was the use of large quantities of fossil fuel in diesel generator sets. Recent advancements in technology, however, have changed this situation. Methods now exist which would enable reliable quantities of energy to be produced locally at the bases from renewable energy sources. Advantages associated with a move towards renewable energy systems include reduced atmospheric emissions from the burning of fossil fuels; reduced shipping demand; reduced costs associated with fuel purchasing, handling and

storage; and reduced risk of fuel spills. These are issues of major environmental and logistical concern to all Antarctic operators (Brown, 1997).

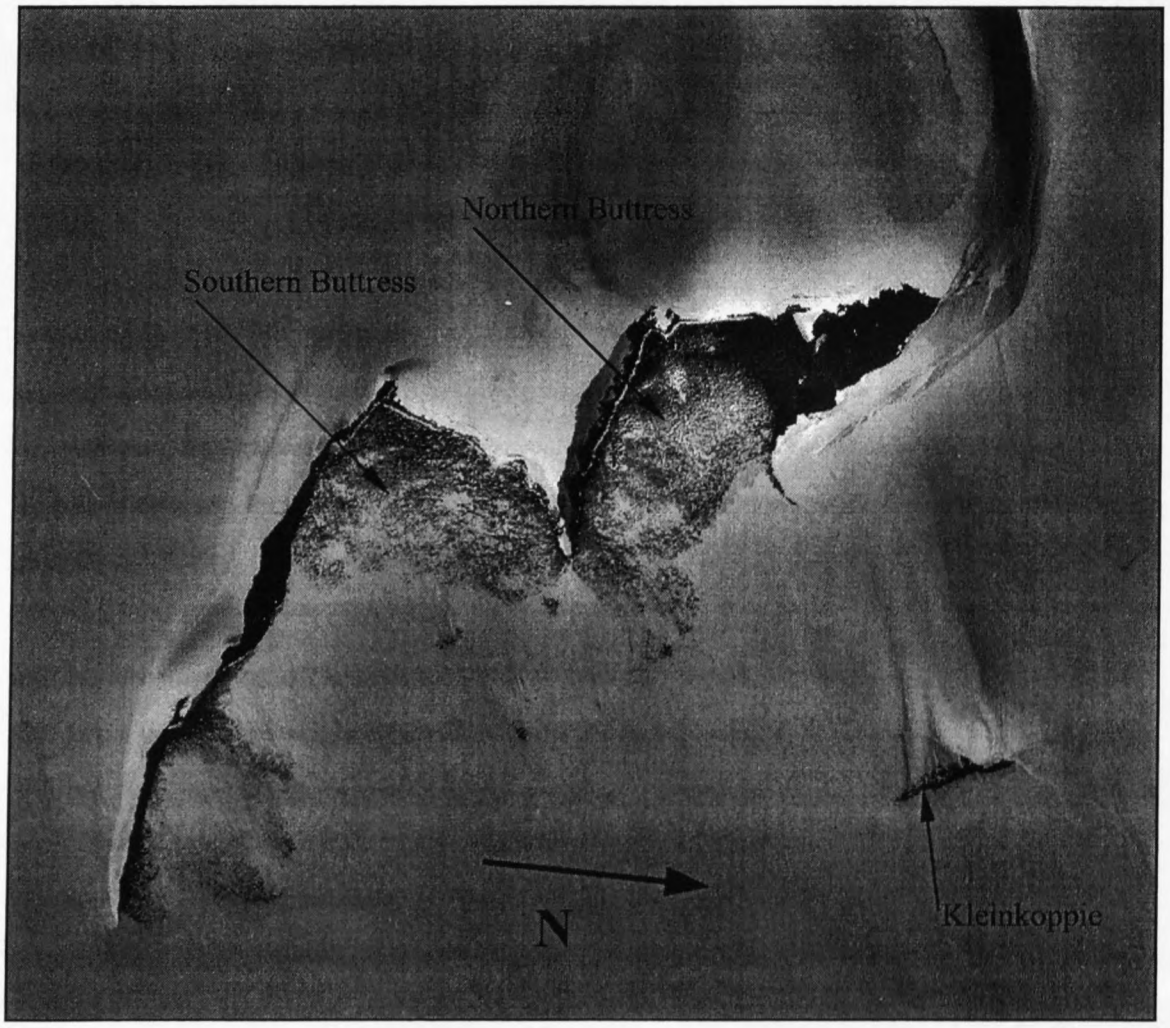

Figure 1-1: Arial photograph of Vasleskarvet, Antarctica

1.1 Problem Statement

The cost of powering Antarctic research stations by conventional diesel electric generator systems is high. A significant financial cost is associated with transporting fuel long distances by sea and storing and handling large quantities of bulk fuel in Antarctic conditions (Steel, 1993). Another cost factor involved is the mixing of special blends of diesel fuel that can be used in Antarctic conditions. These costs are taking up a major part of the yearly budget allocated for SANAE IV.

Diesel combustion for electricity generation is the single largest local contributor to Antarctic produced airborne pollution. Also, the influence of diesel fuel spillage in the Antarctic leads to pollution. From a survey for the Australian stations, it was assumed that the contribution of emissions from the diesel electric generators amounts to about 80% of the total emissions, while the remaining portion of the emissions are produced by boilers, skidoos, snow trucks, etc (Steel, 1993).

In order to reduce these kinds of pollution, a reduction in fossil fuel use is required. This has been the objective for many nations involved in Antarctica. There are many ways of reducing fossil fuel use, a few examples being technological advanced diesel electrical generator systems with low diesel fuel consumption and low emissions, solar energy, wind energy or other kinds of renewable energy systems (Brown, 1997).

1.1.1 Objective of the thesis

Reduced fuel usage would lead to savings in transportation time and cost, lower atmospheric emissions and reduce the risk of fuel spills. This thesis focuses on the partial energy supply by making use of wind turbine technology.

The objective of this thesis is to investigate the feasibility of utilizing wind energy, in terms of technical and economical factors at the SANAE IV base. Another important consideration that has to be taken into consideration when doing this feasibility analysis is the analysis of the impact of a wind turbine system on the Antarctic environment.

In order to get all the information, regarding the wind conditions, the energy demand of the base and possible environmental aspects, a trip to the SANAE IV was undertaken in December 2001. This aided in the successful completion of this thesis.

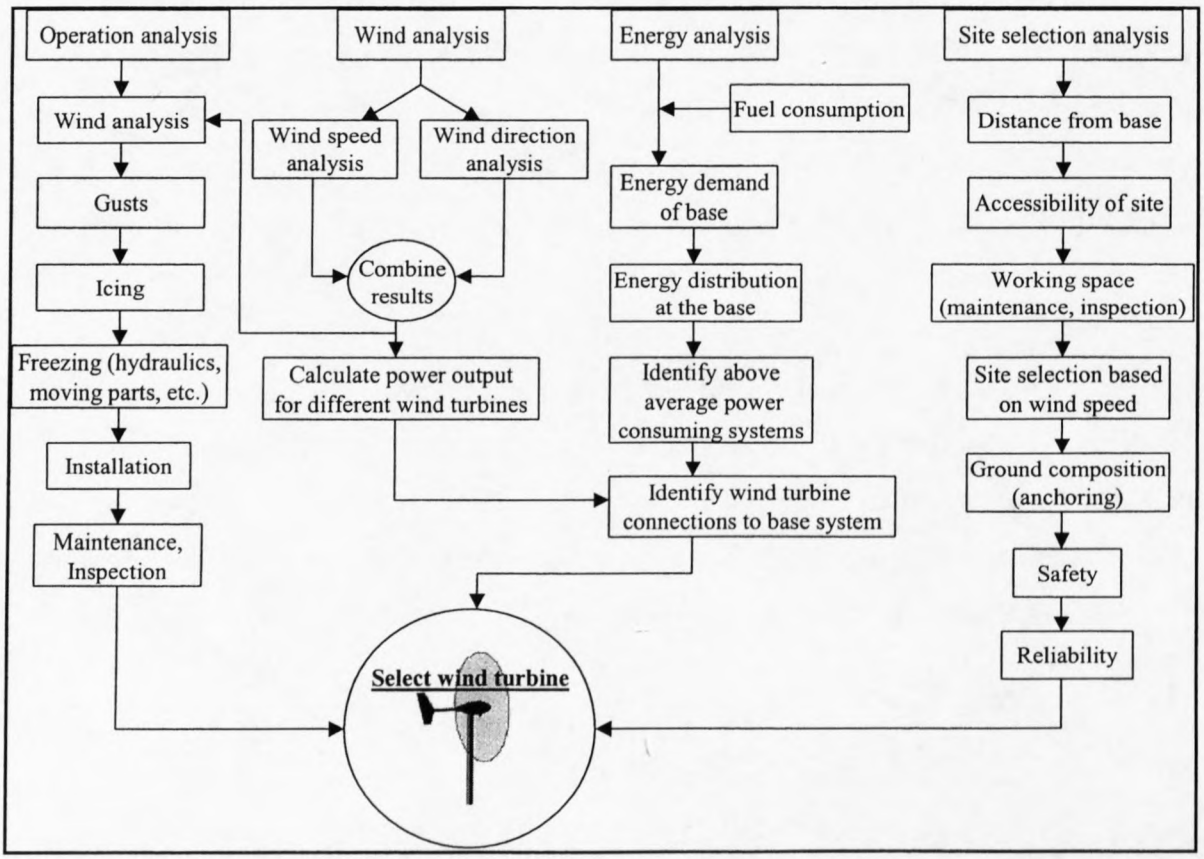

Figure 1-2: Technical layout of thesis

Also included in this thesis are sample calculations regarding the energy demand of the base and energy calculations regarding the wind turbine setup. The layout of the technical part of this report can be seen in figure 1-2.

The second part of this thesis is the economical analysis. The economical analysis will deal mainly with the breakeven analysis, associated with the installion of a wind energy system. Environmental aspects concerning a wind turbine setup and a time schedule for the development of this thesis are included. Finally a conclusion follows.

1.1.2 Limitations

The information needed to do a wind turbine feasibility study was obtained during the trip to SANAE IV. The base has an existing weather station, with an anemometer, which is

located 10 m above ground level. However, this weather tower is fixed in position and is therefore not well suited for determining wind profiles at selected wind turbine locations.

It was therefore decided to build a wind measuring tower ourselves, which could be used for work on another project as well. The tower is 6 m high and has 4 wind speed sensors spaced along the length of the tower. This helped in determining the wind profile at a suited location. In order to use the weather data from the past year, the 6 m wind mast was initially positioned close to the 10 m weather station. Thus the data from the 6 m wind mast was correlated with the data of the 10 m tower.

Another limit was that the 6 m tower could only be placed on certain positions around the base. At the moment there are mainly three different ground surfaces, namely blue ice, snow and rocks. The tower was anchored on a snow and a rock surface.

A major aspect of this thesis was to determine how a wind turbine would perform at SANAE IV given the harsh conditions. As it was not possible to take a wind turbine along and install it, the performance levels of turbine situated at other stations or bases were examined. This gave a fairly good idea of what performance factors can be expected for the proposed wind turbine for SANAE IV.

2 *AIMS*

The successful achievement of the objectives and aims is presented in the following chapters and is discussed in the conclusion. The objectives are:

- Technical viability of installing, operating and maintaining a wind turbine at SANAE IV, with the following aims:
    - Obtaining an energy supply from a wind turbine of about 20 - 25% into the existing electricity grid.
    - No need for electricity storage (batteries, etc.).
    - Less fuel transport to the base.
    - Selecting a suitable wind turbine for operation at SANAE IV.
- Economic viability of installing, operating and maintaining a wind turbine at SANAE IV, with the following aims:
    - Achieving a wind turbine system payback period of 10 years.
    - Achieving a lower cost per kWh than for the current system.

The aims have not changed drastically during the assigned time for this thesis. The only change that took place was to shift the emphasis from the economical part more to the technical analysis. The reason for taking this step was due to a lack of information, regarding the financing of this project.

The wind turbine manufacturers need proper details regarding the installation, the systems used at the base and financial information regarding the support of the base. This information is very difficult to obtain and will only be needed once the decision has been taken to install a wind turbine at SANAE IV, and once the funding is provided. The economical analysis will only deal with the payback period of the proposed wind turbine.

2.1 Motivation

There is full agreement about the fact that today's wind turbine is something radically different from what it was 10 years ago. These differences are seen to release improvements in profitability. Profitability has been the main design driver during this development period (Martinez, 1999).

Today's wind turbines are close to half the price, operate with one-fifth of the downtime and achieve about one-third more energy per unit of installed power or even swept surface, when compared to wind turbines built 10 years ago. These figures demonstrate the maturity of today's technology applied to wind energy installations.

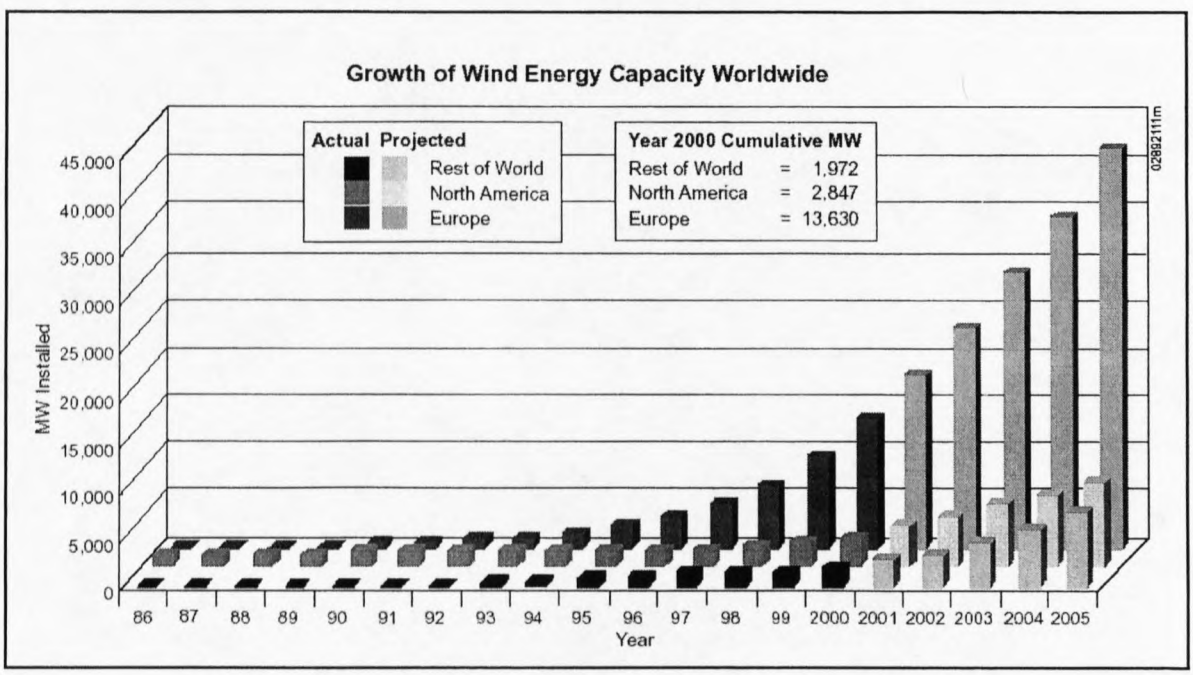

Figure 2-1: Growth of wind energy capacity worldwide (Taylor, 2001)

The growing market for wind energy is an important part of the process to develop advanced technology that will eventually reduce the cost of energy from wind turbines. The growth capacity can be seen in figure 2-1. Data from large wind farm developments, for example, provide valuable operating experience to researchers seeking to improve system performance. Good performance records at these wind farms also lay the foundation for future projects.

2.2 Main Technology Characteristics

Reviewing the development during the last few years, it is easy to detect a trend towards horizontal axis, three bladed wind turbines and cylindrical towers. Only in very specialized situations are vertical-axis wind turbines employed. An example of a vertical axis turbine is the wind turbine based at the German Antarctic research station Neumayer, shown in figure 2-2.

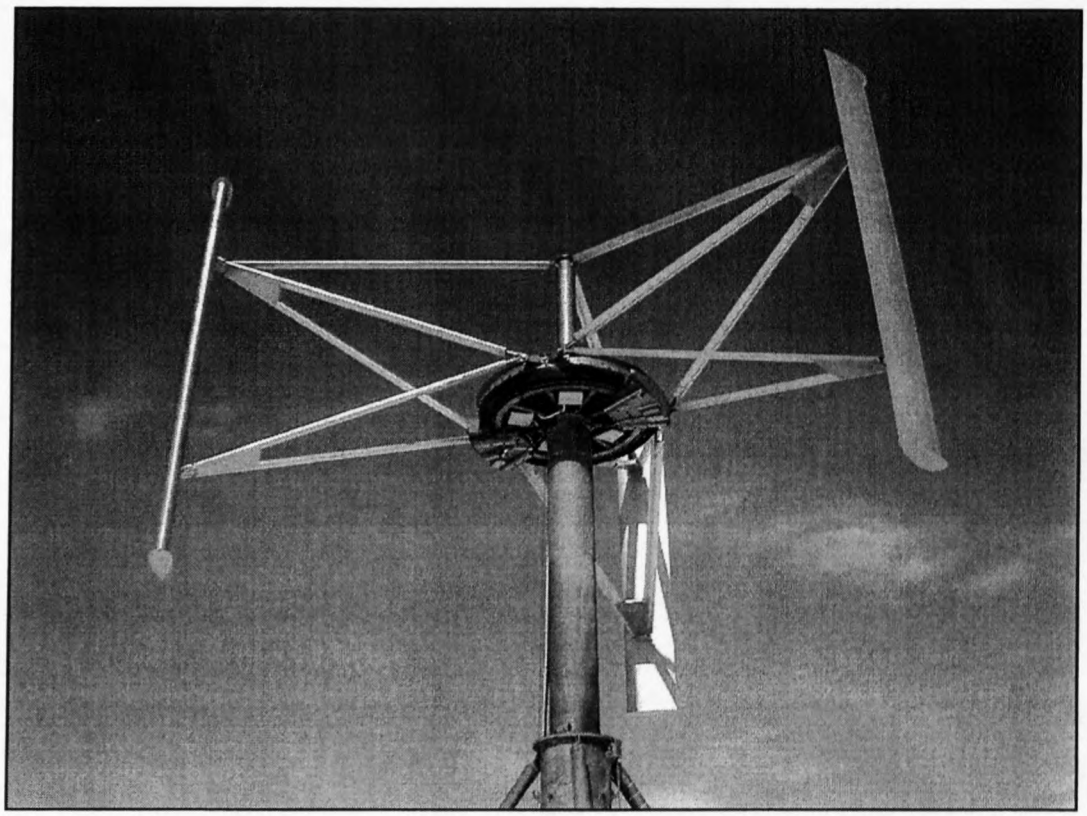

Figure 2-2: Vertical axis wind turbine at Neumayer, Antarctica

In recent years, this trend in the development of wind turbines has also been transferred to Antarctica. Countries like Australia, Germany, USA, Japan, France and Spain are using or testing wind turbines in Antarctica.

This development is due to the environmental concerns facing the stations in Antarctica. The stations are mainly using diesel electricity generators for energy production, but since those generators are polluting the Antarctic environment, due to the emissions and fuel

spills, the focus has shifted onto renewable energy sources, as mentioned beforehand. The implementation of wind energy at SANAE IV has the following potential advantages:

- Savings in supplying less fuel to the base (transport & fuel cost)
- Reliable energy source (in case of down time, the diesel generators can be used)
- Low safety risk
- Relatively ease of operation and maintenance of wind turbines
- Reduction in CO_2 productions and other emissions

3 *LITERATURE REVIEW*

Due to the broad spectrum of the analysis, only literature covering more general aspects of wind turbine engineering will be mentioned in this chapter. Articles that are more detailed and that have been used extensively will be mentioned in the subsequent relevant chapters. In this section only an overview of the articles and publications found to date is presented. Subsections are used to keep track of the large amounts of information.

3.1 General Information

Information concerning the topic of wind energy development in South Africa indicates the reaction of the South African companies to renewable energy and especially wind energy (Lace, 2001). The first wind turbine that is connected to South Africa's electricity grid has started producing energy in August 2002. The turbine is rated at 660kW and has been built by Vestas. Further research wind turbines are due to start operating in November 2002.

A project study for wind parks in Walvis Bay and Lüderitz, Namibia, demonstrates that the wind regime in Lüderitz and to a lesser extend also in Walvis Bay permits the installation and operation of grid-connected wind parks with a wide range of outputs (installed capacity). The study also confirms that the most favorable sites are in Lüderitz where wind energy conversion has a cost advantage over Walvis Bay of up to 55%. The major and probably only factor working against the use of wind energy in Namibia is that NamPower's power purchase agreement (PPA) with ESKOM gives the country access to exceptionally cheap electricity and enables the utility to wholesale electricity at fairly low rates. As a consequence, both the economic and financial value of electricity, which could be displaced by wind parks, appears to be too low to justify wind energy projects (GTZ, 1999).

The literature research revealed a substantial amount of information regarding the design of wind turbines. Martinez and Prats (1999) focus on the main trends of the technology

behind the present wind energy applications. The technology characteristics and main challenges are analyzed. The important links between political decisions and the development to date of wind turbines signal a direction for forecasting future tendencies and possible technical characteristics of future turbines. However, this is not part of the thesis and will only be used as additional information and for important criteria regarding the operation and maintenance aspects of wind turbines.

3.2 SANAE IV Base Information

The report by Teetz (2000) presents the analysis and the redesign of parts of the current heating- and ventilation system at the South African Research Base, SANAE IV, situated in Antarctica. The base has heating and ventilation system problems. During wintertime, the base is too cold, while in summer time, the base seems too hot. Another problem is that the humidity in the base is too low. The design of improvements that can be developed and then be used at SANAE IV is included in the report. The chapter on the results of the calculations clearly points out that the capacities of the fan coil units and the humidifiers are too small and possible solutions to the problems were found. Very useful information regarding the thermal energy requirements were used for this thesis.

Beyers and Harms (2002) describe the experimental modeling procedure and present results to evaluate the snowdrift characteristics surrounding the SANAE IV station. The wind profiles of the prevailing winds were measured with a 6 m wind mast and the characteristic surface roughness and shear velocity functions were derived and analyzed. It was found that the surface roughness and shear velocity functions derived from the wind velocity data compares favorably with other available results. The functions for the surface roughness and shear velocity were used in this thesis to obtain wind speeds at 10 m height.

Taylor et al. (2002) investigated methods of reducing the impact of diesel engines on the Antarctic environment and their associated maintenance benefits. The report provides valuable information regarding the emissions by the diesel generators at SANAE IV. The use of particle traps to reduce particulate matter from the combustion of diesel fuel is

recommended. Improvements to make the polar diesel more visible, in order to aid the spilt fuel clean-up process, are presented. One suggestion was to add a dye to the fuel to make it more visible.

The field trip to SANAE IV, as mentioned in chapter 5, is the first involvement of a university engineering department at SANAE IV. Information regarding the involvement of engineers in Antarctica has been obtained (Wilks, 2000). The harsh conditions and the remoteness of Antarctica make engineering work at or for Antarctica a difficult task. Wilks (2000) mentions the activities of British Antarctic Survey (BAS) engineers and some of the solutions they have obtained. These solutions include ice core drills, snow depth detection systems and sea ice tracking devices.

3.3 Other Antarctic Stations Involved with Wind Power

Australia currently occupies three Antarctic stations (Guichard et al., 1995). A significant amount of research and experimentation on wind energy utilization for these stations have been done. Therefore much of this information has been used. Steel (1993) concluded that the large scale of an alternative energy system involving hydrogen as the prime 'energy carrier' is initially prohibitive. An alternative energy system centered on a wind farm producing energy for a station is the most practical means to reduce the consumption of fossil fuels. Periods of excess electrical production by the wind farm can be used for the production of hydrogen by the electrolysis of water. The hydrogen can be stored and later used by a fuel cell power plant to produce energy during periods of low electrical production by the wind farm.

Information regarding current wind energy projects at Antarctic stations for several different countries was obtained from another Australian source (Brown, 1997). This information is very useful, since the development of wind turbine research for Antarctic conditions can be compared. Two countries and their current wind turbine projects are listed below:

Germany, Neumayer:

- Vertical axis wind turbine in operation for more than 1 year
- Very robust wind turbine
- System is fairly reliable
- Size: 10 kW
- Energy penetration into grid: ~5 - 10% per year.

Australia, Casey:

- 10 kW test turbine in operation for 5 years

Australia, Mawson:

- Current project of installing 3 wind turbines
- 300 kW output per turbine
- Current aim: 80% energy penetration into existing electricity grid
- => Trying to save ~500000 L of fuel per year
- Future aim: 100% energy penetration into grid

Brown (1997) shows that the analysis of the wind energy indicated high resources for Mawson and Macquarie Islands, while low resources for Casey and Davis. Fieldwork to validate his results was initiated at Casey, including the installation of a 10 kW wind turbine.

This thesis is dealing with the technical and economic feasibility of utilizing wind energy for the South African Antarctic station SANAE IV. This involves medium-scale wind turbines, compared to the current intensive research on big scale wind turbines at the Australian station Mawson (Magill, 2000). Research done on the technical aspects of wind turbine design, installation and operation are given in the next section.

3.4 Technical Information

Rogers et al. (2001) provide an overview of the design requirements for medium-sized wind turbines intended for use in a remote hybrid power system. The recommendations are based on first hand experience acquired at the University of Massachusetts through the

installation, operation, and upgrade of a 250 kW turbine on a mountain top with difficult access in Western Massachusetts. Experience with the operation of this turbine and the design of its control system, together with a long history in the design and analysis of hybrid power systems, has made it possible to extend the work in Western Massachusetts to remote or hybrid power systems in general. The University test site has many attributes of more remote sites and the overall wind turbine installation is typical of one that could power a hybrid wind system. For example, access to the site is limited due to steep terrain, snow, and environmental restrictions. Also, the power lines feeding the turbine exhibit voltage sags and phase imbalances, especially during start-up. The paper is based on the experience gained from the operation of this wind turbine and assesses the requirements for the design and operation of medium to large wind turbines in remote locations. The work summarizes lessons learned relative to: (1) sensors, communication, and control capabilities; (2) grid connection issues; and (3) weather-related problems. The final section of the paper focuses on design requirements to ensure successful installation and the completion of maintenance and repairs at remote sites. This article has many aspects that were considered, like accessibility problems, grid connections issues and maintenance problems, when the feasibility of this thesis was analyzed.

The paper by Maalawi and Badawy (2000) presents a direct approach for the determination of aerodynamic performance characteristics of horizontal axis wind turbines. Based on Glauert's solution of an ideal windmill along with an exact trigonometric function method, analytical closed form equations are derived and given for preliminary determination of the optimum chord and twist distributions. The variation of the angle of attack of the relative wind along blade span is then obtained directly from a unique equation for a known rotor size and refined blade geometry. A case study including the analysis of an existing turbine model is given and results are discussed and compared with those obtained by other investigators. It is shown that the approach used in the study is efficient and saves much of the computational time as compared with the commonly used iterative procedures. The determination of aerodynamic performance was not included in this thesis, since a wind turbine was proposed that meets the requirements for operation at SANAE IV.

The realization of a wind turbine as a source of clean, non-polluting and renewable energy may depend on the optimum design of turbine blades that can operate efficiently under extreme variations in wind conditions (Ahmed and Archer, 2001). In this paper the results of an experimental investigation to examine the effectiveness of a highly loaded theory for the design of a horizontal axis wind turbine for optimum power production over a wide range of advance ratios is presented. It is found that the theory, which can be used to set up design curves easily and requires only hand held calculators for calculation, offers a rational basis for the design of propeller wind turbines for peak performance.

Selected results of a study concerning the load bearing capacity and the seismic behavior of a prototype steel tower for a 450 kW wind turbine with a horizontal power transmission axle are presented in an article by Bazeos et al. (2002). The main load bearing structure of the steel tower rises to almost 38 m in height and consists of thin-wall cylindrical and conical parts of varying diameters and wall thicknesses, which are linked together by bolted circular rings. The behavior and the load capacity of the structure have been studied with the aid of a refined finite element and other simplified models recommended by appropriate building codes. The structure is analyzed for static and seismic loads representing the effects of gravity, the operational and survival aerodynamic conditions, and possible site-dependent seismic motions. Comparative studies have been performed on the results of the above analyses and some useful conclusions are drawn pertaining to the effectiveness and accuracy of the various models used in the work. Although a topic of interest for Antarctic conditions, this thesis did not take structural analyses into account, since again a complete wind turbine was found.

The article by Winterstetter and Schmidt (2002) discusses the stability of circular steel shells under combined loading. Circular cylindrical shells made of steel are used in a large variety of civil engineering structures, e.g. in off-shore platforms, chimneys, silos, tanks, pipelines, bridge arches or wind turbine towers. They are often subjected to combined loading inducing membrane compressive and/or shear stress states, which endanger the local structural stability (shell buckling). A comprehensive experimental and numerical investigation of cylindrical shells under combined loading has been performed which

yielded a deeper insight into the real buckling behavior under combined loading. Beyond that, it provided rules how to simulate numerically the realistic buckling behavior by means of substitute geometric imperfections. A comparison with existing design codes for interactive shell buckling reveals significant shortcomings. A proposal for improved design rules is put forward.

The main objective of the paper by Maalawi and Badr (2002) is to categorize practical families of horizontal-axis wind turbine rotors, which are optimized to produce the largest possible power output. Refined blade geometry is obtained from the best approximation of the calculated theoretical optimum chord and twist distributions of the rotating blade. The mathematical formulation is based on dimensionless quantities so as to make the aerodynamic analysis valid for any arbitrary turbine models having different rotor sizes and operating in different wind regimes. The selected design parameters include the number of blades, type of airfoil section and the blade root offset from hub center. The effects of wind shear as well as tower shadow are also examined. A computer program has been developed to automate the overall analysis procedures, and several numerical examples are given showing the variation of the power and thrust coefficients with the design tip speed ratio for various rotor configurations.

Craig and Van Reenen (1996) describe the generation of both unstructured and structured surface grids for use in the numerical simulation of air pollution and atmospheric flows. The topographical features of a terrain are captured using Global Positioning System (GPS) data. Unstructured grids are generated using this data. Various interpolation and post-processing techniques are used to construct a structured grid. The structured grid is used for numerical simulation with Computational Fluid Dynamics (CFD) techniques and for the manufacturing of wind tunnel models for the terrain. The grid generation methods presented are shown to be able to capture intricate topographical features, thereby increasing the accuracy of wind field predictions required for air pollution simulation. The techniques developed can be used for the conversion of any unstructured grid to a structured grid. The use of structured grid to obtain contour maps were not needed in this thesis, since the program MathCAD version 8 is able to plot contour maps from

unstructured girds. Another very important subject for this thesis is the ice accretion on wind turbines. This is discussed in the next paragraph.

The objective of the paper by Brahhimi et al. (1998) is to develop a computer code capable of simulating the shape and amount of ice that may accumulate on horizontal axis wind turbine blades when operating in icing conditions. The resulting code is able to predict and simulate the formation of ice in rime and glaze conditions, calculate the flow field and particle trajectories, and perform a thermodynamic analysis. It also gives the possibility to study the effect of different parameters that influence the ice formation such as temperature, liquid water content, droplet diameter and accretion time. The analysis has been conducted on different typical airfoils as well as on the NASA/DOE Mod-0 wind turbine. Results showed that ice accretion on wind turbines might reduce the power output by more than 20 %.

3.5 Wind Analysis Information

Wind data information from SANAE IV is very important for this thesis, as the technical evaluation will be based on wind data at SANAE IV. Some useful data was found on the website http://www.geocities.com/sanaeiv/weather/weather.html. However, the thesis will not be based solely on this information, since a comprehensive amount of wind data measurements were taken during the trip to SANAE IV.

In order to analyze the data gathered, wind profiles have to be obtained and power densities have to be calculated from the given wind speeds (Beyers and Harms (2002), Seguro and Lambert (1999), Garcia et al. (1997) and Ahmed and Abouzeid (2001)).

The paper by Lu et al. (2002) discusses the potential for electricity generation on the Hong Kong islands through an analysis of the local weather data and typical wind turbine characteristics. An optimum wind speed, u_{op}, is proposed to choose an optimal type of wind turbine for different weather conditions. A simulation model has been established to describe the characteristics of a particular wind turbine. A case study investigation allows

wind speed and wind power density to be obtained using different hub heights, and the annual power generated by the wind turbine to be simulated. The wind turbine's capacity factor, being the ratio of actual annual power generation to the rated annual power generation, is shown to be 0.353, with the capacity factor in October as high as 0.50. The simulation shows the potential for wind power generation on the islands surrounding Hong Kong. The information regarding the optimum wind speeds and the derivation of the energy output of a wind turbine has been found to be very useful for this thesis. The derivation of the Weibull parameters are described next.

Three methods for calculating the parameters of the Weibull wind speed distribution for wind energy analysis are presented in the paper by Seguro and Lambert (1999): The maximum likelihood method, the proposed modified maximum likelihood method, and the commonly used graphical method. The application of each method is demonstrated using a sample wind speed data set, and a comparison of the accuracy of each method is also performed. The maximum likelihood method is recommended for use with time series wind data, and the modified maximum likelihood method is recommended for use with wind data in frequency distribution format. Since time series data was used for the wind analysis, the maximum likelihood method to determine the Weibull parameters was used in this thesis.

In the study by Mathew et al. (2001), a method for characterizing wind regimes and bringing out their energy potential is discussed. A Rayleigh distribution was adopted for defining the distribution of wind velocity in terms of its probability density and cumulative distribution functions. Expressions to compute the energy density, energy available in the wind spectra in a time period and the energy received by turbine have been developed. A method to identify the most frequent wind speed and velocity that carries maximum amount of energy with it is also discussed. The analysis of wind energy potential of eight sites in Kerala, India, adopting this procedure is presented. The performance of three wind turbines, differing in their working velocity band, at these sites, are compared. The effect of cut-in and cut-out wind speeds on wind turbine performance is also analyzed and the results were also used in this thesis.

The wind speed data represented in the form of frequency curves show the shape of a potential model. The Weibull and Lognormal models are used for this purpose, with hourly mean wind speed data. The study by Garcia et al. (1997) deals with the estimation of the annual Weibull and Lognormal parameters from 20 locations in Navarre. The suitability of both distributions is judged from the R^2 coefficient with linear regression for the Weibull distribution and nonlinear regression for the Lognormal distribution. Both approaches give a good fit, but better results are obtained for the Weibull distribution. A comparison between the estimation and the production for a wind farm is offered.

The paper by Ahmed and Abouzeid (2001) presents a study for the utilization of wind energy in Egypt at coastal and some remote desert areas. The available wind energy data at the north coast, the Red Sea coast and east of Oweinat were collected and analyzed and are presented in a form useful for wind energy study. The investigation aimed at evaluating average wind speed for the most promising sites. Moreover, the possible amount of captured energy for each site is determined. Average and r.m.s. values of power are calculated in order to determine the power form factor. These parameters at any site are essential for choosing the appropriate wind turbine. The assessment reveals that these remote sites offer sufficient wind energy for economic utilization and represent a good example for utilizing wind energy to supply a part of the energy requirements to those communities. The design of a wind chart is presented in detail. The study confirms that the Capacitor Self-Excited Induction Generator, Reluctance Generator and Permanent-Magnet Generator emerged as suitable candidates for utilizing wind energy in isolated and remote areas.

The article by Balouktsis et al. (2001) presents a nomogram method for estimating the energy produced by wind turbine generators. A simple nomogram is constructed to estimate the power generated by a wind turbine generator (WTG) operated at near maximum efficiency using optimum tip-speed ratio between cut-in and rated wind speed, and at constant power using optimum pitch control between the rated and cut-out wind speed. The nomogram is based on information that is readily available for commercial

WTGs as well as some simple statistical quantities for the wind at the site. When the wind speed is described by a Weibull distribution, the power of a WTG is estimated in terms of three generalized non-dimensional parameters. When a Rayleigh distribution is employed only two parameters are necessary. A mathematical analysis is presented which allows for the construction of single chart nomograms without sacrificing the necessary accuracy. Two application examples demonstrate the degree of accuracy achieved by the nomograms and the advantages they offer for parametric analyses as regards convenience and labor. The nomogram method to determine the output of a wind turbine was initially used in this thesis. However, a more accurate technique (integration of the Weibull distribution) was found and was used in the thesis.

The paper by Pryor and Barthelmie (2001) presents analyses of flow characteristics in the near-shore and offshore environment using data from the Danish wind-monitoring network. In this relatively high wind speed environment the temporal auto-correlation of wind speeds measured in the offshore coastal zone at or above a height of 40 m is not significantly higher than that from land masts. However, the persistence of wind speeds above typical wind turbine cut-in speeds is higher at coastal and offshore masts. The parameters of wind speed distributions, calculated for the onshore and offshore data, indicate that both the mean and form of the distribution are modified during offshore flow. It is shown that in the near-surface layer vertical propagation of the modified momentum flux differentially affects the body and tails of the wind speed distribution. These analyses further indicate that at a height of 50 m under stable stratification the flow has not fully adjusted to the differing fluxes over the sea even after an over water fetch of at least 11–20 km.

Another type of important information has been found on the website called http://www.geocities.com/Yosemite/Geyser/3161/tech/tech.html. This website contains the major technical information regarding SANAE IV. Form this website additional information regarding the energy systems at the base has been obtained.

3.6 Energy, Electrical and Grid Connection Information

The article by Lenzen and Munksgraad (2001) presents energy and CO_2 life cycle analyses of wind turbines. Despite the fact that the structure and technology of most modern wind turbines differs little over a wide range of power ratings, results from existing life cycle assessments of their energy and CO_2 intensity show considerable variations. While the range of energy intensities reflects economies of scale, their scatter is due to discrepancies in the energy contents of materials and the analyses' methodology and scope. Furthermore, energy intensities depend crucially on the country of manufacture, turbine recycling or overhaul after the service life, and the choice of tower material. In addition, CO_2 intensities vary with national fuel mixes. Measures of life-cycle energy or CO_2 emissions can be employed in policy and planning, especially for comparative risk and sustainability assessments, and source switching and capacity growth scenarios. If these measures are to assist decision-making, uncertainties in life-cycle assessments should be minimized by compliance to a standardized methodology, and by use of input–output-based hybrid techniques. Although the CO_2 life cycle technique was not used in this thesis, it provided valuable information regarding similar techniques. The integration of wind turbines, based on the level of energy penetration, is presented in the following paragraphs.

It is tempting to view the addition of wind turbines to a diesel mini-grid as a straightforward task, only slightly more complicated than a conventional grid-connected installation, requiring only a few ancillary components at a relatively modest cost (Drouilhet, 1999). While this is true for low penetration wind-diesel systems, where the wind turbine output averages no more than about 15% of the load, high penetration systems, in which the average wind power generated can approach or even exceed the average load, require much more sophisticated controllers and more extensive components in addition to the wind turbines. This additional cost and complexity can often be justified by the much greater fuel savings (and associated environmental benefits) and reduced diesel-operating time made possible by high wind penetration. This article is intended as an introduction to some of the control challenges faced by developers of high penetration wind-diesel systems, with a focus on the management of power flows in order to achieve precise regulation of frequency and voltage in the face of rapidly varying wind power input

and load conditions. The control algorithms presented in the paper are being implemented in the National Renewable Energy Laboratory (NREL) high penetration wind-diesel system controller that was installed in the village of Wales, Alaska, in early 2000.

Hourly mean wind-speed data for the period 1986-1997 recorded at the solar radiation and meteorological monitoring station, Dhahran, Saudi Arabia, have been analyzed to investigate the optimum size of battery storage capacity for hybrid (wind-diesel) energy conversion systems at Dhahran. The results exhibit a trade-off between size of the storage capacity and diesel power to be generated to cope with specific annual load distribution (41500 kWh) and for given energy generation from wind energy conversion systems (WEC). The energy to be generated from the back-up diesel generator and the number of operational hours of the diesel system to meet a specific annual electrical energy demand have also been presented. The diesel back-up system is operated at times when the power generated from wind energy conversion systems fails to satisfy the load and when the battery storage is depleted. The present study shows that for economic considerations, for optimum use of battery storage and for optimum operation of the diesel system, storage capacity equivalent to one to three days of maximum monthly average daily demand needs to be used. It has been found that the diesel energy to be generated without any storage is considerable; however, use of one day of battery storage reduces diesel energy generation by about 35%; also the number of hours of operation of the diesel system is reduced by about 52%.

The paper by Tariq (2002) describes a hybrid energy system consisting of a 5 kW wind turbine and a fuel cell system. Such a system is expected to be a more efficient, zero emission alternative to a wind-diesel system. Dynamic modeling of various components of this isolated system is presented. Selection of control strategies and design of controllers for the system is described. Simnon is used for the simulation of this highly nonlinear system. Transient responses of the system for a step change in the electrical load and wind speed are presented. System simulation results for a pre-recorded wind speed data indicates the transients expected in such a system. Design, modeling, control and limitations of a wind fuel cell hybrid energy system are discussed.

The paper by Jurado and Saenz (2001) deals with the development of a neuro-fuzzy controller for a wind–diesel system composed of a stall regulated wind turbine with an induction generator connected to an AC bus-bar in parallel with a diesel generator set having a synchronous generator. A gasifier is capable of converting tons of wood chips per day into a gaseous fuel that is fed into a diesel engine. The controller inputs are the engine speed error and its derivative for the governor part of the controller, and the voltage error and its derivative for the automatic voltage regulator. These are readily measurable quantities leading to a simple controller, which can be easily implemented. It is shown that by tuning the fuzzy logic controllers, optimal time domain performance of the autonomous wind–diesel system can be achieved in a wide range of operating conditions compared to fixed-parameter fuzzy logic controllers and PID controllers. Since controllers for the wind turbine system were recommended to be purchased from NPS the design of such equipment was not performed in this thesis.

In the article by Papathanassiou and Papadopoulos (2000) the dynamics of a small autonomous system, comprising a diesel generator and a wind turbine, are investigated. The analysis is performed both in the frequency and time domain, using simplified models of the system components and taking into account the diesel engine speed governor and the wind turbine pitch controller (for pitch regulated machines). The investigation is extended to include different types of wind turbines, equipped with induction or synchronous generators and using pitch or stall regulation, as well as operation of the wind turbine in an autonomous or infinite system. The objective is to determine the main factors affecting the behavior of the system and to illustrate the effect of the speed governor and pitch controller settings on the expected performance. Particular emphasis is placed on identifying the main modes of the system and determining their dependence on the controllers' parameters. A comparative assessment of the dynamic characteristics of different types of wind turbines is also included and the operation of the wind turbine in a small system and against an infinite bus is addressed and discussed.

The paper by Valtchev et al. (2000) briefly reviews the need for renewable power generation and describes a medium-power Autonomous Renewable Energy Conversion

System (ARECS), integrating conversion of wind and solar energy sources. The objectives of the paper are to extract maximum power from the proposed wind energy conversion scheme and to transfer this power and the power derived by the photovoltaic system in a high efficiency way to a local isolated load. The wind energy conversion system operates at variable shaft speed yielding an improved annual energy production over constant speed systems. An induction generator (IG) has been used because of its reduced cost, robustness, absence of separate DC source for excitation, easier dismounting and maintenance. The maximum energy transfer of the wind energy is assured by a simple and reliable control strategy adjusting the stator frequency of the IG so that the power drawn is equal to the peak power production of the wind turbine at any wind speed. The presented control strategy also provides an optimal efficiency operation of the IG by applying a quadratic dependence between the IG terminal voltage and frequency: $V \sim f^2$. For improving the total system efficiency, high efficiency converters have been designed and implemented. The modular principle of the proposed DC/DC conversion provides the possibility for modifying the system structure depending on different conditions. The configuration of the presented ARECS and the implementation of the proposed control algorithm for optimal power transfer are fully discussed. Again, much information in the article refers to designs and their evaluation, and was not used in this thesis.

Most of the articles found on economics are based on grid connected wind turbines, producing energy for the local grid (Gupta, 2000, Cavall, 1995 and Habali et al. 2000). This however is not relevant to this project since the operation of a wind turbine at SANAE IV is a typical example of a remote, hybrid, and off-grid wind power system. Also, a wind turbine system for SANAE IV is of the small-scale type, which has to be connected to a weak grid. This is explained in detail in the chapter on grid connection.

3.7 Economic Information

The economic evaluation of a wind energy system for Antarctic conditions is a very specialized subject and very little information regarding this topic is available. However, a substantial amount of information has been obtained on economic evaluations of wind energy systems in third world countries (Jagadeesh, 2001) and remote villages.

The paper by Isherwood et al. (1999) presents an analytical optimization of a remote power system for a hypothetical Alaskan village. The analysis considers the potential of generating renewable energy (e.g., wind and solar), along with the possibility of using energy storage to take full advantage of the intermittent renewable sources available to these villages. Storage in the form of either compressed hydrogen, or zinc pellets can then provide electricity from hydrogen or zinc–air fuel cells whenever wind or sunlight is low. The renewable system is added on to the existing generation system, which is based on diesel engines. Results indicate that significant reductions in fossil fuel consumption in these remote communities are cost effective using renewable energy combined with advanced energy storage devices. A hybrid energy system for the hypothetical village can reduce consumption of diesel fuel by about 50% with annual cost savings of about 30% by adding wind turbines to the existing diesel generators. Adding energy storage devices can further reduce fuel use, and depending on the economic conditions potentially reduce life-cycle costs. With optimized energy storage, use of the diesel generator sets can be reduced to almost zero, with the existing equipment only maintained for added reliability. However, about one quarter of the original fuel is still used for heating purposes. Very useful information was used from this article and was integrated in chapter 11. Another method to assign a value to emissions is given in the next article.

The economics of renewable energy is the largest barrier to renewable energy penetration. Nevertheless, the strong desire to reduce environmental emissions is considered a great support for renewable energy sources. In the paper by El-Kordy et al. (2001), a full analysis for the cost per kWh of electricity generated from different systems actually used in Egypt is presented. Also renewable energy systems are proposed and their costs are analyzed. The analysis considers the external cost of emissions from different generating systems. A proposed large scale PV plant of 3.3 MW, and a wind farm 11.25 MW grid connected at different sites are investigated. A life cycle cost analysis for each system was performed using the present value criterion. The comparison of results showed that wind energy generation has the lowest cost, followed by a combined cycle natural gas fired system. A photovoltaic system still uses comparatively expensive technology for electricity

generation; even when external costs are considered the capital cost of photovoltaic needs to be reduced by about 60% in order to be economically competitive.

The aim of the investigation by Papadopoulos and Dermentzoglou (2001) is the development and implementation of a general and systematic procedure for the evaluation of the economic viability of planned installation of wind energy converters (WEC) for the purpose of electrical power production. The procedure is based on: the assessment of wind energy potential of an area; the limitations involved in selecting specific locations/sites for the system installation in this area; the technical specification of a candidate WEC system; and the assessment of the economic viability of such electrical power production systems by applying suitable economic/financial analysis techniques.

The influence of the governing techno-economic parameters on the economic behavior of commercial wind parks is investigated in the article by Kaldellis and Gavras (1999). For this purpose, a complete cost-benefit analysis model, properly adapted for the Greek market, is developed in order to calculate the payback period and the economic efficiency of similar investments in the energy production sector. Moreover, the impact of various parameters - such as capital cost, return on investment index, local inflation rate index, electricity price escalation rate, installation capacity factor, maintenance and operation cost, turn-on key cost of the power plant, size of wind turbines used - on the economic viability and attractiveness is extensively investigated, using a well-elaborated simple "expert system" type numerical code. Finally, the prediction results are summarized in a representative sensitivity analysis map, including the most reasonable economic scenarios. Taking into account the analytical results of the proposed study along with the existence of high wind potential regions in Greece, a remarkable growth of the wind energy sector is expected in the near future, leading to considerable investment profits and offering a strong position (share) of the liberalized local power market.

The paper by Bakos and Tsagas (2002) reports the technical feasibility and economic viability of a hybrid solar/wind grid connected system for electrical and thermal energy production, covering the energy demand of a typical residence in the city of Xanthi

(Greece). The technical characteristics of the solar and wind energy subsystems are given. The energy output provided by the hybrid energy system was estimated using a simulation program, which is based on the Monte Carlo method, for reading the solar radiation and wind potential data. The auxiliary energy supply is based on the output of a combined-cycle natural gas power plant, recently constructed in the Thrace region. The economic analysis of the proposed hybrid solar/wind system is performed using the life cycle savings (LCS) method and the payback period (PBP) of the initial capital cost is determined.

An integrated time-dependent feasibility analysis is presented by Kaldellis (2002) in order to improve the reliability of the computational methods to simulate the economic behavior of commercial wind parks in Greece, in view of the continuous technological improvements of the sector and the important worldwide political and economic transformations. According to the proposed model, the time dependency of the governing parameters is taken into account, based on almost 20-years data from the local market records. Additionally, information concerning the technology dependent parameters from several European and local wind parks is also incorporated. The application of the developed computational frame to several cases, concerning the economic behavior of wind parks erected during 1985–95 in Greece, significantly improved the accuracy of predictions in comparison with the results based on time-mean values of the corresponding parameters. Finally, the proposed model satisfactorily explains the evolution of wind energy applications in Greece during the last 15 years, on the basis of pure economic terms. The information of the articles mentioned in this section was used extensively in chapter 11, as they are the basis for an economic evaluation.

4 SANAE IV ENERGY DEMAND

Doing the energy demand calculations for the wind turbine and for the SANAE IV base is very challenging, since very little information was available regarding the energy demand, the fuel consumption, the weather data, etc. Most of this data had not been logged in the previous years, or it had been logged at intervals only. During the field trip, apparatus like the wind mast, the wind measurement equipment and kVA loggers were taken along to get the vital data needed for this thesis. This data was, to a certain extent, obtained during the trip to Antarctica.

In this chapter the thermal energy demand is mentioned, since Teetz (2000) calculated it in a final year thesis on the heating and ventilation system of SANAE IV. In addition to the thermal energy demand, the electrical energy demand there has to be taken into account when doing an energy audit of the SANAE IV base.

4.1 Introduction

South Africa's Antarctic station, SANAE IV, is a large, modern and extremely well equipped facility, consuming significant amounts of energy, both electrical as well as thermal. Thermal energy is the energy recovered by the exhaust heat exchangers on the diesel electric generators. The research station has special needs for reliable, safe, efficient and environmentally friendly power systems to provide electricity, heat and potable water.

Since the 1950s and 1960s when most of the research stations were developed, the energy demands were met by diesel electric generator sets and oil fired boilers. At the time these methods were the most convenient, established and reliable means of supplying power where reliability and safety were, and still are of highest priority. The rationale has persisted that, as the current system works, there is no need to drastically change it. With the shifting environmental emphasis of the activities conducted in Antarctica, the substantial use of fossil fuels in the current energy system has come under increasing scrutiny.

4.2 Current Energy System

The main power demand at the base is in the form of electrical power. ADE diesel electric generators meet the power demand. Mostly only one diesel electric generator is in use, the second generator is automatically switched on when the power demand exceeds 162 kW and is switched off again should the demand drop below 140 kW. The third diesel electric generator is a standby unit. The use of each diesel electric generator is approximately equally balanced, by switching the mode of each diesel electric generator from standby unit to main unit at certain intervals of time.

Two types of engines are used, namely:

- 2 x ADE 442T (Turbo charged)
- 1 x ADE 442Ti (Turbo charged and intercooled)

The detailed information regarding the diesel generators and controllers can be viewed in appendix E. In addition to electrical energy, the station needs large quantities of thermal energy. Estimating the amount of this requirement is not straightforward. At the moment fan coil units are used to heat the ventilation air for each block of the base. In addition, electrical resistance heaters are used, if the outside temperature drops too much. At the moment about 72 kW of energy is needed to keep the base at a temperature of 18 °C, during wintertime. During very cold periods, the energy demand for heating can increase up to about 120 kW.

Heating is one of the largest energy requirements for the operation of the research station. Water jackets on the engines provide heat recovery from the diesel engine cooling water and exhausts. This is supplemented, if necessary, with additional electrical water heating elements located in water tanks in the hangar and water is distributed through the station by a continuously running water circuit.

4.3 Fuel Consumption

Due to extreme temperatures at Antarctica, being –50 °C at times, a special blend of diesel fuel has to be used at the base. Engen supplies the special blend, called 'Special Antarctic Blend', in short SAB. The details for this fuel are given below.

- Specific viscosity: 1.4
- Density: 800 kg/m^3
- Sulfur content: 0.1% m/m max
- Freezing point: -65 °C
- Lower heating value (LHV): 9.8 kWh/L

The fuel consumption is being measured indirectly each day. The base has a day tank, where fuel levels are recorded each day, when fuel is pumped from the main fuel tanks to the day tanks. Therefore a daily average is being obtained, and possible faults with the diesel generators can be recognized early. However, if the day tank is not refilled each day, then there also is no fuel consumption being measured. Thus this data can only be used to represent the fuel consumption accurately for a period longer than a few days, typically one week. This data has been captured for the last 2 years, but only the fuel consumption for 2001and the beginning of 2002 will be used. Figure 4-1 shows the monthly fuel consumption for the years 2000, 2001 and the beginning of 2002. The fuel consumption for the beginning of 2002 has been used for the curve fit between fuel consumption and power production, as can be seen in the following section.

The total yearly diesel consumption can be seen in table 4-1. From the diesel consumption for the 2 years it can be safely assumed that the yearly fuel consumption is about 300000 L.

YEAR	FUEL CONSUMPTION [LITERS]
2000	296072
2001	298416

Table 4-1: Yearly generator diesel consumption

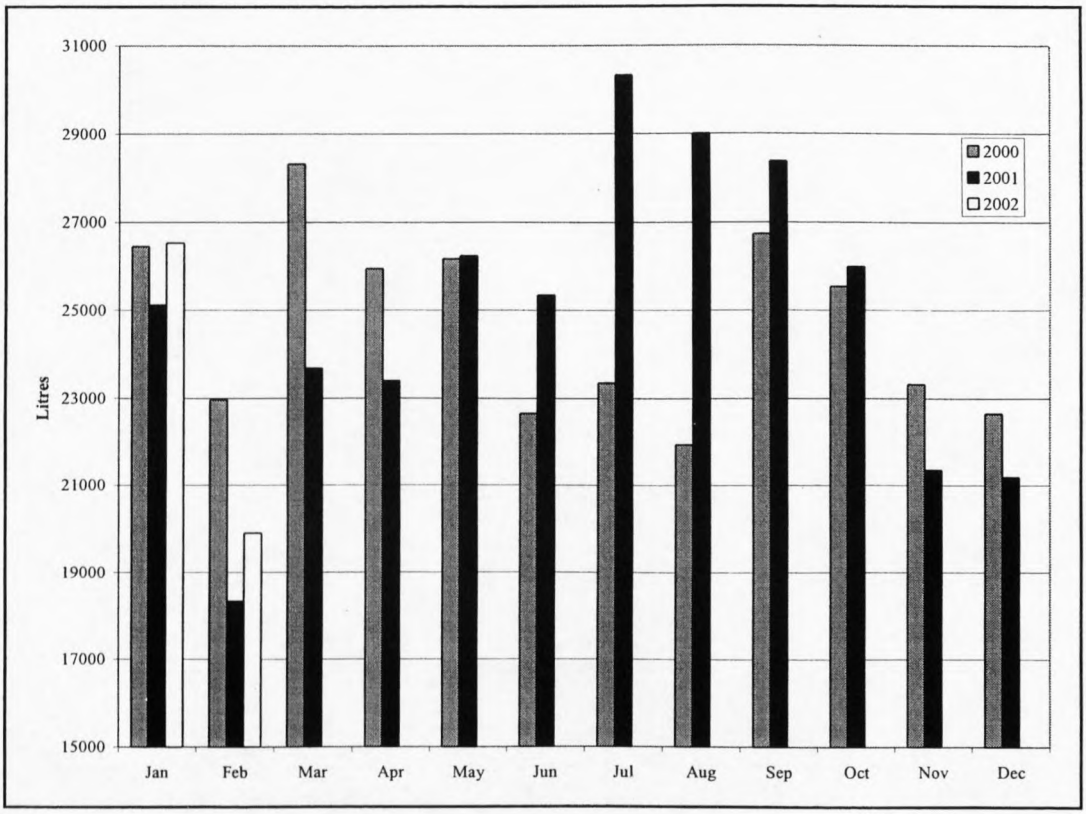

Figure 4-1: Monthly diesel consumption at SANAE IV for power generation

4.4 Electrical Energy Production

As mentioned above, only one diesel electric generator is producing electricity, until the demand exceeds 162 kW and a slave diesel electric generator is switched on. A typical duty-cycle can be seen in figure 4-2.

The rotation of the master and slave diesel electric generator is done every week so that an even power production is achieved between all three generators.

The electrical energy production level of the diesel electric generators was measured during the field trip by Taylor et al. (2002) for about 5 days. From this data, a daily trend can be followed. No data exists for continuously measured energy demand at the base. The only measured data is that of the daily fuel consumption of the diesel electric generators.

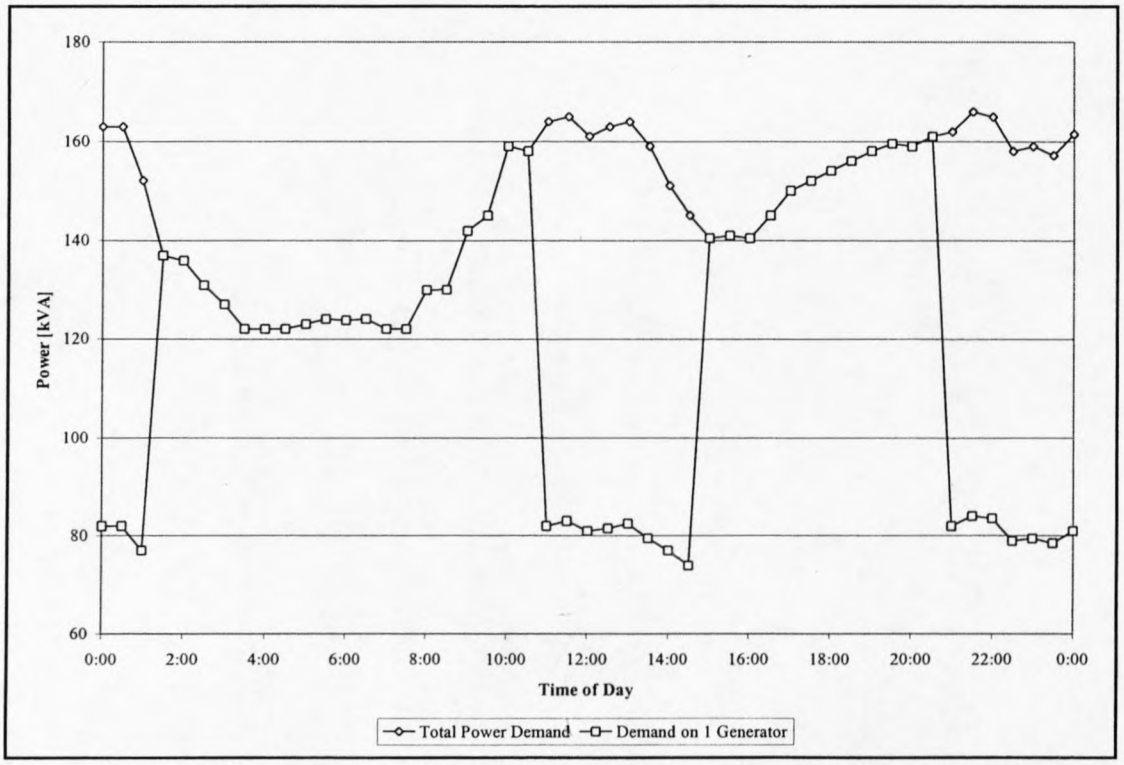

Figure 4-2: Typical duty-cycle of SANAE IV diesel generators (Taylor et al. 2002)

Thus the 5 days of energy demand data was compared to the respective fuel consumption, and a linear relationship in terms of fuel consumption was obtained, by performing a regression analysis. The fuel consumption can be used to evaluate the daily average energy production by the diesel electric generators. The equation is:

$$P := 3.3890 \cdot FC + 167.756 \quad \textbf{(4-1)}$$

where P is the energy production and FC is the fuel consumption, with a regression coefficient of $R^2 = 0.97313$. The comparison graph can be seen in appendix D. Equation (4-1) is only applicable in the range of FC = 300 L – 1300 L.

It remains questionable, if the relationship between the fuel consumption and energy demand is really linear. Normally a diesel electric generator has its highest efficiency when it operates close to its peak output, and with lower efficiency when it operates at a lower output. This would mean that the relationship between fuel consumption and power production would not necessarily be linear. However, since a second diesel electric generator is switched on, when the power demand exceeds 162 kW, the relationship can

still be fairly linear, because then the fuel consumption of 2 diesel electric generators has to be considered. The linear relationship can also be verified by the fact that the regression coefficient of 0.9731, which is fairly high. The regression coefficient was determined by comparing the actual fuel consumption with the linear model described above.

With the fuel consumption data available for 2 years (2000 and 2001), the average power demand of the base can be established. This can be seen in figure 4-3. The following has been evaluated from this power demand data set:

- Maximum power: 215kW x 24 h = 5160 kWh/day
- Minimum power: 60kW x 24 h = 1440 kWh/day
- Average power: 122kW x 24 h = 2930 kWh/day

Although 2 years of fuel consumption and power demand is available, only the power demand data for the year 2001 will be used for the following reasons:

The wind data is available for just longer than one year; therefore it will only be necessary to work with the respective year of power demand data, which is 2001. The other reason is that the fuel consumption follows the power demand, as can be seen from figure 4-3.

The total power demand for 2000 and 2001 can be seen in table 4-2. From the table, it is also obvious that the yearly power demand is nearly the same for both years.

YEAR	TOTAL POWER DEMAND [MWh/year]
2000	1145
2001	1153

Table 4-2: Total yearly power demand

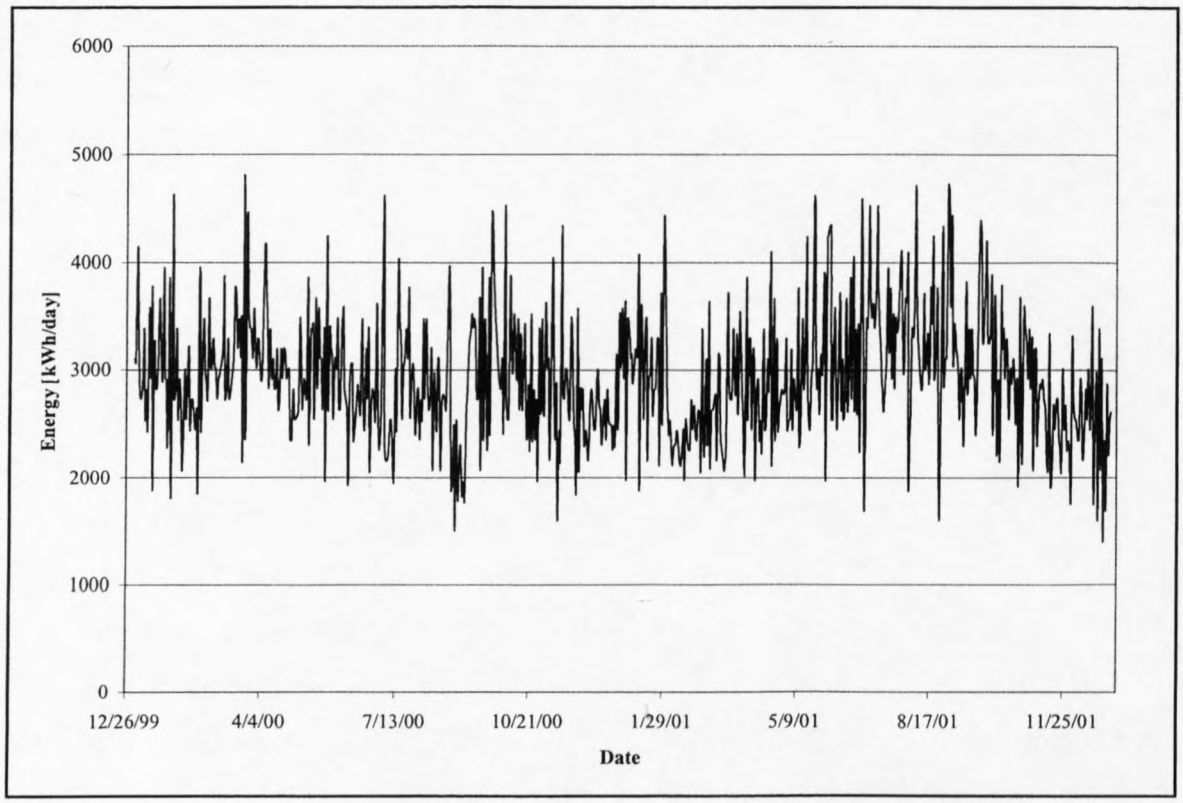

Figure 4-3: Energy demand for 2000 and 2001

The electrical efficiency of the generators can be determined from the linear model used to generate the power demand form the available fuel consumption. It is based on the lower heating value (LHV) of Special Antarctic Blend (SAB) diesel fuel, which is 9.8 kWh/L. It has been determined as follows:

Using the average daily energy production P = 3160 kWh/day with the linear fuel consumption model, we can calculate the fuel consumption. By transforming equation (4-1), we get

$$FC := 0.2951 \cdot P - 49.50 \qquad \textbf{(4-2)}$$

Therefore, the average fuel consumption is FC = 883.016 L/day, resulting in an efficiency of

$$E := \frac{P}{FC} := \frac{3160}{883.016} \cdot \frac{kWh}{day} \cdot \frac{day}{L} := 3.57 \frac{kWh}{L} \qquad \textbf{(4-3)}$$

The efficiency, as a percentage of the LHV of SAB is defined as follows:

$$E_{electrical} := \frac{E}{LHV} := \frac{3.575}{9.8} \cdot 100\ \% := 36.5\ \% \qquad \textbf{(4-4)}$$

The efficiencies are shown in table 4-3.

ELECTRICAL EFFICIENCY OF GENERATOR SETS	
[kWh/L]	**[%]**
3.57	36.5

Table 4-3: Electrical efficiency of generator system (based on LHV of SAB diesel of 9.8 kWh/L)

4.5 Electrical and Thermal Energy Distribution

The electrical and thermal energy distribution at SANAE IV was determined during the takeover period in 2001/2002 by Cencelli (2002). This is part of an energy audit that Cencelli performed during the takeover period. The energy distribution was done as follows. The maximum rating of all the electrical and thermal equipment was written down and from that a distribution scheme was created, because it is known where every piece of equipment is positioned in the base. It is also approximately known when and for how long the equipment is used. Thus the quantified energy distribution was evaluated and is shown in figure 4-4.

Figure 4-4 clearly shows that much more power is used for thermal purposes, than for purely electrical purposes. An example is that about 57 kW is used for the skirting heaters, 120 kW is used for the inline water heaters and 34.28 kW is used for humidification, ventilation and heating of the base. Significantly lower values, like dining room equipment using 6.5 kW, water purification plant using 6.5 kW, are taken up by electrical rather than thermal/electrical equipment. Dining room equipment includes a toaster, a kettle, a refrigerator, a microwave oven and a perculator.

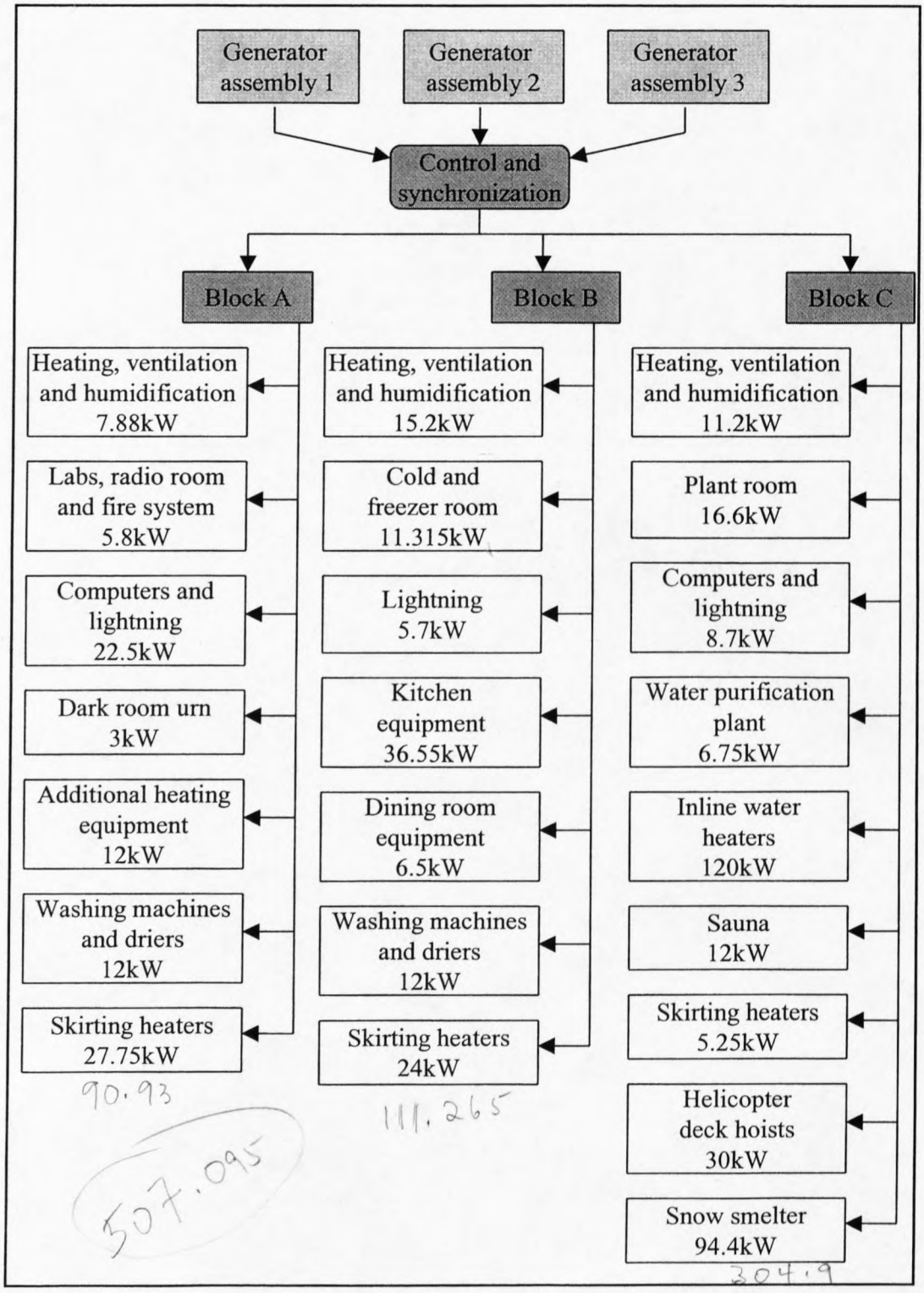

Figure 4-4: SANAE IV base electrical energy distribution

Another important aspect of the energy distribution of SANAE IV is highlighted in figure 4-5. This is the energy flow from the generators to the main distribution boards of blocks A, B and C of the base. Also shown in the figure is the energy flow to the snowsmelter. The reason for showing the energy flow to the snowsmelter is that the snowsmelter uses about 94 kW of electrical power, when all 6 heating elements and the circulation pumps are switched on. This is more than 2/3 of the average energy production during summer season. The reason for highlighting the snowsmelter is not just because of the big power demand, but also because it is ideally suited as a dump load. This dump load, however, will be discussed in chapters 7 and 10.

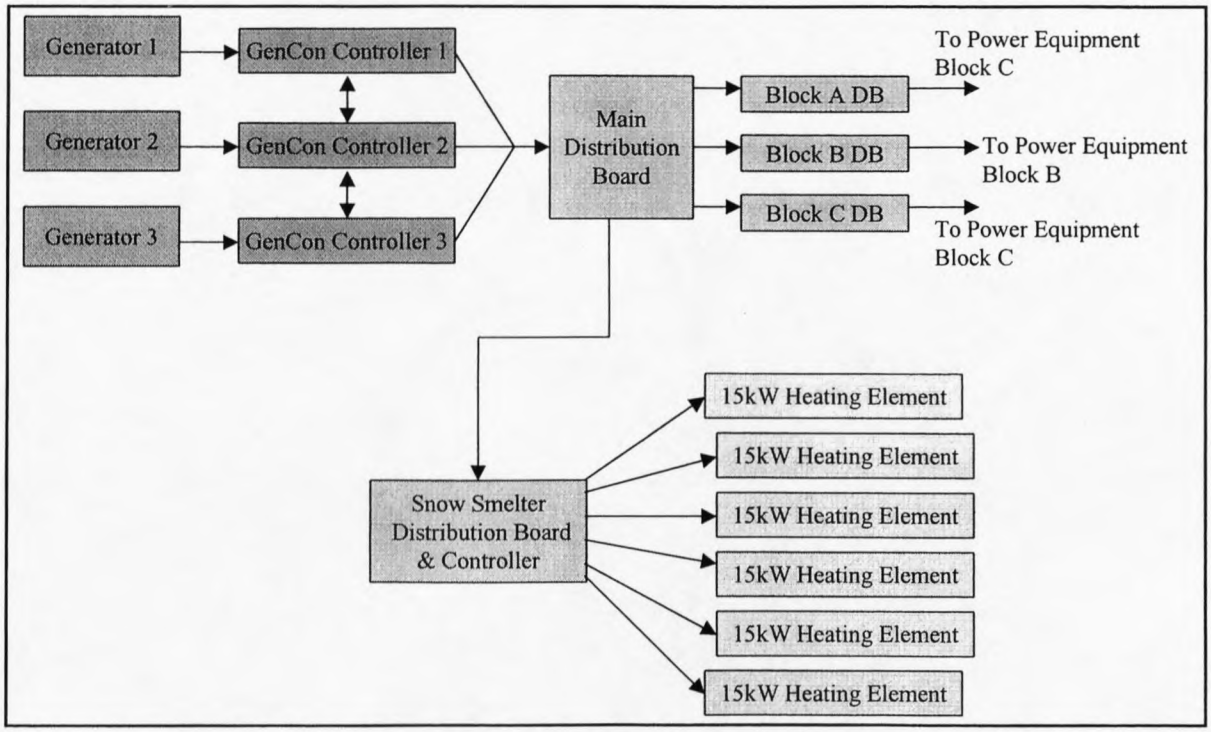

Figure 4-5: Energy flow from generators to the main distribution boards and snow smelter

4.6 Energy Demand Variation

Energy production levels are not constant over a period of time. Daily and seasonal variations occur, due to the number of people at the base and climatic conditions. Energy needs throughout the year are influenced by two main factors: the level of activity on the base, which is highest in summer, and the thermal and lightning needs which are highest in winter.

4.6.1 Constant and varying power demand equipment

The power consuming equipment at the base has been classified into two categories. One category is the constant power demand equipment and the other one is the varying power demand equipment. They have been identified during the summer field trip period, and the varying power demand equipment is:

- Kitchen equipment: 36.55 kW
- Dining room equipment: 6.5 kW
- Sauna: 12.0 kW
- Helideck hoist: 30.0 kW
- Snowsmelter: 94.4 kW
- Washing facility: 24.0 kW
- Low demand equipment uses, like workshop equipment, entertainment equipment, ice machines, etc.: approximately 50 kW

Added to the varying power demand equipment is the equipment with a constant power demand. Although this equipment may not be using constant power, it is referred to as a constant power user, since this equipment will remain switched on permanently. This equipment is:

- Base heating, ventilation and humidification equipment for blocks A, B and C: 34.28 kW
- Cold and freezer room equipment: 11.315 kW
- Computers: 19.8 kW
- Lighting: 17.1 kW
- Plant room pumps and equipment: 16.6 kW
- Laboratory equipment: 2.42 kW
- Radio room equipment: 3.3 kW
- Fire system: 0.08 kW
- Water purification plant: 6.75 kW

- Heating elements for the hot and cold water storage tanks: 30 kW
- Inline water heaters for the fan coil units (FCU): 90 kW
- Additional heating requirement in the form of skirting heaters: 57 kW

Together the constant and the varying power demand equipment produce the total power demand of the base. By using different equipment at different times, daily and seasonal demand levels of varying magnitude are established.

4.6.2 Daily and seasonal variations

Daily variation in energy demand occurs due to the use of different power equipment at different times during the day. A pattern evolves at the base, where certain equipment is used at certain times during the day, day after day, and the pattern is usually kept for each season.

In the summer season the pattern is disturbed, because of the takeover period, which is in itself a separate season. Therefore, one can say that there are roughly 2 seasons: one is the winter season, where only 10 people occupy the base and the takeover season, when about 80 people occupy the base. The takeover period is also known as the summer period. During the summer period an average day power demand was created from the power equipment data at the base, with average power demand, and then also a day with maximum energy demand was created. Figure 4-6 shows the estimated daily energy demand variations for a typical, average summer day and figure 4-7 shows the estimated daily energy demand variations for a maximum power demand summer day.

The two aforementioned graphs clearly show the same pattern. During the night, the constant power load dominates, because everybody is sleeping and nobody is varying any loads. During the day there are three peaks. These peaks originate from the snowsmelter. During the take over period, the snowsmelter is switched on three times a day, thus creating peaks loads at about 10h00, 17h00 and 21h00. Other variations during the day occur due to the kitchen use at about 7h00, 9h00 and 18h00. There are also some minor

variations due to small-scale power demand equipment use. Figures 4-6 to 4-8 clearly show an increased power demand during nighttime than during parts of daytime. During the day the bedrooms are not occupied and do not need any heating. During night the skirting heaters are switched on for additional heating purposes, thus increasing the power demand.

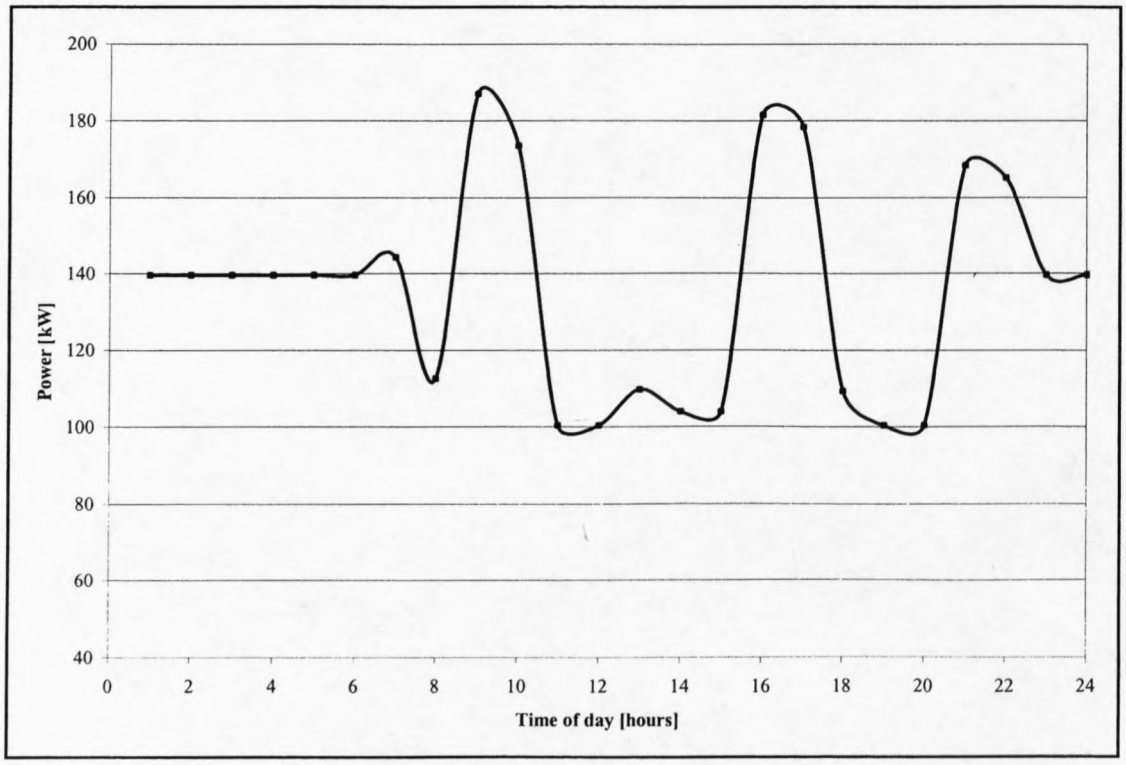

Figure 4-6: Estimated daily energy demand for an average summer day

Unlike during the take over period, the snowsmelter will only be switched on between one and two times a day during the winter period. Thus there are only two power load peaks in figure 4-8.

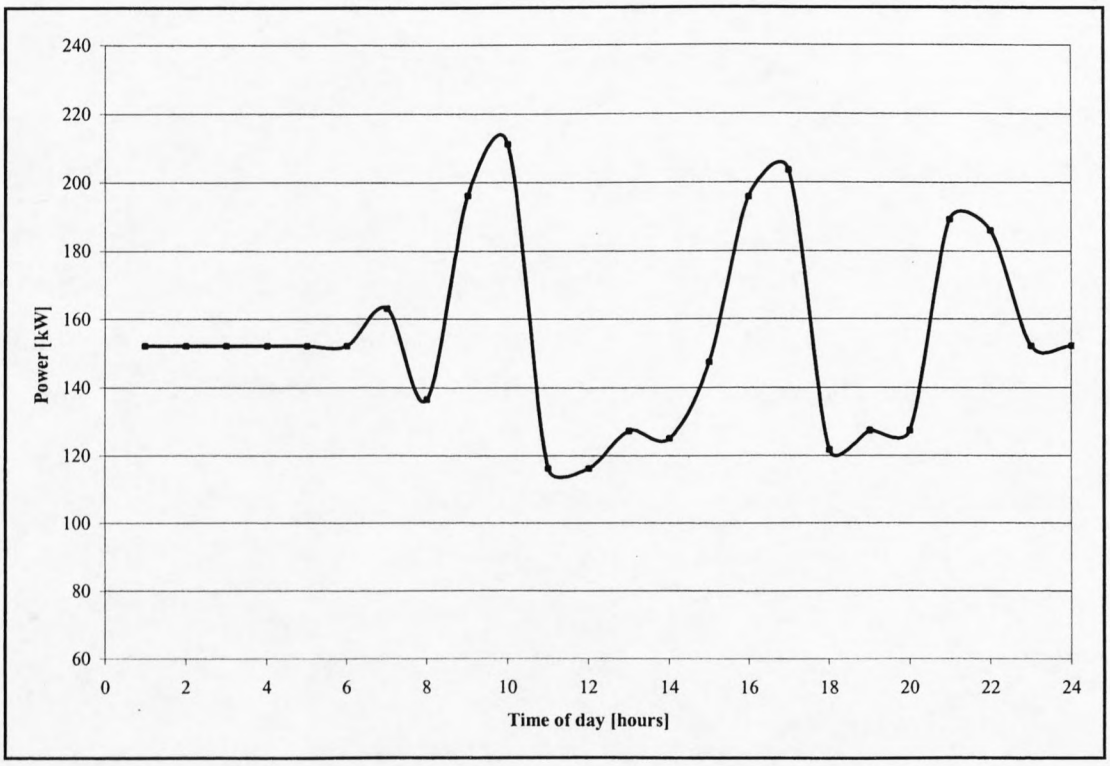

Figure 4-7: Estimated daily energy demand for a maximum power demand summer day

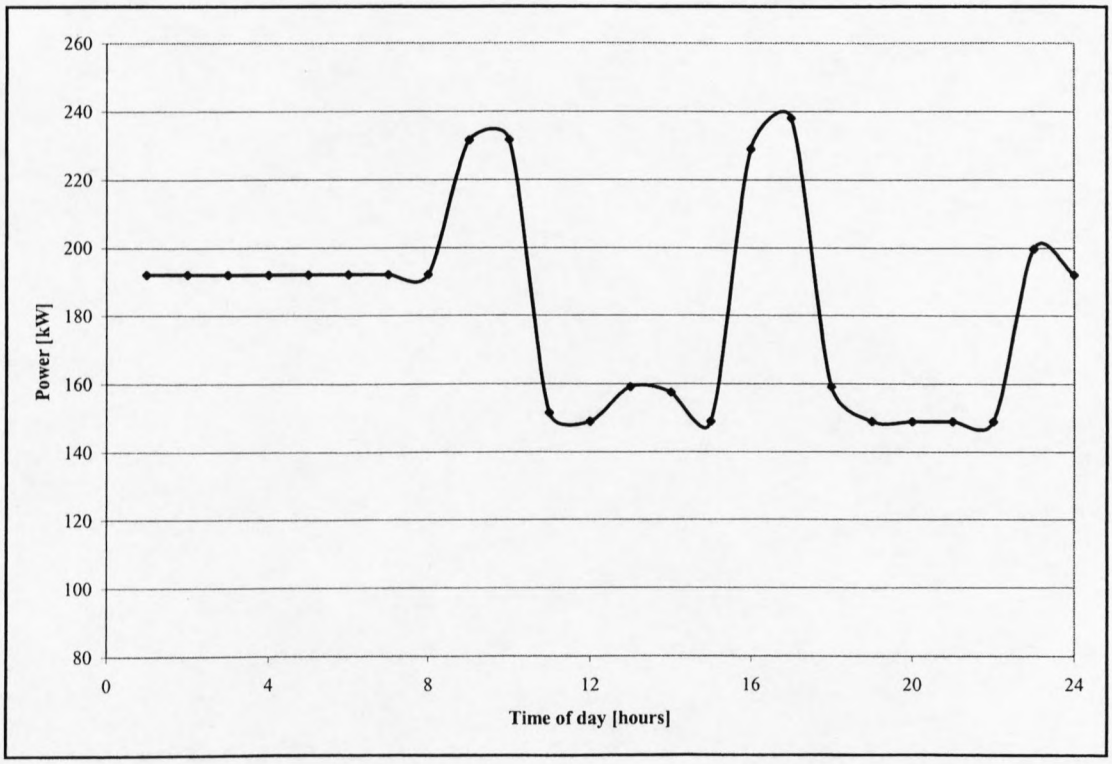

Figure 4-8: Estimated daily energy demand for an average winter day

For the winter period only the average day has been created, although this is only an estimate. The reason for just estimating the winter season is that activity is strongly influenced by the weather conditions. For example, if a storm is blowing for 1 week, no one can go to the outside, in order to refill the snowsmelter. Thus once the storm has cleared, the snowsmelter will be refilled and will be working longer than usual, since the water reserves have to be replenished. From this example it becomes obvious that it is not a straightforward task to make an accurate estimate for a typical winter day's power demand. The estimated energy demand for an average winter day can be seen in figure 4-8.

As mentioned above, this data has been obtained and evaluated by Cencelli (2002). The estimated daily energy demand variations are based on the maximum power demand, specified by the equipment on the base. Since it is quite obvious that the equipment at the base will seldom operate at the maximum power rating, a correction factor has to be incorporated into the power demand data.

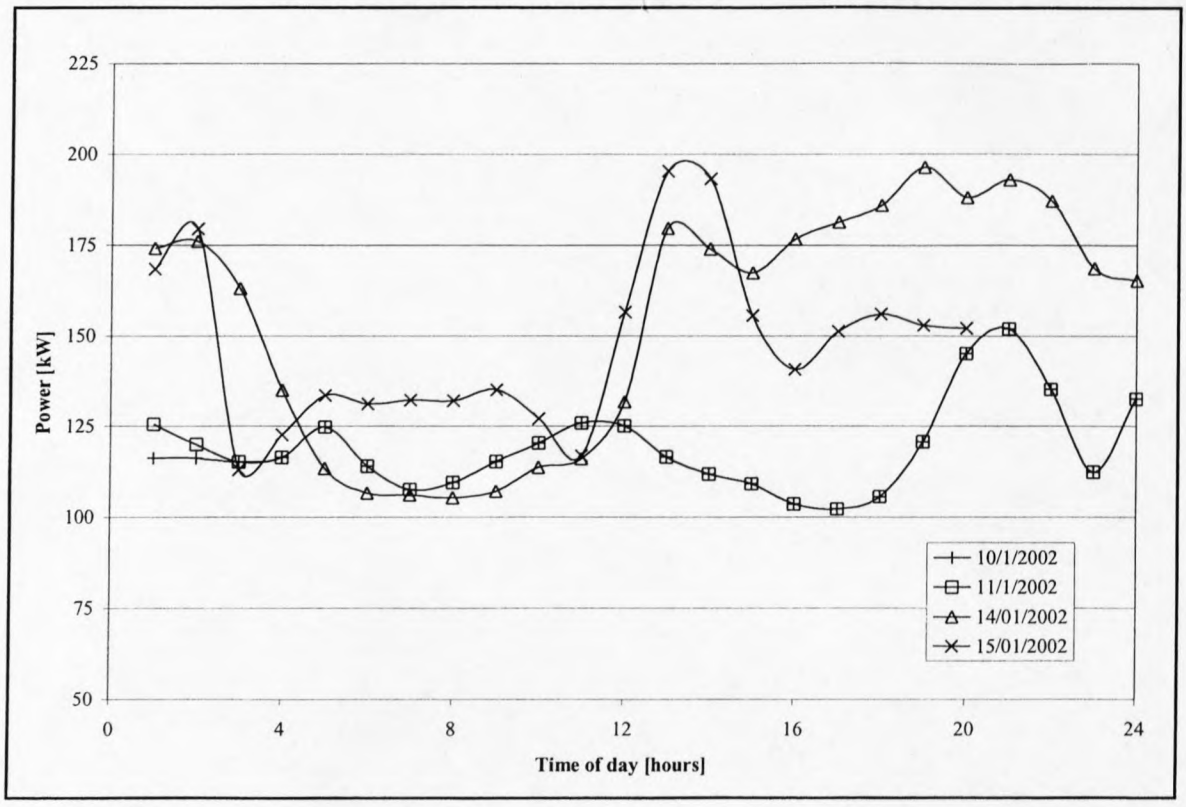

Figure 4-9: Measured power demand data

From the fuel consumption data, a model has been found to correlate the power demand of the base to the fuel consumption. From this power demand data, the average daily power demand can be calculated. This can be compared to the estimated models of Cencelli (2002) and the appropriate correction factors can be found. Another very important correlation is the comparison of the measured power demand data to the estimated models. The energy demand was logged for about 5 days during the takeover period. This data shows the average summer day power demand and the maximum power demand during the takeover period and can be seen in figure 4-9.

In the figure shown above, it can be seen that there are two different power demand variation patterns. One is the average summer day pattern, which happened on the 10th and 11th of January 2002, and the other pattern is the maximum power demand pattern for a summer day, which happened on the 14th and 15th of January 2002. From this data the average and maximum summer day correction factors have been obtained. A sample calculation for the summer day maximum power demand was performed.

Time	Constant Load	Snowsmelter	Kitchen	Miscellaneous	Total
1:00	193.97	0.00	0.00	9.00	202.97
2:00	193.97	0.00	0.00	9.00	202.97
3:00	193.97	0.00	0.00	9.00	202.97
4:00	193.97	0.00	0.00	9.00	202.97
5:00	193.97	0.00	0.00	9.00	202.97
6:00	193.97	0.00	0.00	9.00	202.97
7:00	193.97	0.00	14.50	9.00	217.47
8:00	139.40	0.00	3.00	39.55	181.95
9:00	139.40	94.40	18.28	9.55	261.62
10:00	139.40	90.00	43.05	9.02	281.47
11:00	139.40	0.00	6.50	9.02	154.92
12:00	139.40	0.00	6.50	9.02	154.92
13:00	139.40	0.00	21.12	9.02	169.54
14:00	139.40	0.00	18.28	9.00	166.67
15:00	139.40	0.00	18.28	39.00	196.67
16:00	139.40	94.40	18.28	9.00	261.07
17:00	139.40	90.00	32.90	9.00	271.29
18:00	139.40	0.00	13.81	9.00	162.21
19:00	139.40	0.00	9.50	21.00	169.90
20:00	139.40	0.00	9.50	21.00	169.90
21:00	139.40	94.40	9.50	9.00	252.30
22:00	139.40	90.00	9.50	9.00	247.90
23:00	193.97	0.00	0.00	9.00	202.97
24:00	193.97	0.00	0.00	9.00	202.97
				Average [kW]:	**205.98**

Table 4-4: Energy demand breakup for a typical summer day maximum power demand

Table 4-4 shows the power demand breakup for a summer day with maximum power demand. The 2nd column displays the constant load while columns 3 to 5 display the varying load and column 6 shows the total power demand. At the bottom of the table the average power demand was calculated and is $P_{average}$= 205.98 kW.

From the measured data, shown in figure 4-9, the average power demand can be calculated. The 14th of January 2002 will be used to represent a maximum power demand day in the summer period. The average values can be seen in table 4-5. The estimated and measured averages are compared and the correction factor can be calculated, as follows:

$$\text{Difference} = \frac{\left(P_{theo} - P_{meas}\right)}{P_{theo}} \cdot 100\% := \frac{(205.98 - 154.66)}{205.98} \cdot 100\% := 24.92\ \% \qquad \textbf{(4-5)}$$

Thus the estimated data has to be lowered by about 25%, and the correction factor (CF) for the summer day maximum power demand is

$$CF := \frac{100 - 25}{100} := 0.75 \qquad \textbf{(4-6)}$$

The correction factors (CF) will be multiplied with the estimated models. Thus the estimated models correspond to the measured data. The correction factors for the three estimated models are shown in table 4-6.

Measured average summer day power demand	134.56kW
Measured summer day maximum power demand	154.66kW
Measured average winter day power demand	166.05kW
Estimated average summer day power demand	188.46kW
Estimated summer day maximum power demand	205.98kW
Estimated average winter day power demand	226.05kW

Table 4-5: Estimated and measured power demand data (daily averages)

This is one power demand model. In order to analyze and predict the feasibility of using wind power at SANAE IV, one also has to look at the future use of SANAE IV. Therefore

an overpopulated base will be assumed. This was done so that this project will still be relevant, even when the base will be overpopulated by current standards and practices (SANAE Technical, 1999).

The second scenario is discussed in appendix F.

Description of day	Correction factor
Average summer day power demand	0.72
Summer day maximum power demand	0.75
Average winter day power demand	0.85

Table 4-6: Correction factors for different models

4.7 Electrical Energy Dump Locations

As mentioned earlier, electrical energy dumps are a necessity for the efficient operation of wind turbines. An energy dump is defined as a sink for electrical energy. This sink has to have the property to accept or dissipate electrical energy whenever the wind turbine produces excess electrical energy. This happens when the electrical energy production by the wind turbine is exceeding the energy demand of, in our case, the base. A potential electrical dump has to fulfill the following criteria:

- It has to be in constant operation, or
- It has to be able to be switched on whenever needed.
- It has to be able to be loaded immediately, possibly with a full load.
- It must be on standby for a power influx at any time.
- It must be able to handle the maximum rating of the selected wind turbine, either
    - By a single load, or
    - By load sharing between different dumps.
- It has to be controlled automatically.

- The control system should be similar to the existing control system at the base.
- The control system should not be linked to the existing control system, because the existing control system could become unstable.

From the energy distribution outlined in section 4.5 the bigger power demand sources were identified. This was done so that possible dump locations could be analyzed according to the criteria mentioned above. These possible dump locations are:

- Snow smelter
- Helicopter deck vehicle hoists
- Inline water heaters of the FCU
- Kitchen

After analyzing the possible dump location with the given criteria, it becomes obvious that the only efficient electrical energy dump would be the snowsmelter. The helicopter deck vehicle hoists are operated very seldom and irregularly. Also, the kitchen equipment energy demand is very high only during the take over period. The inline heaters for the fan coil units are only additional heaters, for times when there is not enough heat produced by the generator water jacket heat exchangers to heat up the base.

However, by supplying the inline water heaters with power by the wind turbine the current system instability could be eliminated. At the moment this system is operated as follows. The base obtains its heating capacity by water jacket heat exchangers that are fitted to the generator liquid cooling circle and the exhaust pipes. This heated water is run through fan coil units that heat up the ventilation air supplied to the base. When the temperature of the return water is too low, the electrical elements are switched on (Teetz, 2000).

By switching on the electric heating elements, the generators have to produce more power, thus generating more heat, which in turn is absorbed by the water for the fan coil units. This has the effect of being an unstable system, because once the water reaches a certain

temperature the elements are switched off and the generators produce less power and heat, thereby cooling down the water for the fan coil units. Thus the temperature could fall below the limit again and the electrical heaters are switched on again. This creates a loop that is continued over and over again, thereby creating an unstable system. By using the power from the wind turbine to meet the power demand of the electrical inline heaters, this loop is eliminated and the system becomes stable. As mentioned earlier, the inline heating elements are used too irregularly and another dump location has to be found.

The main dump location would be the snow smelter. Although the snow smelter is not used permanently, the key point is that there is always water in the snowsmelter that has to be heated in order to pump it to the base via unheated, insulated pipes.

The wind turbine could be connected to the snow smelter in two different ways, as can be seen in figure 4-10. One way is to connect the wind turbine directly to the snow smelter and supplying all the power that is generated directly to the snow smelter. The second way is to connect the wind turbine to the main distribution board of the base and use the snowsmelter only as a pure dump location. This decision cannot be made now since it depends on the size of the wind turbine. The decision will be made in chapter 13.

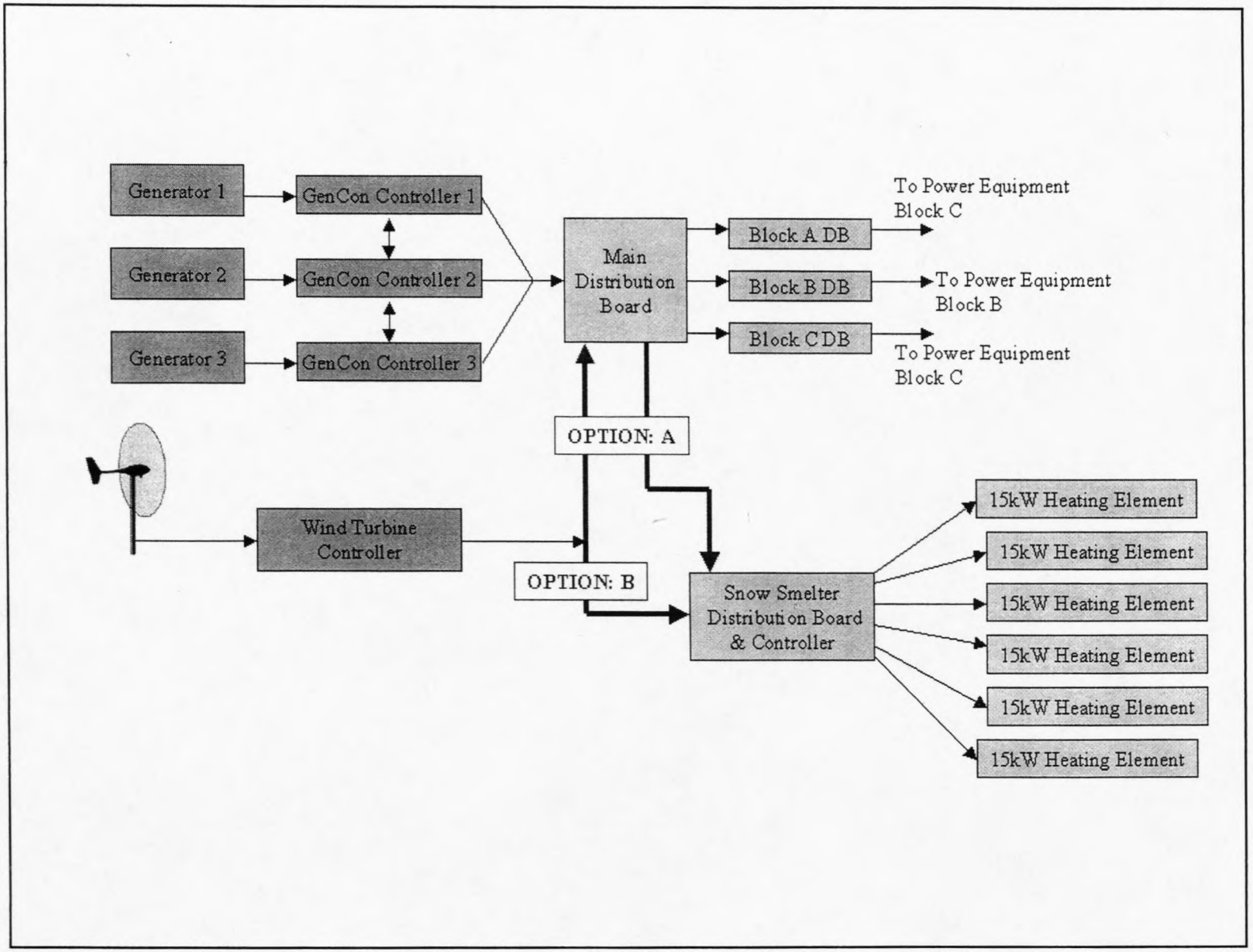

Figure 4-10: Wind turbine connection to the snow smelter

5 *ACTUAL WIND MEASUREMENTS*

5.1 Introduction

In order to get the wind measurements, a field trip was done, which was conducted during the summer period at the South African research base SANAE IV in Antarctica.

The Antarctic field trip started on the 7th of December 2001 with a three weeklong ship voyage to Antarctica. During that time little work could be done, but some theoretical work was done and also the wind measurement equipment was checked and repaired. Some of the cables from the hand-held anemometer had to be resoldered, due to wear and tear of the equipment.

The actual time period during which measurements could be taken and information could be gathered was about 4 weeks. This reduced the initial planned period of 6 weeks, allocated for experimental work, by 2 weeks. The reason for the reduced experimental time was due to the prolonged stay on the ship. The ship got stuck in the pack ice a few times and bad weather forced some of the people, including the author, to stay longer on the ship before being airlifted to the base.

It was thus decided to set up the 6 m wind mast at only 2 positions, instead of the planned 3 positions. Therefore, the wind tower was placed on a snow surface for the first 3 weeks and then on a rocky outcrop for another 10 days.

The general weather data can be taken from the existing data from the 10 m weather tower. However, suitable locations for the proposed wind turbine position have to be found and certain criteria influence the determination of a suitable location. Criteria such as ground composition (rocks, snow or blue ice), topographical information and prevailing wind directions all influence the determination of a suitable location.

The set-up of the wind tower began on the 1st of January 2002. Wind profiles were measured on the ice and snow surface for 20 days. On the 21st of January 2002, the wind tower was shifted closer to the SANAE IV base on the rocky outcrop. This shift was done to get wind profiles for rocky surfaces as well. The wind measurements lasted for about 10 days, after which the experimental equipment was dismantled and the container packed for shipment back to South Africa.

Other work during the field trip included taking regular wind measurements at 16 different positions around the base. The wind speeds of these different positions was linked to the 6 m wind mast data, in order to get the wind speeds on the same time frame. Then the best position, i.e. the position with the maximum wind energy potential was evaluated.

During the second last week GPS positions were taken around the base. These GPS positions in connection with elevation recordings has been used to plot contour maps.

Other work included the collection of the weather data from the weather bureau, electrical system investigations, generator set-ups, base layout and energy consumption. Also included in the fieldwork was assessing the energy demand of the base for a couple of days, the diesel consumption of the generators, inventory and maintenance lists of the generators.

5.2 Activities Performed During SANAE IV Field Trip

During the field trip a substantial amount of information gathering was done. Information gathering at the base included:

- Wind speed and direction data covering more than a year from the existing 10 m weather station from SAWS
- Wind profiles from a wind mast that was positioned on two different locations during the field trip. The one being on an ice and snow surface and the other a snow surface with protruding rocks

- Wind profile survey of existing weather station
- Wind speed measurements at 16 different locations around the base
- Ground survey at these locations
- GPS position and elevation loggings of the terrain around the base, so that a three-dimensional contour map can be established
- Generator diesel consumption for 2000, 2001, and the beginning of 2002
- Power demand logging during the field trip period
- Temperature, pressure and humidity data from the SAWS weather station
- General information regarding the power systems at the base, power distribution at the base and operating information of the power consuming systems at the base

In order to get all this information, a great deal of practical work was done. The general weather data was taken from the existing data from the 10 m weather tower. However, suitable locations for the proposed wind turbine position were found and certain criteria influencing the determination of a suitable location were analyzed. Criteria such as ground composition (rocks, snow or blue ice), topographical information and prevailing wind directions all influence the determination of a suitable location.

In order to get a proper insight into the wind distribution and the magnitude of the prevailing winds at these locations, a 6 m high wind tower with 4 wind sensors distributed along the towers length, was built. This tower was anchored at different locations and the wind velocity profile was determined. The velocity profile was used to estimate the surface roughness of the surrounding surfaces. The wind data was taken from a data logger onto a PC and was transformed into useful information.

5.3 Summer 2001/2002 Period: 6 m Wind Mast Measurements

The wind mast in figure 5-1 was manufactured by Stellenbosch Meganiese Dienste (SMD) and has a height of 6 m. The wind profiles were measured with four MCS177 aluminium cup type anemometers, which were positioned 0.5 m, 1.4 m, 2.7 m and 5.5 m above the

snow surface. The wind sensors were mounted on horizontal arms, 0.5 m in length, to the wind tower. The arms were orientated in a north-south direction, as to minimize the interference by the wind mast, at least for the prevailing wind direction (Beyers, 2003).

The wind speeds were logged at 15-minute intervals with a MCS 120 RS232 digital data logger, which was supplied by the Council for Scientific and Industrial Research (CSIR), Stellenbosch branch. The wind mast drawings can be seen in appendix L.

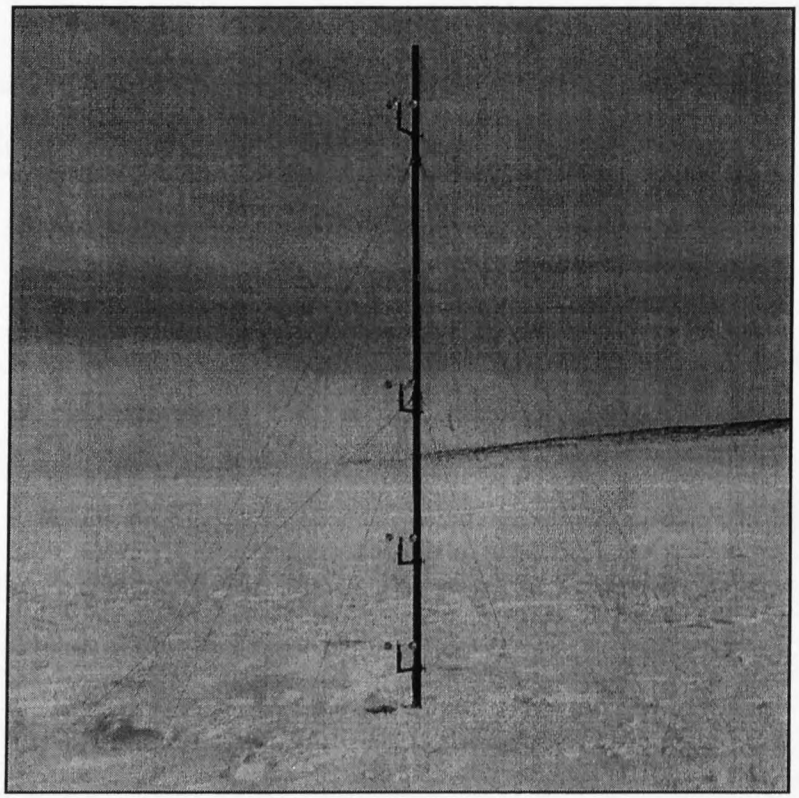

Figure 5-1: Wind tower positioned on snow surface (looking to the southwest)

5.3.1 Wind mast locations

The first location of the wind mast was about 2 km east of the base on a flat snow surface, as shown in figure 5-1. The wind mast was positioned on the snow surface for a duration of 20 days. During this time data of two storms were captured onto the data logger. This means that a full spectrum of wind speeds have been captured and proper velocity profiles have been established.

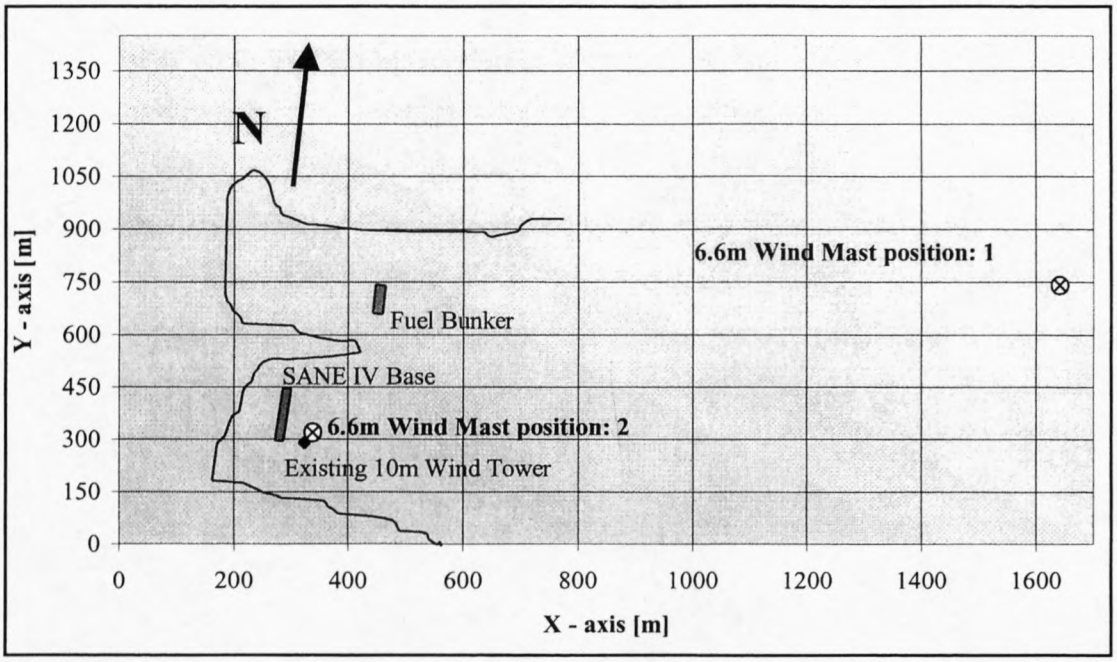

Figure 5-2: The 2 positions of the 6 m wind mast

The second location was on a rocky outcrop, about 200 m east of the base. Both measuring positions can be seen in figure 5-2. At the second position, the wind data necessary to establish a velocity profile for a typical rocky outcrop has been gathered for about 10 days. Figure 5-3 shows the wind mast positioned on the rocky outcrop.

The surface of the hill is covered in snow and ice with scattered rocks protruding approximately 0.3 m above the snow.

Both wind mast locations are measuring positions. The wind mast was assembled at the university and the anemometers were tested in Stellenbosch. Therefore no test position was necessary during the field trip. The wind mast was assembled at the first location and worked perfectly from the start.

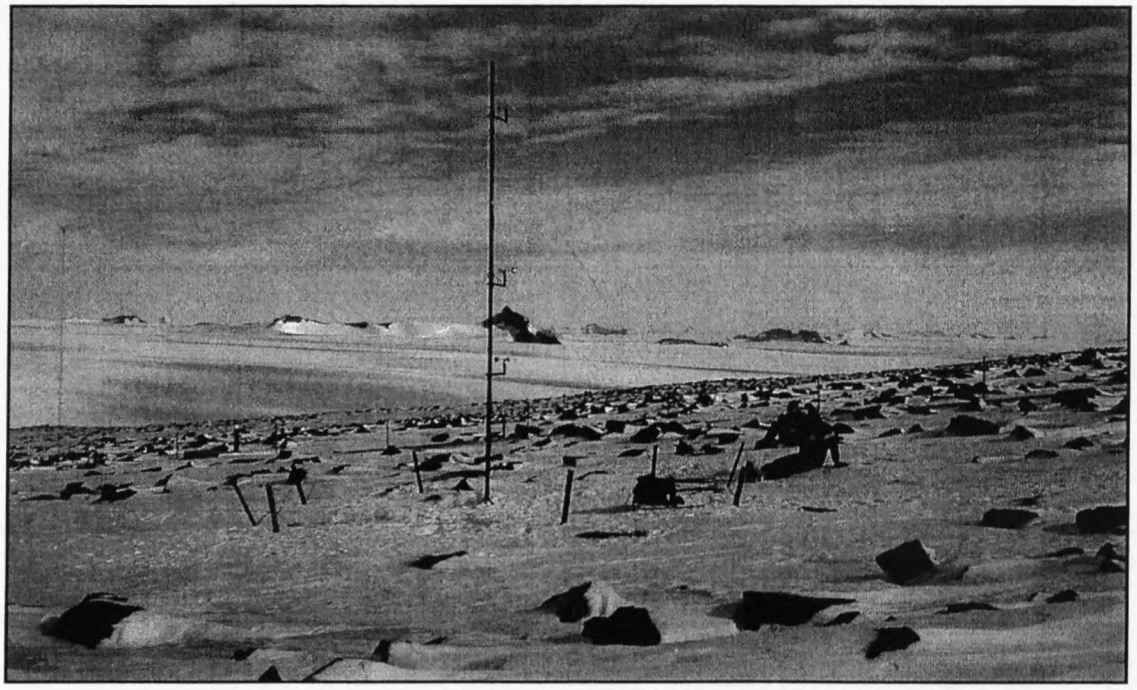

Figure 5-3: Wind tower positioned on rocky outcrop (looking to the south)

The data gathered during the two measurement periods provides the necessary wind data for the velocity profiles for a snow covered area and a rocky outcrop. Also, the second aim of positioning the wind mast on the rocky outcrop was to position the wind mast close to the existing automatic weather station located near the research base. Thus the wind speeds of the 6 m wind mast can be compared to measured wind speeds of the existing weather station.

In order to fully analyze the wind data, a wind direction has to be available. The wind mast has no wind direction sensor, therefore the data was obtained from the automatic weather station, as will be explained in section 5.5.

5.3.2 Data analysis

The wind data analysis will be presented in detail in chapter 6. The data from the 6 m wind mast will primarily be used to connect the measurements taken by the hand-held anemometer and the existing 10 m weather station.

Another use of the wind mast was to verify both the data from the 6 m wind mast and the data from the existing 10 m wind mast. The wind data from the 1st to the 28th of February 2002, measured at 5.5 m height can be seen in figure 5-4.

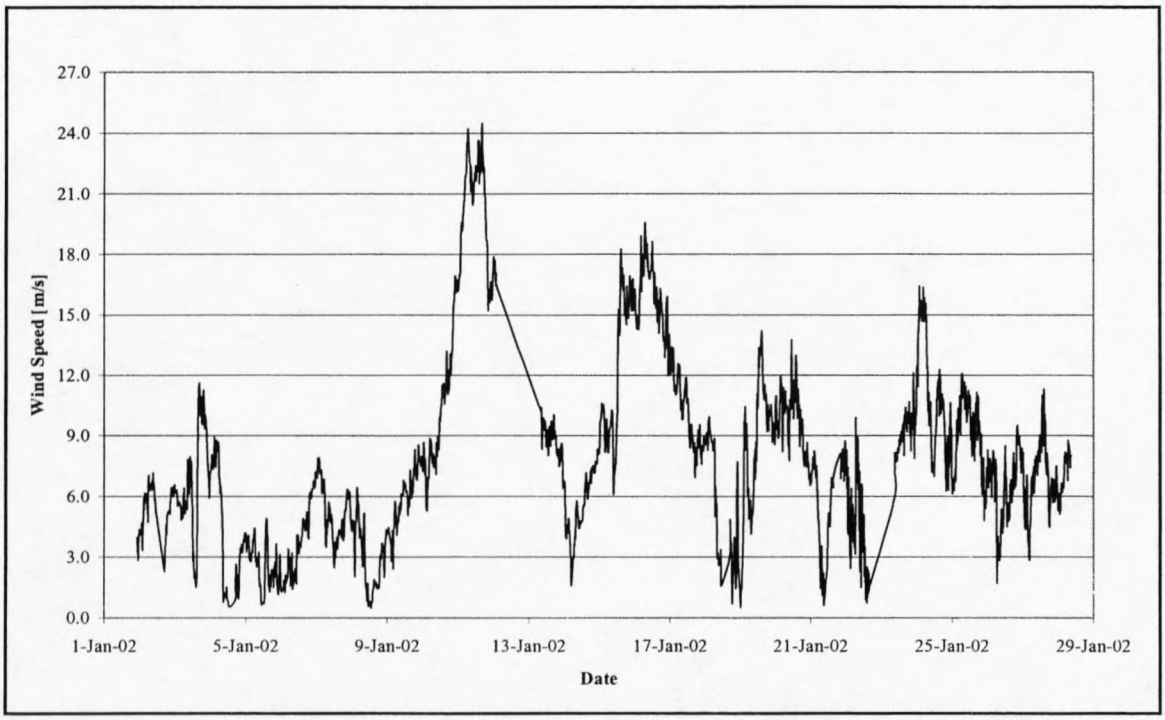

Figure 5-4: Wind speed data for the 6 m wind mast, measured at 5.5 m height

The third use of the wind mast was to establish wind velocity profiles for different surfaces encountered around the base.

Figure 5-4 does not show all the data that was captured during the field trip with the 6 m wind mast. Due to cluttering of the graph, the data from the other three heights have been omitted. Since 4 weeks of measured data is not enough to establish the feasibility of using a wind turbine at SANAE IV, this data will be linked to the automatic weather station, which has measured data for the complete year 2001 and part of the year 2002.

5.4 Summer 2001/2002 Period: Hand-held Anemometer Measurements

During the field trip wind speed data was logged with the 6 m wind tower. Another method of gathering wind data was to use a hand-held anemometer, and to write down the measured wind speed by hand. The reason for using this method is that 16 positions around the base were selected, mostly outcrops, where the wind speed was measured with the hand-held anemometer. Since the surface structure of the area around the base is classified into a snow-covered surface and a snow-covered surface with protruding rocks, it was decided to take wind measurements at different positions. Also difference in elevations of up to 60 m of the area around the base, presented the need to measure wind speed at different positions. The 16 positions can be seen in figure 5-5. This data was linked to the 6 m wind mast, so that velocity maps can be created. From there the data was linked to the year data from the existing 10 m automatic weather station and the best position, according to wind speeds, were chosen.

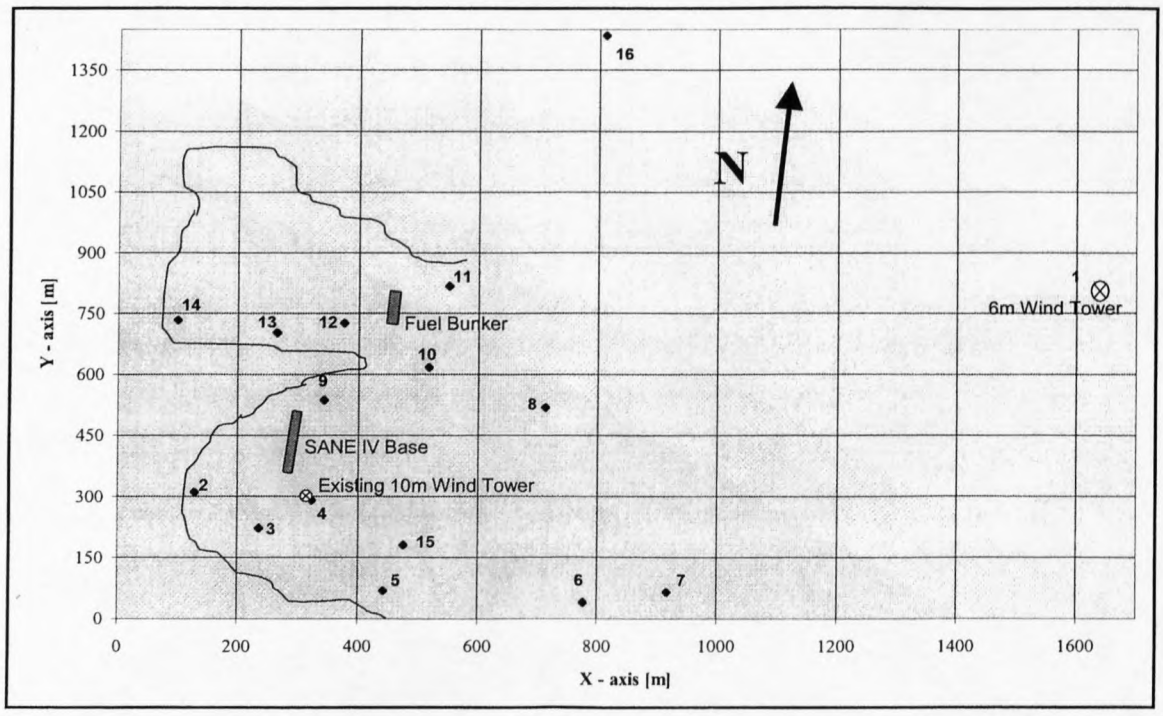

Figure 5-5: Hand-held anemometer measurement positions

5.5 Year 2001: Automatic Weather Station Measurements

The existing automatic weather station from the South African Weather Service (SAWS) has a wind mast of 10 m height. One wind speed and direction sensor is installed at 10 m height. This data will be primarily used for the evaluation of the energy potential from the winds at the research station.

The weather station records hourly averages of wind speeds to an accuracy of 1 decimal place. The wind direction is accurate to 10° intervals. In figure 5-6 one can see the wind sped data for the year 2001. Note, that this figure represents the daily averages of the hourly data.

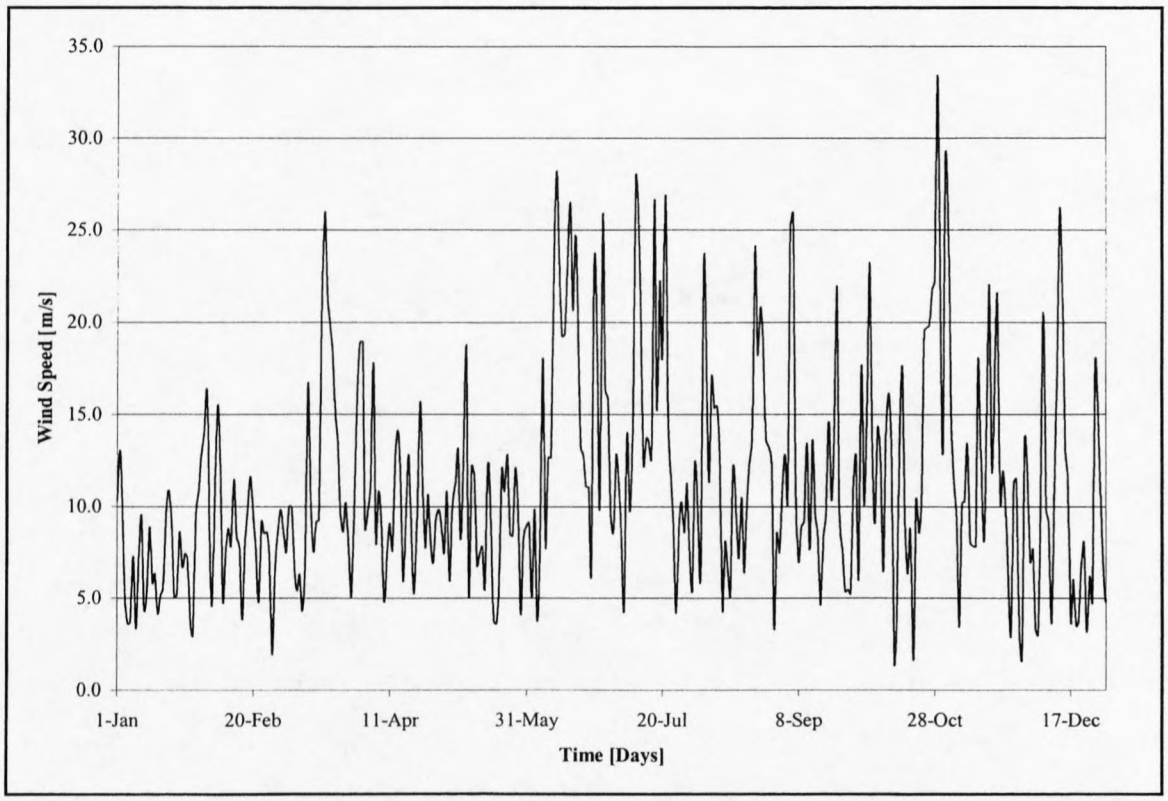

Figure 5-6: Average daily wind data for the year 2001

6 *WIND ANALYSIS*

The wind analysis is based on the wind data, as mentioned in the chapter on actual wind measurements, i.e. chapter 5. There are three main categories of data that will be used in the wind data analysis. They are:

- Hourly measured wind speed and direction data, for a period from 1st of January 2001 until the 28th of February 2002. This data is measured by the existing, automatic weather station from SAWS. The height of measurement is 10 m above ground level.
- Quarter hourly measured wind speed data, for a period, during the field trip, from the 1st of January 2002 until 28th of January 2002. A 6 m high wind mast, which was designed and built at the University of Stellenbosch, was used to measure this data.
- A hand-held anemometer was used at 16 different locations, in order to get an insight of the wind speed distribution around the base.

The data from the above mentioned measuring devices was analyzed and linked together as follows. The data from the existing 10 m weather station was the most important data set, because this data set has a period of more than a year and thus was used to calculate the power that a typical wind turbine will produce at the base. The data from the hand-held anemometer was used to produce wind maps of the area surrounding the SANAE IV base. The wind data analysis is outlined in figure 6-1. The data from the 6 m wind mast was partly used to create the wind maps from the hand-held anemometer and to extrapolate the wind speeds to higher heights. This was possible since the 6 m wind mast had four wind speed sensors, spaced vertically on the mast and thus velocity profiles have been calculated from the data.

The analysis of the data is divided into 3 parts:

- Analysis of the data from the 6 m wind mast
- Analysis of the data from the existing 10 m weather station
- Analysis of the data from the hand-held anemometer

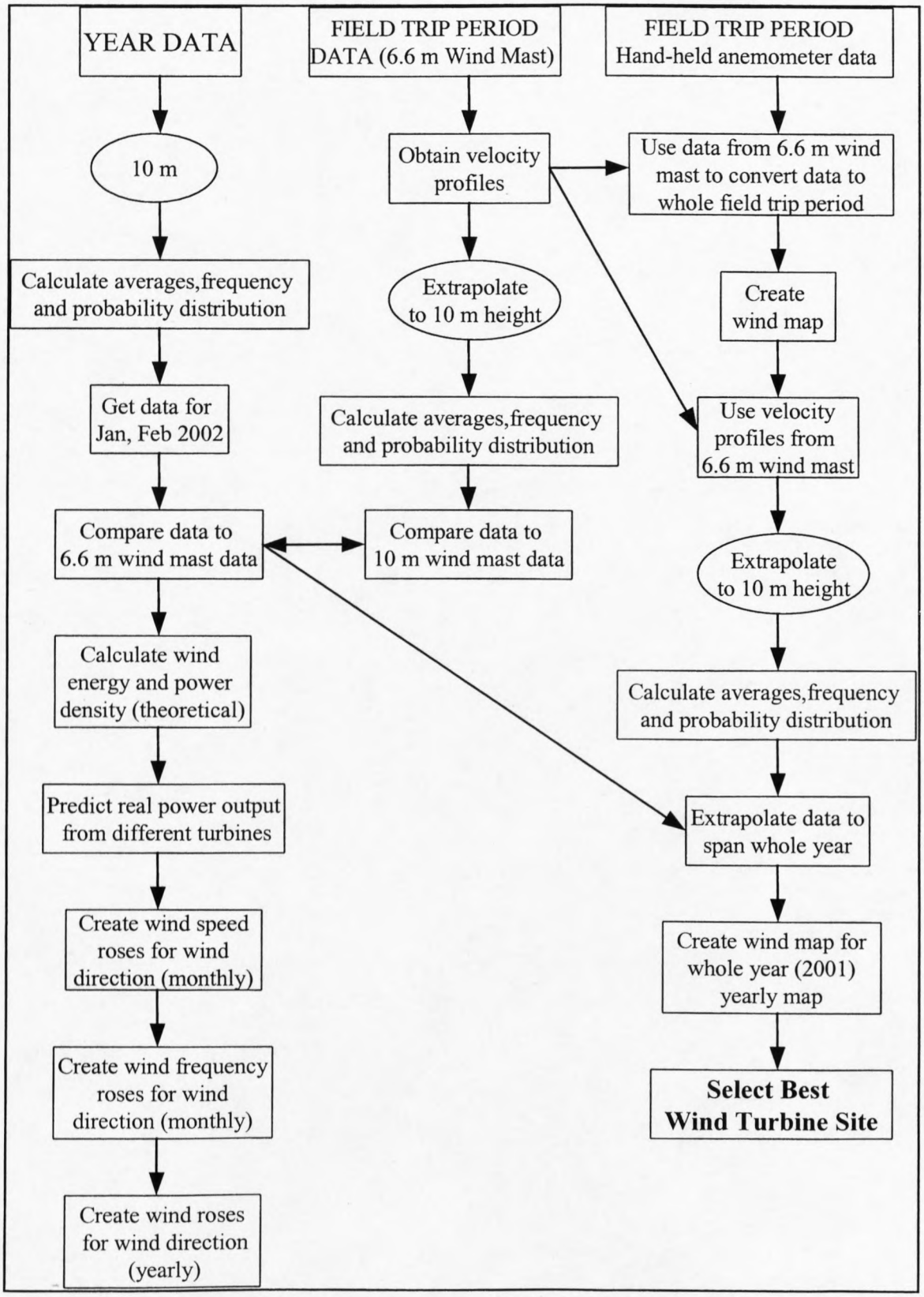

Figure 6-1: Wind data analysis overview

6.1 Data Analysis of the 6 m Wind Mast

The measurement time during the field trip was divided into two periods of observation, carried out at 2 different locations. The first set of wind measurements was carried out on a large snow covered area, in the vicinity of the SANAE IV base (71° 39' S 2° 48' W).

The second set of measurements was carried out on a rocky just upwind of the base (71° 40.45' S 2° 50.34' W). The first set of measurements was taken from the 1st of January 2002 to the 18th of January 2002, while the second set of measurements was taken from the 18th of January 2002 to the 28th of January 2002.

The reason for having two measurement sites around the base is that two different surface roughnesses are prevalent there. One is the snow-covered surface and the other one is the snow surface with protruding rocks. The first set of measurements was done on a snow surface while the second set of measurements was done on a surface with protruding rocks. See chapter 5 on actual wind measurements for photos of the different surfaces.

6.1.1 Wind mast locations

The equipment that was used for the wind measurements and data capture has already been described in detail in the chapter on actual wind measurements (see chapter 5). The heights of the four wind sensors however will be given now. During one of two storms during the field trip, there was a snow accumulation of about 0.5m in total. This happened during the 11th and the 12th of January 2002. Also during the second setup phase, different heights of the wind sensors were used, in order to compensate for the different surface roughness, as can be seen in table 6-1.

		SENSOR HEIGHTS [m]			
Day (January)	**Time**	**Height 1**	**Height 2**	**Height 3**	**Height 4**
1 – 18	22:30	0.5	1.4	2.7	5.6
11	10:45	0.5	1.4	2.7	5.6
11	15:30	0.34	1.24	2.54	5.34
:	:	:	:	:	:
12	1:30	0.03	0.93	2.23	5.03
13 – 18	8:45	0.5	1.4	2.7	5.0
18 – 28	16:45	1.2	1.9	3.4	5.7

Table 6-1: Different heights of wind sensors during field trip data acquisition

6.1.2 Theoretical derivations

The law of the wall as derived by Blackadar (1998) can be used to describe the ratio of the average wind speed divided by the shear velocity as

$$\frac{u}{u^*} := \frac{1}{\kappa}\cdot\ln\left(\frac{z + z_0}{z_0}\right) \qquad \textbf{(6-1)}$$

The near ground turbulent velocity profile for stable atmospheric conditions can be derived from the logarithmic near wall velocity profile and is commonly presented in the form of

$$\frac{u}{u^*} := \frac{1}{\kappa}\cdot\ln\left(\frac{z}{z_0}\right) \qquad \textbf{(6-2)}$$

for situations where the surface roughness is small in comparison to the height scale. By performing a regression analysis an exponential curve of the form $z = bm^u$ is fitted through the wind speed data, which was obtained from the four wind sensors of the 6 m wind mast. The exponential curve was used by the program Excel version 2000 to perform the regression analysis. From the regression analysis and equation (6-2), the surface roughness and shear velocity functions are found from

$$z_0 := b \tag{6-3}$$

$$u^* := \frac{\kappa}{\ln(m)} \tag{6-4}$$

With these equations and the data from the 6 m wind mast, the wind speed can be extrapolated to 10 m. The equation is as follows, with $\kappa = 0.41$ and $z = 10$ m (White, 1991)

$$u_{10} := \frac{u^*}{\kappa} \cdot \ln\left(\frac{z}{z_0}\right) \tag{6-5}$$

The extrapolated data is then compared to the data measured by the existing automatic weather station, which measures at a height of 10 m. The average regression coefficient for the measured data is $R^2 = 0.9772$ for $u_{10} > 0.0$ m/s. The comparison of the extrapolated data from the 6 m wind mast and the data from the existing weather station is shown in figure 6-2.

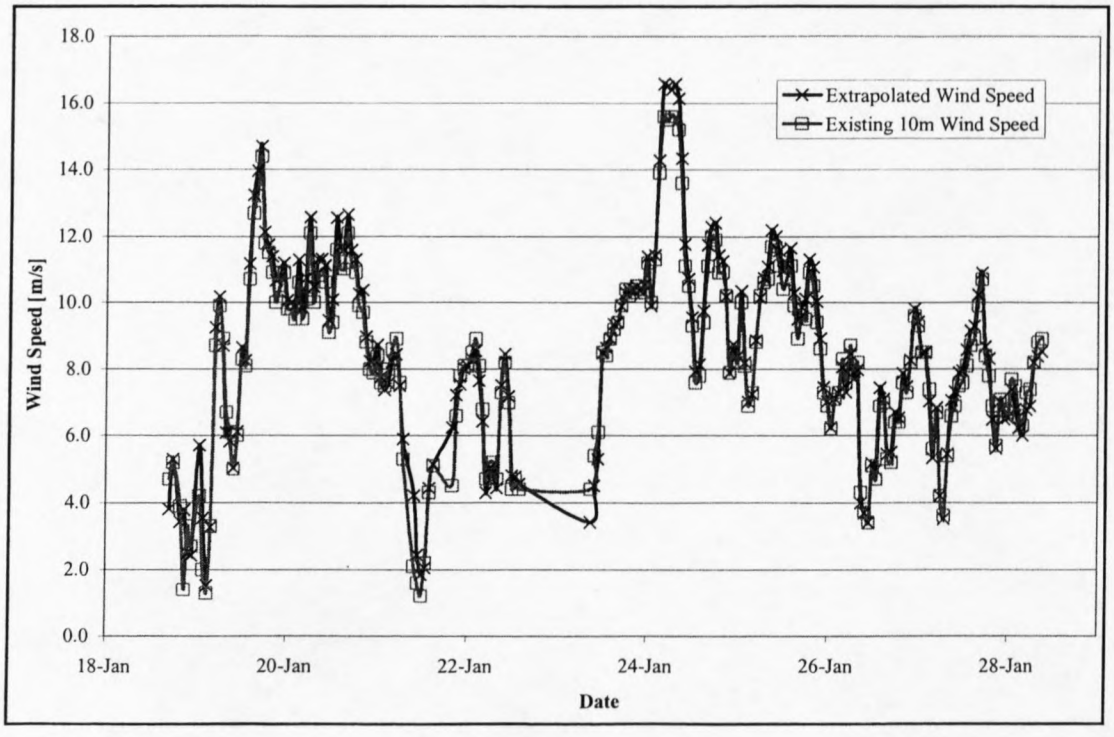

Figure 6-2: Comparison of extrapolated and measured wind speed u_{10}

From the regression coefficient and from figure 6-2 it can be seen that the two data sets are in very close agreement. It should be noted that the existing automatic weather station is situated on a snow-covered area with protruding rocks. Therefore, only the second data set of the 6 m wind mast has been used to compare the data.

Another interesting fact that was observed during the wind data analysis is that the velocity gradients for both the snow and rock covered surfaces are very steep, as can be seen in section 7.2.6. This means that the difference in the measured 5.7 m height wind speed and the extrapolated 10 m wind speed is relatively small.

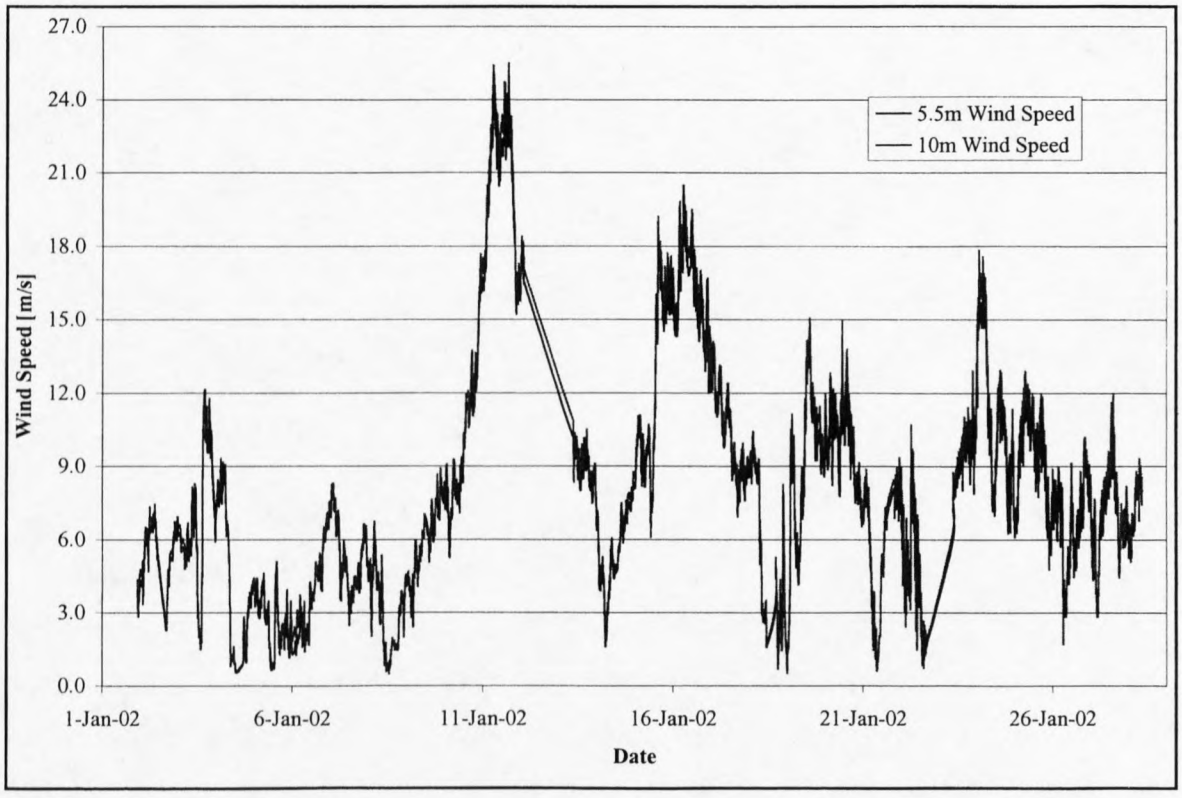

Figure 6-3: Comparison of 5.5 m and extrapolated 10 m wind speeds

The small difference can be seen in figure 6-3, where the wind speeds at heights of 5.7 m and extrapolated 10 m are displayed.

For flow over a smooth plate one may find from equation (6-1)

$$z_0 := \frac{\nu}{9.53 \cdot u^*} \tag{6-6}$$

The present data can be grouped into two categories, the data gathered in the snow-covered area before the 18 January 2002 and the data gathered on the Vesleskarvet to the 28 January 2002. During the period before 18 January 2002, the first storm occurred after three days of exceptionally warm weather, day temperatures of approximately +4 °C. This means that the old snow test area 'thawed'. This should result in higher threshold wind speeds and smaller effective surface roughness due to less snow saltation at lower wind speeds, according to Beyers and Harms (2002). This data, measured for the snow-covered area, fits the curve

$$z_0 := \frac{0.0022 \cdot u^{*2}}{2 \cdot g} \qquad u^* \geq 0.2 \qquad R^2 := 0.896 \tag{6-7}$$

The data obtained shows scattering for $0.2 \leq u^* \leq 0.4$ which may be due to the initiation of snow saltation and follows the trend of data collected for similar experiments in similar regions.

During the course of the wind measurements carried out from the 10-12 January 2002 a heavy deposition of blown snow, approximately 0.5 m deep, occurred throughout the test area, as well as on the rock covered hill at SANAE IV during the later stages of the storm. Therefore the subsequent wind conditions may have corresponded to slightly lower threshold wind speeds to entrain snow particles from the surface. The surface roughness parameters calculated from the data gathered after 18 January 2002 fits the curve

$$z_0 := \frac{0.04 \cdot u^{*2}}{2 \cdot g} \qquad u^* \geq 0.2 \qquad R^2 := 0.896 \tag{6-8}$$

which is applicable to the snow-covered area with protruding rocks (k = 0.3 m).

Equations (6-7) and (6-8) are applicable for $u^* \geq u^*_t$ and describe the effective surface roughness and include the effects of the natural surface quality as well as the additional roughness due to the presence of creeping and saltating snow. Furthermore it is known that for single-phase flow over rough surfaces, the following equation can be used

$$z_0 := \frac{\nu}{9.53 \cdot u^*} + 0.0315 \cdot k \tag{6-9}$$

where k is the effective height of the surface roughness (Beyers and Harms, 2002). Equations (6-7), (6-8) and (6-9) may converted to a single function to describe the velocity profile for saltating snow over surfaces with varying roughness, namely

$$\frac{u}{u^*} := \frac{1}{\kappa} \cdot \ln\left(\frac{z \cdot u^*}{\nu}\right) + B - \Delta B\left(k^+, s^+\right) \tag{6-10}$$

where B = 5.5 and in similar manner to White (1992) for rough flow in pipes,

$$\Delta B\left(k^+\right) := \frac{1}{\kappa} \cdot \ln\left(1 + 0.3 \cdot k^+ + 9.53 \cdot s^+\right) \tag{6-11}$$

$$k^+ := \frac{k \cdot u^*}{\nu} \tag{6-12}$$

and introducing the additional parameter

$$s^+ := \frac{c_1 \cdot u^{*3}}{2 \cdot g \cdot \nu} \tag{6-13}$$

where c_1 is a constant from Beyers and Harms (2002) and is given as $c_1 = 0.0022$ (for snow-covered area, with $k \approx 0.0$) and $c_1 = 0.04$ (for snow-covered nunatak with protruding rocks, with $k \approx 0.3$).

The effective surface roughness function calculated from equation (6-10) is given as

$$z_0 := \frac{\nu}{9.53 \cdot u^*} + 0.0315 \cdot k + \frac{c_1 \cdot u^{*2}}{2 \cdot g \cdot \nu} \tag{6-14}$$

The equations for the surface roughness are shown in figure 6-4 for the snow-covered area.

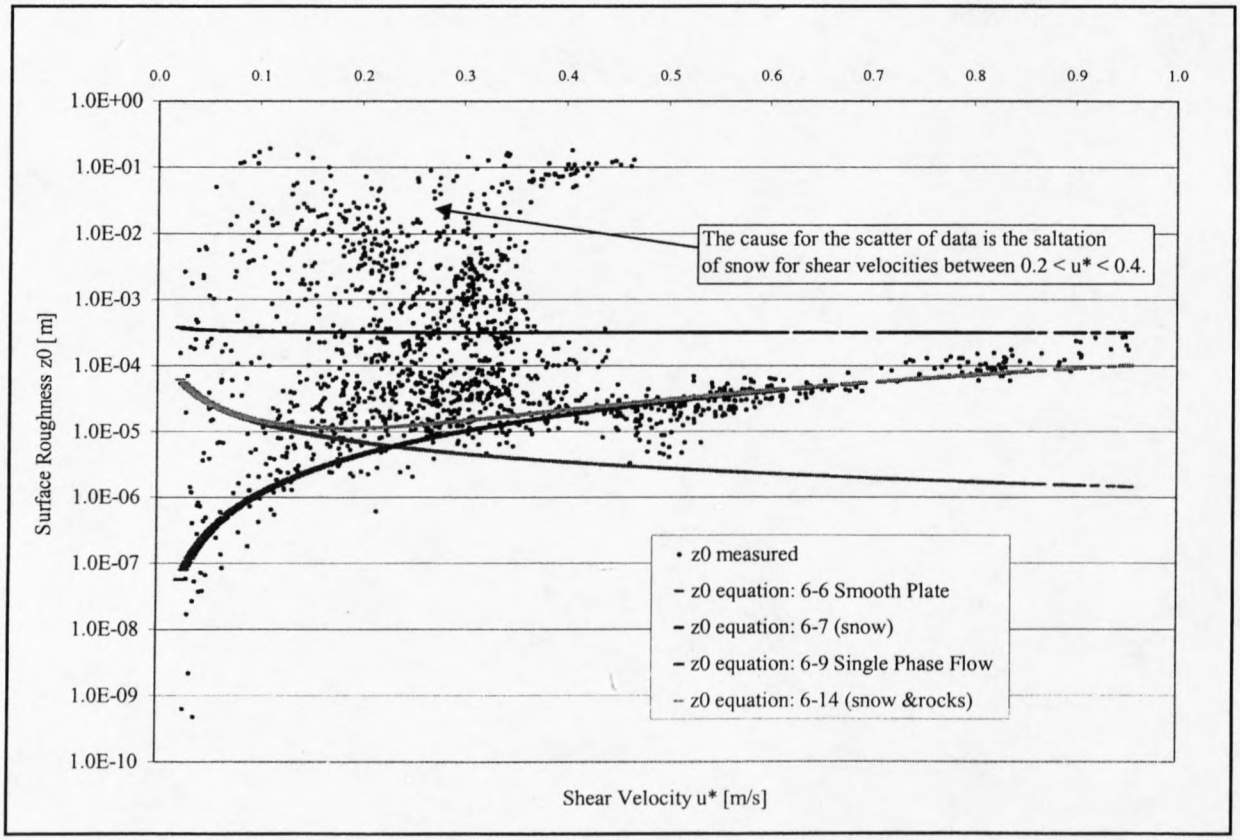

Figure 6-4: Surface roughness against shear velocity for snow-covered area

Figure 6-5 shows the equations for the snow-covered area with protruding rocks. Note that the curve for the rocky area was found with an effective roughness of k = 0.01 instead of the earlier mentioned k = 0.3.

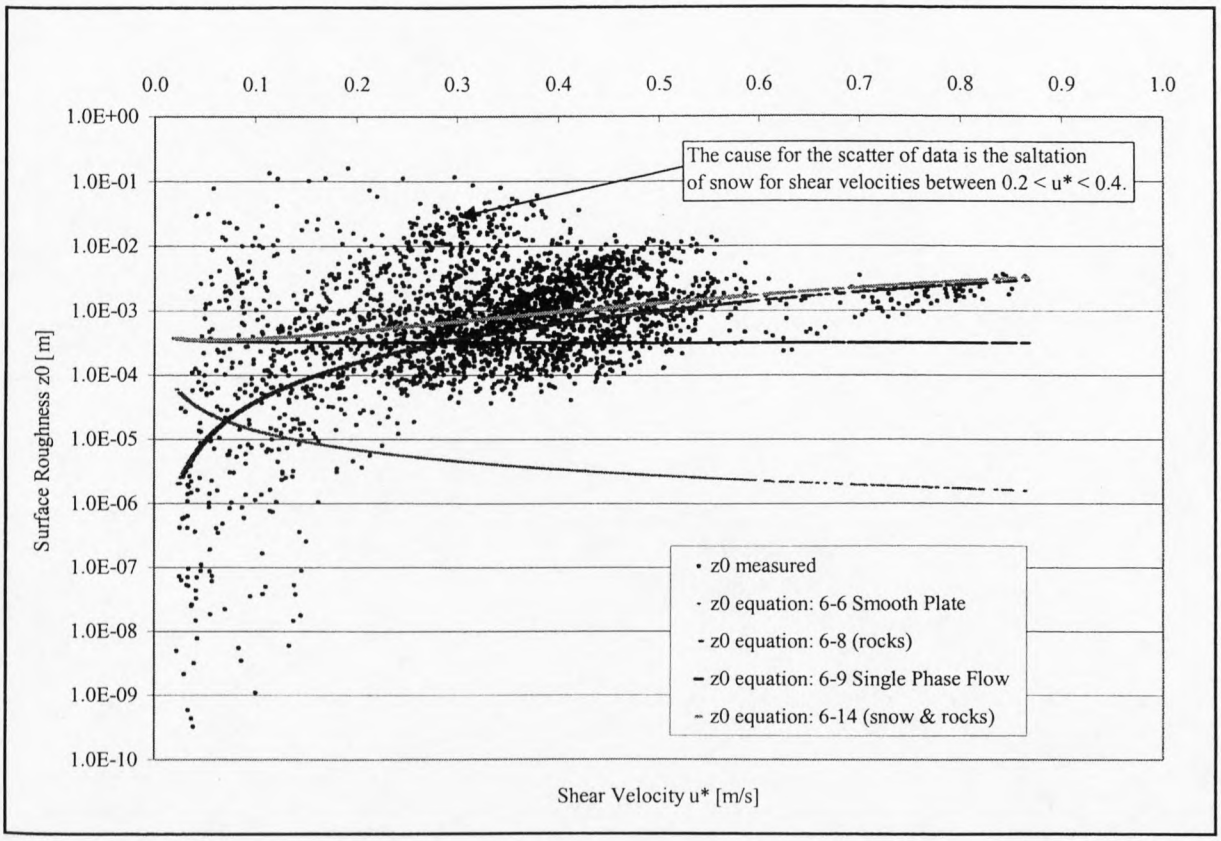

Figure 6-5: Surface roughness against shear velocity for snow-covered area with protruding rocks

In conjunction with the derivations above, another important correlation is found from the evaluation of the shear velocity as a function of the 10 m wind speed. Here commonly used power functions have been fitted through both data sets, one for the snow-covered area and one for the rocky area. The data gathered before 18 January 2002 in the snow-covered area follows the curve

$$u^* := 0.02 \cdot \left(u_{10}\right)^{1.18} \qquad z_0 = \frac{0{,}0072 \cdot u^{*2}}{2g} \qquad \textbf{(6-15)}$$

The data gathered after 18 January 2002 on top of the rocky hill fits the curve

$$u^* := 0.025 \cdot \left(u_{10}\right)^{1.23} \qquad z_0 = \frac{0{,}044 \cdot u^{*2}}{2g} \qquad \textbf{(6-16)}$$

Figure 6-6 shows the comparison between the shear velocity function results derived from the data gathered at SANAE IV and those obtained from the correlations described above.

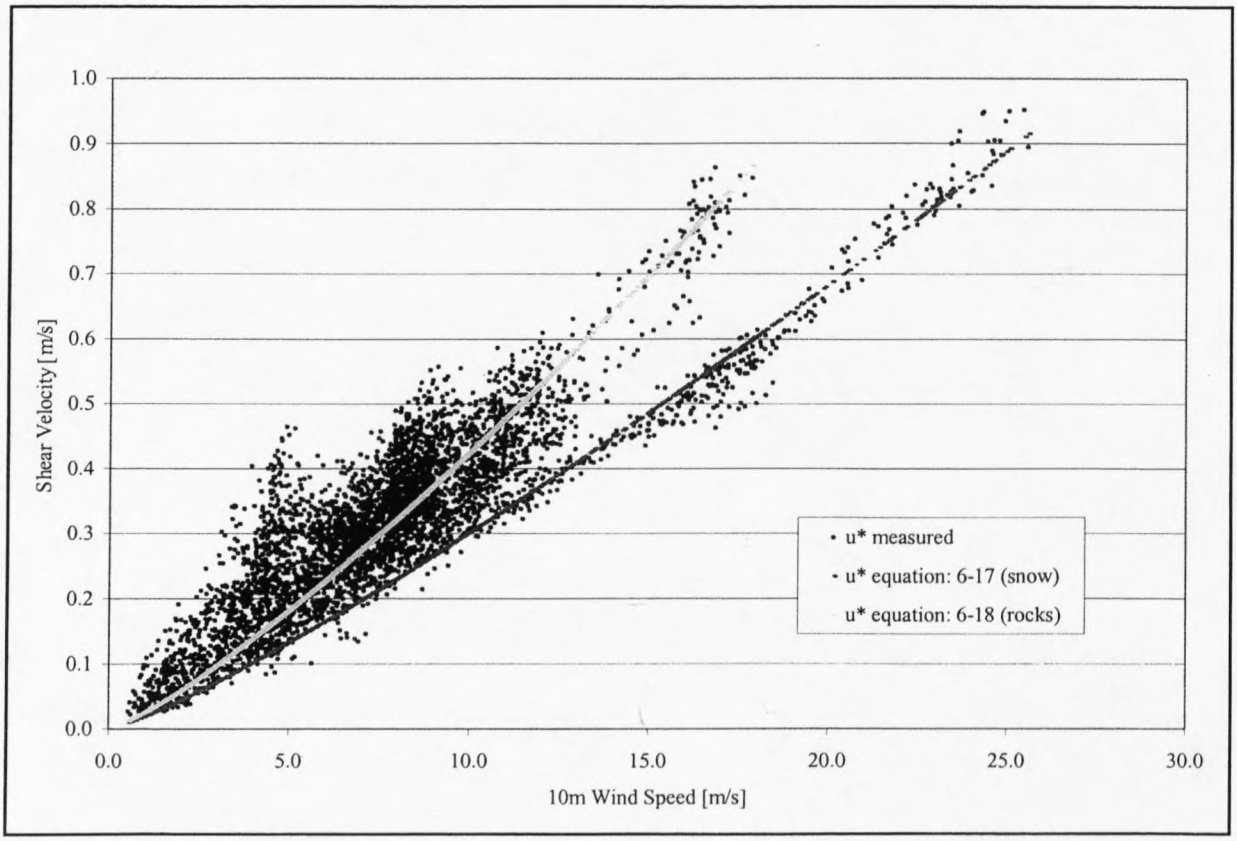

Figure 6-6: Shear velocity against 10 m wind speed for both areas

As already assumed, equation (6-16) follows the larger u* profile due to the presence of the protruding rocks on the snow-covered area. From equation (6-15) and (6-16) the equations for the 10 m wind speed can be derived as follows

$$u_{10} := \left(\frac{u^*}{0.02}\right)^{\frac{1}{1.18}} \qquad \textbf{(6-17)}$$

for the snow-covered area and for the snow-covered area with protruding rocks

$$u_{10} := \left(\frac{u^*}{0.025}\right)^{\frac{1}{1.23}} \qquad \textbf{(6-18)}$$

Figure 6-3 shows the extrapolated 10 m wind speed for 1 January 2002 to 28 January 2002.

6.1.3 Results of wind data from 6 m wind mast

With the 10 m wind speeds evaluated, the frequency distribution, cumulative distribution, average wind speed, mode, median, variance and standard deviation were calculated.

The median is the wind speed such that 50% of the data is larger than the median and 50% is smaller. The relevance of calculating the average wind speed, mode and median for this project is that they present a fairly easy description of the wind speeds at the base. The variance and standard deviation present a more difficult, but more accurate and detailed description of the distribution of wind speeds at the base, when used in conjunction with the average wind speed. The median for the 6 m data, based on hourly averages is:

n = number of data points => n = 558
Therefore the median is the wind speed at (n + 1)/2.
v_{median}= 7.96 m/s.

The mode is the wind speed that occurred the most during the observation. The mode is
v_{mode} = 7.5 m/s.

The average wind speed for this data is
$v_{average}$ = 8.56 m/s.

In order to calculate the variance and the standard deviation, the theory for the Weibull function has to be established and then the equations for the variance and the standard deviation can be calculated.

Weibull function theory

The Weibull distribution is a two-parameter function commonly used to fit wind speed frequency distributions. The Weibull function provides a convenient representation of the wind speed data for wind energy calculation purposes.

Before sufficiently powerful computers were widely available, the preferred method of calculating the Weibull parameters was a graphical technique, which entailed generating the cumulative wind speed distribution, plotting it on special Weibull graph paper, and drawing a line of best fit. This procedure is now commonly implemented by performing a linear regression on a computer. A more accurate and robust approach that will be used in this analysis is given by the maximum likelihood method (Seguro and Lambert, 1999).

The accuracy of the maximum likelihood method has been shown to be better than the graphical method (Seguro and Lambert, 1999). The Weibull distribution can be characterized by its cumulative distribution function F(V) and probability density function f(V) where

$$F(v) := 1 - \exp\left[-\left(\frac{v}{c}\right)^{k}\right] \tag{6-19}$$

and

$$f(v) := \frac{dF}{dv} := \frac{k}{c}\left(\frac{v}{c}\right)^{k-1} \exp\left[-\left(\frac{v}{c}\right)^{k}\right] \tag{6-20}$$

The use of Weibull distribution requires that the shape factor k and the scale factor c, should be determined, for which adequate field data collected at short intervals of time is necessary. In this case, hourly data has been used.

The two Weibull parameters and the average wind speed are related by

$$v_{ave} := c \cdot \Gamma\left(1 + \frac{1}{k}\right) \tag{6-21}$$

where v_{ave} is the average wind speed and $\Gamma(\ )$ is the gamma function.

Measured wind data is commonly available in time-series format, in which each data point represents either an instantaneous sample wind speed or an average wind speed over some period of time. An example of such data (giving hourly averages over a 24 h period) was

taken by the year 2001 data set and is given in table 6-2. The method that works best with the time-series format data is the maximum likelihood method.

DAY 1				DAY 2				DAY 3			
Hour	Speed [m/s]	Hour	Speed [m/s]	Hour	Speed [m/s]	Hour	Speed [m/s]	Hour	Speed [m/s]	Hour	Speed [m/s]
1	3.3	13	5.7	1	4.0	13	4.5	1	4.7	13	6.3
2	3.8	14	8.3	2	4.0	14	5.8	2	4.5	14	9.4
3	4.2	15	8.9	3	2.0	15	4.8	3	4.2	15	7.7
4	3.3	16	9.3	4	2.7	16	4.8	4	5.7	16	6.0
5	2.8	17	6.5	5	2.7	17	5.5	5	2.7	17	8.9
6	3.0	18	4.2	6	3.3	18	5.7	6	4.3	18	7.7
7	4.0	19	4.3	7	2.7	19	5.0	7	4.3	19	6.2
8	2.7	20	3.7	8	2.7	20	4.3	8	4.5	20	5.7
9	5.2	21	4.0	9	5.8	21	4.0	9	4.5	21	5.7
10	6.7	22	2.8	10	5.7	22	3.5	10	6.0	22	7.5
11	6.8	23	3.7	11	6.2	23	5.0	11	10.4	23	7.5
12	6.8	24	3.3	12	6.5	24	3.7	12	6.7	24	5.3

Table 6-2: Wind speed data sample in time-series format

The shape factor k and the scale factor c are estimated using the following two equations:

$$k := \left[\frac{\sum_{i=1}^{n} v_i^{k} \cdot \ln(v_i)}{\sum_{i=1}^{n} v_i^{k}} - \frac{\sum_{i=1}^{n} \ln(v_i)}{n} \right]^{-1} \qquad \textbf{(6-22)}$$

$$c := \left(\frac{1}{n} \cdot \sum_{i=1}^{n} v_i^{k} \right)^{\frac{1}{k}} \qquad \textbf{(6-23)}$$

where v_i is the wind speed at time step i and n is the number of nonzero wind speed data points. Equation (6-22) has been solved using an iterative procedure on a spreadsheet, using k = 2 as an initial guess, after which equation (6-23) can be solved explicitly. Care must be taken to apply equation (6-22) only to the nonzero wind speed data points. The Excel sheet can be seen in appendix G.

In this section, an example of the solving procedure to determine the Weibull parameters is shown. Using the three days of hourly wind speed data from table 6-2, n = 72 and an initial guess of k = 2.0, successive applications of equation (6-22) to the data in table 6-2 gives k = 4.07, 2.30, and 3.60, converging after several iterations to 2.93. Equation (6-23) then gives c = 5.75 m/s.

Determination of the variance and standard deviation

From the Weibull equations (6-19) and (6-20) the equations for the variance σ^2 and the standard deviation σ can be derived as follows:

$$\overline{v^n} := \int_0^{\infty} v^n \cdot \frac{k}{c} \cdot \left(\frac{v}{c}\right)^{k-1} \cdot e^{-\left(\frac{v}{c}\right)^k} dv \qquad \textbf{(6-24)}$$

$$\overline{v^n} := c^n \cdot \Gamma\left(1 + \frac{n}{k}\right) \qquad \textbf{(6-25)}$$

Therefore, for n = 1,

$$\overline{v} := c \cdot \Gamma\left(1 + \frac{1}{k}\right) \qquad \textbf{(6-26)}$$

and for n = 2,

$$\overline{v^2} := c^2 \cdot \Gamma\left(1 + \frac{2}{k}\right) \qquad \textbf{(6-27)}$$

The variance of the wind speed is defined as

$$\sigma^2 := \overline{v^2} - \left(\overline{v}\right)^2 \tag{6-28}$$

Therefore the variance can be written in terms of c and k as follows:

$$\sigma^2 := c^2 \left[\Gamma\left(1 + \frac{2}{k}\right) - \left(\Gamma\left(1 + \frac{1}{k}\right)\right)^2 \right] \tag{6-29}$$

The standard deviation is then

$$\sigma := \sqrt{c^2 \left[\Gamma\left(1 + \frac{2}{k}\right) - \left(\Gamma\left(1 + \frac{1}{k}\right)\right)^2 \right]} \tag{6-30}$$

From the equations above, the variance and the standard deviation can be calculated. For the data from the 6 m wind mast, k = 1.90 and c = 9.67 m/s. The standard deviation is calculated as follows:

The variance is $\sigma^2 = 22.09\ m^2/s^2$.

Therefore the standard deviation $\sigma = 4.70$ m/s.

The above mentioned wind speeds and the Weibull frequency distribution can be seen in figure 6-7.

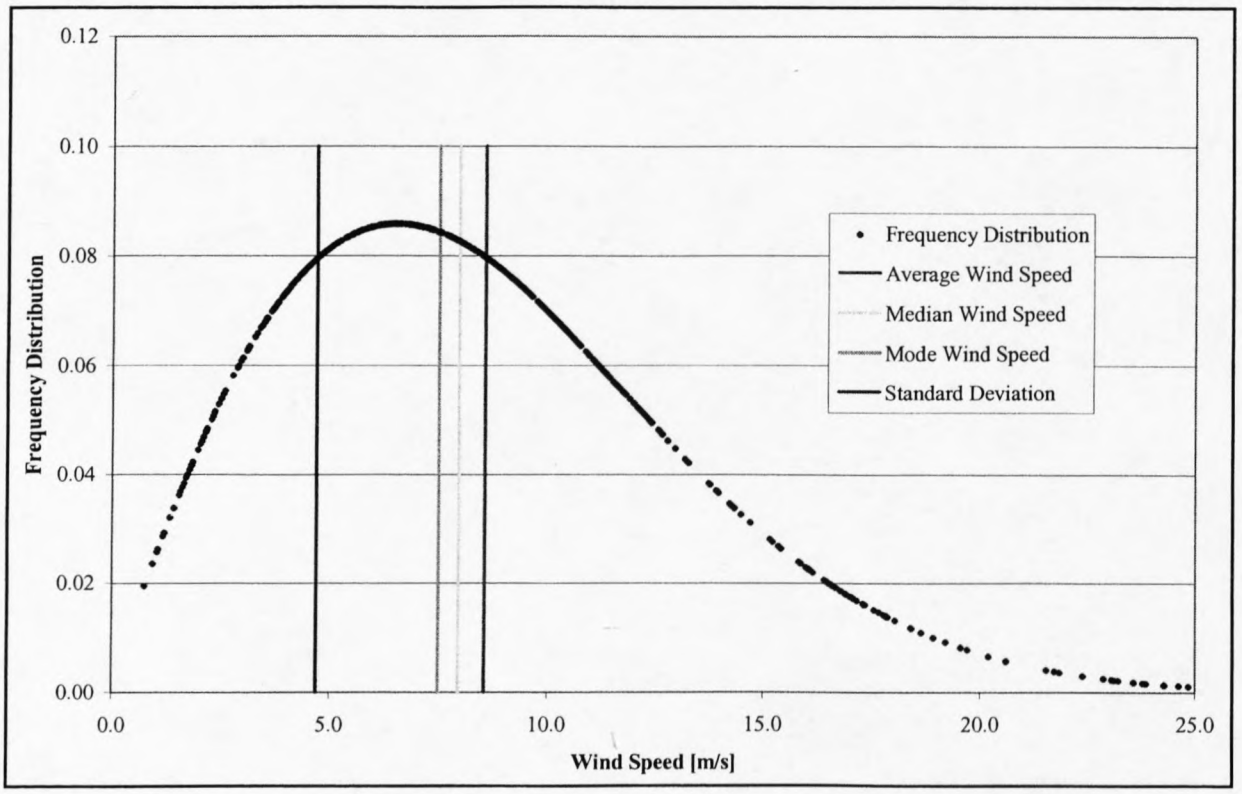

Figure 6-7: Weibull frequency distribution for 6 m wind mast data

6.2 Data Analysis of 10 m Weather Mast

The data from the automatic weather station was obtained from SAWS. The data stretches over a period from January 2001 to February 2002. The data includes wind speed and wind direction.

In order to analyze the data, Visual Basic programs were written to sort and to convert the data into workable form. The Visual Basic programs can be found in appendix A.

Attempts were made to define the wind regime characteristics using probability functions by fitting field data with standard mathematical functions describing frequency distributions. Weibull distributions are often used to characterize wind regimes in terms of its probability density and cumulative distribution functions (Mathew et al., 2001, Garcia et al., 1997, Sulaiman et al., 2000, Seguro and Lambert, 1999,

Balouktsis et al., 2001). Although efforts were made to fit field data with other distributions like Pearson type IV distribution, exponential distribution, gamma distribution and logistic distribution, the Weibull distribution is well accepted and widely adopted for wind data analysis. The Weibull function was applied to the wind data of the 6 m wind mast, as can be seen in chapter 6.1. The Weibull theory will not be repeated here, only the results will be shown.

6.2.1 Weibull distribution analysis

The determination of the Weibull parameters was applied firstly to the year 2001, January 2002 and February 2002 data for the complete period and then for each month. Thereby a comparison between the complete data and the monthly data can be made. First the average wind speeds for the relevant period has to be evaluated and then the Weibull parameters are calculated, as explained for the example in section 6.1. The results can be seen in table 6-3.

In order to verify the results of the Weibull parameters, a simple check is performed for the data of the complete period. The average wind speed of the measured data is compared to the average wind speed obtained by using the Weibull parameters. From table 6-3, k = 1.71 and c = 12.17 m/s. Therefore

$$v_{ave} := c \cdot \Gamma\left(1 + \frac{1}{k}\right) \tag{6-31}$$

$$v_{ave} := 10.854 \frac{m}{s}$$

The average wind speed from the measured complete period is $v_{avemeas}$ = 10.84 m/s. Therefore, the error made is

$$error := \left(\frac{v_{avemeas} - v_{ave}}{v_{avemeas}}\right) \cdot 100\ \% \tag{6-32}$$

$$error := -0.129\ \%$$

Therefore it can be seen that the Weibull parameters are correct in the order of 0.1%.

Year	Average	k	c [m/s]
2001	10.84	1.71	12.17
Month	**Average**	**k**	**c [m/s]**
January	6.97	2.19	7.87
February	8.88	2.26	9.99
March	11.60	2.07	13.14
April	10.04	2.35	11.31
May	9.19	2.15	10.36
June	15.97	2.07	18.00
July	12.90	1.91	14.57
August	12.32	2.00	13.85
September	10.90	1.83	12.29
October	13.85	1.71	15.44
November	11.95	1.69	13.36
December	9.52	1.44	10.53
January	8.04	1.58	8.99
February	9.48	1.61	10.60

Table 6-3: Weibull shape factor k and scale parameter c

From the equations above, the variance and the standard deviation can be calculated for the complete data period and for each month. The results are shown in table 6-4. The parameters calculated in this section are all evaluated for a height above ground level of h = 10 m.

	k	c [m/s]	Variance [m/s]	Standard Deviation
Complete Period:	1.71	12.17	42.76	6.54
Month:				
Jan-01	2.19	7.87	11.28	3.36
Feb-01	2.26	9.99	17.18	4.14
Mar-01	2.07	13.14	34.80	5.90
Apr-01	2.35	11.31	20.55	4.53
May-01	2.15	10.36	20.20	4.49
Jun-01	2.07	18.00	65.30	8.08
Jul-01	1.91	14.57	49.61	7.04
Aug-01	2.00	13.85	41.17	6.42
Sep-01	1.83	12.29	38.25	6.19
Oct-01	1.71	15.44	68.78	8.29
Nov-01	1.69	13.36	52.70	7.26
Dec-01	1.44	10.53	45.41	6.74
Jan-02	1.58	8.99	27.29	5.22
Feb-02	1.61	10.60	36.52	6.04

Table 6-4: Tabulation of the variance and standard deviation

6.2.2 Results of the wind data from the 10 m weather station

The data from the 10 m automatic weather station was analyzed similar to the data analysis of the 6 m wind mast. The results of the analysis are shown in table 6-5.

The variation of each of the minimum, maximum, average, median, mode, k, c, variance and standard deviation can be seen in the figures in appendix B.

	Min [m/s]	Max [m/s]	Average [m/s]	Median [m/s]	Mode [m/s]	k	c [m/s]	Variance [m/s]	Standard Deviation [m/s]
Complete Period:	0.80	38.90	10.84	9.80	8.90	1.71	12.17	42.76	6.54
Month:									
Jan-01	1.10	19.20	6.97	7.30	8.80	2.19	7.87	11.28	3.36
Feb-01	1.10	23.70	8.88	8.90	8.40	2.26	9.99	17.18	4.14
Mar-01	1.10	29.60	11.60	10.00	8.40	2.07	13.14	34.80	5.90
Apr-01	1.20	24.70	10.04	9.70	8.60	2.35	11.31	20.55	4.53
May-01	1.10	27.30	9.19	9.45	11.40	2.15	10.36	20.20	4.49
Jun-01	1.20	37.70	15.97	15.40	10.70	2.07	18.00	65.30	8.08
Jul-01	1.20	38.90	12.90	11.45	9.50	1.91	14.57	49.61	7.04
Aug-01	1.10	27.70	12.32	12.25	13.30	2.00	13.85	41.17	6.42
Sep-01	1.10	34.90	10.90	10.00	10.00	1.83	12.29	38.25	6.19
Oct-01	1.00	38.90	13.85	13.20	8.80	1.71	15.44	68.78	8.29
Nov-01	1.10	31.90	11.95	10.80	13.20	1.69	13.36	52.70	7.26
Dec-01	1.10	31.30	9.52	7.60	8.90	1.44	10.53	45.41	6.74
Jan-02	0.80	27.70	8.04	7.35	8.90	1.58	8.99	27.29	5.22
Feb-02	1.10	30.10	9.48	8.60	7.90	1.61	10.60	36.52	6.04

Table 6-5: Results of 10 m weather station data analysis

The Weibull probability density and cumulative frequency distribution function for the complete data period is shown in figure 6-8 and figure 6-9, respectively. From the cumulative frequency distribution one can see that about 17% of all the wind data lies below a wind speed of 5 m/s. This 5 m/s is a typical cut-in wind speed. The cut-in wind speed means that at this certain speed, for example 5 m/s, the wind turbine will start to produce power. At the cut-out wind speed, usually in the range of about 25 – 30 m/s, the wind turbine stops and discontinues to produce power. The percentage of wind speed above a cut-out wind speed of 30 m/s, as seen from the cumulative frequency distribution, is about 5%. Thus for a wind turbine with a cut-in and a cut-out wind speed of 5 m/s and 30 m/s, respectively, the total amount of time, the turbine will not be producing electricity, is about 22%.

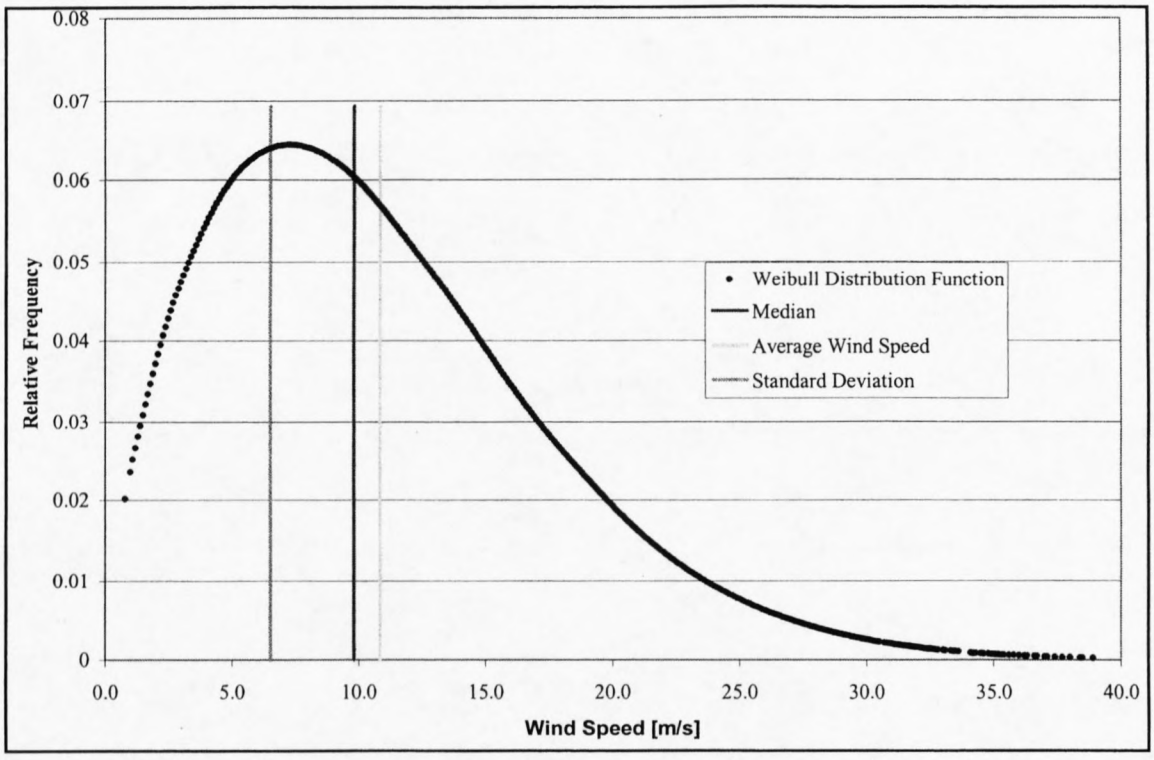

Figure 6-8: Weibull probability density

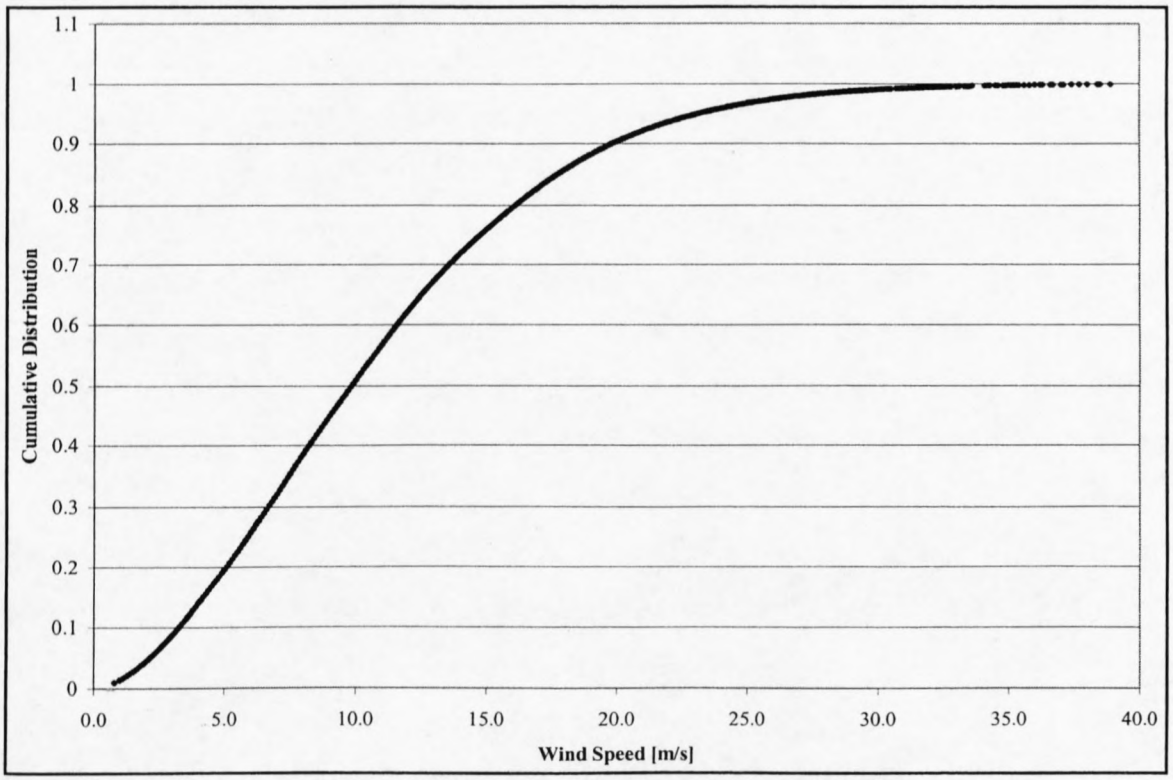

Figure 6-9: Weibull cumulative frequency distribution

6.2.3 Wind direction analysis

Strong winds usually come from a particular direction. To show the information about the distributions of wind speeds, and the frequency of the varying wind directions, a so-called wind rose has been created on the basis of meteorological observations of wind speeds and wind directions (Cheng 1999).

Wind roses vary from one location to the next. They actually are a form of meteorological fingerprint. Wind roses from neighboring areas are often fairly similar, so in practice it may sometimes be safe to interpolate (take an average) of the wind roses from surrounding observations. If complex terrain exists, i.e. mountains and valleys running in different directions, or coastlines facing in different directions, it is generally not safe to make simple assumptions like these. The wind rose, once again, only displays the relative distribution of wind directions, not the actual level of the mean wind speed (Potts et al., 2001).

A look at the wind rose is extremely useful for siting wind turbines. If a large share of the energy in the wind comes from a particular direction, then there should be as few obstacles as possible, and as smooth a terrain as possible in that direction, when placing wind turbines in the landscape. At the SANAE IV base most of the wind is coming from the east and southeast. Therefore there is no particular need to be very concerned about obstacles to the west or northwest of wind turbines, since practically no wind energy is coming from those directions. However, wind patterns may vary from year to year, and the energy content may vary (typically by some 10%) from year to year, so it is best to have observations from several years to make a credible average (DWEA, 2001).

For SANAE IV we can use the measurements made during the field trip for the different locations and take the data from the previous year from the existing wind tower. The data from the previous year and from 2002 indicate that the wind direction does not change significantly. Also from the observations made by previous year teams, it has been noted that the main wind directions always were from the east and southeast.

For the purposes of this analysis, the complete data, from January 2001 to February 2002, was analyzed to estimate average wind speeds and directions such that wind roses could be developed. To develop wind roses, the velocity records were separated into 36 different directional compartments. Then, the average velocity and relative frequency of occurrence were determined for each of these directional compartments. In order to simplify the explanation of the wind roses, a table has been created to identify the direction values.

N	350° to 11°	S	170° to 191°
NNE	12° to 34°	SSW	192° to 214°
NE	35° to 56°	SW	215° to 236°
ENE	57° to 79°	WSW	237° to 259°
E	80° to 101°	W	260° to 281°
ESE	102° to 124°	WNW	282° to 304°
SE	125° to 146°	NW	305° to 326°
SSE	147° to 169°	NNW	327° to 349°

Table 6-6: Classification of direction values into direction bins

Two different kinds of wind roses were used to display the data that is being analyzed. The one is a wind speed wind rose that shows the average wind speed in each sector or bin, and the other is the wind frequency rose that shows the number of occurrence of wind speeds in each direction sector.

Firstly the complete data period was incorporated into one wind speed rose and one wind frequency rose, and then the whole procedure was repeated for each month. This has was so that each month can be evaluated separately and any changes in wind direction pattern can be observed for each month. Figure 6-10 and figure 6-11 show the wind speed and wind frequency rose, respectively.

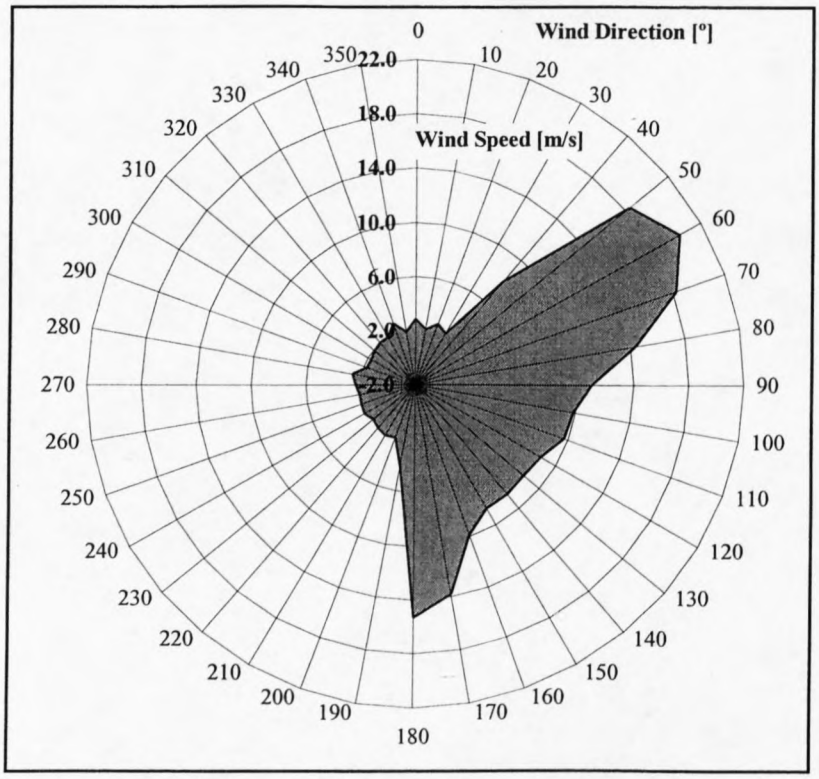

Figure 6-10: Wind speed rose (January 2001 – February 2002)

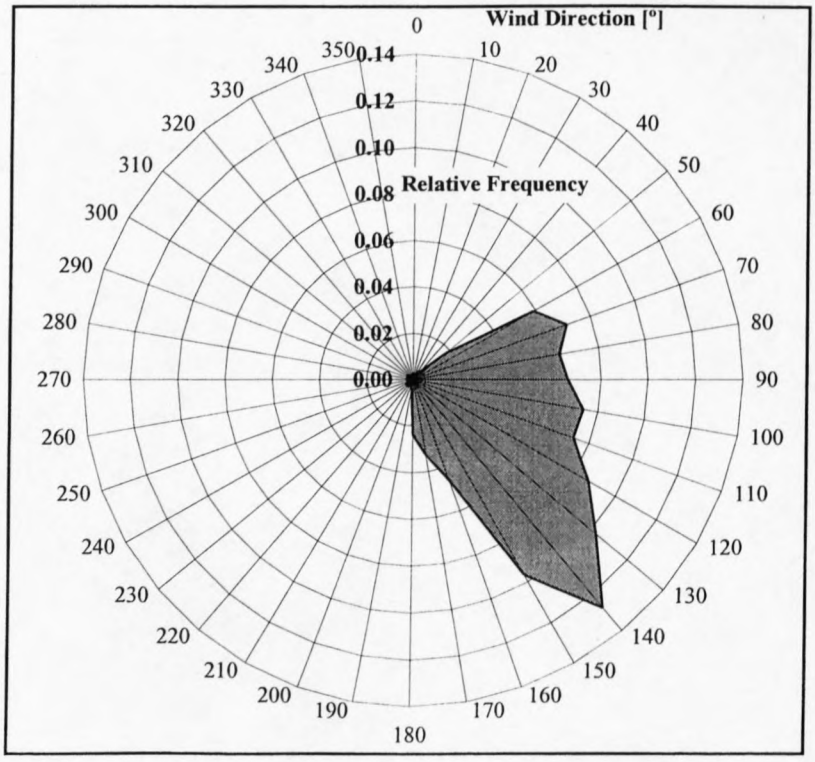

Figure 6-11: Wind frequency rose (January 2001 – February 2002)

In the following two figures the wind speed and wind frequency roses have been evaluated for each month and then been incorporated into one diagram. This has been done so that possible changes occurring during each month can be observed.

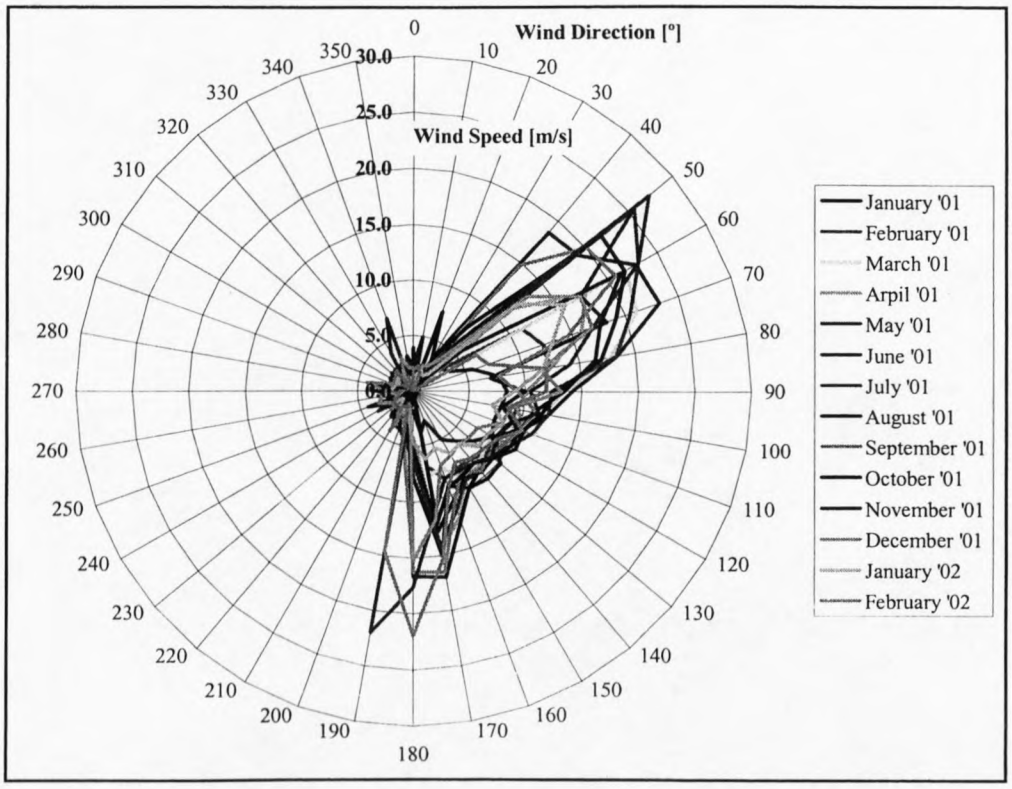

Figure 6-12: Monthly wind speed rose (January 2001 to February 2002)

It can be seen from figure 6-12 and figure 6-13 that there is no significant change in frequency or direction during each month. The highest wind speeds are coming from NE to ENE and from S as can be seen in figure 6-12. The wind speed and frequency roses generated for each month separately can be seen in appendix C.

From figure 6-13 it can be seen that most of the wind is coming from ENE to SE. Taking this information into account, as well as the main direction for the highest wind speeds, then the most power in the wind lies between ENE and S. As can be seen from the wind roses, is that nearly all the wind is coming from an easterly direction with a range of 150°. This means that the wind at SANAE IV is highly directional and well suited for wind turbine power production.

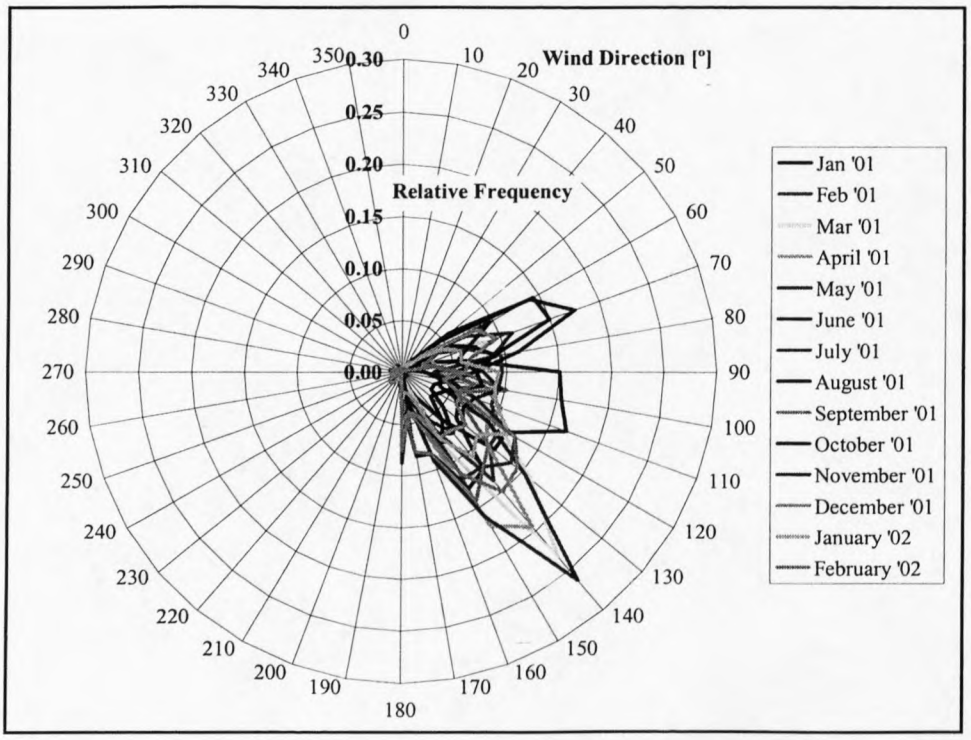

Figure 6-13: Monthly wind frequency rose (January 2001 to February 2002)

The reason for being well suited for wind turbine application is that a more directional wind pattern increases the chances of a wind turbine capturing the energy in the wind. With a highly directional wind pattern, a horizontal axis wind turbine does not need to turn to the right wind direction first in order to start operating. With a highly varying directional wind pattern, the yaw system of the wind turbine has to turn the turbine into the wind first and only then it can start producing energy. This can take up a lot of time if the wind is not highly directional and varying all the time.

Another reason why this wind pattern is well suited for wind turbine application is that when a wind comes mainly from one direction sector, then one only has to be concerned with the surface structure and obstacles in the direction sector. This means that in this case, only the eastern direction should be as clear as possible, with as little obstacles as possible, in the path of the oncoming winds. Therefore the wind turbine should be installed at a position, where there are no obstructions for the wind in the easterly direction, when looking from the wind turbine.

6.3 Data Analysis of Hand-held Anemometer Data

The data of the hand-held anemometer measurements was used primarily to generate a wind map of the area around SANAE IV. The measurements were done, using an analog hand-held anemometer. With this sensor the wind speeds at each of the 16 positions at a height of 2.5 m above ground level were measured. The sensor is mounted on a 1m long rod, so that it can be lifted up by a person to a height of about 2.5 m. The measurements taken are about 1-minute averages of wind speed at each location.

6.3.1 Data analysis and sample calculation

The surface structure can be roughly divided into two parts. One is the snow-covered area and the other one is the snow-covered area with protruding rocks, about 0.3 m in height. Therefore the velocity profiles, calculated for the 6 m wind mast can be used to extrapolate the hand meter wind measurements to a standard height of 10 m. Since the approximation has been made that only two different surfaces exist, only two different wind profiles are needed to be worked with, in order to extrapolate to 10 m height. In table 6-7 the surface type of each position is given.

Position	GPS Coordinates	Surface
1	71° 40.19' S 2° 47.85' W	Snow
2	71° 40.44' S 2° 50.67' W	Snow with protruding rocks
3	71° 40.49' S 2° 50.49' W	Snow with protruding rocks
4	71° 40.45' S 2° 50.34' W	Snow with protruding rocks
5	71° 40.57' S 2° 50.14' W	Snow
6	71° 40.59' S 2° 49.57' W	Snow
7	71° 40.58' S 2° 49.33' W	Snow
8	71° 40.33' S 2° 49.67' W	Snow with protruding rocks
9	71° 40.32' S 2° 50.30' W	Snow with protruding rocks
10	71° 40.28' S 2° 50,21' W	Snow
11	71° 40.17' S 2° 49.94' W	Snow
12	71° 40.22' S 2° 50.24' W	Snow with protruding rocks
13	71° 40.23' S 2° 50.43' W	Snow with protruding rocks
14	71° 40.21' S 2° 50.71' W	Snow with protruding rocks
15	71° 40.51' S 2° 50.08' W	Snow
16	71° 39.84' S 2° 49.48' W	Snow with protruding rocks

Table 6-7: Surface types for different positions

The derivation of the function for wind profiles of the two different surfaces is given in section 6.1.2. As mentioned above, the time step for the hand measurements is about one minute. In order to compare the data from the 6 m wind mast with the data from the hand meter, the time steps have to be the same. The data of the 6 m wind mast however has been logged at different time steps. They are listed in table 6-8. It can be seen from the table that most of the time the time step was 15 minutes.

Date		Time step
Start	**End**	**[min]**
1/1/2002 20:40	2/1/2002 11:20	5
2/1/2002 16:45	21/1/2002 15:30	15
21/1/2002 20:00	22/1/2002 15:45	1
23/1/2002 8:50	28/1/2002 8:50	5

Table 6-8: Time steps used for the 6 m wind mast

The wind speed difference between each measurement in the 15-minute time step has to be evaluated in order to see if these time steps can be used for comparison with the hand meter data. For example the wind speed on the 17th January 2002 at 14h30 is $v_1 = 9.4$ m/s at 10 m height and the wind speed on the 17th January 2002 at 14h45 is $v_2 = 9.9$ m/s at 10 m height. Thus the change in wind speed is:

$$\text{Difference} = \frac{|v_1 - v_2|}{v_1} \cdot 100\ \% := \frac{|9.4 - 9.9|}{9.4} \cdot 100\ \% := 5.32\ \% \qquad \textbf{(6-33)}$$

This example is representative for the complete data set of the 6 m wind mast. The example indicates a change in wind speed of about 5 %, which is fairly small. Thus it is safe to compare the 1-minute time step hand measured data to the 6 m wind mast data.

The data set of the hand meter contains a minimum, an average and a maximum reading for each measurement. During the 1-minute time step, the minimum has been noted, as well as the maximum. The average for the whole period has then been noted. For the wind speed extrapolation to 10 m height, the average wind speeds will be used.

A sample calculation is given next to show the procedure that has been used to get a wind map. The data set of the 6 m wind mast has been taken and extrapolated to 10 m height as explained in chapter 6.1. Then the wind speeds of the hand measured wind sensor have to be extrapolated to 10 m height, using the two wind profiles, corresponding to the two different surfaces, from the 6 m wind mast. For this sample calculation position 12 will be used. As can be seen from table 6-7, position 12 is located on a snow surface with protruding rocks. Therefore only the equations for a rocky surface apply here.

The 10 m wind speed can be obtained by calculating the shear velocity u^* and the surface roughness z_0 for the wind speeds at 2.5 m height first. Adapting equation (6-16), we get

$$u^* := 0.03 \cdot u_{10}^{1.23} := 0.03 \cdot 8.8^{1.23} := 0.435 \qquad \textbf{(6-34)}$$

and

$$z_0 := \frac{\nu}{9.53 \cdot u^*} + 0.0315 \cdot k + \frac{c_1 \cdot u^{*2}}{2 \cdot g} \qquad \textbf{(6-35)}$$

$$z_0 := \frac{0.0000131}{9.53 \cdot 0.435} + 0.0315 \cdot 0.01 + \frac{0.04 \cdot 0.435^2}{2 \cdot 9.81} := 0.0007046 \text{ m}$$

Therefore the wind speed at 10 m height is

$$v_{10} := \frac{u^*}{\kappa} \cdot \ln\left(\frac{10}{z_0}\right) := \frac{0.435}{0.41} \cdot \ln\left(\frac{10}{0.0007046}\right) := 10.15 \frac{\text{m}}{\text{s}} \qquad \textbf{(6-36)}$$

This procedure has been done for every measurement and all of the 16 positions. Since there are only about 10 measurements that have been done for each position during the field trip, the relevant date and time has to be found, when comparing the hand measured data to the 6 m wind mast data set. For the sample calculation, the date is the 14th of January 2002 at 19h57. The closest time at which a measurement has been recorded with the 6 m wind mast is 20h00. The wind speed is v = 7.81 m/s.

After this procedure has been repeated for each data point, a relationship has been established between the hand measured wind speeds and the 6 m wind mast wind speeds. This model will be different for each position, since the wind speeds are not the same at each position. For position 12 a regression analysis has been performed and a linear relationship has been found:

$$v_{hand} := 1.2434 \cdot v_{mast} + 0.00592 \tag{6-37}$$

with a regression coefficient of $R^2 = 0.9442$. Figure 6-14 shows the linear relationship between the wind mast and position 12 wind speeds. The graphs, regression coefficients and functions for the other 15 positions are shown in appendix H.

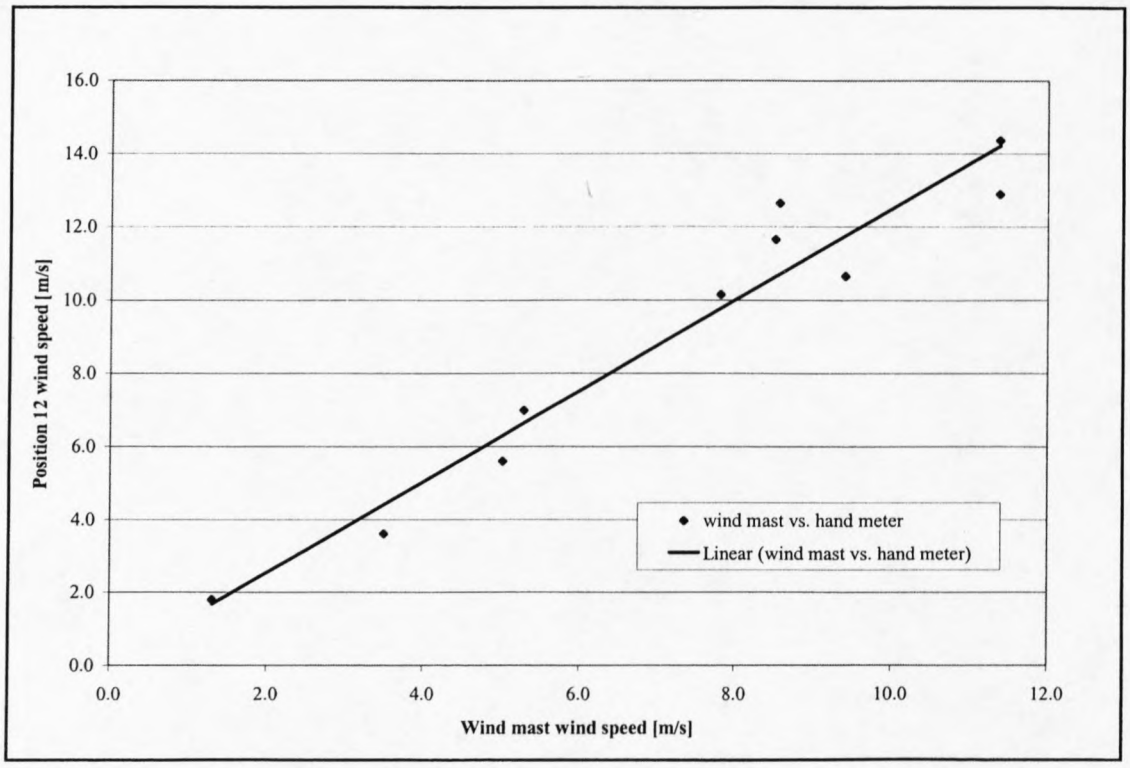

Figure 6-14: Linear relationship between wind mast and position 12 wind speeds

Once the 10 m height wind speed functions of all positions have been established, the wind speeds at each position can be calculated. From those data sets the average wind speeds have been calculated. The averages are based on the time during which the 6 m wind mast logged wind speeds. The wind mast logged wind data from the 1st of January 2002 until the

28th of January 2002. The average wind speed for each position is shown in figure 7-15. The figure clearly shows the different wind speeds of each position. Positions 2 to 12 have a similar average wind speed, while position 1 shows the lowest wind speed of the set. Positions 13, 14 and 16 show very high wind speeds.

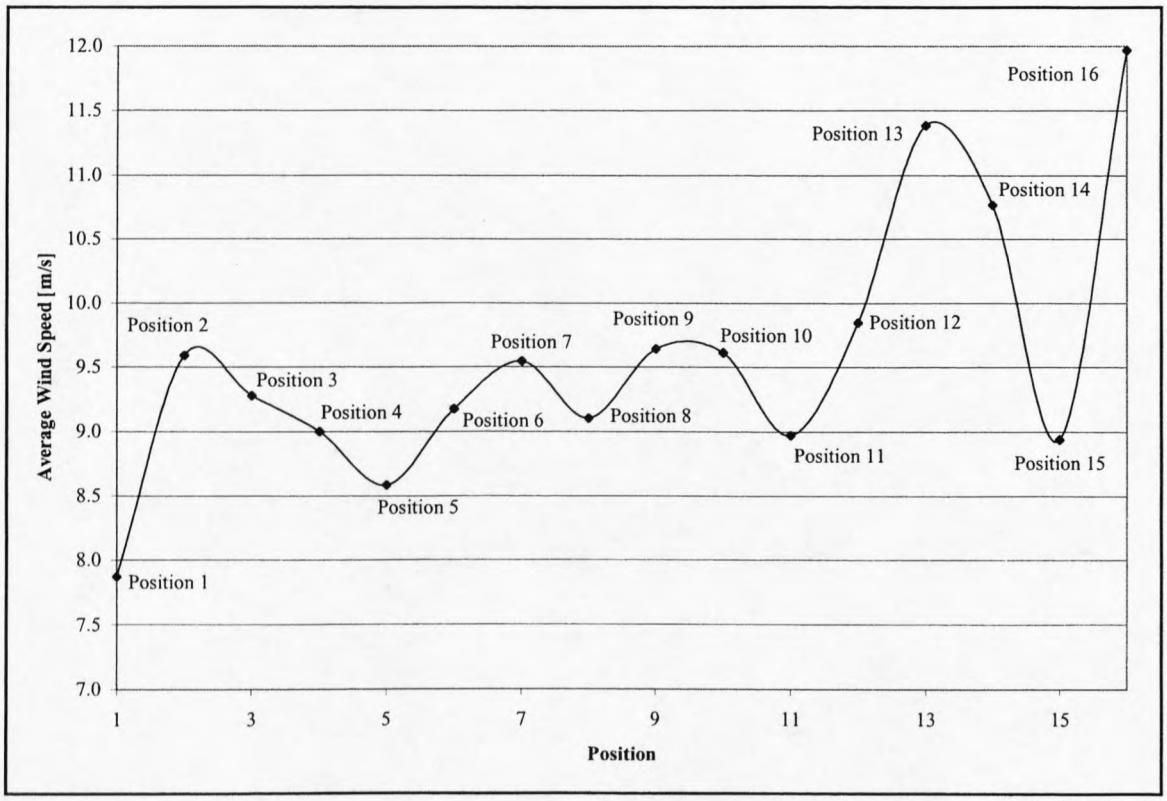

Figure 6-15: Average wind speeds at each position

The reason for those high wind speeds originates from the elevation of the position. Positions 13, 14 and 16 are the highest positions in that area, thus they are on outcrops, or in the case of position 16, which is situated on a small hill called 'Kleinkoppie'. The values for the average wind speed can be obtained from appendix H.

The average wind speed for each position is then taken and inserted into three matrices together with the coordinates of the position. With the aid of the program 'MathCAD' Version 8, wind maps have been created and are shown in figure 6-16 and figure 6-17.

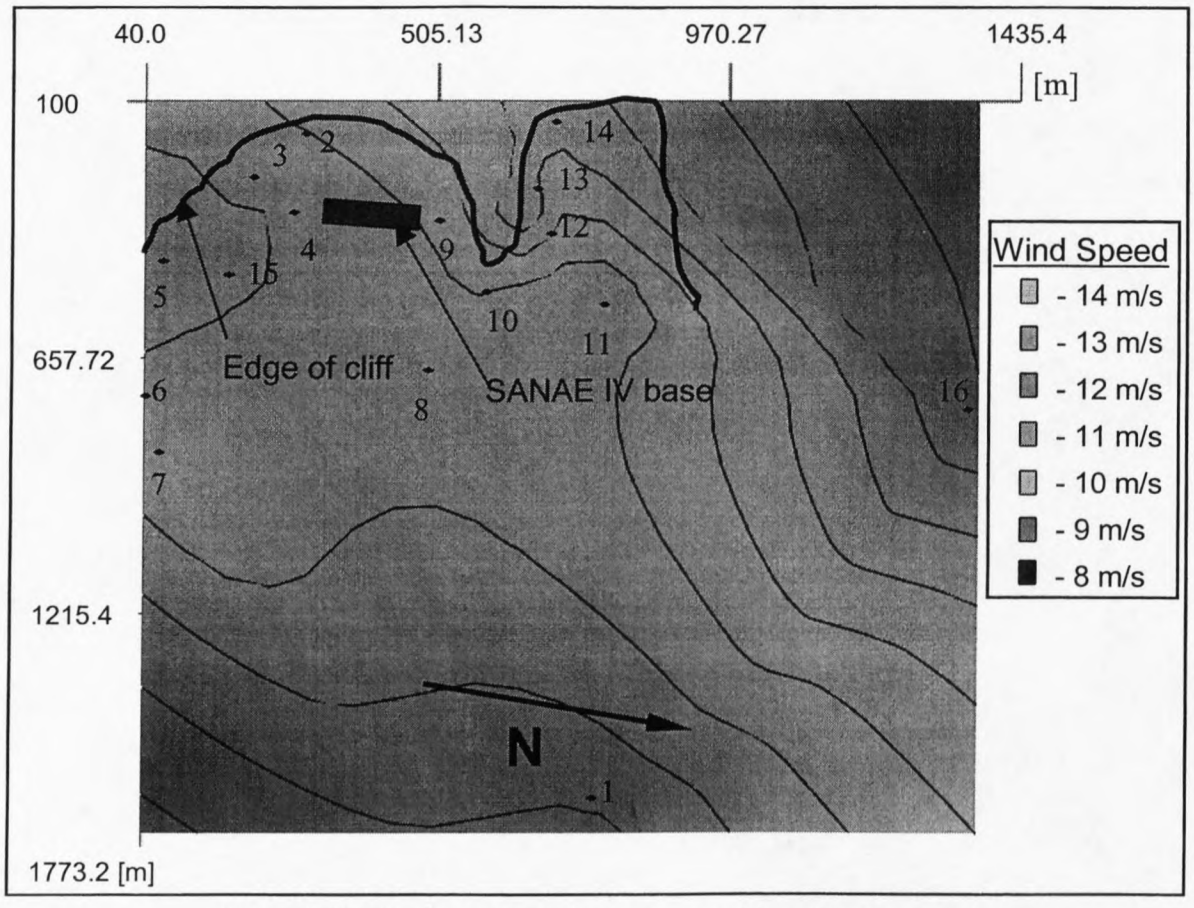

Figure 6-16: Wind speed map for area around base (contour map)

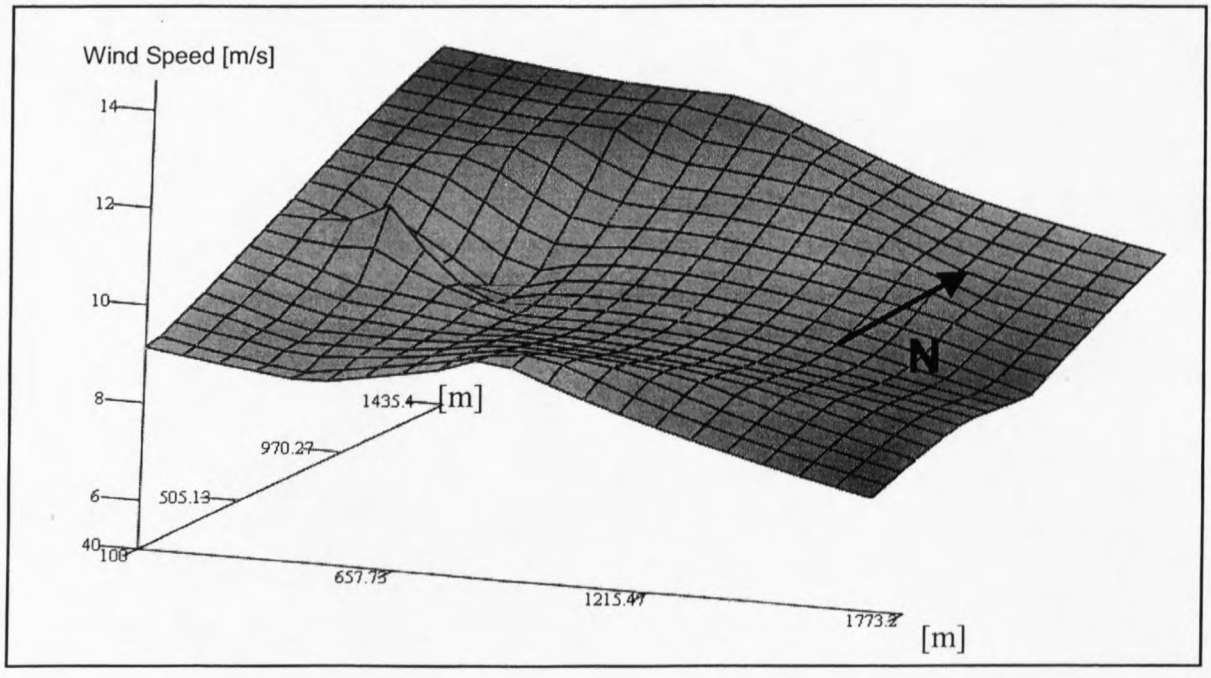

Figure 6-17: Wind speed map for area around SANAE IV (wire mesh map)

The wind speed distribution around the base is clearly visualized in the above figures. Figure 6-16 shows that lower wind speeds occur in the valley east of the base, while higher wind speeds occur north and partly west of the base, which are outcrops and nunataks. The western and northern regions of the base are therefore ideally suited for wind turbine positioning. In order to visualize the measuring position properly, photographs have been taken of each measuring position and can be seen in appendix I.

6.3.2 Error estimation of hand meter data analysis

The hand meter data analysis has been done by setting up relationships and using an analog hand held wind sensor. This can potentially lead to some errors, which can be:

- Analog hand measuring device, reading error
- Analog hand measuring device, accuracy of equipment
- Analog hand measuring device, accuracy of reading/ guessing average, minimum and maximum values
- Conversion of data, data being extrapolated to 10 m height, by using the two wind profiles from the wind mast
- Fitting functions and comparing hand measuring device data to the wind mast data
- Total error for wind speed analysis
- Total error for wind energy analysis ($P = \frac{1}{2}\rho v^3$)

The three errors mentioned first can be calculated measuring wind speeds with the hand-measuring device in close proximity of the wind mast. The wind sensor of the hand held anemometer has to be at the same height as the sensors of the wind mast. This was done during the field trip and the hand held anemometer measurements were compared to the measurements by three sensors of the wind mast. The measurements can be seen in table 6-9. The position of the wind mast was 71° 40.19' S 2° 47.85' W.

	Wind Tower	Hand meter		
Date / Time	3/1/2002 22h00	3/1/2002 21h55		
Wind Sensor Height	**Average [m/s]**	**Min [m/s]**	**Ave [m/s]**	**Max [m/s]**
1) 0.3 m	6.4	5	6	7
2) 1.3 m	7.1	6.5	7	7.8
3) 2.5 m	7.5	7	8	9

Table 6-9: Hand-held anemometer verification measurements

From these measurements the errors at each of the three heights can be evaluated and then the average for the three heights can be calculated as follows.

Height 1:

$$e_1 := \frac{6.0\,\frac{m}{s} - 6.4\,\frac{m}{s}}{6.4\,\frac{m}{s}} \cdot 100\,\% := 6.25\,\% \qquad \textbf{(6-38)}$$

Height 2:

$$e_2 := \frac{7.0\,\frac{m}{s} - 7.1\,\frac{m}{s}}{7.1\,\frac{m}{s}} \cdot 100\,\% := 1.41\,\% \qquad \textbf{(6-39)}$$

Height 3:

$$e_3 := \frac{8.0\,\frac{m}{s} - 7.5\,\frac{m}{s}}{7.5\,\frac{m}{s}} \cdot 100\,\% := 6.67\,\% \qquad \textbf{(6-40)}$$

The total error made is just the average of all three errors and is

$$e_{total} := \frac{6.25 + 1.41 + 6.67}{3} := 4.8\,\% \qquad \textbf{(6-41)}$$

Thus the analog reading error and the accuracy of the equipment error can be approximated as 5%. The next error is the error involved in extrapolating the data to 10 m height. This error, either originating from the hand measuring device or the 6 m wind mast, is due to inaccuracies in the curve fitting through the measured data. In order to calculate the error

involved, the wind speeds obtained from the 10 m weather station were compared to the extrapolated 10 m wind speeds from the 6 m wind mast.

Since the weather station measures hourly average, the data from the 6 m wind mast has to be converted to hourly averages. The averages calculated for the 6 m wind mast may not be very accurate, since some of the data has not been measured on the hour and is averaged in the next hour. The data set that has been compared is from the 18th of January 2002 until the 28th of January 2002.

	6.6m Wind Mast		10m Weather Station		
Date	Average Hourly Wind Speed [m/s]	Wind Direction	Average Hourly Wind Speed [m/s]	Acumulated Error Made	No of Hours
1/18/2002 17:00	3.8	180	4.7	0.19	1
1/18/2002 18:00	5.3	140	5.2	0.21	2
1/18/2002 20:00	3.44	160	3.9	0.33	3
1/18/2002 21:00	3.78	110	1.4	2.03	4
1/18/2002 22:00	2.50	70	3.3	2.27	5
1/18/2002 23:00	2.43	50	2.7	2.37	6
1/19/2002 1:00	5.72	80	4.2	2.73	7
1/19/2002 2:00	3.55	50	2	3.51	8
1/19/2002 3:00	1.53	200	1.3	3.68	9
⋮	⋮	⋮	⋮	⋮	⋮
1/27/2002 10:00	7.33	110	6.9	12.49	184
1/27/2002 11:00	7.89	110	7.5	12.54	185
1/27/2002 12:00	7.95	110	7.6	12.58	186
1/27/2002 13:00	8.58	110	8.1	12.64	187
1/27/2002 14:00	9.14	100	8.7	12.69	188
1/27/2002 15:00	9.30	90	8.9	12.74	189
1/27/2002 16:00	10.23	90	9.9	12.77	190
1/27/2002 17:00	10.89	80	10.7	12.79	191
1/27/2002 18:00	8.66	90	8.4	12.82	192
1/27/2002 19:00	8.31	100	7.8	12.89	193
1/27/2002 20:00	6.48	90	6.9	12.95	194
1/27/2002 21:00	5.62	90	5.7	12.96	195
1/27/2002 22:00	7.03	100	7.1	12.97	196
1/27/2002 23:00	6.49	90	6.8	13.01	197
1/28/2002 0:00	6.54	90	6.7	13.04	198
1/28/2002 1:00	7.38	110	7.7	13.08	199
1/28/2002 2:00	6.80	110	7.5	13.17	200
1/28/2002 3:00	6.23	100	6.6	13.23	201
1/28/2002 4:00	6.01	120	6.3	13.27	202
1/28/2002 5:00	6.79	140	7.3	13.34	203
1/28/2002 6:00	6.90	140	7.4	13.41	204
1/28/2002 7:00	8.19	150	8.2	13.41	205
1/28/2002 8:00	8.38	140	8.8	13.46	206
1/28/2002 9:00	8.53	140	8.9	13.50	207
	8.5		**8.3**	**6.52%**	
Average wind speed from 6.6m wind mast, extrapolated to 10m.		**Average wind speed from 10m weather station.**		**Average error for this data set.**	

Table 6-10: Error involved in extrapolating wind speeds to 10 m height

The error for each hourly measurement is calculated first. Then the errors for the complete data set are added and the result is divided by the number of hours for the data set. The result is shown at the bottom of table 6-10. The error is e = 6.52%.

The last error is due to finding relationships between the hand meter data and the 6 m wind mast data. An example for the curve fitting can be seen in figure 6-14. The same procedure as described for the previous error will be used here as well. The error for each measurement of one position is calculated first. Then the errors are added and the sum is divided by the number of measurements. The errors made for each position are shown in table 6-11.

Measuring Position	Calculated Error [%]
1	0.0
2	11.4
3	10.4
4	9.2
5	6.9
6	5.6
7	7.4
8	2.5
9	7.5
10	7.1
11	8.5
12	9.5
13	6.3
14	8.3
15	6.4
16	3.7
Average Error	6.9

Table 6-11: Curve fitting errors for each wind measurement position

From the calculations above the total error made for the hand meter wind speed analysis is

$$\text{Error}_{\text{Total}} := 5\ \% + 6.5\ \% + 6.9\ \% := 18.4\ \% \tag{6-42}$$

Therefore the error made in calculating the wind speed averages for each measurement position (1-16) is roughly 19%. If one combines this error and calculates the error made when the energy density is calculated, the error has to be cubed due to the power density function, which is

$$P := \frac{1}{2} \cdot \rho \cdot v^3 \tag{6-43}$$

The error in calculating the power density is $e = (1.184)^3 - 1 = 1.6598 - 1 = 0.6598$. Thus the error is approximately 66%. This enormous error clearly shows that no energy calculation can be made from the hand meter wind speed analysis. The wind speeds and maps calculated are primarily used to illustrate the differences in wind speeds for each of the 16 positions around the base.

The accuracy of the hand meter wind speed analysis is relatively low (19%) since very crude and basic equipment has been used to measure the wind speeds at each position. The hand meter analysis has been done so that the wind speed maps will show where the best wind energy capturing position will be, which has been established in section 6.3.1.

6.4 Catabatic Winds

Catabatic wind are caused by gravity slowly accelerating cold air along the long smooth slopes of the Antarctic continent until it reaches enormous speeds near the shores, sometimes augmented by funneling effects of valleys. The Catabatic winds are claimed to be the fastest wind on the planet. The duration of a Catabatic wind is normally between one day and one week, having nearly constant wind speeds of about 35 – 45 m/s. On Antarctica, they should come from a southerly to southeasterly direction. As mentioned in the wind direction analysis, most of the winds are coming from the NE to the SE. Very seldom, the winds come from a southerly direction.

It is not known at this stage, how Catabatic winds affect the wind regimes at SANAE IV, which is situated 150 km from the shore. However, since the Catabatic winds reach their maximum levels close to the shores, they should not influence the wind regimes at SANAE IV in a drastic manner. This can be seen from the wind direction analysis, which shows that the fastest winds are coming from a northeasterly and southerly direction, but most of the winds are coming from the southeasterly direction.

During the summer period from December 2001 until February 2002, fine scale wind speed measurements have been logged with the 6 m wind mast, taking average measurement every 5 minutes or less. Only two storms have been recorded, but both storms originated from an easterly direction, thus giving rise to the question whether these storms were Catabatic or not. No fine scale wind speed data measurements are logged at the SANAE IV base at the moment. The wind speed and direction measurements are hourly averages. These measurements cannot be used to identify gusts.

SAWS state that Catabatic winds should not have a significant effect on the wind regime at SANAE, since the base is built on a nunatak. It is recommended that the occurrence of gusts should be investigated and fine scale wind measurements should be logged for at least one year, before the budget, to install a wind turbine at SANAE IV, is allocated.

Useful information can be obtained from the Weibull shape parameter k. Normally k is in the range 1.5 to 3.0. A smaller k corresponds to a gustier wind, while a bigger k means that the winds are more even at a specific site. From the year data, $k = 1.71$, measured at a height of 10 m. The value of k for the year data clearly shows that the winds encountered at SANAE IV are gusty, but they are still within levels encountered at many locations around the world, where 'normal' wind turbines are operational.

The predecessor of the Northern Power Systems NW100/19 wind turbine has been tested at the South Pole and Antarctic coasts and the experiences gained in these harsh conditions has been incorporated into the design of the NW100/19 wind turbine. As the predecessors have been running at Antarctic coasts, where the Catabatic wind are the strongest, there

should be no problem running the NW100/19 wind turbine at SANE IV, which due to its distance from the coast is much less influenced by Catabatic winds.

7 *WIND TURBINE POWER PRODUCTION*

In the preceding chapters the wind data and the information, regarding the wind turbine set-up at SANAE IV have been analyzed in order to predict the power output of a wind turbine, which will be handled in this chapter.

7.1 Introduction

There are two acceptable systematic approaches that may be used for the evaluation of the wind energy potential of an area of interest. The first approach is analytical and it is based on specially developed mathematical models ("mass consistent models", e.g. as in the WasP computer program), which take into account the orography and roughness of the area under study (by using special digitized maps) and use data taken from meteorological station(s) located in the above area or with reasonable proximity to it (Papadopoulos and Dermentzoglou, 2001). The aim is to predict the wind characteristics, i.e. the distribution of wind speeds expected annually, in scale and frequency in each direction sector and at different heights above ground level, the mean annual expected wind speed in m/s at different heights above ground level and finally the annual expected wind energy potential (energy density in W/m^2) at different heights above ground level in order to reveal sites with favorable wind energy potential.

A preliminary evaluation follows by choosing the most suitable sites, which seem to be more attractive for application purposes and deserve further investigation. The criteria used in this example are as follows:

- Sites with suitable mean annual wind speed (e.g. for SANAE IV greater than 5m/s) at the hub-height of the wind turbine system;
- Proximity of the site to the station's electric grid should preferably not exceed 2.0 km; and
- Accessibility of the site, in order to avoid expensive road construction must be guaranteed.

Finally, a series of investigations is performed, by assuming possible commercially available candidate wind turbine systems, in order to predict the mean annual expected power production (in kWh) for possible installation in the examined location of interest.

The second approach uses real, on site measurements taken from a meteorological station installed at the site under examination and for a duration period of at least 1 year. Then, an evaluation similar to the above method is performed in order to obtain information about the wind energy potential of the site and the mean annual expected power production from various wind turbine systems, which might be installed in the location/site under study. In any case it is recommended that real (on site) measurements must always accompany the results of the analytical approach, in order to validate them and thus avoid possible unreasonable investment risks from the exploitation of the examined location/site (Papadopoulos and Dermentzoglou, 2001).

7.2 Wind Energy Resources

A wind turbine obtains its power by converting the kinetic energy of the wind into torque, through the rotor blades. The amount of energy that the wind transfers to the rotor, depends on the density of the air, the rotor area, and the wind speed. Figure 7-1 shows how a cylindrical slice of air 1m thick moves through a 1500 m^2 rotor of a typical 600 kW wind turbine.

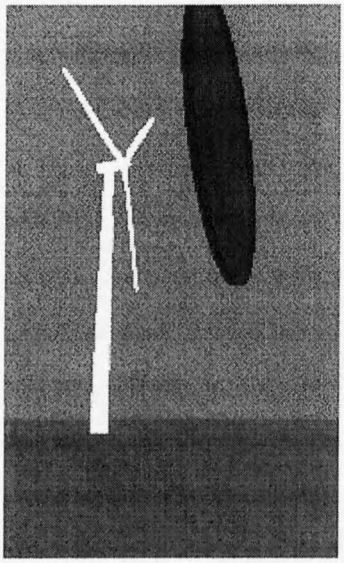

Figure 7-1: Cylindrical slice of air, 1m thick, moving through a wind turbine (DWEA, 2001)

7.2.1 Density of air

The kinetic energy of a moving body is proportional to its mass. The kinetic energy in the wind thus depends on the density of the air, i.e. its mass per unit of volume. In other words, the "heavier" the air, the more energy is received by the turbine. At normal atmospheric pressure and at 15 °C air has a density of 1.225 kg/m^3, but the density decreases slightly with increasing humidity.

Also, the air is denser when it is cold than when it is warm. At high altitudes, (in mountains) the air pressure is lower, and the air is less dense. For the SANAE IV case, the atmospheric pressure varies between 88 kPa and 92 kPa. Taking the air temperature to be an average value of T = -20 °C = 253.16 K and the gas constant for air is R = 0.2870 kJ/kgK, the density is calculated as follows. From P = ρRT, where T is the temperature measured in Kelvin, the density of air at SANAE IV is

$$\rho := \frac{P}{R \cdot T} := \frac{90\ \text{kPa}}{0.2870\ \frac{\text{kJ}}{\text{kg} \cdot \text{K}} \cdot 253.16\ \text{K}} := 1.24\ \frac{\text{kg}}{\text{m}^3} \qquad \text{(7-1)}$$

Although the density changes, these changes are not big and the air density is taken as a constant throughout all the calculations in this project.

7.2.2 Rotor area

A typical 100 kW wind turbine has a rotor diameter of 19-21 m, i.e. a rotor area of some 290 m^2. The rotor area determines how much energy a wind turbine is able to harvest from the wind. Since the rotor area increases with the square of the rotor diameter, a turbine which is twice as large will receive four times as much energy.

$$A = \pi/4 * D^2 \qquad \textbf{(7-2)}$$

7.2.3 Wind deflection by turbine

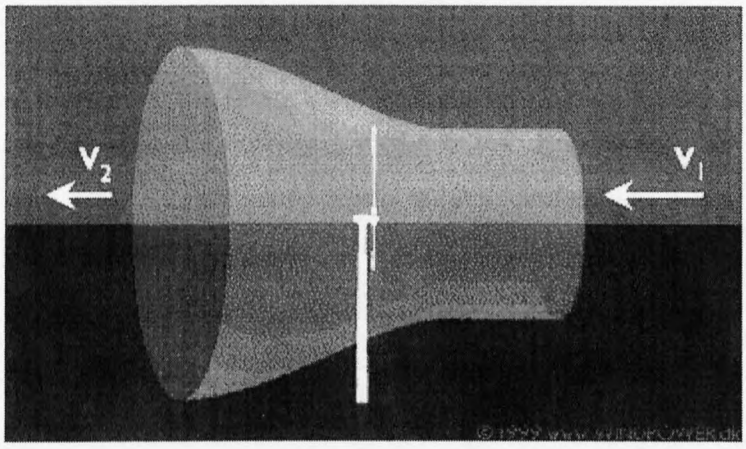

Figure 7-2: Wind deflection by a horizontal axis wind turbine (DWEA, 2001)

The image in figure 7-2 is a bit simplified, because in reality, a wind turbine will deflect the wind, even before the wind reaches the rotor plane. This means that one will never be able to capture all the energy in the wind using a wind turbine. This will be discussed later, when Betz's Law is introduced. In figure 7-2 the wind is coming from the right, and a device to capture part of the kinetic energy in the wind is used. (In this case a three bladed, horizontal axis rotor is used, but it could be some other mechanical device).

7.2.4 The stream tube

The wind turbine rotor must obviously slow down the wind as it captures its kinetic energy and converts it into rotational energy. This means that the wind will be moving slower behind the rotor than in front of the rotor. Since the amount of air entering through the swept rotor area from the right (every second) must be the same as the amount of air leaving the rotor area to the left, the air will have to occupy a larger cross section (diameter) behind the rotor plane.

In figure 7-2 a tube of the airflow is shown, which is known as a steam tube. The stream tube shows how the slow moving wind to the left in the picture will occupy a large volume behind the rotor. The wind will not be slowed down to its final speed immediately behind the rotor plane. The slowdown will happen gradually behind the rotor, until the speed becomes almost constant.

7.2.5 The air pressure distribution in front of and behind the rotor

The graph in figure 7-3 shows the air pressure plotted vertically, while the horizontal axis indicates the distance from the rotor plane. The wind is coming from the right, and the rotor is in the middle of the graph. As the wind approaches the rotor from the right, the air pressure increases gradually, since the rotor acts as a barrier to the wind.

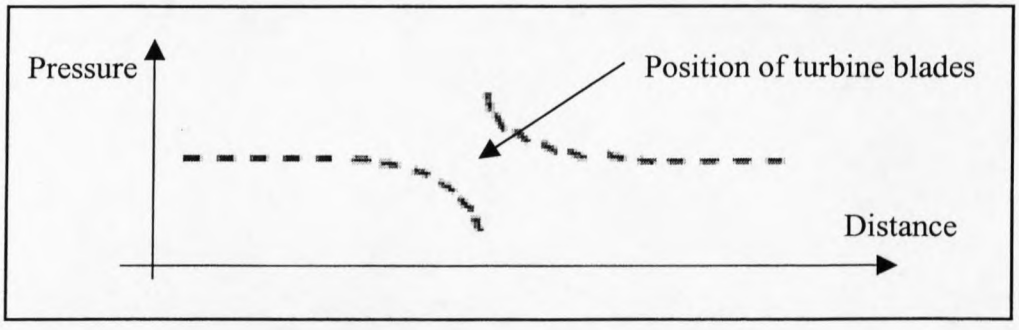

Figure 7-3: Pressure distribution in front and behind a wind turbine

Note, that the air pressure will drop immediately behind the rotor plane (to the left). It then gradually increases to the normal air pressure level in the area.

7.2.6 Roughness

In general, the more pronounced the roughness of the earth's surface, the more the wind will be slowed down. Forests and large cities obviously slow the wind down considerably, while concrete runways at airports will only slow the wind down a little. Water surfaces are even smoother than concrete runways, and will have even less influence on the wind, while long grass, shrubs and bushes will slow the wind down considerably.

As the wind profile was measured, the surface roughness was calculated from the measured wind profile. Thus there is no need to estimate the surface roughness and get a wind profile from the estimated surface roughness.

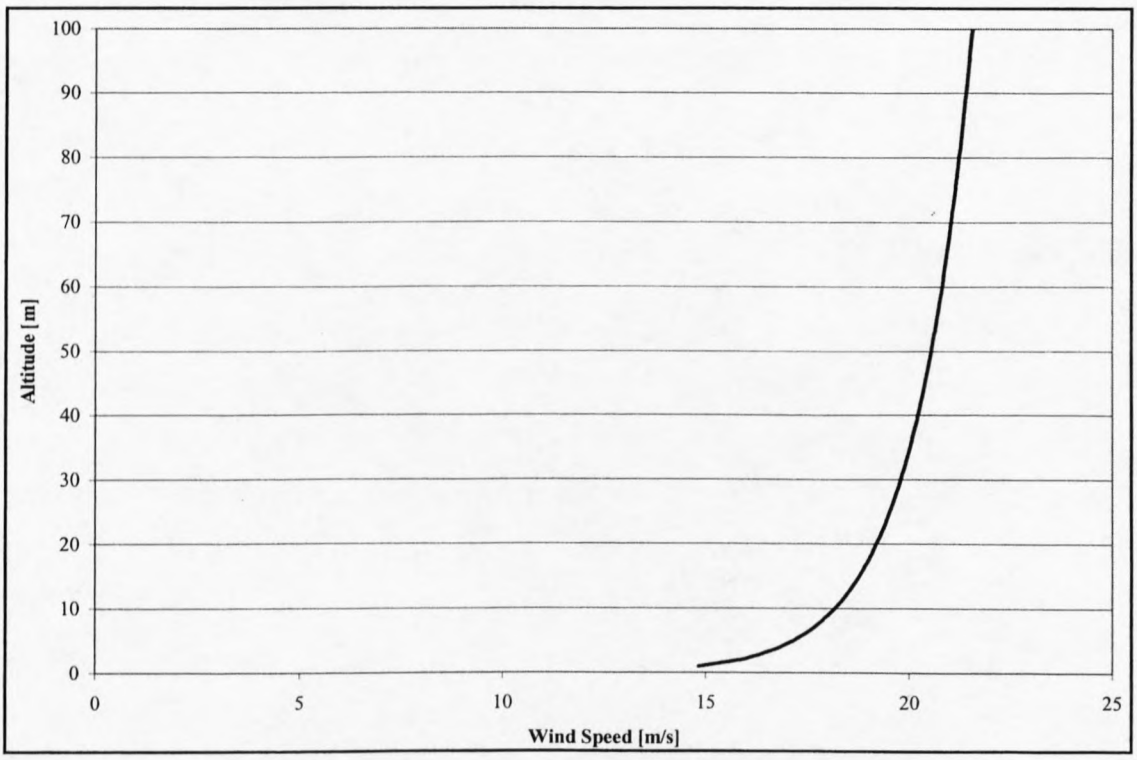

Figure 7-4: Wind profile for a typical surface roughness of z_0 = 0.00004 m (snow surface)

A typical wind profile up to a height of 100 m is shown in figure 7-4. The wind profile was created using a shear velocity u* = 0.6, yielding a surface roughness of z_0=0.00004 m. This surface roughness corresponds to the snow covered area and is calculated using equation (6-1). The wind profile for a snow covered area with protruding rocks looks very similar to figure 7-4.

7.2.7 Large scale turbulence

It is well known that hail storms or thunder storms, in particular, are associated with frequent gusts of wind, which both change speed and direction. In areas with a very uneven terrain and behind obstacles such as buildings, a lot of turbulence is similarly created, with very irregular wind flows, often with whirls or vortexes in the neighborhood. Turbulence decreases the possibility of using the energy in the wind effectively for a wind turbine. It also imposes more wear and tear on the wind turbine. Towers for wind turbines are usually made tall enough to avoid turbulence from the wind close to ground level.

Due to the steep velocity profile, as can be seen in figure 7-4, originating from very low surface roughnesses at the potential positions, the turbulence effect does not have a great impact on the wind turbine height. Therefore a relatively low tower can be used, in the order of 15 to 20 m.

7.2.8 Wind shade

Figure 7-5 gives an estimate of how wind speeds decrease behind a blunt obstacle, i.e. an obstacle that is not properly streamlined. In this case an obstacle is used, which is 6 m tall and 100 m wide, placed at a distance of 300 m upwind of a wind turbine with an 8 m hub height. The wind shade, as different shades of gray, can be seen quite literally. The blue numbers indicate the wind speed in percent of the wind speed without the obstacle. At the top of the yellow wind turbine tower the wind speed has decreased by some 5.8 % to 94.2 % of the speed without the obstacle. It should be noted that this means a loss of wind energy of some 17.4 % at the top of the tower. This example illustrates the effect of obstacle situated in front of a wind turbine. The main wind direction at SANAE IV is east. In order for the wind turbine to have as little obstacles in front of it, the turbine should be placed east of the base. The area east of the base is relatively smooth with only few obstacles like small outcrops.

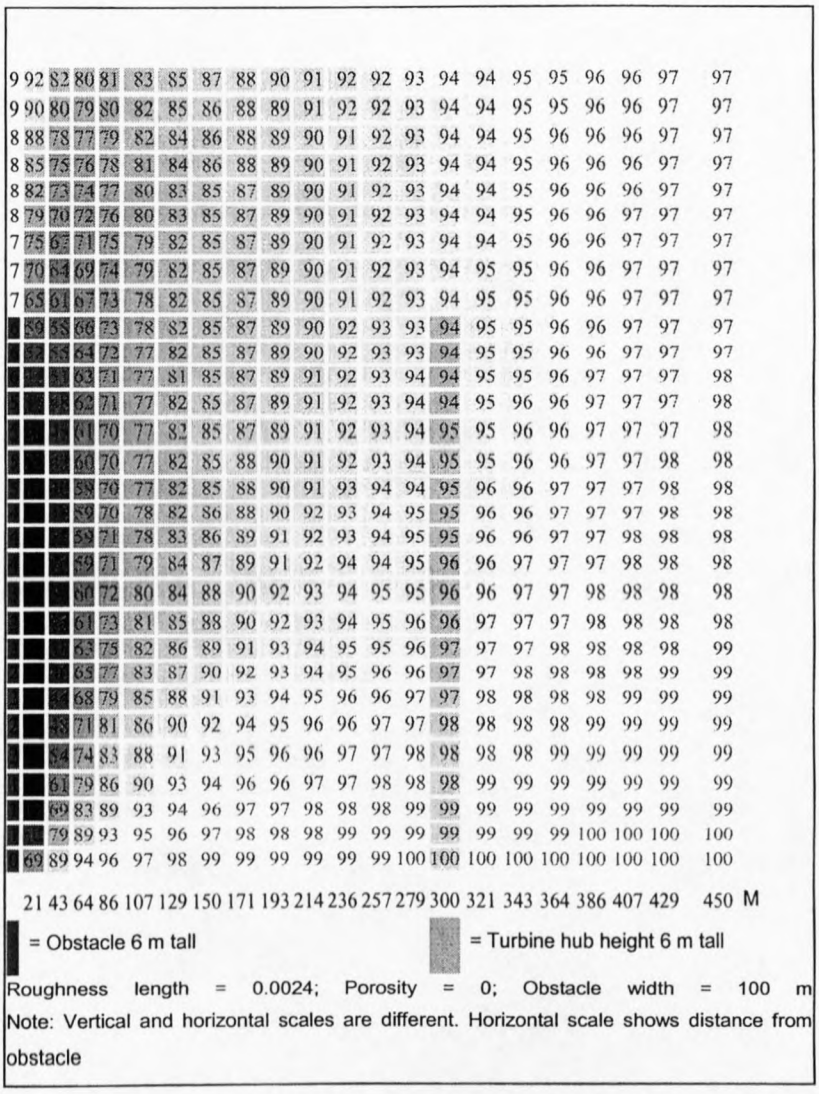

Figure 7-5: Wind speed in percent of wind speed without obstacle (DWEA, 2001)

7.2.9 Wind turbine site selection

From the previous pages, it becomes obvious that the best site would be as open a possible in the prevailing wind direction. Thus the fewer the obstacles and the lower the surface roughness upstream of the wind turbine, the better. If one can find a rounded hill to place the turbine, one may even get a speed up effect. Both the feasibility of building the foundation of the turbine, and accessibility to the site must be taken into account with any wind turbine project.

7.3 Wind Turbine Energy Output

It is very important for the wind industry to be able to describe the variation of wind speeds. Turbine designers need the information to optimize the design of their turbines, so as to minimize generating costs. Turbine investors need the information to estimate their income from electricity generation.

7.3.1 Weibull distribution

If wind speeds are measured throughout a year, it will be noticed that in most areas strong gale force winds are rare, while moderate and fresh winds are quite common.

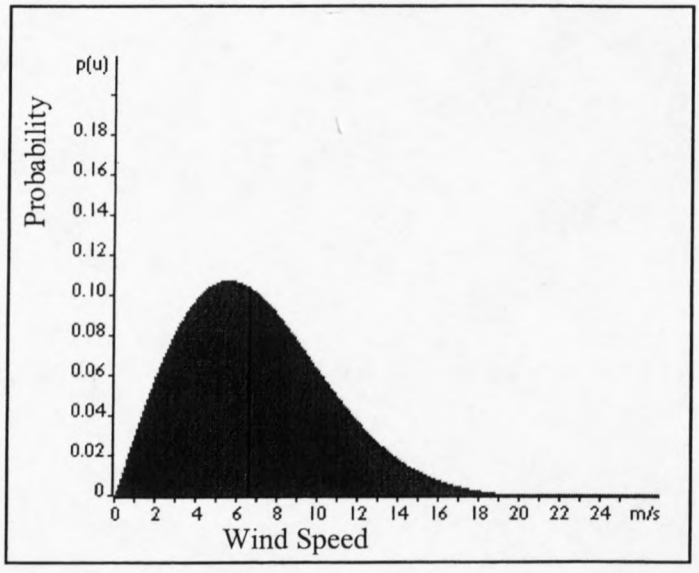

Figure 7-6: Weibull distribution example (DWEA, 2001)

The wind variation for a typical site is usually described using the so-called Weibull distribution, as shown in figure 7-6. The Weibull distribution function has been derived in chapter 1. This particular site has a mean wind speed of 7 m/s, and the shape of the curve is determined by a so-called shape parameter of 2.

Figure 7-6 shows a probability density distribution. The area under the curve is always exactly 1, since the probability that the wind will be blowing at some wind speed including zero must be 100%. Half of the gray area is to the left of the vertical black line at 6.6 m/s. The 6.6 m/s is called the median of the distribution. This means that half the time it will be blowing less than 6.6 m/s, the other half it will be blowing faster than 6.6 m/s. The mean wind speed is the average of the wind speed observations recorded at this site. The figure shows that the distribution of wind speeds is skewed, i.e. it is not symmetrical. Sometimes very high wind speeds occur, but they are very rare. Wind speeds of 5.5 m/s, on the other hand, are the most common ones. The value of 5.5 m/s is called the modal value of the distribution. If each incremental small wind speed interval is multiplied by the probability of getting that particular wind speed, and is added up, the mean wind speed is obtained.

The statistical distribution of wind speeds varies from one place to the next around the globe, depending upon local climate conditions, the landscape, and the surface. The Weibull distribution may thus vary, both in its shape, and in its mean value. If the shape parameter is exactly 2, as in figure 7-6, the distribution is known as a Rayleigh distribution. Wind turbine manufacturers often give standard performance figures for their machines using the Rayleigh distribution. However the Rayleigh distribution assumes a constant shape parameter of k = 2, describing the wind pattern as moderately gusty. While this may seem accurate for certain regions in the world, the winds at SANAE IV are gustier, resulting in a smaller shape parameter. As shown in section 7.2.1 the shape parameter for the period from January 2001 to February 2002 is k = 1.71, measured at 10 m height. Comparing this to the assumed value of the Rayleigh distribution of k = 2.0 results in a deviation of 17 % when the Rayleigh distribution is used. The Rayleigh distribution would describe the winds at SANE IV as moderately gusty, which is not accurate. Thus the Weibull distribution function will be used in this analysis.

An important thing to note is that the energy cannot by calculated by taking the average wind speed and using

$$P = a \times v^3 \qquad \textbf{(7-3)}$$

where a is the rotational area and v the average wind speed. Each wind speed probability has to be weighed with the corresponding amount of power.

7.3.2 Theoretical power in the wind

The power available in a wind stream per unit area is given by

$$P := \frac{1}{2}\cdot\rho\cdot v^3 \tag{7-4}$$

Wind power density of a site can be expressed as

$$P_D := \int_0^\infty P(v)\cdot f(v)\, dv \tag{7-5}$$

From equations (6-19), (6-20) and (7-5)

$$P_D := \int_0^\infty \frac{1}{2}\cdot\rho\cdot v^3\cdot\frac{k}{c}\cdot\left(\frac{v}{c}\right)^{k-1}\cdot e^{-\left(\frac{v}{c}\right)^k} dv \tag{7-6}$$

Simplifying equation (7-6) yields

$$P_D := \frac{1}{2}\cdot\rho\cdot c^2\cdot k\cdot\int_0^\infty \left(\frac{v}{c}\right)^{k+2} e^{-\left(\frac{v}{c}\right)^k} dv \tag{7-7}$$

At this point, a substitution is needed to solve this integral. From (Mathew et al., 2001) it is seen that a Gamma function has been employed where an analysis has been based on the Rayleigh function. As the Rayleigh function has only one parameter, it is much easier to solve than the Weibull function.

From (Zill and Cullen, 1996), the Gamma function is defined as follows

$$\Gamma := \int_0^{\infty} t^{x-1} \cdot e^{t-1}\, dt \tag{7-8}$$

for $x > 0$. Making the substitution

$$t := \left(\frac{v}{c}\right)^k \tag{7-9}$$

Differentiating equation (7-9) with respect to v yields

$$dt := \frac{k}{c^k} \cdot v^{k-1} \cdot dv$$

and transforming gives

$$dv := \frac{1}{v^{k-1}} \cdot \frac{c^k}{k} \cdot dt \tag{7-10}$$

Substituting equation (7-10) into equation (7-7) yields after some simplifying

$$P_D := \frac{1}{2} \cdot \rho \cdot c^3 \cdot \int_0^{\infty} \left[\left(\frac{v}{c}\right)^k\right]^{\frac{3}{k}} \cdot e^{-\left(\frac{v}{c}\right)^k} dt \tag{7-11}$$

Substituting equation (7-9) yields

$$P_D := \frac{1}{2} \cdot \rho \cdot c^3 \cdot \int_0^{\infty} (t)^{\frac{3}{k}} \cdot e^{-t}\, dt \tag{7-12}$$

From the definition of the Gamma function, one obtains $x - 1 = 3/k$, therefore $x = 1 + 3/k$. Thus the power density can be written as

$$P_D := \frac{1}{2} \cdot \rho \cdot c^3 \cdot \Gamma\left(1 + \frac{3}{k}\right) \tag{7-13}$$

Once the power density is estimated, energy that is available in the wind spectra for a duration (that is in a month for this analysis) can be expressed as

$$P_{Dt} := T \cdot P_D := \frac{1}{2} \cdot T \cdot \rho \cdot c^3 \cdot \Gamma\left(1 + \frac{3}{k}\right) \tag{7-14}$$

As in the wind analysis chapter, the calculations are first performed for the complete data period (January 2001 to February 2002), and then for each month. A sample calculation will be given for each derivation, using the complete period data.

Another fact that has to be considered is the height of the wind turbine. Thus the height has to be included in the energy calculations. For the sample calculations a height of 25 m will be used. The reason is that the Northern Power Systems NW100 100 kW wind turbine will be used to calculate the real wind turbine power output and the hub height of this turbine is 25 m. The Weibull parameters for a turbine height of 25 m are given in table 7-1. The Weibull shape and scale parameter, k and c, respectively, for different turbine hub heights are given in appendix J. The heights used for each of the 5 wind turbines, are 9, 18, 25 and 35 m.

For the case of the complete data period, c = 13.15 m/s and k = 1.57. Therefore, using a density of $\rho = 1.24$ kg/m^3 and a time period of one year T = 12 months * 30 d * 24 h = 8640 h. Therefore the power density is

$$P_D := \frac{1}{2} \cdot 1.24 \cdot 13.15^3 \cdot \Gamma\left(1 + \frac{3}{1.57}\right) := 2601.07 \frac{W}{m^2} \tag{7-15}$$

And for the complete period, the energy density is

$$P_{Dt} := \frac{1}{2} \cdot 8640 \cdot 1.24 \cdot 13.15^3 \cdot \Gamma\left(1 + \frac{3}{1.57}\right) := 22473.26 \frac{kWh}{m^2 \cdot year} \tag{7-16}$$

The results for each month can be viewed in table 7-1.

	Average Wind Speed	k	c [m/s]	Power density	Power density per year/months
	[m/s]		[m/s]	[W/m²]	[kWh/m²/year]
Complete Year:	11.81	1.57	13.15	2601.07	22473.26
Month:	[m/s]		[m/s]	[W/m²]	[kWh/m²/month]
Jan-01	7.28	1.90	8.21	482.72	347.56
Feb-01	9.50	2.02	10.72	1007.60	725.47
Mar-01	12.73	1.93	14.35	2530.76	1822.14
Apr-01	10.87	2.15	12.27	1422.89	1024.48
May-01	9.88	1.93	11.14	1181.95	851.00
Jun-01	17.65	1.97	19.91	6593.93	4747.63
Jul-01	14.20	1.81	15.98	3777.42	2719.74
Aug-01	13.48	1.83	15.17	3179.50	2289.24
Sep-01	11.89	1.70	13.32	2386.70	1718.42
Oct-01	15.18	1.58	16.91	5446.26	3921.31
Nov-01	13.05	1.56	14.52	3557.30	2561.25
Dec-01	10.28	1.30	11.13	2331.74	1678.85
Jan-02	8.57	1.41	9.41	1167.42	840.54
Feb-02	10.23	1.45	11.29	1891.81	1362.10

Table 7-1: Theoretical power in the wind stream.

7.3.3 Most frequent wind speed and speed carrying maximum energy

From the Weibull distribution function (6-19) and (6-20) the wind speed that occurs most frequently can be calculated as follows

$$\frac{d}{dv} f(v) = 0 \tag{7-17}$$

Therefore substituting equation (6-20) into equation (7-17) and differentiating

$$\frac{d}{dv}\left[\frac{k}{c}\cdot\left(\frac{v}{c}\right)^{(k-1)}\cdot\exp\left[-\left(\frac{v}{c}\right)^{k}\right]\right] := 0 \tag{7-18}$$

Thus

$$\frac{k}{c}\cdot\left(\frac{v}{c}\right)^{(k-1)}\cdot\frac{(k-1)}{v}\cdot\exp\left[-\left(\frac{v}{c}\right)^{k}\right] - \frac{k^2}{c}\cdot\left(\frac{v}{c}\right)^{(k-1)}\cdot\frac{\left(\frac{v}{c}\right)^{k}}{v}\cdot\exp\left[-\left(\frac{v}{c}\right)^{k}\right] = 0 \tag{7-19}$$

Solving the above equation for the most frequent wind speed v_{Fmax} yields

$$V_{Fmax} := c \cdot \left(\frac{k - 1}{k}\right)^{\frac{1}{k}} \tag{7-20}$$

For the complete data period, the most frequent wind speed is

$$V_{Fmax} := 13.15 \cdot \left(\frac{1.57 - 1}{1.57}\right)^{\frac{1}{1.57}} := 6.90 \frac{m}{s} \tag{7-21}$$

Since the power available from a wind stream is proportional to the cube of its velocity, it is not the most frequent wind speed but a wind speed usually higher than that would carry the maximum amount of energy in it. A wind turbine is designed to work at its maximum efficiency point at a wind velocity usually termed the design wind speed (v_D). Hence it is advantageous that the design wind speed of a machine and the wind speed corresponding to the maximum amount of energy is made as close as possible. Once the velocity responsible for the maximum energy is identified for a particular site, in this case SANAE IV, the designer can design the wind turbine system to be most efficient at this velocity. The energy corresponding to a particular wind speed can be expressed as

$$E_v := P(v) \cdot f(v) \tag{7-22}$$

Hence from equations (6-20) and (7-4), one gets

$$E_v := \frac{1}{2} \cdot \rho \cdot v^3 \cdot \frac{k}{c} \cdot \left(\frac{v}{c}\right)^{k-1} \cdot e^{-\left(\frac{v}{c}\right)^k} \tag{7-23}$$

From equation (7-23) E_v would be a maximum at wind speed V_{Emax} such that

$$\frac{dE_v}{dv} := 0 \quad \text{at } V_{Emax}. \tag{7-24}$$

Thus

$$\frac{d}{dv}\left[\frac{1}{2} \cdot \rho \cdot c^2 \cdot k \cdot \left(\frac{v}{c}\right)^{k+2} \cdot \exp\left[-\left(\frac{v}{c}\right)^k\right]\right] = 0 \tag{7-25}$$

$$\frac{1}{2}\cdot\rho\cdot c^2\cdot k\cdot\left(\frac{v}{c}\right)^{(k+2)}\cdot\frac{(k+2)}{v}\cdot\exp\left[-\left(\frac{v}{c}\right)^k\right]-\frac{1}{2}\cdot\rho\cdot c^2\cdot k^2\cdot\left(\frac{v}{c}\right)^{(k+2)}\cdot\frac{\left(\frac{v}{c}\right)^k}{v}\cdot\exp\left[-\left(\frac{v}{c}\right)^k\right]=0 \quad \textbf{(7-26)}$$

Therefore the wind speed that produces the most energy is defined as

$$V_{Emax} := c\cdot\left(\frac{k+2}{k}\right)^{\frac{1}{k}} \quad \textbf{(7-27)}$$

For the complete data period, with c = 13.15 m/s and k = 1.57, the wind speed with the most energy is

$$V_{Emax} := 13.15\cdot\left(\frac{1.57+2}{1.57}\right)^{\frac{1}{1.57}} := 22.19\,\frac{m}{s} \quad \textbf{(7-28)}$$

The results of this analysis and the power density including Betz' Law are shown in table 7-2. The derivation of Betz Law can be seen in appendix J.

	Power density	Power density per year/months	Power density (Betz Law)	V e max	V f max
	[W/m²]	[kWh/m²/year]	[kWh/m²/year]	[m/s]	[m/s]
Complete Year:	2601.07	22473.26	13317.49	22.19	6.90
Month:	**[W/m²]**	**[kWh/m²/month]**	**[kWh/m²/month]**	**[m/s]**	**[m/s]**
Jan-01	482.72	347.56	205.96	11.99	5.54
Feb-01	1007.60	725.47	429.91	15.09	7.63
Mar-01	2530.76	1822.14	1079.79	20.74	9.83
Apr-01	1422.89	1024.48	607.10	16.69	9.16
May-01	1181.95	851.00	504.30	16.08	7.65
Jun-01	6593.93	4747.63	2813.41	28.37	13.93
Jul-01	3777.42	2719.74	1611.70	24.10	10.25
Aug-01	3179.50	2289.24	1356.59	22.67	9.88
Sep-01	2386.70	1718.42	1018.32	21.05	7.91
Oct-01	5446.26	3921.31	2323.74	28.30	9.02
Nov-01	3557.30	2561.25	1517.78	24.71	7.48
Dec-01	2331.74	1678.85	994.88	22.89	3.55
Jan-02	1167.42	840.54	498.10	17.61	3.92
Feb-02	1891.81	1362.10	807.17	20.46	5.08

Table 7-2: Power by Betz' Law, most frequent wind and wind speed carrying maximum energy

7.3.4 Wind turbine selection and specification

In order to give some diversity to the energy calculations, 5 different wind turbines have been selected, which potentially meet the requirements for installation, operation and maintenance at SANAE IV. The different wind turbines and the rated power output are given in table 7-3. Only the North Wind NW100/19 wind turbine will be used in this chapter to calculate the power that can be captured from the wind at the base. The energy calculations regarding the other wind turbines can be seen in appendix J. This has been done so that this section will not be cluttered with information.

Wind Turbine Manufacturer	Wind Turbine Description	Nominal Power Rating
Bergey Windpower Co., Inc.	Bergey BWC Excel	10 kW
Fuhrländer	Fuhrländer FL 30	30 kW
Atlantic Orient	Atlantic Orient 15/50	50 kW
Fuhrländer	Fuhrländer FL 100	100 kW
Northern Power Systems	North Wind NW100/19	100 kW

Table 7-3: Wind turbines used for energy calculations and nominal power ratings

As can be seen from table 7-3, the North Wind NW100/19 wind turbine has a 100 kW nominal power rating which is the highest of all the wind turbines. Thus the wind turbine is fairly big and special precaution has to be taken whether this or any of the other turbines can be installed at SANAE IV.

7.3.5 Wind turbine power curve

The power curve of a wind turbine is a graph that indicates how large the electrical power output will be for the turbine at different wind speeds. Figure 7-8 shows a power curve for the North Wind NW100/19 wind turbine.

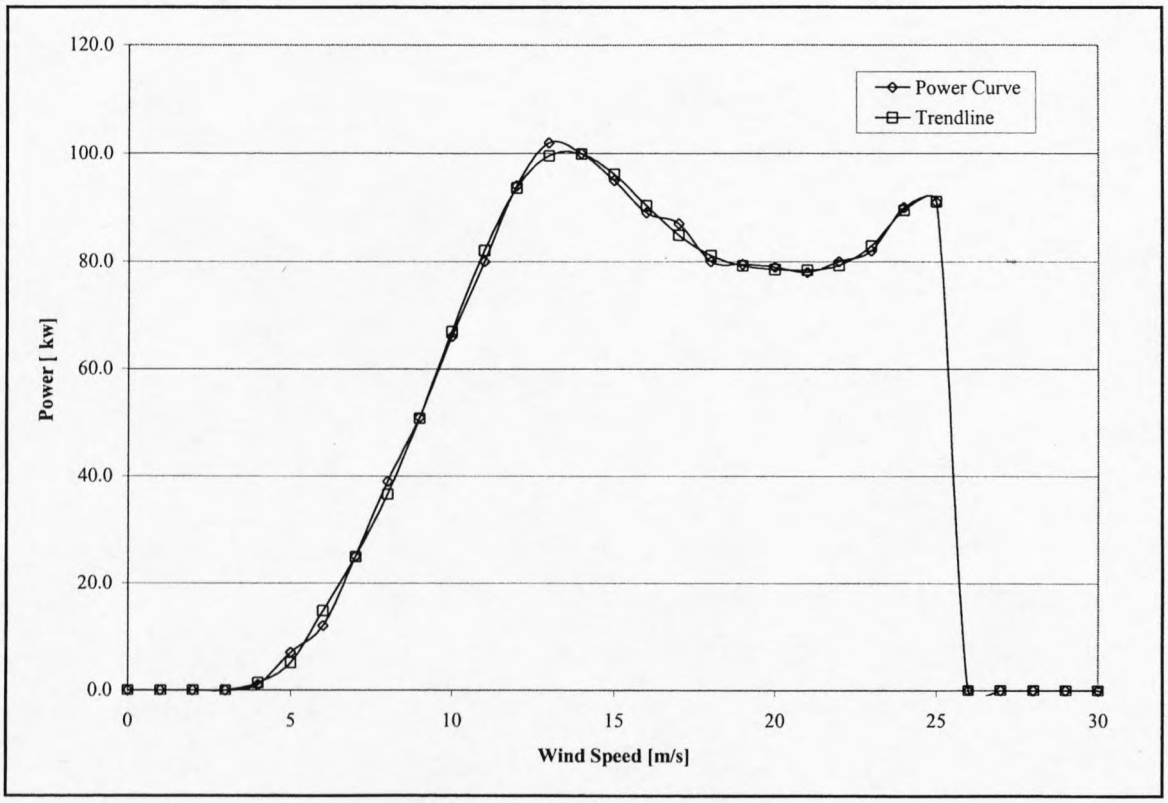

Figure 7-7: Power curve of the North Wind NW100/19 wind turbine

Power curves are found by field measurements, where an anemometer is placed on a mast reasonably close to the wind turbine (not on the turbine itself or too close to it, since the turbine rotor may create turbulence, and make wind speed measurement unreliable). If the wind speed is not fluctuating too rapidly, then the wind speed measurements from the anemometer may be used, the electrical power output from the wind turbine recorded and the two values plotted together in a graph like in figure 7-7.

The trendline curve in figure 7-7 is a curve fit to the power curve data. The function for the curve called trendline has been found by doing a regression analysis. The function is a 9-degree polynomial.

$$y := -3.0469 \cdot \exp^{-7} \cdot x^9 + 3.9870 \exp^{-5} \cdot x^8 - 0.0022345 \cdot x^7 + 0.07006 \cdot x^6 - 1.34645 \cdot x^5 + 16.3685 \cdot x^4 - 125.5419 \cdot x^3 + 586.3445 \cdot x^2 - 1508.6508 \cdot x + 1624.7065 \quad \textbf{(7-29)}$$

The reason for creating such a high degree polynomial is that the power curve will be used to calculate the true power output of a wind turbine and therefore a function for this power curve has to be found, which has to be as accurate as possible. Equation (7-29) features a regression coefficient of $R^2 = 0.9981$.

In reality, a swarm of points spread around the power curve line will be seen, and not the neat curve, as in figure 7-7. The reason is that in practice the wind speed always fluctuates, and the column of wind that passes through the rotor of the turbine cannot be measured exactly.

It is not a workable solution just to place an anemometer in front of the turbine, since the turbine will also cast a "wind shadow" and brake the wind in front of itself. In practice, therefore, the average of the different measurements for each wind speed has to be taken, and the graph has to be plotted through these values. Furthermore, it is difficult to make exact measurements of the wind speed itself. If an error of 3 % in wind speed measurement occurs, then the energy in the wind may be 9 % higher or lower (remembering that the energy content varies with the third power of the wind speed). Consequently, there may be errors up to plus or minus 10 % even in certified power curves.

Power curves are based on measurements in areas with low turbulence intensity, and with the wind coming directly towards the front of the turbine. Local turbulence and complex terrain (e.g. turbines placed on a rugged slope) may mean that wind gusts hit the rotor from varying directions. It may therefore be difficult to reproduce the power curve exactly in any given location.

It is very important to note that a power curve does not tell how much power a wind turbine will produce at a certain average wind speed. It would not even be close, if this method were used. The energy content of the wind varies very strongly with the wind speed, as was seen in the section on the wind energy resources. It matters a lot how that average came about, i.e. if winds vary a lot, or if the wind blows at a relatively constant speed.

Also, remembering from the example in the section on the power density function that most of the wind energy is available at wind speeds, which are twice the most common wind speed at the site.

Finally, the fact that the turbine may not be running at standard air pressure and temperature has to be considered. Consequently corrections for changes in the density of air have to be made. In this case the density is 1.24 kg/m^3.

7.3.6 Power density function

In order to calculate the energy output from a wind turbine, the Northern Power Systems North Wind NW100/19 wind turbine was chosen. Although this is a fairly large wind turbine, it could be used to cover part of the energy demand of the base. This wind turbine is a three bladed self-supporting construction, mounted on a tapered tubular steel tower. Some of the important technical specification for the energy analysis is given in table 7-4.

The hub height of this wind turbine is 25 m. The wind data is based on a height of 10 m only. As mentioned before the wind speed data, captured between January 2001 and February 2002, has been extrapolated to 25 m height. The energy potential per second (the power) varies in proportion to the cube of the wind speed, and in proportion to the density of the air.

Rotor:		**Performance:**	
Diameter	19.1 m	Nominal power rating	100 kW
Swept area	284 m^2	Rated wind speed	13 m/s
Power regulation	Variable Speed Stall	Cut-in wind speed	4 m/s
Tower:		Cut-out wind speed	25m/s
Type	Tubular	Survival wind speed	70 m/s
Height	25 m		

Table 7-4: Technical specifications of the North Wind NW100/19 wind turbine

Therefore, if the power of each wind speed is multiplied with the probability of each wind speed from the Weibull graph, then the distribution of wind energy at different wind speeds = the power density has been calculated.

$$P_D := \sum_{i=1}^{n} P_i \cdot f(v_i) \qquad \textbf{(7-30)}$$

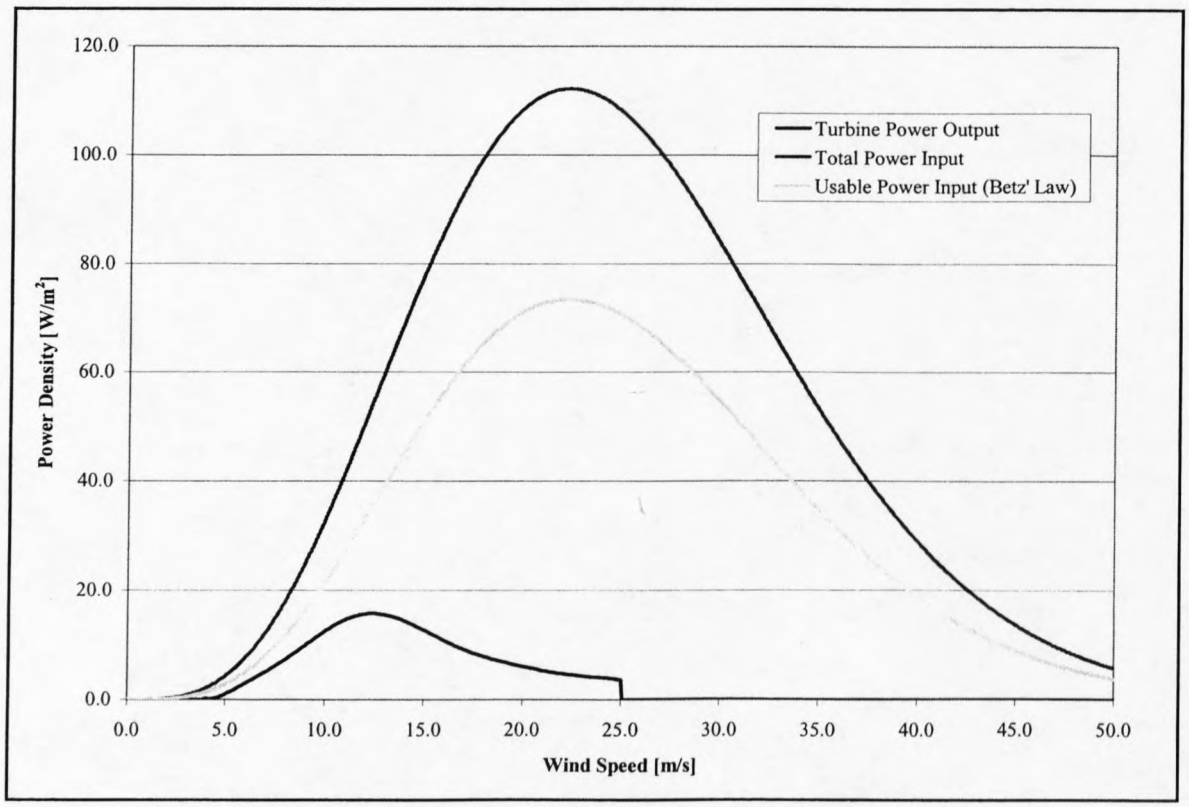

Figure 7-8: Power density curve for North Wind NW100/19 wind turbine

The area under the red curve, in figure 7-8, (all the way to the axis at the bottom) gives the amount of wind power per square meter wind flow expected at this particular site. This curve has been calculated as follows:

In this case there is a mean wind speed of 11.81 m/s and a Weibull k = 1.57 and c = 13.15 m/s, so we get 2601.07 W/m^2, as calculated in equation (7-15). This is more than twice as much power as the wind has when it is blowing constantly at the average wind speed, as can be seen from the following calculation.

$$P_D := \frac{1}{2} \cdot 1.24 \cdot (11.81)^3 := 1021.27 \frac{W}{m^2} \quad \textbf{(7-31)}$$

The graph consists of a number of narrow vertical columns, one for each 0.1 m/s wind speed interval. The height of each column is the power (number of W/m^2), which that particular wind speed contributes to the total amount of power available per square meter. The area under the yellow curve indicates how much of the wind power can be theoretically converted to mechanical power, According to Betz' law, this is 16/27 of the total power in the wind. The total area under the blue curve indicates how much electrical power the NW100/19 wind turbine will produce at this site. The blue curve was calculated by multiplying the power produced at a certain wind speed with the probability of that wind speed distribution, using equation (7-30).

The most important thing to notice is that the bulk of wind energy will be found at wind speeds above the mean (average) wind speed at the site. Usually, wind turbines are designed to start running at wind speeds somewhere around 3 to 5 m/s. This is called the cut-in wind speed. The area under the blue curve in figure 7-9 shows the small amount of power lost due to the fact the turbine only cuts in after, in his case, 5 m/s.

The wind turbine will be programmed to stop at high wind speeds above, in this case 25 m/s, in order to avoid damaging the turbine or its surroundings. The stop wind speed is called the cut-out wind speed. This is only a small part as can be seen to the right of the blue power curve shown in figure 7-8.

In Antarctic conditions, the wind speed is usually very high and wind speeds of more than 35 m/s occur quite frequently. Thus the wind turbine has to be designed in such a way as to have a relatively high cut-out speed and that the turbine is appropriately secured after that.

7.3.7 Power coefficient

The power coefficient indicates how efficiently a turbine converts the energy in the wind to electricity. Very simply, the electrical power output is divided by the wind energy input to measure how technically efficient a wind turbine is. In other words, if the power curve is taken, and it is divided by the area of the rotor, the power output per square meter of rotor area is obtained. For each wind speed, the result is divided by the amount of power in the wind per square meter.

For example, using again the North Wind NW100/19, at a wind speed of 10 m/s. The theoretical power in the wind is

$$P_{wind} := \frac{1}{2}\cdot\rho\cdot v^3 := \frac{1}{2}\cdot 1.24\cdot(10)^3 := 620\ \frac{W}{m^2} \qquad \textbf{(7-32)}$$

From equation (7-29), the power of the turbine at a wind speed of 10 m/s is $P_t = 66.9$ kW. Dividing this by the area and converting to Watts, the power density is obtained, which is $P_{turbine} = 235.65\ W/m^2$. To calculate the power coefficient, the following formula will be employed:

$$c_P := \frac{P_{turbine}}{P_{wind}} := \frac{235.65}{620} := 0.38 \qquad \textbf{(7-33)}$$

By repeating this calculation for all wind speeds under consideration, the curve in figure 7-9 is obtained.

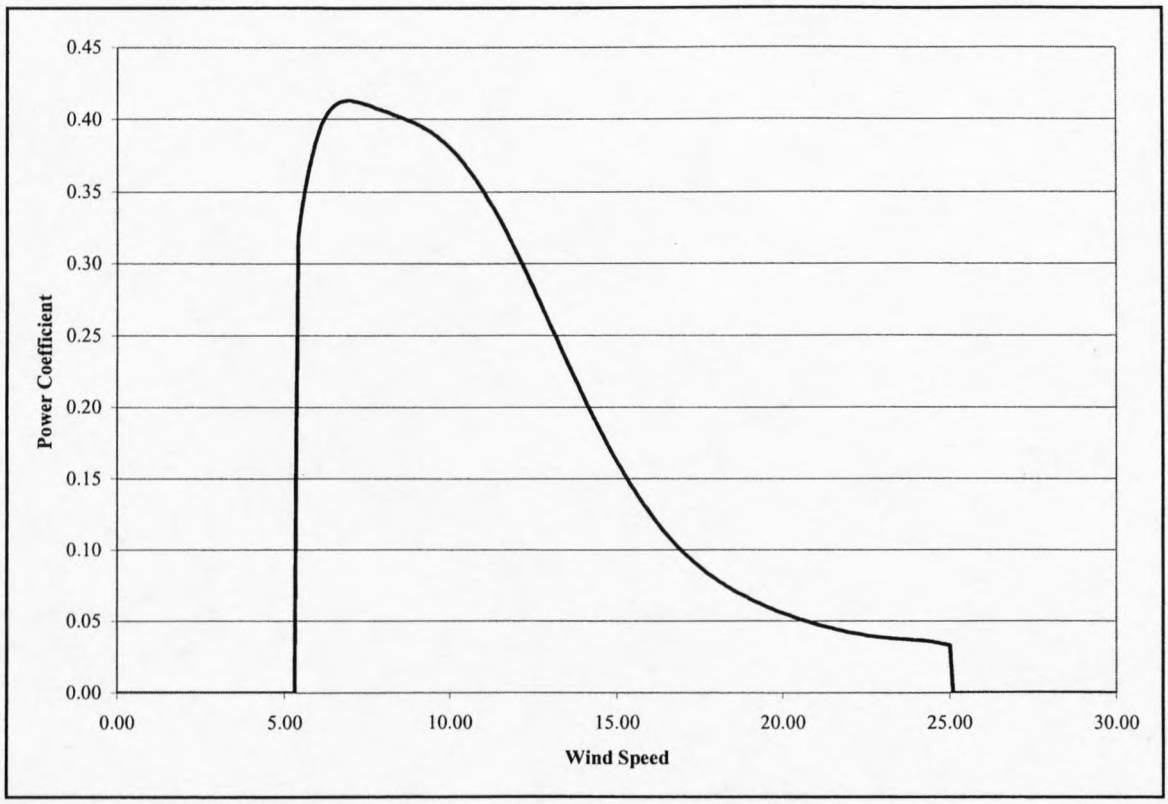

Figure 7-9: Power coefficient curve for North Wind NW100/19 wind turbine

Figure 7-9 shows a power coefficient curve for a typical North Wind NW100/19 wind turbine. Although the average efficiency for these turbines is somewhat above 20 %, the efficiency varies very much with the wind speed. If there are small kinks in the curve, they are usually due to measurement errors. From figure 7-9 it can be seen that the mechanical efficiency of the turbine is largest (in this case 41 %) at a wind speed of about 7 m/s. This is a deliberate choice by the engineers who designed the turbine. At low wind speeds efficiency is not so important, because there is not much energy to harvest. At high wind speeds the turbine must waste any excess energy above what the generator was designed for. Efficiency therefore matters most in the region of wind speeds where most of the energy is to be found.

7.3.8 Annual energy output from a wind turbine

Taking the previous sections into account, it is now possible to calculate the relationship between average wind speeds and annual energy output from a wind turbine.

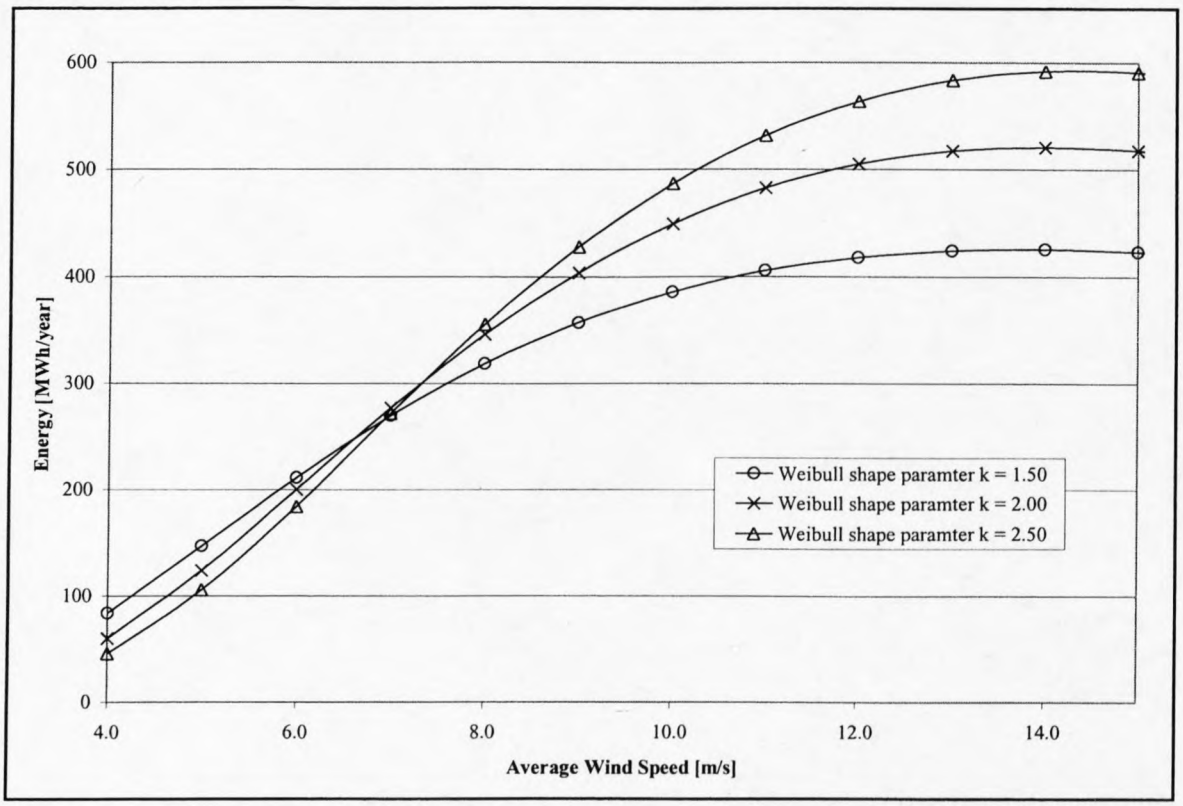

Figure 7-10: Annual energy versus wind speed, using different Weibull shape parameters k

To draw figure 7-10, the power curve from the North Wind NW100/19 wind turbine has to be used. A standard atmosphere with an air density of 1.24 kg/m^3 is used. For each of the Weibull parameters k = 1.5, 2.0, and 2.5 the annual energy output for different average wind speeds at turbine hub height are calculated. From figure 7-10, it can be seen that the output may vary up to 45 % depending on the shape parameter at a low average wind speed of 4.0 m/s, while it may vary some 26 % at a very high average wind speed of 14 m/s at hub height. These values are calculated as follows. The difference between k = 1.5 and k = 2.5 at low wind speeds, say 4.0 m/s is

$$D_1 := \frac{P_{1.5} - P_{2.5}}{P_{1.5}} \cdot 100\ \% := \frac{83.77 - 45.68}{83.77} := 45\ \% \qquad \textbf{(7-34)}$$

From figure 7-10 it can be seen that at low average wind speeds the mentioned wind turbine can capture more energy, when there is a small k. At higher average wind speeds, a bigger k is favorable, regarding the annual energy output of a wind turbine. At an average

wind speed of 12 m/s, there is a difference in annual power output between a k = 1.5 and k = 2.5, of

$$D_2 := \frac{P_{2.5} - P_{1.5}}{P_{2.5}} \cdot 100\ \% := \frac{545.0 - 402.5}{545.0} := 26\ \% \qquad (7\text{-}35)$$

The curve with k = 2, is the curve, which is normally shown by manufacturers: With an average wind speed of 4.5 m/s at hub height the machine will generate about 60 000 kWh per year. With an average wind speed of 9 m/s it will generate 400 000 kWh per year. Thus, doubling the average wind speed has increased energy output 6.6 times. If the 5 and 10 m/s are compared instead, almost exactly 4 times as much energy output is obtained. The reason why not exactly the same results are obtained in the two cases, is that the efficiency of the wind turbine varies with the wind speeds, as described by the power curve.

With the weather data from SANAE IV, the Weibull shape parameter is k = 1.57 as mentioned previously. A smaller k corresponds to a more variable wind, while a bigger k, in the region of 2.5, corresponds to a more even wind speed distribution.

	Average Wind Speed	k	c [m/s]	Power Output	Power Output	Turbine Power Output	Yearly / Monthly Turbine Power Output
	[m/s]		[m/s]	[W/m²]	[kW]	[MWh/m²/year]	[MWh/Year]
Complete Year:	11.81	1.57	13.15	175.30	49.79	1514.59	430.14
Month:	[m/s]		[m/s]	[W/m²]	[kW]	[MWh/m²/month]	[MWh/Month]
Jan-01	7.28	1.90	8.21	120.77	34.30	86.96	24.70
Feb-01	9.50	2.02	10.72	174.97	49.69	125.98	35.78
Mar-01	12.73	1.93	14.35	205.33	58.32	147.84	41.99
Apr-01	10.87	2.15	12.27	201.91	57.34	145.38	41.29
May-01	9.88	1.93	11.14	178.70	50.75	128.67	36.54
Jun-01	17.65	1.97	19.91	197.07	55.97	141.89	40.30
Jul-01	14.20	1.81	15.98	198.66	56.42	143.03	40.62
Aug-01	13.48	1.83	15.17	200.42	56.92	144.30	40.98
Sep-01	11.89	1.70	13.32	185.56	52.70	133.61	37.94
Oct-01	15.18	1.58	16.91	179.37	50.94	129.15	36.68
Nov-01	13.05	1.56	14.52	177.71	50.47	127.95	36.34
Dec-01	10.28	1.30	11.13	144.10	40.92	103.75	29.47
Jan-02	8.57	1.41	9.41	134.96	38.33	97.17	27.60
Feb-02	10.23	1.45	11.29	156.24	44.37	112.50	31.95

Table 7-5: Annual and monthly wind turbine energy output

With a k = 1.57, the wind speeds distribution is relatively variable and gusty. The results for the monthly and annual energy output from the North Wind NW100/19 wind turbine can be seen in table 7-5.

7.3.9 Wind turbine operating percentages

To analyze the effect of the wind turbine's height on the wind power generation, the NW100/19 wind turbine power output was calculated using different turbine heights for the analysis. The rated electrical power of the turbine is 100kW (at a rated wind speed of 13 m/s), and there are three options for the tower height: 25 m, 30 m and 35 m. For these heights, with additional heights of 9 m, 13 m, 18 m and 27 m chosen for comparison, the wind power density and probability are calculated, and the results are given in table 7-6 and figure 7-11.

Hub height [m]	**Average wind speed** [m/s]	**Shape parameter** k	**Scale parameter** c [m/s]	**Average power density** [W/m^2]
9	10.85	1.60	11.80	1821.11
13	11.02	1.59	12.28	2073.78
18	11.41	1.58	12.71	2323.63
25	11.81	1.57	13.15	2601.07
30	12.02	1.57	13.38	2739.95
35	12.20	1.57	13.58	2864.67

Table 7-6: Power density for different hub heights

The values of average wind speed and average power density increase with height. Obviously, to obtain more wind power, the higher the hub height of the wind turbine should be.

For different hub heights, the average wind speed and power density are different. In assessing the wind power potential, or choosing the suitable type of wind turbine, not only

the wind data but also the site circumstances (terrain, different referred height, surface roughness) should be considered.

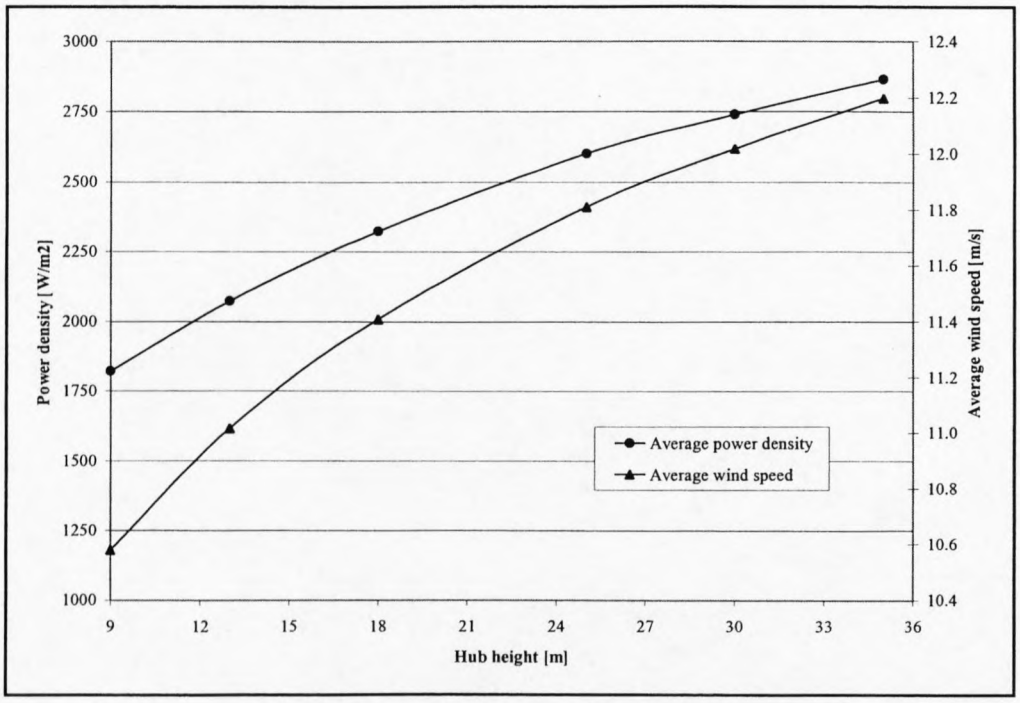

Figure 7-11: Annual power density versus average wind speed for different hub heights

Operating hours of wind turbine

For the North Wind NW100/19 wind turbine the cut-in speed is 4.0 m/s and the cut-out wind speed is 25 m/s. For the three tower heights and other heights for comparison, the operating hours of the wind turbine in a year can be calculated and are shown in figure 7-12. The percentage of the operating hours can be obtained as follows. From table 7-6 the values of c and k can be obtained for the different hub heights under consideration. Using a hub height of 25 m for the sample calculation, the operating percentage (OP) of the wind turbine is

$$OP := \left(F\left(v \geq v_{ci}\right) - F\left(v \geq v_{co}\right)\right) \cdot 100\ \%$$

$$:= \left[1 - \exp\left[-\left(\frac{v_{ci}}{c}\right)^{k}\right] - 1 + \exp\left[-\left(\frac{v_{co}}{c}\right)^{k}\right]\right] \cdot 100\ \% \qquad \textbf{(7-36)}$$

$$:= \left[\exp\left[-\left(\frac{25.0}{13.15}\right)^{1.57}\right] - \exp\left[-\left(\frac{4.0}{13.15}\right)^{k}\right]\right] \cdot 100\ \% := 79.25\ \%$$

From the operating percentage, the operating time per year can be simply calculated by multiplying the operating fraction with the amount of hours in a year, which is 8760 h. Thus the operating time for the given example at 25 m hub height is OT = 0.7925 8760 h = 6942 h.

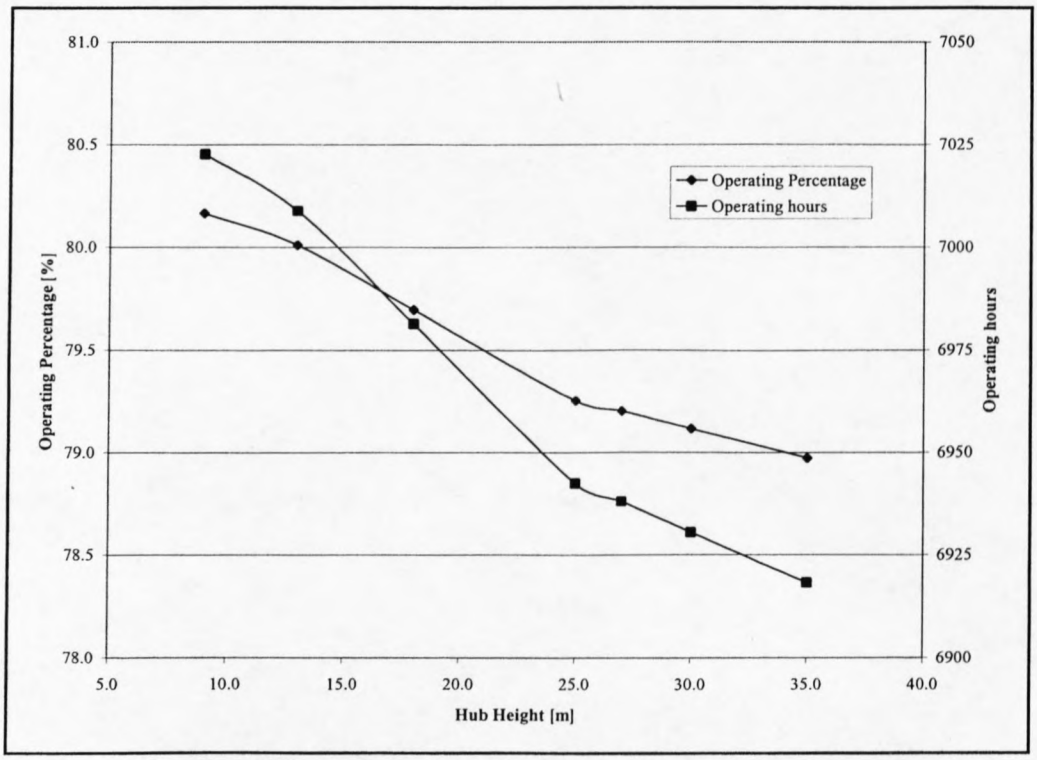

Figure 7-12: Operating percentage versus wind turbine hub height

Figure 7-12 shows that, for different tower heights, the operating hours of the wind turbine are also different. For an 18-m-high tower, the total operating hours are 6981 h (79.70%) in a year, but 6918 h (78.97%) for a 37 m high tower, a difference of 63 hours. Normally,

the higher the tower is, the bigger is the operating time. The reason why this is not the case for our example is, that the cut-out wind speed is 25 m/s and at higher tower heights, the wind speeds more often exceed the cut-off speed, the wind turbine has to be shut down and thus the operating time is decreased.

Figure 7-13 shows that the operating percentage changes for different months during the year. The highest of 90.36 % occurs in April, while the lowest is 70.89 % in December. The trend is not in accordance with the monthly wind power density, because the operating percentage is not only determined by the wind data distribution, but also by the performance of the wind turbine and specifically the cut-in and cut-out speeds of the wind turbine.

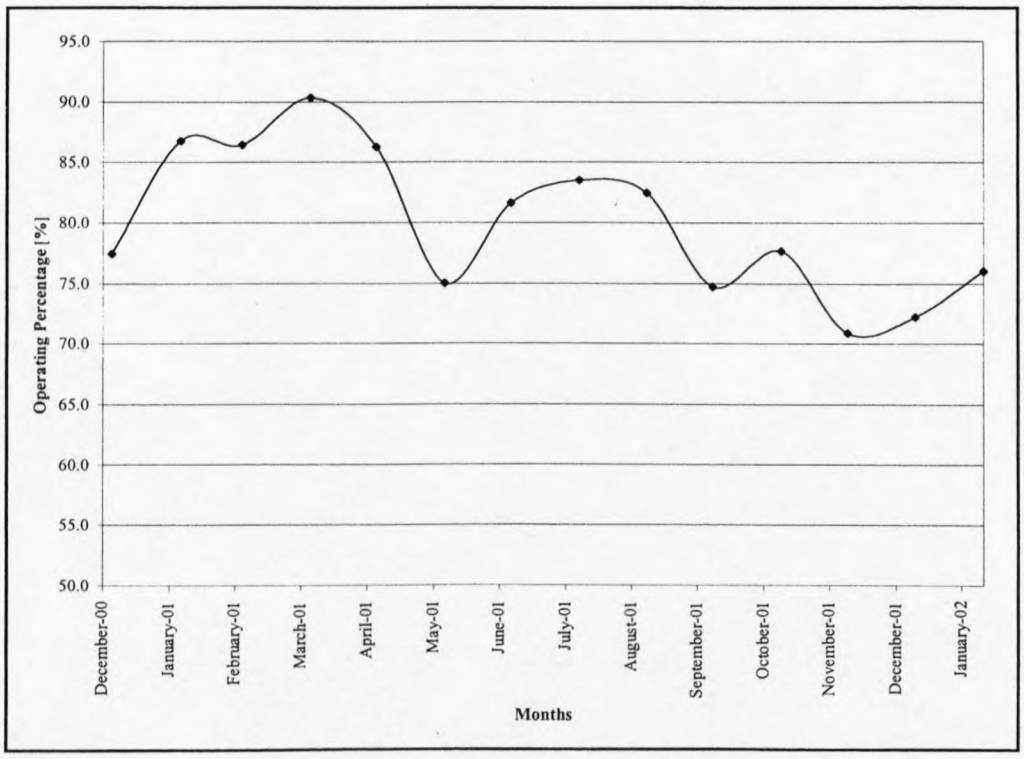

Figure 7-13: Monthly operating percentage of the NW100/19 wind turbine (25 m high tower)

Power output of wind turbine

Using the Weibull function and the polynomial regression function, from equation (7-29), the average annual power generated by the wind turbine can be estimated. The wind

turbine can generate electrical energy amounting to 430.14 MWh per year, at 25 m hub height. For different hub heights, the yearly power generated is calculated and the results are given in figure 7-14. For a hub height of 35 m, the power output of 435 MWh is 1.14 times greater than for a hub height of 18 m. The power difference between the two hub heights is relatively small since, again, the cut-out speed limits the wind turbine of producing more energy due to higher wind speeds at higher hub heights.

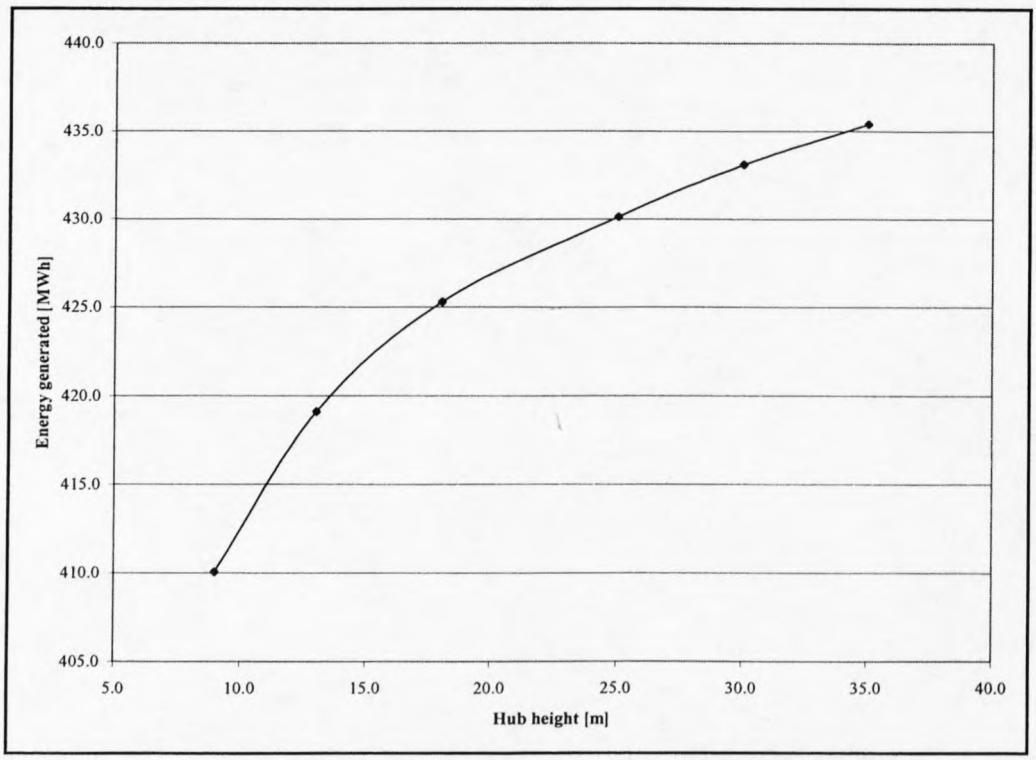

Figure 7-14: Annual energy output of the wind turbine for different hub heights

Similarly, taking the 25 m high tower as an example, the monthly power output is calculated and is shown in figure 7-15. For ease of comparison 30 days are chosen for each month. The result shows that the power generated per month is different and varies from 24.70 MWh to 41.99 MWh. The highest power output is generated in March, which is 1.7 times the lowest, which is in January. From the graph, it can be seen that the months of highest power production are from February to November and the lowest are from December to January. The peaks in March and April are due to the higher wind speeds than in January, but are not high enough to make the cut-out wind speeds a critical factor.

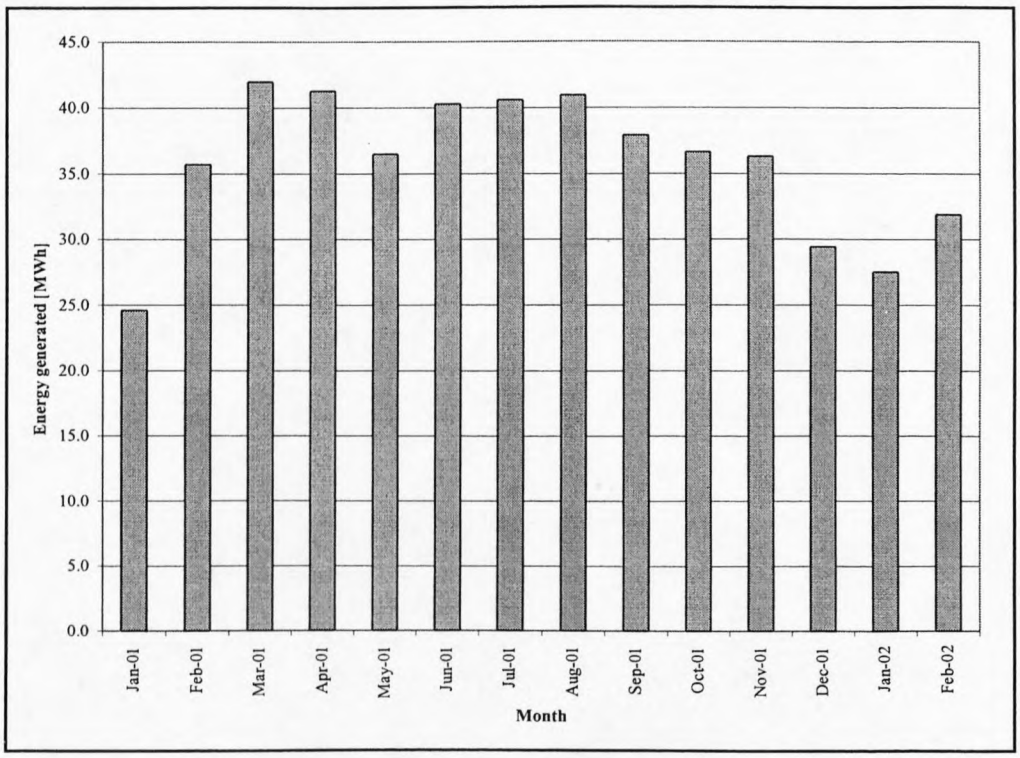

Figure 7-15: Monthly energy output distribution (25 m high tower)

7.3.10 The capacity factor

Another way of stating the annual energy output from a wind turbine is to look at the capacity factor for the turbine in its particular location. Capacity is the actual annual energy output divided by the theoretical maximum output, if the machine was running at its rated (maximum) power during all of the 8760 h of the year. Example: If a 100 kW turbine produces 270 MWh in a year, its capacity factor is = 270000 : (365· 24· 100) = 270000 / 876000 = 0.308 = 30.8%.

Capacity factors may theoretically vary from 0% to 100%, but in practice they will usually range from 20% to 70%, and mostly be around 25-30%. In this case the North Wind NW100/19 100 kW turbine produces 430.14 MWh in a year, therefore its capacity factor is 430140 / (365 24 100) = 0.491 = 49.1%. Thus we have achieved a relatively high capacity factor of nearly 50%. The capacity factors for each month can be seen in table 7-7.

	Average Wind Speed	k	c	Yearly / Monthly Turbine Power Output	Capacity Factor
	[m/s]		[m/s]	[MWh/Year]	
Complete Year:	11.81	1.57	13.15	430.14	0.49
Month:	[m/s]		[m/s]	[MWh/Month]	
Jan-01	7.28	1.90	8.21	24.70	0.33
Feb-01	9.50	2.02	10.72	35.78	0.48
Mar-01	12.73	1.93	14.35	41.99	0.56
Apr-01	10.87	2.15	12.27	41.29	0.55
May-01	9.88	1.93	11.14	36.54	0.49
Jun-01	17.65	1.97	19.91	40.30	0.54
Jul-01	14.20	1.81	15.98	40.62	0.55
Aug-01	13.48	1.83	15.17	40.98	0.55
Sep-01	11.89	1.70	13.32	37.94	0.51
Oct-01	15.18	1.58	16.91	36.68	0.49
Nov-01	13.05	1.56	14.52	36.34	0.49
Dec-01	10.28	1.30	11.13	29.47	0.40
Jan-02	8.57	1.41	9.41	27.60	0.37
Feb-02	10.23	1.45	11.29	31.95	0.43

Table 7-7: Annual and monthly capacity factors.

Although one would generally prefer to have a large capacity factor, it may not always be an economic advantage. In a very windy location, for instance, it may be an advantage to use a larger generator with the same rotor diameter (or a smaller rotor diameter for a given generator size). This would tend to lower the capacity factor (using less of the capacity of a relatively larger generator), but it may mean a substantially larger annual production. Whether it is worthwhile to go for a lower capacity factor with a relatively larger generator, depends both on wind conditions, and on the price of the different turbine models.

Another way of looking at the capacity factor paradox is to say that to a certain extent there may be a choice between a relatively stable power output (close to the design limit of the generator) with a high capacity factor - or a high-energy output (which will fluctuate) with a low capacity factor. Thus by having a relatively high capacity factor for the NW100/19 wind turbine indicates, that there will be a fairly stable power output, and the turbine is run very close to its design limits, as indicated by the average wind speeds in the range of 12 m/s and the rated wind speed of the wind turbine of 13 m/s.

7.3.11 Wind turbine selection, based on wind analysis and power output

In order to make a proper wind turbine selection, all 5 different wind turbines chosen were analyzed. However, looking only at the technical specifications of the different wind turbines, it can be seen that the North Wind NW100/19 wind turbine features the best specifications. The first one is that it has a rated wind speed of 13 m/s, which is fairly close to the average wind speed at SANAE IV.
at hub height 25 m

The cut-off wind speed is 25 m/s, which all the other wind turbines, except for the Bergey Excel, also feature. The rated power output of the NW100/19 is 100 kW and the only other wind turbine with the same power output is the Fuhrländer FL100 wind turbine. The disadvantage of the Fuhrländer FL100 is that it only features one hub height, which is 35 m. The NW100/19 feature three hub heights, which are 25 m, 30 m and 35 m. Referring to the results obtained in section 7.3.9, it is obvious that a hub height is required that will allow the turbine to run inside its limits for most of the time. Thus by choosing a wind turbine with a lower hub height, increases the operating percentage considerably, while decreasing the annual power output only slightly. Selecting a group of smaller wind turbines, having lower hub heights, is another option.

The annual operating percentage of 80 % for the NW100/19 wind turbine, as calculated in section 7.3.9, is more than wind turbines are generally designed for. It is very difficult to determine at this stage what the implications of this result will be on the design life of the wind turbine. It will be assumed that either the design life of the wind turbine will be reduced, or the wind turbine would need several refurbishments during its design life time. As a result the design life has to be considered when a wind turbine is selected. The NW100/19 is designed for 30 years thus making it an excellent candidate for operation at SANAE IV. A shorter design life could have the effect that the wind turbine will not survive the pay back period. Due to the high number of turbine stoppages at high wind speeds a pitch controlled blade arrangement should result in far less wear and tear than stall controlled wind turbines, which need to be stopped with disc brakes. This has to be considered when selecting a turbine.

8 *WIND TURBINE SITE SURVEY AND SELECTION*

The cold weather issues do not apply to the site selection analysis, as there obviously is, to some degree, the same snow flow, icing and temperatures around the base. The 16 positions of the hand-held anemometer measurements are taken for the site selection process, since care has been taken that they are potential wind turbine sites. In order to do a proper site selection, certain criterion have to be considered. The most important criterion is the wind speed analysis, since the energy output from a wind turbine is dependent on the average wind speed at the site in question. This will be handled in section 8.1, whereas the contours of the area around the base are analyzed in section 8.2. In order to ensure proper transport, installation and maintenance of the wind turbine, section 8.3 is dedicated to the accessibility and the operation area of the 16 sites. Another important factor is the anchoring of the wind turbine and will be handled in section 8.4.

8.1 Site Selection Based on Wind Analysis

In section 6.3 the details regarding the wind analysis of all the 16 positions are given. In order to distinguish between well-suited wind turbines sites and sites with lower average wind speeds only sites with an average wind speed of more than 9.5 m/s will be further evaluated. The reason for using 9.5 m/s as the cut-off value is that exactly 50 % of the sites still have to be evaluated and this therefore seems a reasonable decision. These positions are shown in table 8-1.

Position	Average Wind Speed [m/s]
2	9.6
7	9.5
9	9.6
10	9.6
12	9.8
13	11.4
14	10.8
16	12.0

Table 8-1: Positions with average wind speeds more than 9.5m/s

The table on the previous page shows the average wind speeds of the mentioned positions extrapolated to 10 m height. If a wind turbine, like the North Wind NW100/19 is installed at one of the sites, the average wind speeds has to be determined at a height of 25 m, which is the hub height of the wind turbine. Therefore, the wind speeds at each position will increase considerably, when being measured at 25 m height.

8.2 Contour Maps

As mentioned in chapter 5, GPS measurements were taken, so that a contour map could be created of the area around the base. With the help of German scientists, who also performed their research during the field trip period at SANAE IV, the GPS coordinates were transformed to 3-dimensional Cartesian coordinates. A total of 284 GPS measurements were taken. The relative positions and paths that were taken during measurements can be seen in figure 8-1.

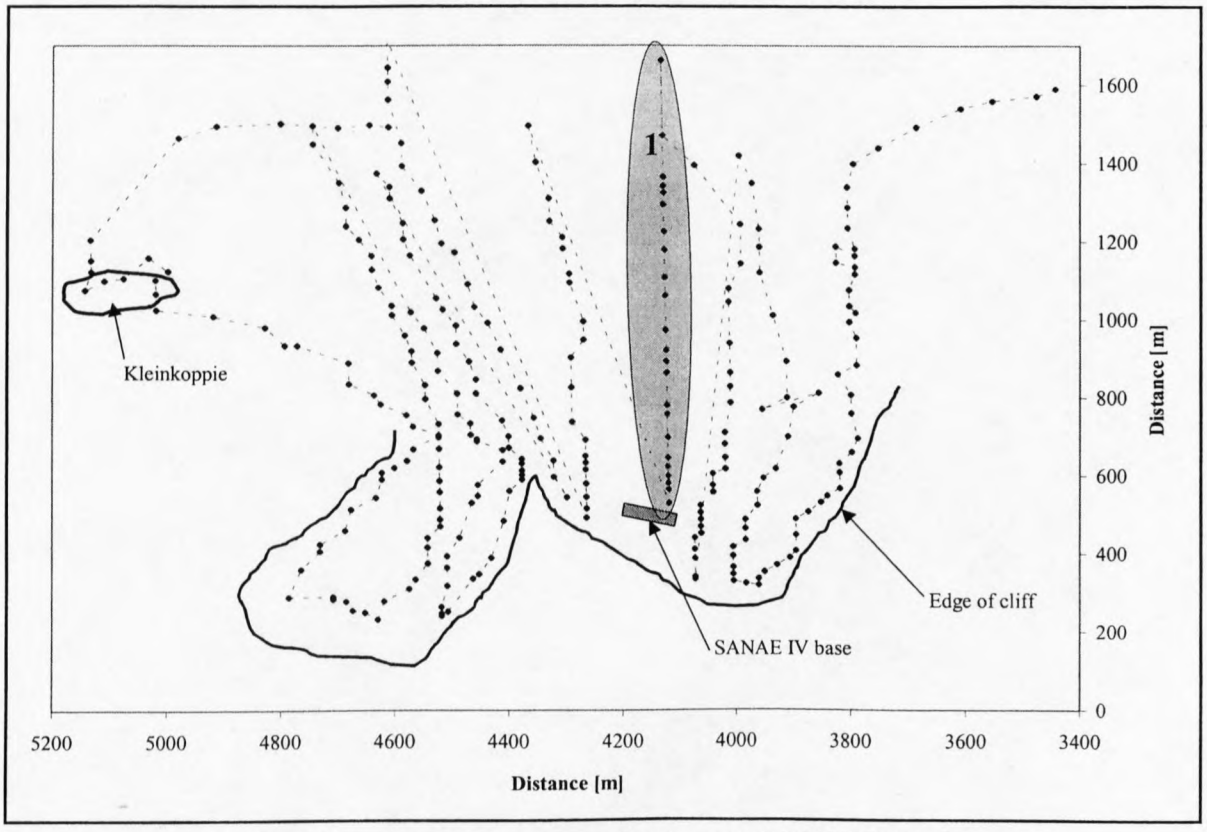

Figure 8-1: GPS measurements of area around SANAE IV base

It is important to note that the indication of the edge of the cliff, the mountain 'Kleinkoppie' and the base are only approximate and not to scale. The advantage of having figure 8-1 is that it shows the amount of measurements taken and the direction of lines that were walked during measurements. They all go from east to west thus going in the main wind direction. This has the advantage that the elevation can be plotted from east towards west.

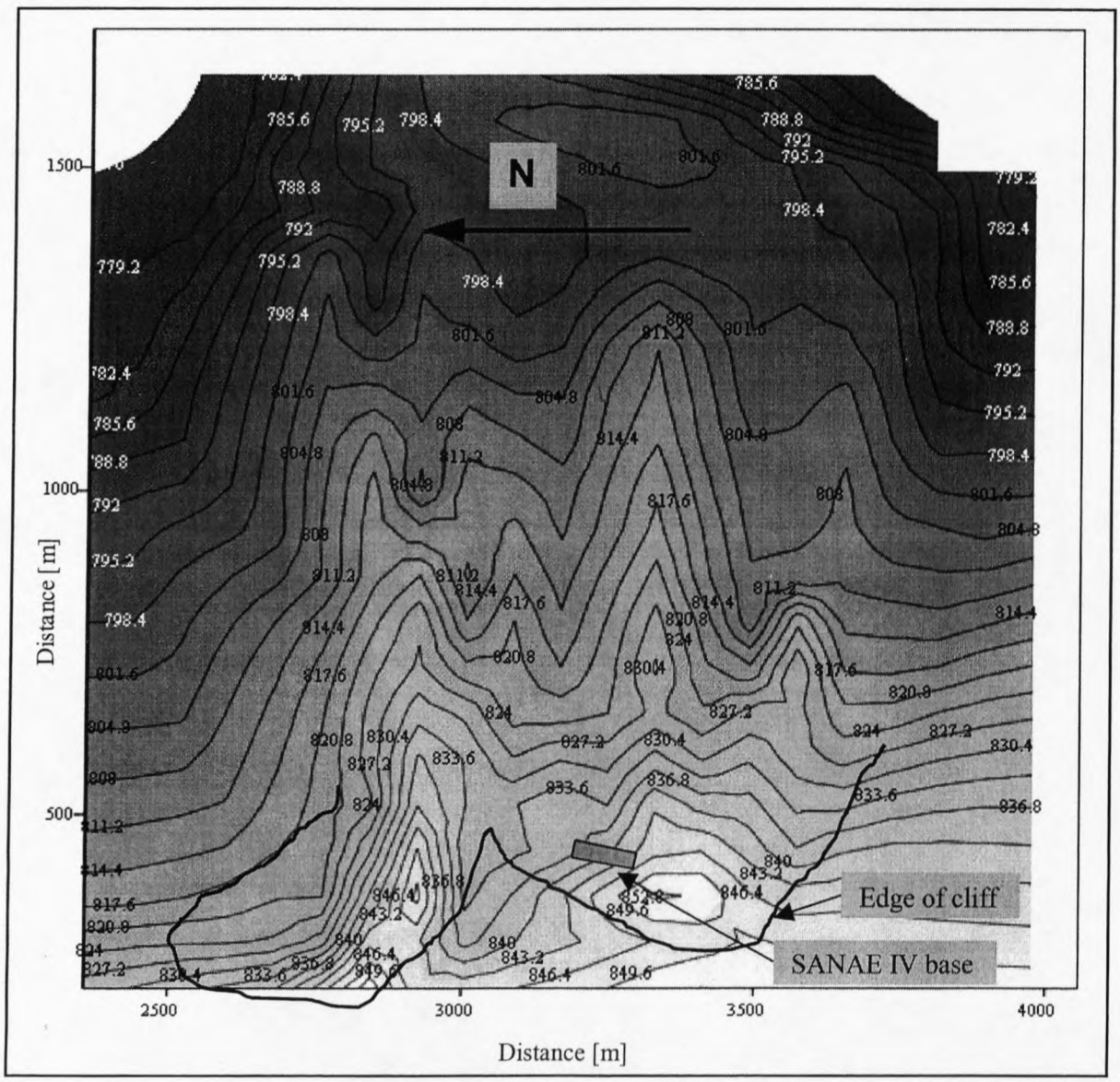

Figure 8-2: Contour plot of area around base

The contour plot is done using the same area around the base. The plot can be seen in figure 8-2. The contour plot has been created with the program MathCAD Version 8. MathCAD linearly interpolates the values of the x, y and z coordinates to form level curves in such a way that no two curves cross. Using a grayscale to indicate the difference in elevation visualizes the gradual rise in elevation from east towards west, until the sudden drop at the edge of the cliff. The drop at the edge of the cliff was not incorporated into the contour map, since it was too dangerous to take measurements at the bottom of the cliff. Another way of visualizing the elevation from east to west, until the base has been reached, is given in figure 8-3. The height difference from the starting point to the base is about 40 m, covering a distance of almost 800 m, along the line, marked 1, in the shaded area.

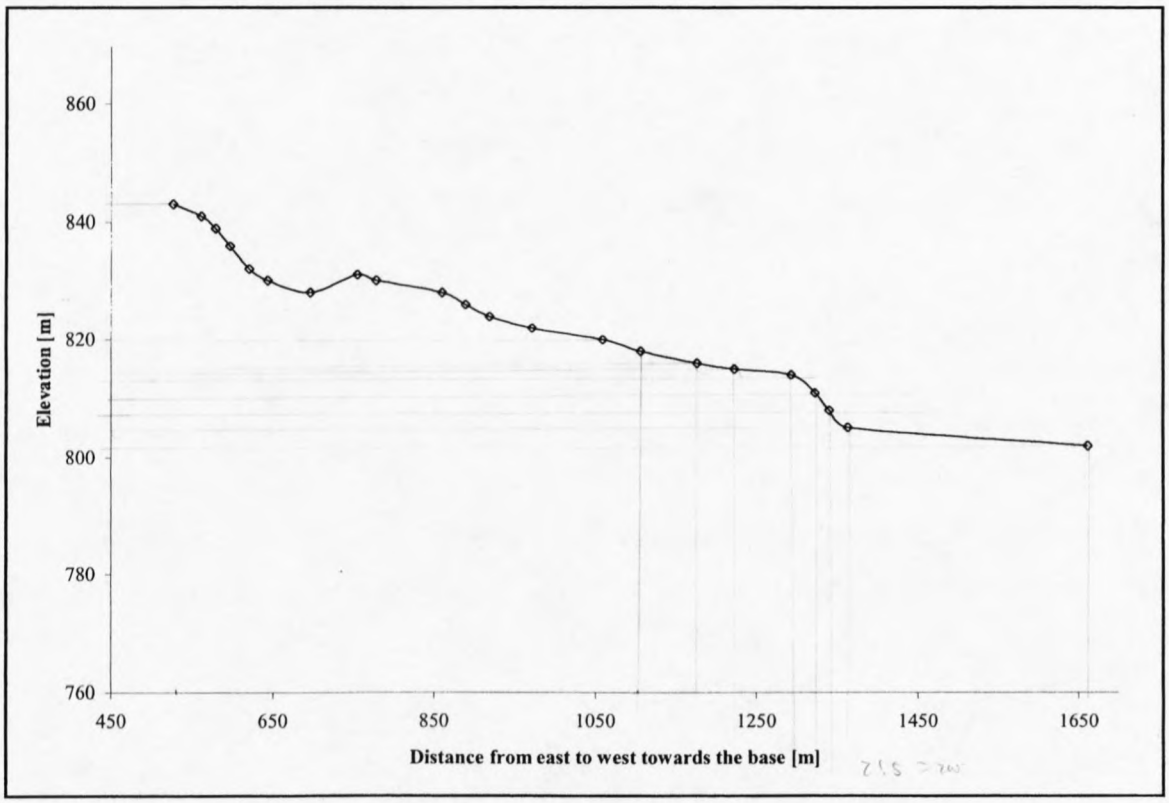

Figure 8-3: Elevation from east to west towards the base

Figure 8-2 does not properly present the elevation of the mountain called 'Kleinkoppie'. The reason for that is that not enough measurements have been taken to accurately create contour lines for Kleinkoppie. The elevation of Kleinkoppie can be seen from the

photographs in appendix I. For better wind speed distributions at the wind turbine sites, higher elevations are preferable. However, looking at the average wind speeds measured at each position, it can be seen that the higher elevations are not always adequate.

The elevations thus do not present an important constraint to the site selection analysis. The contour map merely serves as an orientation tool that helps visualizing the area surrounding the base.

8.3 Accessibility and Operation Area of Sites

Due to the fact that positions 13 and 14 are situated on restricted area, which is the northern buttress, they cannot be used as a wind turbine site. Access has to be provided to the site and due to the fact that the northern buttress is covered with rocks and boulders, positions 13 and 14 have to be eliminated from the list of potential wind turbine sites. The surface of the northern buttress can be seen from the photographs showing positions 13 and 14 in appendix I.

Position 16, which is situated on Kleinkoppie, has also been eliminated from the list because the summit of the mountain is very small, thus making it difficult to install and maintain the wind turbine. However, the final decision can only be made, once it has been decided, which wind turbine will be installed at SANAE IV. This will only happen once this thesis has been accepted and the planning phase for a wind turbine installation commences. However, this is out of the scope of this project.

Position 2 is also a site with lots of space, situated just south of the base, but this area is also covered with rocks, making accessibility of the site difficult. The best position, based on elevations, accessibility and space are positions 7, 9, 10 and 12. Positions 9 and 10 are potentially the best suited positions, since they are also close to the base. In section 8.4 only positions 7, 9, 10 and 12 will be further evaluated, since the other positions do not meet the requirements mentioned above.

8.4 Anchoring of Wind Turbine

A very important aspect of installing and operating a wind turbine at SANAE IV is the anchoring of the turbine, so that it can survive the storms that are frequently experienced at the base. The following criteria have to be met by the remaining sites:

- The tower must not be erected within 1 1/2 times the tower height of electric power lines, radio mast or any structures that can impose installation and operation problems. Most overhead power lines are not insulated, so they pose a life-threatening shock hazard.
- The anchoring system must be able to withstand, without appreciable creep, the steady and vibratory loads of the tower through all weather conditions for the life of the installation. Site conditions will dictate the type of anchoring system used. Soil type, water level, freeze depth, and weather variations all have an effect on the holding capacity of the anchors.
- The appropriate anchoring technique has to be employed, considering the wind turbine specifications and the soil type. The soil classifications are provided in table 8-2.

All of the above mentioned sites are situated on rocky nunataks. The rock found at the base is mostly granite, but some of the rock is severely weathered. From the soil classifications it is obvious that the soil type class for the potential wind turbine sites, is class 2. During the implementation stages, the designers will have to consider the soil type, when designing the foundations of the wind turbine, in this case soil class 2. The type and size of the foundations would have a large bearing on the project cost.

It has to be said again that a final position of the wind turbine can only be made during the implementation stages of installing a wind turbine at SANAE IV, which are beyond the scope of this project. The observations made above should only be used as recommendations.

Class	Common Soil Type Description	Geological Soil Classification
0	Sound hard rock, unweathered	Granite, Basalt, Massive Limestone
1	Very dense and/or cemented sands; coarse gravel and cobbles	Caliche, (Nitrate bearing gravel/rock)
2	Dense, fine sand; very hard silts and clays	Basal till; boulder clay; caliche; weathered laminated rock
3	Dense clays, sands and gravel; hard silts and clays	Glacial till; weathered shales, schist, gneiss and sandstone
4	Medium dense sandy gravel; very stiff to hard silts and clays	Glacial till; hardpan; marls
5	Medium dense course sand and sandy gravel; stiff to very stiff silts and clays	Saprolites; residual silts
6	Loose to medium dense, fine to coarse sand; firm to stiff silts and clays	Dense hydraulic fill; compacted fill; residual soils
7	Loose fine sand; Alluvium; Loess; soft to firm clays; varied clays; fill	Flood plain soils; lake clays; adobe; gumbo; fill
8	Peat; organic silts; inundated silts; fly ash	Miscellaneous fill; swamp marsh

Table 8-2: Soil classification (Wilke, 2001)

Designed specifically for high reliability and low maintenance, the North Wind NW100/19 wind turbine features industry proven robust components with innovative design features to maximize wind energy capture in severe and remote locations, like Antarctica. The turbine features a minimum of moving parts and vulnerable subsystems to deliver high system availability. The uncomplicated rotor design allows safe, efficient turbine operation (NPS2, 2002).

The innovative tilt-up tower erection system allows the NW100/19 to be installed without a crane, which is often costly and site prohibitive. At SANAE IV, using a crane would be an almost impossible task because of all the snow and ice prohibiting its movement. Therefore the accessibility of the site does not pose such a big problem with a wind turbine that does not require a crane and working space at the site can be reduced.

9 COLD WEATHER ISSUES

There are three general issues important to the operation of wind turbines in cold weather that can be classified as follows:

- The impact of low temperatures on the physical properties of materials
- The ice accretion on structures and surfaces
- The presence of snow in the vicinity of a wind turbine

Cold weather operation of wind turbines require that these issues be examined in the design or at least in the phase preceding the installation of the turbines in their working environment. Not doing so would mean prolonged periods of inactivity required for safety purposes or turbine inability to perform satisfactorily (Lacroix and Manwell, 2000).

9.1 Low Temperatures

Low temperatures affect the different materials used in the fabrication of wind turbines usually adversely. Structural elements such as steel and composite materials have their mechanical properties changed by low temperatures. Steel becomes more brittle; its energy absorbing capacity and deformation prior to failure are both reduced. Composite materials, due to unequal shrinkage of their fiber/matrix components, will be subjected to a residual stress. If this stress is sufficient, it can result in micro cracking in the material. These micro cracks reduce both the stiffness and the impermeability of the material, which can contribute to the deterioration process.

Low temperatures can also damage the electrical equipment such as generators, yaw drive motors and transformers. When power is applied to these machines after they have been standing in the cold for a long period, the windings can suffer from a thermal shock and become damaged.

Gearboxes, hydraulic couplers and dampers suffer from long exposure to cold weather. As the temperature goes down, the viscosity of the lubricants and hydraulic fluids increases up to a point where at -4°C, heavy gear oil could be described as being almost solid. Damage to gears will occur in the very first seconds of operation where oil is very thick and cannot freely circulate. In addition, due to an increase in internal friction, the power transmission capacity of the gearbox is reduced when the oil viscosity has not reached an acceptable level.

Seals, cushions and other rubber parts loose flexibility at low temperatures and oil seals will leak. This may not necessarily result in part failure but can cause a general decline in performance. A typical rubber part can see its stiffness augmented by a factor of 8 at a temperature of –4°C. Brittleness also increases, which changes impact resistance and makes the part prone to cracking.

9.2 Icing

Icing represents the most important threat to the integrity of wind turbines in cold weather. Based on the duration of inoperative wind measuring equipment at one surveyed mountain in western Massachusetts, it was determined that icing weather can occur as much as 15 % of the time between the months of December and March, in the northern hemisphere. Wind turbines must therefore be able to sustain at least limited icing without incurring damage, preventing normal operation. Furthermore, it is advisable that power production be maintained in moderate icing for the following reasons:

- To minimize downtime period and benefit from the more favorable winter winds
- To keep the rotor turning and therefore limit the ice growth on the leading edge part of the blade that is likely to be fitted with some ice protection equipment

The icing likely to form on wind turbine blades is of two kinds: glaze and rime. Glaze ice is the result of liquid precipitation striking surfaces at temperatures below the freezing point.

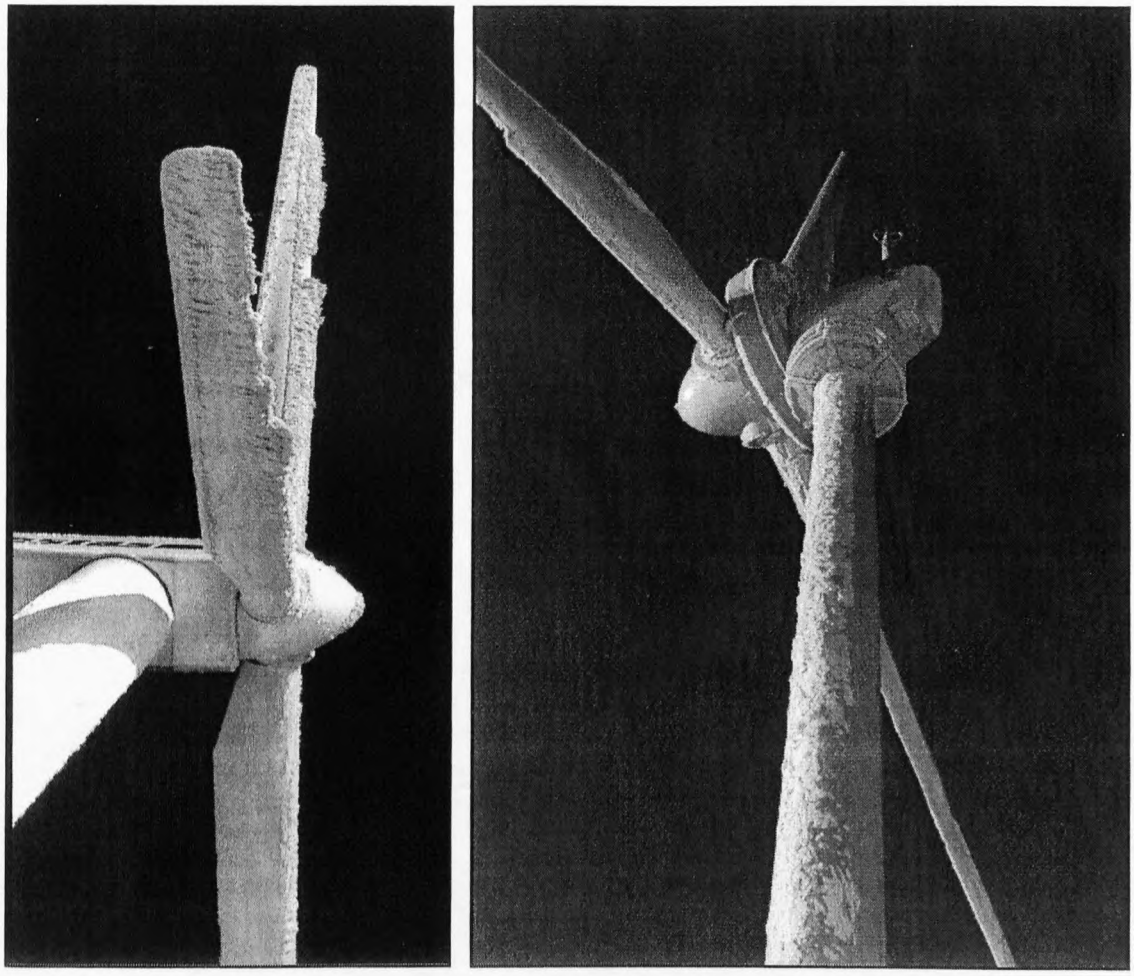

Figure 9-1: Severe icing on a medium sized wind turbine (Arnold, 2001)

Glaze is rather transparent, hard and attaches well to surfaces. It is the type of icing encountered during ice storms. New England and especially Massachusetts is an area of high occurrence for glaze storms. A study covering a period of fifty years of glaze precipitation in the United States conducted by Tattelman and Gringorten supports this claim, as repeated by Arnold (2001). They have established the probability of an ice storm causing glaze ice of thickness greater or equal than 0.63 cm for the Pennsylvania, New York and New England regions during one year to be 0.88 cm, i.e. almost once per year.

Rime ice occurs when surfaces below the freezing point are exposed to clouds or fog composed of super cooled water droplets. Its white and opaque appearance is caused by the presence of air bubbles trapped inside. Rime ice is of primary importance in high elevation locations such as hills or mountaintops.

Ice collects on both the rotating and non-rotating surfaces. The most adverse effect of icing occurs on the rotor itself. Its consequences on the rotor are the following:

- Interferes with the deployment of speed limiting devices such as tip flaps or movable blade tip
- Increases the static load on the rotor
- Changes the dynamic balance of the rotor, thereby accelerating fatigue
- Reduces the energy capture by altering the aerodynamic profile of the rotor

Ice fragments can be propelled and represent a safety hazard for population and property in the vicinity of wind turbines. Larger chunks can also strike the rotor and damage it. Ice also accumulates on fixed structures such as nacelles, towers and ladder, making periodic maintenance more difficult by preventing easy access to turbine components. It can interfere with the normal functioning of pitch control and orientation mechanisms. Finally, the presence of ice on structural elements increases both the static loading and the wind loading due to an augmentation in surface area.

9.3 Snow

Due to its very low specific gravity, snow is easily carried by wind. It can infiltrate almost any unprotected openings where airflow can find its way. Wind turbine nacelles, i.e. the housings that contain the gearbox and the generator, are not necessarily airtight compartments. In fact, they incorporate many openings in order to provide a supply of fresh air for cooling purposes. Hence, snow can accumulate inside the nacelle and damage

the equipment. This could prove to be very detrimental for the electrical machinery. On the other hand, snow could also obstruct these openings and prevent normal circulation of air. It is suggested to use deflectors or baffles in order to keep these openings free of obstruction. Another method to decrease the accumulation of snow inside the wind turbine is to provide a positive pressure inside the nacelle and tower. This method however requires the use of additional equipment that has to be operated and thus decreases the availability of the wind turbine. In order to keep additional equipment inside the turbine at a minimum, an airflow could be established inside the nacelle so that the snow is either blown through the nacelle or accumulated snow in the nacelle is blown out. Also better seals around the openings could reduce the accumulation of snow inside the nacelle and turbine tower.

9.4 Wind Turbine Assessment

From section 7.3.11 it has become evident that the North Wind NW100/19 is the best-suited wind turbine, based on the wind and power analysis. This wind turbine is the only wind turbine that has been designed taking Antarctic conditions into account. Thereby the NW100/19 wind turbine is the only turbine that meets the requirements regarding cold weather issues. Thus, only the North Wind NW100/19 will be analyzed in this section.

The main consideration of the above mentioned is the low temperatures experienced at SANAE IV. Since the precipitation at SANAE IV is close to zero, very little snowfall has been experienced in the past. The only form of snow that occurs at SANAE IV is snow carried by strong winds and storms. Snow flow starts at a wind speed of about 8 m/s. However, at a wind speed of 8 m/s, the snow barely moves over the surface. At higher wind speeds, the snow flow starts elevating. Thus at very high wind speeds, the wind turbine is subjected to snow flow.

As mentioned in section 9.3, this snow can accumulate inside the nacelle through ventilation openings in the nacelle. To reduce this effect, deflectors have to be fitted to these openings. Apart from snow accumulating inside the nacelle, no other harm can be

done by snow flow. The recommendations made in section 9.3 have to be presented to the wind turbine manufacturers so that the penetration of snow inside the wind turbine can be prohibited and the design life of the turbine can be realized.

Icing also has to be taken into account when operating a wind turbine at SANAE IV. Since the nacelle can be reached from inside the tower, it is important that the door leading inside the tower can be opened at any time. The possibility of installing some heating device for the locking mechanism and hinges of the door eliminates the possibility of a frozen up door. The biggest concern, however, is the icing of the turbine blades. It is not mentioned in the system description of the North Wind NW100/19 that the rotor blades are heated. Blade heating should be recommended to Northern Power Systems, as this will keep the blades at optimum performance levels. Information obtained from the 2001 year team shows that icing is not a problem for the existing radio and radar towers, which are in close proximity of the base. It can thus be concluded that icing should not pose problems with the operation of a wind turbine at SANAE IV.

Referring back to the low temperature issues, the North Wind NW100/19 wind turbine has some design features to eliminate problems associated with low temperatures. The turbine features a minimum of moving parts and vulnerable subsystems, in order to deliver high system availability. A direct drive system eliminates the gearbox that is a big problem with low temperatures. A dual fail-safe disk brake and electro-dynamic braking system eliminates blade brakes. Another feature is the advanced FRP-resin infusion molding process that ensures a high-quality blade that will endure extreme temperatures.

The NW100/19 wind turbine has an allowance of ice accretion of up to 30mm. Thus the turbine is well suited for Antarctic use. According to the manufacturers, Northern Power Systems, it is stated that the NW100/19 is well suited for Antarctic use, and that predecessors of the NW100/19, on which the design of the NW100/19 is based, have been tested at the South Pole and Antarctic coasts (NPS3, 2002). These turbines have been running in temperatures of –80 °C and from that point of view, the North Wind NW100/19 is ideally suited for operation at SANAE IV.

10 CONNECTION TO SANAE IV ELECTRICITY GRID

The potential for large fuel savings using renewable energy systems is in part dependent on the match between consumption periods and renewable energy production periods. High renewable energy reserves are only useful if the power that can be extracted from them is usable. By sizing the renewable energy plant correctly, the match between production and consumption can be optimized, maximizing returns for a given investment. To enable optimal sizing, the available energy from the wind turbine has to be used by the base. Since the case may develop, that the wind turbine will supply more power than is needed at SANAE IV, a dump location has to be found, as described in chapter 4. A suitable dump location is the snow smelter.

10.1 Wind Turbine Electrical Specifications

The most common generator utilized in the wind industry is a gear driven asynchronous (induction) generator. Induction generators must be connected to a stable voltage source for excitation and reactive power (VAR) support. While large power grids can easily provide this support, power quality and system stability is compromised in distributed generation and village systems where the power grid is typically "soft and unbalanced."

NPS has solved this issue with the NW100/19. The synchronous, variable speed, direct drive generator and integrated power converter increases energy capture, while eliminating current in-rush during control transitions. This turbine can be connected to large power grids and remote wind-diesel configurations without inducing surges, effectively providing grid support rather than compromising it.

The direct drive generator is a salient pole synchronous machine designed specifically for high reliability applications. Electrical output of the generator is converted to high quality AC power that can be synchronized to conventional or weak isolated grids. The advanced power conversion system also eliminates the inrush currents and poor power factor of conventional wind turbines. The output complies with IEEE 519-1992 power quality specifications. The variable speed direct drive generator / converter system is tuned to

operate the rotor at the peak performance coefficient, and also allows stall point rotor control to contend with wide variation in air density found in the target applications. Table 10-1 provides some of the electrical specification of the NW100/19 wind turbine. In appendix K, the complete wind turbine specifications are given.

General Configuration:	
Rotation axis	Horizontal
Orientation	Upwind
Yaw control	Active
Drive train	Direct Drive
Power Regulation	Variable speed stall
Drive Train:	
Configuration	Variable speed direct drive
Tilt angle	4°
Generator type	Salient pole synchronous
Insulation class	NEMA H
Generating speed	45 – 69 RPM
Generator rating	100 kW w/ 1.15 service factor
Generator Output	575 VAC
Speed control	IGBT control
Grid Connection:	
Grid voltage	480 VAC standard / 380 – 30 kV available
Grid frequency	50 / 60 Hz

Table 10-1: Electrical specifications of NW100/19 wind turbine

The safety system consists of a spring applied, pressure released disk brake mounted on the generator shaft for emergency conditions, and an electrodynamic brake system that provides both normal shutdown and emergency braking backup functions. The above-mentioned information has been obtained from NPS2 (2002).

10.2 Availability

Wind generation has a fluctuating power output, due to the variability of the wind speed. The fluctuations in the available wind energy caused by gusts result in power output fluctuations from the wind turbine. Such power fluctuations may affect the power quality of the network. A reduction of short-term power fluctuations can be achieved using variable-speed operated wind turbines, as they are able to absorb short-term power variations by the immediate storage of energy in the rotating masses of the drive train, hence, a smoother power output is achieved than with strongly grid-coupled turbines.

It is even found that wind turbines with directly grid-connected induction generators in a wind farm could fall into synchronism with their rotor azimuth position. This synchronism can cause high amplitudes in voltage fluctuations. Both situations can be avoided by coordinating the operation of the different wind turbines in a wind farm and by varying the electrical parameters of the wind farm grid.

The medium-term variations (hours) are also very important for network operation, as network operators have to dispatch other generation sources, if the wind energy power output varies strongly.

Long-term variations in wind speed, between 1 year and the next, are usually quite low.

10.3 Energy Storage

Wind turbines, when used with diesel electric generators, significantly reduce the cost of fuel consumption and greenhouse gas emissions, but the part load efficiency of the diesel generator is low and this can be a source of pollution. Fuel cells are electrochemical power generators with high overall efficiency and part load efficiency. Additionally, they operate quietly with minimal polluting emissions. The excess heat from a fuel cell can also be used for space heating or for domestic hot water. If fuel cells are used in conjunction with a wind turbine, environmental pollution can be reduced to almost zero (Tariq, 2002).

Fuel cells are not the only form of power storage that exists on the market today. Batteries are also used in hybrid systems (Bowen et al., 2001), but they are not an option for SANAE IV, since the energy to mass ratio is low compared to other storage devices, like hydrogen fuel cells and zinc-air fuel cells (Isherwood et al., 1999). Also, lead acid batteries are generally not designed to be transported and operated at temperatures that occur at SANAE IV. However, specially designed lead acid batteries are very expensive and newer technologies like hydrogen fuel cells are being tested at this stage and are becoming an attractive option.

The use of storage facilities to capture the maximum amount of wind energy is a very costly exercise, since rooms have to be made available for the storage of space consuming batteries or fuel cells. In addition, fuel cells have to be maintained, leading to additional man-hours and maintenance plans. It is therefore advised to install the North Wind NW100/19 wind turbine first, have it operating for a couple of years and then investigate the feasibility of adding power storage facilities.

At this stage, the implementation plan would be to connect the wind turbine directly in parallel with the generators and have the wind turbine supplying power whenever a second generator is needed. This will eliminate the effect of a part-loaded generator, therefore eliminating excess fuel consumption.

10.4 Power Quality

Wind turbines as well as all other equipment connected to a grid affect the quality of the power in the grid. These effects include voltage fluctuations due to power fluctuations and flicker effects, voltage asymmetry and harmonics. To study the impact of wind turbines on the power network, detailed computer models of wind turbines are used.

The evaluation of the impact of wind turbines on the power quality is a complex problem, due to the unique design of each distribution network as well as the different types of wind turbines, e.g. variable speed or fixed speed, stall or pitch-regulated. Fixed-speed wind

turbines, for example, produce a power pulsation emanating from the wind share over height, and the tower shadow effect. Such a power pulsation will cause voltage fluctuations on the grid, which in turn may cause flicker. Variable-speed as well as limited variable-speed turbines, e.g. with induction generators with variable slip, significantly reduce the power fluctuations due to wind share and tower shadow effect.

The start-up of wind turbines is also an important issue. The grid connection during the start-up of stall-regulated fixed-speed wind turbines can cause high inrush currents, as the rotor torque cannot be exactly controlled to meet the required generator torque. Pitch-regulated fixed-speed as well as variable-speed wind turbines are able to achieve a smoother grid connection during start-up [Ackermann and Söder, 2000].

The problems associated with the power quality of the grid have been solved by Northern Power Systems, by using a salient pole synchronous generator. There are no electricity surges and power fluctuations, due to a sophisticated control system, which will be mentioned in section 10.6.

10.5 System Overview

The primary components of a wind-diesel hybrid power system include (Stover, 2002):

- Diesel generators
- One or more wind turbines
- A synchronous condenser or rotary converter and battery bank
- Secondary loads
- Engine and wind system controllers

The wind-diesel systems are defined as being either low penetration or high penetration based on the amount of installed wind capacity as compared to the average load from the community. Modern wind turbines are available in a variety of sizes between 5 kW and 600 kW for a wind-diesel system.

10.5.1 Introduction

The incorporation of a renewable energy generation component into the diesel generation systems results in a hybrid system. Small-scale hybrid systems, involving wind electricity generation plants in conjunction with diesel generators, have been established in many places around the world (Brown, 1997).

There are many ways to connect the wind turbine to the electrical grid. In the simplest arrangement, power from the wind turbine is used to displace diesel fuel that would have been used by diesel generators sets. In these systems the diesel generators are kept operational at all times, with periods of low wind adequately covered. When high winds are present, the wind turbine is synchronized onto the grid in parallel with the diesel generator. Use of an induction generator directly connected to the AC power network as indicated in figure 10-1 allows for a very simple arrangement.

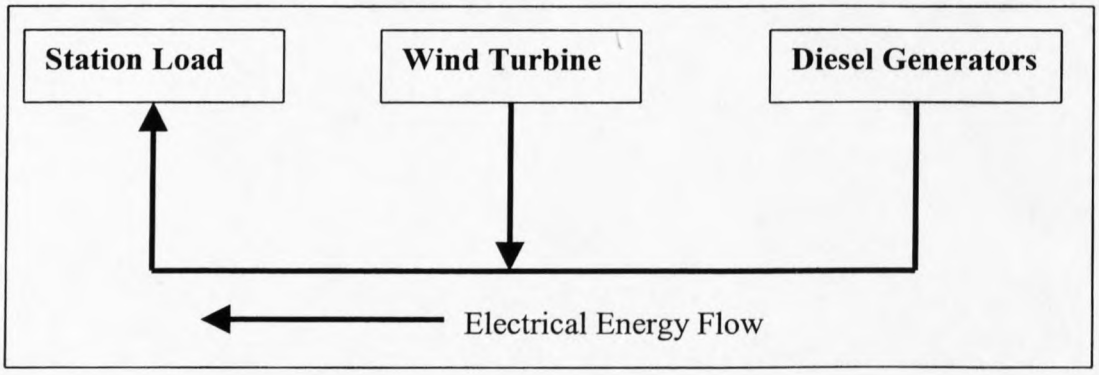

Figure 10-1: Hybrid energy system: wind / diesel

In hybrid systems the penetration level is defined as the fraction of the load generated by the renewable plant. Fuel savings in hybrid systems are a function of the renewable resources and the penetration level.

The use of variable speed DC wind turbines together with DC to AC inverters as indicated in figure 10-2 is one method to increase the renewable penetration level. Provision for a load dump, allowing power to be diverted from the system, may be required if oversupply is an issue.

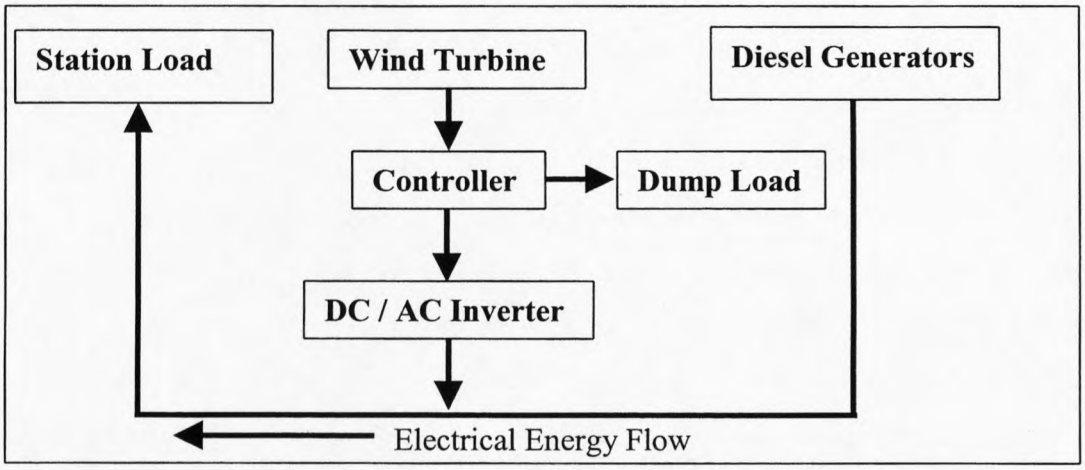

Figure 10-2: Hybrid energy system: wind / diesel with dump load

10.5.2 Low penetration hybrid systems

In a conventional diesel power system the generator power level follows the load demand. If more than one generator is on line, the load is shared in proportion to the rated power of each generator. The engine speed governor controls fuel to the engine to regulate it to its rated speed, and consequently the desired generator frequency. A balance of mechanical and electrical power occurs at the generator; as load demand and generator electrical load increases, the shaft mechanical torque increases, which tends to reduce shaft speed and generator frequency. The governor responds by increasing fuel to the engine to maintain speed and frequency, increasing mechanical power at the generator shaft to follow the demand of the electrical load. The engine, governor, actuator, and fuel distributor represent a stable closed loop control system to regulate frequency. Field experience has proven the stability of this control loop.

When a small amount of wind power is added to a system, the engine governors adjust to the reduced load; tolerating the small contribution provided by the fluctuating wind power. This mode of operation is acceptable until the installed turbine capacity exceeds 15 % to 30 % of the load demand. This operating scenario is defined as a low-penetration hybrid system (Stover, 2002).

10.5.3 High-penetration hybrid systems

When the installed wind capacity exceeds between 15 % - 30 % of the load demand, the uncontrolled wind power begins to play havoc with the engine governors and dispatch control. As installed wind capacity is increased, peak wind power could potentially exceed the load demand on occasion, causing the engines to be back-driven and the system to become unstable. This occurs because induction generator wind turbines contribute power according to the wind passing the rotors, irrespective of load demand. In addition, the variability of the wind often creates large power fluctuations over short time periods. Consequently, a wind-diesel system must increase or reduce diesel-generated power quickly to accommodate the wind power and keep frequency constant. Since the diesel cannot absorb excess wind turbine power, frequency control requires the addition of an active load element, herein defined as a secondary load. The additional wind power influence, the active load element and a closed-loop control circuit, complicate the system and provide opportunity for control loop interactions and unstable operation.

In a remote island power system, stability is power quality as defined by the constancy of voltage and frequency of the electric power produced. High penetration wind-diesel systems are inherently unstable and require active control to make them work at constant frequency. The challenge is the large uncontrolled power source presented by the induction wind turbine. To meet this challenge a synchronous condenser or rotary converter must be included in the hybrid configuration to provide reactive power (VAR) support for the induction (asynchronous) wind turbine generators.

A rotary converter combines the function of a synchronous condenser and a power converter, allowing power to be transferred to and from a DC battery bank. The main advantage of incorporating a rotary converter in a hybrid system is that the margin required, to operate in a wind-only mode, is reduced. Without access to the battery storage provided by a rotary converter, the variability of wind and the consequent variability of power supplied by the wind turbine(s) will prevent the diesel generators from shutting down, often even during periods of high wind (Stover, 2002).

10.5.4 Secondary and optional loads

As discussed above, high-penetration hybrid systems require some form of load element to accommodate the excess energy in the system during periods when wind generated electricity exceeds the load. The secondary load or "dump" load must always be on-line in the system to absorb any energy that is in excess of the system load at any time. For example, the dump load may heat water that can be used for space heating. Another way to accommodate excess energy in the system is with the addition of optional load air conditioners. Optional load heaters are different from the secondary or "dump" load in that they are located within the local grid, are thermostatically controlled, and consequently can be overridden when heating is not needed. Optional load heaters are only available for use when there is excess energy available in the system.

An optional load heater placed in a school or other public building can serve to reduce fuel costs during winter months during periods when wind energy exceeds the local load. If the wind power exceeded the load during such a period, the secondary water heater would be called upon to make up the difference between the load demand and the wind power output. Secondary load heaters in general must be placed near the power plant. The economics of wind-diesel hybrid power systems are often very favorable when a value is placed on this secondary load heat (Stover, 2002).

10.6 Modes of Operation

Most wind-diesel hybrid power systems have the ability to operate in three distinct modes:

- Diesel-only mode
- Wind-diesel mode
- Wind-only mode

10.6.1 Diesel-only mode

In the diesel-only mode of operation, the power system will function as a typical diesel generator providing the electrical load with the diesel generator controls providing the

frequency and voltage regulation. The optional load unit heaters are recommended in order to maintain minimum operating levels (25 % of rated diesel power). At most locations appropriate for incorporating wind, operation in the diesel-only mode is infrequent.

10.6.2 Wind-diesel mode

In the wind-diesel mode, the wind turbine and the diesel operate in parallel. The electrical power from the wind turbine and the diesel generator are combined to provide power to the grid. Voltage and frequency regulation are provided by the diesel generator controls assisted by the system secondary load controller. In this mode it is anticipated that there will be an abundance of heat energy provided to the optional heat load and secondary load. The amount of optional and/or secondary load will be equivalent to the instantaneous energy produced minus the electrical demand by the base. Essentially the secondary load provides the energy balance to maintain system frequency stability without unloading (or negatively loading) the diesel engine.

10.6.3 Wind-only mode

When there is sufficient wind energy for the wind turbine to carry the entire electrical load and provide an adequate margin to account for the variation in the wind speed and anticipated variations in base load, the diesel engine can be shut down. When the diesel is shut off, the synchronous condenser (or rotary converter) provides reactive power to the grid to maintain voltage stability. The secondary load controller communicates with the secondary heaters so that the system frequency does not deviate.

The amount of time that a system can operate in each mode will fluctuate and is based on:

- The average wind speed
- The wind speed variation, measured as turbulence intensity and causing the turbine's power output to vary
- The average electrical load and the variation of that load

- The allowable margin, defined as the amount of wind energy in excess of the load power required. An average - positive margin is required in a system to insure frequency stability. The average wind power must exceed the utility demand (during Wind Turbine Only mode) or the spinning components will slow down and the frequency of the system will drop.

One of the obvious goals of a wind-diesel hybrid system is to minimize the run-time of the diesel generators. This can occur when a sufficiently steady wind can allow the wind turbines to carry the primary loads. However, the reality of a wind-diesel hybrid power system is that often times exist when there is sufficient wind to carry a system load, but the variability in the wind is such that the diesels are not allowed to completely turn off. During the design phase of a wind-diesel project, Northern Power System conducted modeling activities whereby a minimum diesel run-time is specified to avoid scenarios where diesels are required to turn on and off in short time intervals. As a result, it is typical to conduct modeling scenarios where a system is sized so that wind provides over 90 % of the energy demand, yet the variability in the wind keeps the diesel facility operating over 90 % of the time as well. The uncontrolled nature of wind power simply does not allow for wind-only mode except during the rare wind events.

As a rule of thumb, the installed wind capacity needs to be over twice the average load if significant wind-only periods are desired. The incorporation of a rotary converter and battery bank will compensate for this variability and result in significant wind-only time (Stover, 2002).

10.7 Control Strategies

Northern Power Systems developed a Universal Wind Diesel Controller for stand-alone wind-diesel "village power" applications. This unit provides supervisory control of diesel generators and wind turbines to provide seamless utility-grade power in remote locations. Its modular, pre-integrated design allows it to adapt to a variety of applications without expensive custom engineering. The Universal Wind Diesel Controller combines a proven,

robust microprocessor control module with Northern's own refined control software. The result of its reliable control and monitoring functions is stable, high quality, utility grade power (NPS1, 2002).

10.7.1 Controller features

- Proven, mature technology from the generator control industry. The hardware modules are interchangeable and readily available.
- Easy integration of a variety of system elements including synchronous condensers, rotary converters, electrical storage components, and critical/non-critical load controls. Custom hardware design costs are eliminated.
- Automatic generator-only operation in the event of a failure. The loss of the control system will not result in a loss of power.
- Flexible system architecture able to accommodate the range of existing diesel generator and wind turbine control packages.

10.7.2 Operation

- The Universal Wind Diesel Controller will switch a wind / diesel hybrid system between four states of operation.
- In times of no wind, the system will operate "diesel only," bringing generators on and off line for maximum fuel efficiencies.
- When there is enough wind to produce power, the controller will reduce the output of the diesel generators to match the load.
- If the wind increases just to the point where the wind turbine can match the load by itself, the controller will set one diesel generator to a minimum level and dump excess wind power to a secondary heat load. The addition of battery storage would allow the generator to be shut down in this state.
- When the wind power is ample enough to allow a margin of safety, the controller will switch off the last diesel generator and use the heat load to absorb the excess power production.

The heat load is variable, and acts along with the synchronous condenser or rotary converter to maintain power stability. The controller ensures seamless transitions between operating states and the most efficient use of both diesel fuel and the wind resource (Stover, 2002).

Control and operation of these systems is not straightforward. A number of complex and expensive problems exist, potentially compromising any financial savings brought about through reduced fuel use. Issues of concern include (Brown, 1997):

1. Frequent diesel cycling: The fluctuating nature of power output from wind turbines, combined with variable consumer load, can result in unacceptable high levels of diesel start / stop cycles with corresponding short running periods. This can lead to regular cold starting of diesel plant, overuse of starting battery, and increased wear and tear on the generator sets, thereby reducing the life of the generator sets.
2. Diesel underloading: In systems where diesels are used to meet any load deficits, unfavorable load conditions can result in prolonged periods of low loading. Operation of diesel plant at less than 30-50% of their rated power is not recommended as it gives rise to increased wear and maintenance and leads to lower efficiencies.
3. Low utilization of renewable energy system: In poorly designed systems, where production periods do not correspond with demand periods, large quantities of renewable energy will be dumped.
4. Poor quality of supply: Short-term variations in output from renewable power plant (particular wind turbines) can result in large voltage and frequency excursions.

If a limit is imposed on the amount of renewable power production, these problems can be minimized. Low penetration systems avoid diesel under loading and allow adequate power regulation to be maintained by the governor systems of the remaining diesel plant online.
A heating dump load could be used to maintain a 40 % penetration level limit, an approach that should be considered for Antarctic stations. Another approach that can be run

independently from the control system of SANAE IV base, is to use the snow smelter as a dump load.

10.7.3 Components

The wind diesel controller consists of a range of digital based control modules especially designed for power control applications (NPS1, 2002). These are:

- Universal wind diesel controller
- Wind Power Controller
- Secondary Load Controller (SLC)
- Energy Storage Controller (ESC)
- Engine/Generator Modules
- Synchronous Condenser Controller (SCC)
- Communications Processing Module (CPM)
- Networked I/O

The details for each of the components mentioned above can be seen in appendix K.

11 ECONOMIC FACTORS

11.1 Introduction

The economics of renewable energy is the largest barrier to renewable energy penetration. Nevertheless, the strong desire to reduce environmental emissions, especially in Antarctica, is considered a great support for renewable energy sources.

Wind energy is already competitive with coal or nuclear power across most of Europe, especially when the cost of pollution is taken into account. Also, the cost of wind energy is falling, whilst other energy technologies are becoming more expensive (Ackermann and Söder, 2002).

Most remote Antarctic stations pay economic penalties for electricity because they must import diesel as their primary fuel for electric power production, paying heavy transportation costs and potentially causing environmental damage. Furthermore, the consumption of fossil fuels and the local negative impact caused by spilled oil, leaking tanks and discarded drums must be considered when examining remote energy options. High fuel costs and environmental impacts occur not only in Antarctica but also in many locations worldwide where remote communities need power, regardless of climate. One such area is Alaska (Isherwood et al., 1999).

The following analysis is an outline of the investments and expenses that occur during the design, installation and operation of a wind turbine at SANAE IV. Since this is only a feasibility study and specific design details regarding the wind turbine setup have to be obtained during the implementation stages, it is quite difficult to put figures to the calculations. Also since not all the information regarding the current economic status of the base is available, information has been taken from remote communities with similar electrical need and setups, so that an approximation can be made, regarding the costs of installing and operating a wind turbine at SANAE IV. The cost breakdown for a wind turbine setup and operation can be as follows (GTZ, 1999 and Bakos and Tsagas, 2002):

11.2 Basic Investment Costs

The installation of a wind turbine system at SANAE IV involves two economic parts. One is the initial investment and the second is the annual recurring costs and revenues. The initial investment is broken down into the following components with subsections:

1. Feasibility study including:
    - Site investigation
    - Wind-resource assessment
2. Development including:
    - Permits and approvals
    - Project management
3. Engineering including:
    - Wind turbine system design
    - Mechanical design
    - Electrical design
4. Renewable energy (RE) equipment including:
    - Wind turbine
    - Spare parts and special tools
    - Control system
    - Transportation
5. Balance of plant including:
    - Transport by ship
    - Transport from ship to base
    - Wind turbine foundations
    - Wind turbine erection
    - Electrical connection
    - Commissioning of wind turbine system
6. Miscellaneous including:
    - Training
    - Contingencies

Component number 4 is not actually needed in this economic analysis, since the North Wind NW100/19 wind turbine has already been designed for Antarctic conditions and thus only the purchasing price has to be accounted for. Furthermore, design changes to the wind turbine that potentially have to be made, so that a successful implementation of the wind turbine to SANAE IV's electricity grid is achieved, have to be taken into account as well.

11.3 Investment Cost of Supplementary Infrastructure and Electrical Connections to SANAE IV's Electrical Grid

Also included into the initial costs, are costs due to the connection of the wind turbine to the SANAE IV electricity grid and due to testing of the complete system. These costs are broken down into the following components:

- Cost of access roads
- Cost of cables, poles, transformers, etc. based on existing grid
- Cost of transforming the turbine into the environment
- Testing costs, including:
    - Turbine testing under normal conditions
    - Turbine testing in Antarctic conditions
    - Electrical grid connection testing at SANAE IV
    - Complete system testing

The analyst often forgets these expenses, but they form a crucial part of the successful implementation of a wind energy system. The components mentioned in section 11.2 and 11.3 will be represented in the economic analysis as one item, namely the capital investment. Also included in the analysis are annually recurring costs. They are given in the next section.

11.4 Annual Recurring Costs and Savings

Expenses and revenues that recur each year have to be included in the economic analysis, even if they only represent a fraction of the initial expenses of a wind turbine implementation. These costs and savings are factors that influence whether or not the wind turbine system is economically feasible or not.

From GTZ (1999) the annual operation and maintenance costs of wind turbine setups installed in other countries vary in a wide range. The special conditions regarding the implementation of a wind turbine system at SANAE IV, like cold weather issues and extreme wind conditions, have to be considered.

During the operation of a wind turbine, certain annual expenses and, in the case of SANAE IV, annual revenues occur and have to be accounted for. They include:

- Wind turbine operation and maintenance (O&M) costs
- Wind turbine labor costs
- Interest on initial capital investment
- Fuel savings due to power production by wind turbine
- Operation and maintenance savings due to reduced generator usage
- Labor savings due to reduced generator usage

11.5 Economic Viability Criteria Necessary to Evaluate Investments for Wind Turbine System Installations

The essential economic concepts and criteria which may lead to safe conclusions with respect to the economic and financing viability in terms of investment and operation of a wind turbine system (and not only) at a given site with prescribed wind and other relevant conditions are the following (Papadopoulos and Dermentzoglou 2001):

- Cumulative system cost comparison (CSCC)
- Net Present Value (NPV)
- Benefit/Cost Ratio (BCR)
- Internal Rate of Return (IRR)
- Payback Period (PBP)
- Cost per kWh energy produced (CP)

The computation of the PBP index is a useful approach to obtain a quick and approximate economic viability system evaluation, whereas the computation of the NPV, IRR and BCR indices constitutes a more accurate approach for a similar evaluation procedure.

For an investment project to be properly evaluated the required initial investment for the wind turbine system under study and also the costs and benefits associated with the operation of the system have to be taken into account. The initial investment is usually made up of the following two pertinent costs:

- Cost of equipment being purchased, and
- Cost of associated installation and testing.

The cost of operation of a wind turbine system is mainly made up of the following two cost components:

- Cost of repairs, and
- Cost of operation and maintenance (O&M)

The resulting benefit may be one of the following two or both:

- Diesel Fuel savings and/or
- Avoiding generating electricity by diesel generators

In the SANAE IV case the energy will not be sold, but it will be used for the energy demand of the base, thereby achieving fuel savings by the diesel generators.

11.6 Power Penetration and Fuel Savings

The amount of wind power penetration into the electrical grid of SANAE IV does not only depend on the amount of power produced by the wind turbine, but also on how much power is used at the base and how much power is being dissipated.

The fuel savings in a year, due to wind power penetration, will only reflect the power that has been usefully consumed at the base. In other words the power that originally has been supplied by the generators and that will be supplied by the wind turbine will result in fuel savings. Another criterion that has to be taken into account is that one generator has to run at all times. Thus a power penetration by the wind turbine will only result in a decreased load for the generator and not great fuel savings. However, during most of the wintertime, a second generator is running due to the increased power demand from the added heating load. It has been calculated the annual operating time of the second generator is about 30 %. Therefore, if the power demand of the second generator can be met by wind power, the second generator does not need to operate and significant fuel savings can be achieved.

The power produced by the NW100/19 wind turbine is about 430 MWh per annum. The annual power production of the generators amounted to 1150 MWh. Thus theoretically, the turbine can produce about 37 % of the power demand of the base. As mentioned this value is only a theoretical value since the wind turbine availability and usefulness of the power generated by the wind turbine reduce the penetration factor.

The wind turbine power is assumed to be fed into the grid whenever the turbine produces energy. However, since not all the energy can be used to meet the demand, an energy dump like the snow smelter takes up the rest of the energy available from the wind turbine. This also results in a decreased fuel savings. This reduced fuel saving agrees with the findings in articles of similar circumstances.

McKenna and Olsen (1999) pointed out that the annual energy production is often lower than the calculated value of 430 MWh due to various system losses. These potential system losses can be seen in table 11-1.

Source	Loss Fraction
Operation and maintenance	1 – 5 %
Blade soiling losses	up to 5 %
Turbulence losses	up to 2 %
Control, grid and collection	up to 3 %

Table 11-1: Availability losses during wind turbine power production

Using a 97 % availability, the combination of the sources, mentioned in table 11-1, is significant, having a possible net loss of 11.5 %. McKenna and Olsen (1999) state that only 50 % of the power produced by the wind turbine actually leads to a direct decrease in generator operating time and fuel saving. Isherwood et al. (2000) however state that 60 % of the power produced by the wind turbine leads to a direct decrease in fuel consumption of the generators. Therefore, a reasonable and conservative assumption would be that 50 % of the annual power generated by the wind turbine would lead to a direct fuel saving of the generators.

The annual energy produced by wind turbine is P_{wt} = 430 MWh. Therefore taking the reduction factor mentioned above into account, the reduction in power generation of the generator sets is:

$$P_{gr} := 50\ \% \cdot 430\ \text{MWh} := 215\ \text{MWh} \qquad \textbf{(11-1)}$$

From chapter 4 the electrical generator efficiency is 3.56 kWh/L, based on the LHV of 9.8 kWh/L. Thus the fuel saving that can be achieved is

$$FS := \frac{215\ \text{MWh} \cdot 1000\ \frac{\text{kWh}}{\text{MWh}}}{3.56\ \frac{\text{kWh}}{\text{L}}} := 60393\ \text{L} \qquad \textbf{(11-2)}$$

By integrating the NW100/19 wind turbine into the electricity grid of the base, a total of 60400 L of SAB diesel fuel can be saved per annum.

11.7 Economic Evaluation of Externalities

Externalities are costs associated with pollution caused by emissions and fuel spills. The fuel used in the diesel generators is SAB diesel fuel. During the field trip, Wally Bester and Jessica Gunalsevam, also students at the University of Stellenbosch, measured the fuel consumption. The total amount of emissions produced by the generators, generated in one year, was approximated by Taylor et al. (2002). They are shown in table 11-2.

Source	**VOC**	**CO**	**NO_x**	**SO_2**	**CO_2**	**PM**
	[Tons]	[Tons]	[Tons]	[Tons]	[Tons]	[Tons]
Total (lower estimate)	**0.341**	**0.533**	**13.451**	**0.076**	**744**	**0.198**
Total (upper estimate)	**0.546**	**0.853**	**13.451**	**0.076**	**744**	**0.317**

Table 11-2: Total annual emissions from the generator internal combustion engines at SANAE IV base

The explanations of the abbreviations used in table 11-2 are as follows:

- VOC: Volatile Organic Compounds
- CO: Carbon Monoxide
- CO_2: Carbon Dioxide
- NO_x: Oxides of Nitrogen
- SO_2: Sulphur Dioxide
- PM: Particulate Matter

In order to calculate the value of the emissions produced annually, a price has to be found for each particular emission. Two articles have been obtained, that assign values to these emissions (Isherwood et al., 1999 and El-Kordy et al., 2001). The article by Isherwood et al. (1999) presents a general price to environmental impact, based on diesel generator operation at remote Alaskan communities. This includes emissions, fuel spills and leakages. The price is US$0.80 per liter or R8.60 per liter of diesel fuel used by the

generators, when the current exchange rate (5th September 2002) of R10.75 for US$1.00 is used. This approach is very suitable for the SANAE IV base, since the article is referring to remote Alaskan communities, usually not bigger than SANAE IV.

Pollutants	Unit Cost R/kg	Amount Produced (Lower limit) [Tons]	Amount Produced (Upper limit) [Tons]	Cost of Pollutant [R]
VOC	40.37	0.341	0.546	22042.02
CO	40.37	0.533	0.853	34435.61
NO_x	24.65	13.451	13.451	331567.15
SO_2	60.91	0.076	0.076	4629.16
CO_2	0.19	744	744	141360.00
PM	35.54	0.198	0.317	11266.18
			Total Cost [R]:	**545300.12**

Table 11-3: Cost of each pollutant

The approach used by Isherwood et al. (1999) only takes into consideration the emissions produced by the generators and not the environmental impact caused by fuel spills and leakages. This approach will be used to identify the cost of each pollutant, while the first approach will be used to obtain a figure for the total environmental impact due the diesel fuel emission and spills.

Table 11-3 presents the annual cost of each pollutant. The unit price of VOC and CO could not be obtained and the average of PM, NO_x and SO_2 have been used to do the approximation. The total cost of the emissions is roughly R550 000,00 per annum. The amount of fuel saved due to the power penetration of the wind turbine is used to calculate the amount of externalities that can be saved. It is done as follows:

$$ES := \frac{\text{"Fuel Saved"}}{\text{"Total Fuel Consumption"}} \cdot \text{"Total Cost of Externalities"} \qquad \textbf{(11-3)}$$

$$ES := \frac{60400\ L}{298416\ L} \cdot R550000,00 := R111321,00$$

Thus the externalities saved due to the introduction of the wind turbine is about R110000,00 per year. This however does not include externalities covering the fuel spills, discarded drums and fuel leaks.

The approach that El-Kordy et al. (2001) used, does take the above-mentioned externalities into account. This method is much simpler than the method above, as it only presents a price per liter of fuel used to calculate the externalities due the operation of generators at remote locations. The price of externalities is US$0.80/L or R8.60/L. As we have calculated the amount of fuel used due to the penetration of wind power into the electricity grid of SANAE IV, we can calculate the yearly externalities saved as follows:

$$\text{ES} := \text{"Fuel Saved"}\text{"Total Cost of Externalities"} 60400\ \text{L} \cdot \frac{\text{R8,60}}{\text{L}} := \text{R519440,00} \qquad \textbf{(11-4)}$$

The total amount of externalities saved, taking the total environmental impact of the diesel generator operation into account, amounts to about R520000,00. This is much more than the value calculated for the emissions only. The reason for this enormous amount is that there is a huge process necessary to clean a fuel spill. Once the fuel has been spilt, the total area of the affected snow has to be shoveled into drums that have been cut open. Then the fuel drums have to be stored until the next take-over period. The fuel drums then have to be digged out of the snow, transported to the ship and then the drums are transported back to South Africa. However, since it is very difficult to separate the diesel from the snow, huge quantities of contaminated snow has to be transported to South Africa, which is very costly and time consuming.

The other point that has to be noted is that sometimes it happens that one does not properly clean a fuel spill, or a fuel spill remains unseen. This fuel freezes, but when warmer temperatures occur, the fuel seeps into the ground, and already now it seems that soon the base could experience problems with contaminated water. The snow smelter lies towards the east of the base and has a lower elevation than the base. Thus the fuel can flow down to the snowsmelter and contaminate the water.

This is the reason for the huge amount of externalities and the amount of R500000,00 thus represents a reasonable figure. Although it may seem a lot at a first glance, one has to consider the implications of environmental degradation, especially in Antarctica.

The externalities will only be partly used to calculate the breakeven point of the wind turbine. Two cases will be employed. One is with and the other one is without the externalities. This will present a good comparison of the two cases and one can see the significant change in breakeven time.

11.8 Economic Assessment

11.8.1 Introduction

The cost of any energy delivery process includes all of the items of hardware and labor that are involved in installing the equipment plus the operating expenses. The analysis system that will be used is the life cycle cost (LCC) analysis. There are several reasons to use the LCC analysis rather than simply to compare the initial cost of each supply option. Capital cost (equipment and installation expenses) is one of many cost components. Power systems also require varying amounts of maintenance, repair, and fuel costs. The external costs due to environmental consequences also differ greatly especially when comparing conventional and renewable systems. As an example, a wind turbine system may have a higher initial cost than a diesel generator, but it requires no fuel, and much less maintenance or other external costs. LCC analysis is used to analyze electricity generation systems. LCC analysis allows the evaluation of all the costs associated with installing and operating any power system over its lifetime, thus giving a realistic assessment of a system's lifetime costs and allowing a reasonable comparison of different power sources. LCC analysis permits the study of the impact of changing economic variables, such as interest or inflation rates and escalation rates. The LCC can be represented by:

$$LCC := C_{pw} + M_{pw} + L_{pw} + F_{pw} + X_{pw} \quad \textbf{(11-5)}$$

where pw is a subscript indicates the present worth of each factor. C = capital cost and includes the initial capital expense for equipment, system design, system engineering, system transport and installation. This cost is considered as a single payment occurring in the initial year of the project, regardless of how the project is financed. M = operation and maintenance cost is the sum of yearly scheduled maintenance and operation costs. L = labor costs for operation, inspections, and insurance. F = the fuel cost is the sum of the yearly fuel costs. Differential fuel inflation may be considered. X = the external costs including damage prevention, or damage cost, if occurred. Using the five cost factors, the LCC can be calculated for each type of power generation systems.

Future costs must be discounted because of the time value of money. The following equations are used to calculate the present value.

- Single present worth factors:
  The formula for the single present worth (PW_s) of a future sum of money (F) in a given year (N) at a given discount rate (i) is given by:

$$PW_s := \frac{1}{(1+i)^N} \tag{11-6}$$

  This equation is used to calculate the discounted cost expected to occur in a specific year.

- Uniform present worth factors:
  The formula for the uniform present worth (PW_u) of an annual sum (A) received over a time period (N years) at a given discount rate (i) is:

$$PW_u := A\left[\frac{1-(1+i)^{-N}}{i}\right] \tag{11-7}$$

This equation is used to calculate the discounted annually recurring costs.

Evaluation of the economics of energy systems strongly depends on the four cost factors: capital cost; maintenance cost; fuel cost; and external cost, when considered. Fuel and external costs are sensitive to fuel type and efficiency of the used system. Economic parameters such as discount, inflation and escalation rates, deeply affects the evaluation. Future sums of money must be discounted because of the inherent risk of future events not turning out as planned, the present worth method being considered as a suitable tool for comparing the different alternatives. In order to evaluate the LCC analysis, certain economic boundary conditions and input data are needed.

The essential data, parameters and system characteristics required are given in table 11-5. It is important to note that the interest on capital could potentially be ignored, since the capital invested is financed by a government budget, thus there should be no need for interest. It has to be noted that the annual labor, maintenance and operation costs are only estimates, since these figures strongly depend on the final system installation and cannot be accurately predicted. The wind turbine purchase price was obtained from Northern Power Systems. The fuel price was obtained from DEA&T and was calculated as follows:

Description	**Price**
Diesel fuel purchase price:	1.932 R/L
Diesel fuel transport by ship price:	2.64 R/L
Diesel fuel transport by truck price:	0.275 R/L
Auxiliary expenses:	1.00 R/L
Total diesel fuel price:	**5.847 R/L**

Table 11-4: Evaluation of diesel fuel price

NW100/19 Wind Turbine Characteristics and Data:		
Annual average wind speed:	10.84	m/s
Annual power production:	430.13	MWh
Annual turbine operating hours:	6942	h
Expected design life of wind turbine:	30	years
Wind turbine purchase price:	1505000.00	Rand
Auxiliary equipment. Installation cost:	1505000.00	Rand
Transportation cost:	100000.00	Rand
Feasibility cost by Northern Power Systems:	232092.50	Rand
Complete wind turbine cost:	3342092.50	Rand
Estimated annual maintenance & operation cost:	20000.00	Rand
Estimated annual labor cost:	13626.84	Rand
Wind turbine energy penetration factor:	50	%
Fuel saved annually due to wind turbine energy penetration	60426	L
Diesel Generator Characteristics and Data:		
Average hourly electric demand of base:	122	kW
1-hour peak demand of base:	215	kW
Annual power production:	1153	MWh
Annual power generation hours:	11304	h
Percentage of second generator operating:	30	%
Fuel energy density:	9.80	KWh/L
Fuel cost:	5.847	Rand/L
Annual diesel consumption:	298416	L
Estimated annual maintenance and operation cost:	30000.00	Rand
Estimated annual labor cost:	20000.00	Rand
Estimated annual saving in generator labor, O&M costs due to reduced operating time, as a percentage of yearly costs:	20	%
Economic Data:		
Capital investment:	3342092.50	Rand
Interest rate on capital investment:	14	%
Estimated maintenance and labor cost escalation per year:	2	%
Estimated fuel cost escalation:	4	%
General inflation rate (July 2002):	10.6	%
Exchange rate (US$ to Rand):	10.75	Rand/US$
Estimated escalation of external costs:	3	%

Table 11-5: Essential data and system characteristics

11.8.2 Evaluation of cumulative system cost comparison

Figure 11-1 shows the cumulative system costs for the hybrid wind-diesel system and, for comparison, the baseline generator system. Cumulative system costs are defined as the present value of all the system expenses (capital, fuel and maintenance) from the time of installation of the power plant to a number of years N during the life of the plant. The cumulative system cost for year n is calculated as:

$$C_{cum} := \left[\sum_{j=0}^{N} \left[\frac{C_{cap.j}}{(1+i_{cap})^{j}} + \frac{C_{fuel.j}}{(1+i_{fuel})^{j}} + \frac{C_{maint.j}}{(1+i_{maint})^{j}} + \frac{C_{labor.j}}{(1+i_{labor})^{j}} \right] \right] \quad \textbf{(11-8)}$$

where $C_{cap,j}$, $C_{fuel,j}$, $C_{maint,j}$ and $C_{labor,j}$ are the capital, fuel maintenance and labor costs during the year j, i_{cap} is the interest rate on capital, and i_{fuel}, i_{maint} and i_{labor} are the cost escalation rates for fuel, maintenance and labor costs.

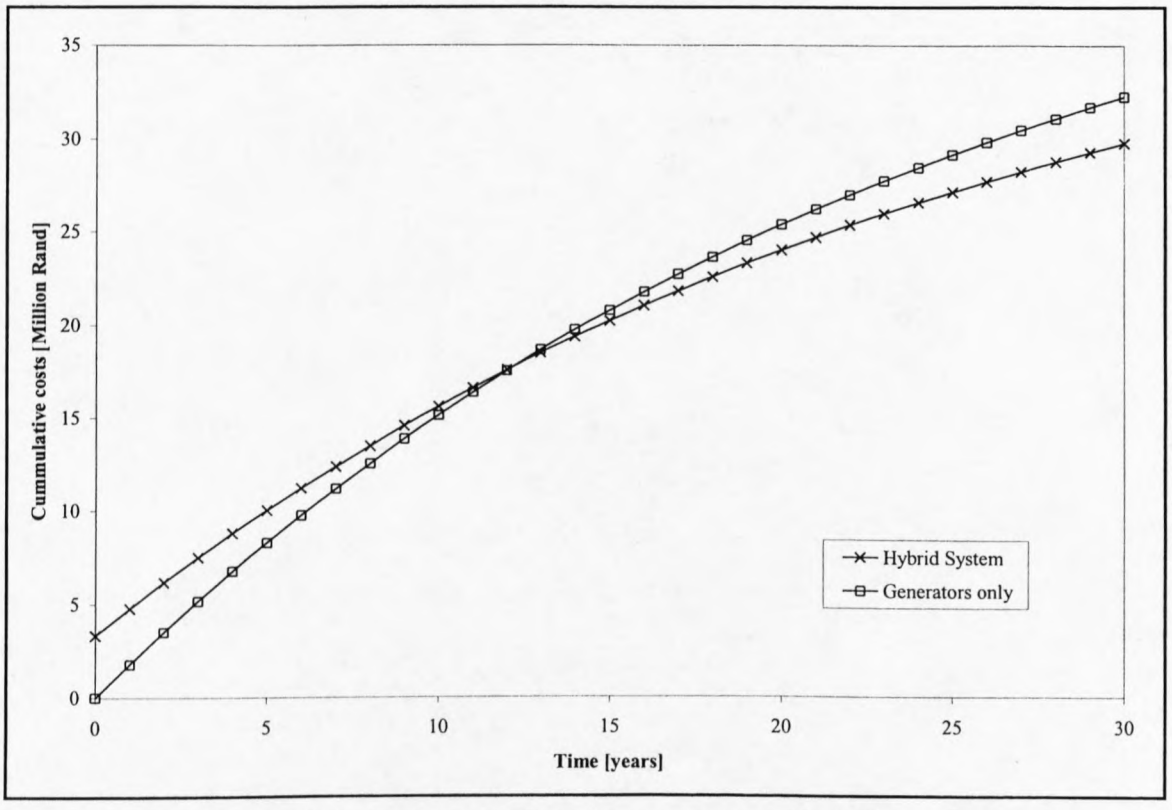

Figure 11-1: Cumulative system cost of baseline generator and hybrid system operation

The initial costs of a wind-diesel system are higher than for just a diesel generator system, but diesel fuel costs are adding up during the life of the system and the wind-diesel

combination is less expensive than the baseline system after about 12 years as can be seen from figure 11-1. In the next section the NPV of the hybrid system will be analyzed.

11.8.3 Evaluation of net present value

Under the net present value method, the present value of all cash inflows is compared against the present value of all cash outflows associated with the investment project. The difference between the present values of these cash flows, called the NPV, determines whether or not the project is generally an acceptable investment. Positive NPV values are an indicator of a potentially feasible project. In order to accurately determine the NPV, the general inflation rate will be introduced and the present worth factors will change to:

$$PWF := \sum_{j=1}^{N} \frac{(1+d)^{j-1}}{(1+i)^{j}} \qquad \textbf{(11-9)}$$

where d is the general inflation rate. The NPV is defined as follows:

$$NPV := \left(\sum_{j=1}^{N} AS_j \cdot PWF \right) - C_{cap} \qquad \textbf{(11-10)}$$

where AS_j is the net annual savings, defined as: AS = Annual Savings – Annual Expenses. The annual savings in our case are the fuel costs that are saved because of the power penetration by the wind turbine and therefore the reduced diesel consumption by the diesel generators and the saved labor and maintenance costs due to the reduced running time of the diesel generators. The annual expenses include interest on capital, labor and maintenance expenses. The cumulative NPV can be seen in figure 11-2. Basically this figure is the same as figure 11-1, except that in figure 11-1 inflation has not been incorporated. For a capital investment of about R3.5 million, the net present value at the end of the design life of the wind turbine is NPV = R20.9 million. Since it is not known, when this project will be implemented, different amounts of capital investment have been

chosen and the NPV resulting from the different capital amounts invested can be seen in figure 11-3.

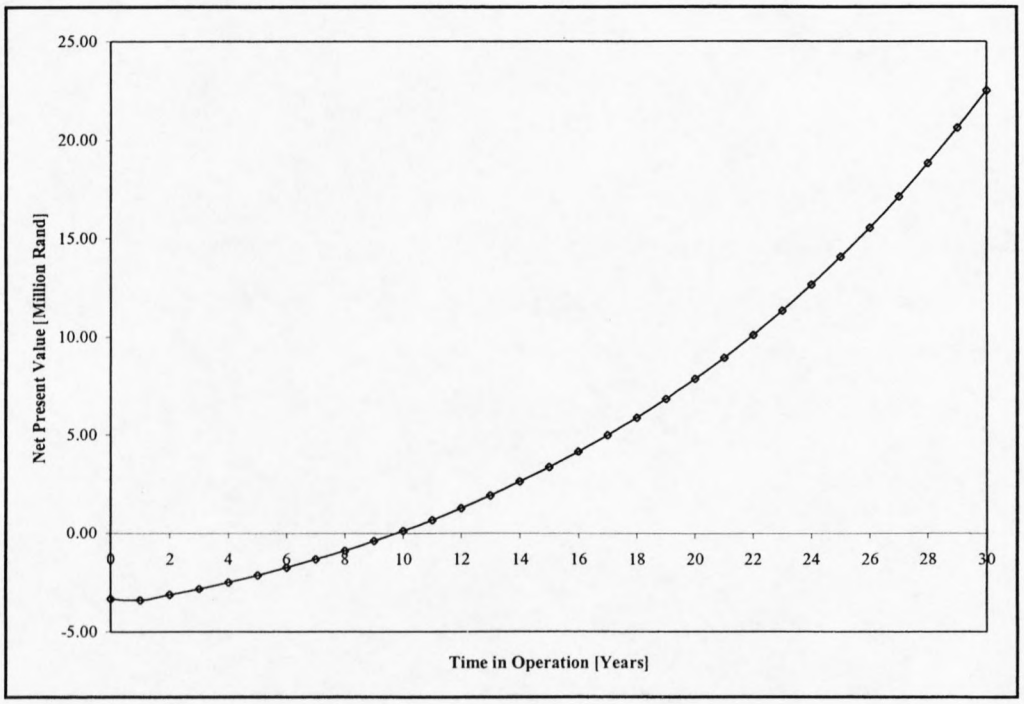

Figure 11-2: NPV of proposed wind turbine system including inflation

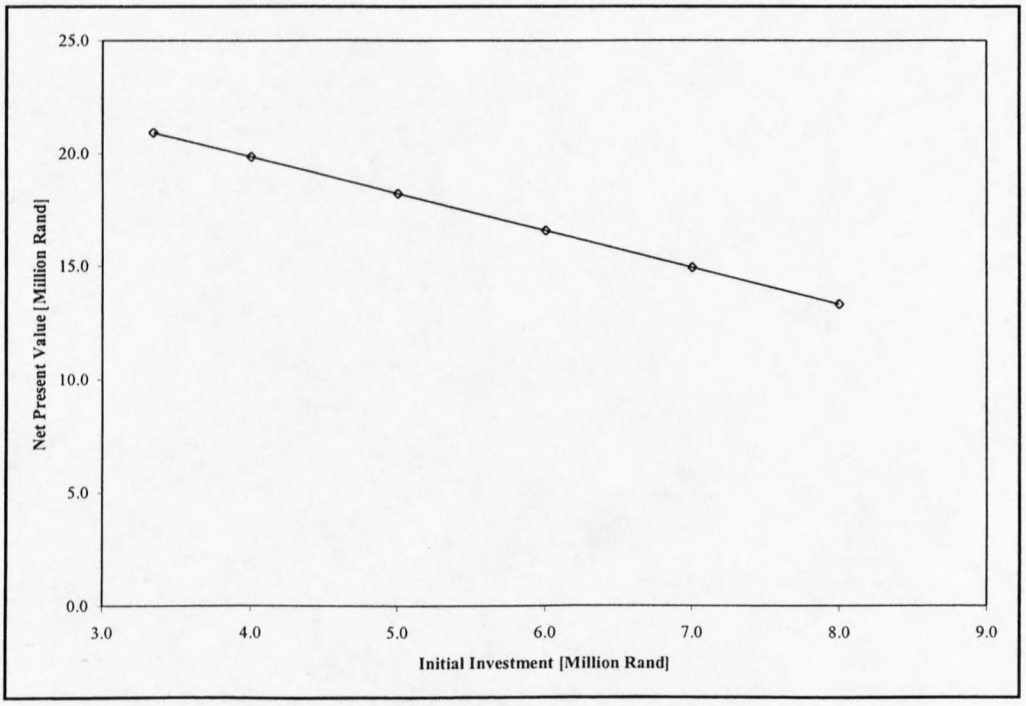

Figure 11-3: NPV for different amounts of capital invested, including inflation

The amount of the capital invested shown in figure 11-3 ranges from R 3.5million to R 8.0million. Even with an initial investment of R 8.0million the NPV is positive, which makes it a favorable investment, if all the other economic factor are favorable.

11.8.4 Evaluation of benefit / cost ratio

As the name implies, the benefit/cost ratio method involves the calculation of a ratio of benefits to costs. Whether evaluating a project in the private sector or in the public sector, the time value of money must be considered to account for the timing of cash flows occurring after the inception of the project (Sullivan et al., 2000). Thus interest, escalation rates and inflation has been incorporated. The BCR is defined as follows:

$$BCR := \frac{\left(\sum_{j=1}^{N} AS_j \cdot PWF \right)}{C_{cap}} \qquad \textbf{(11-11)}$$

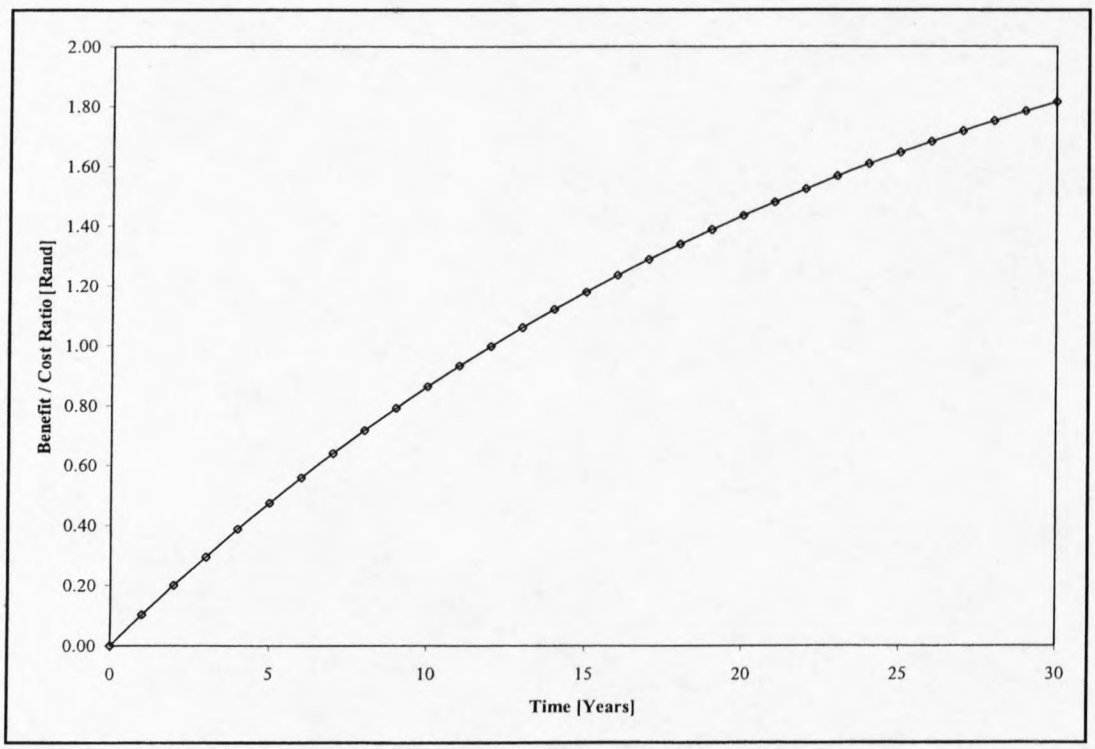

Figure 11-4: BCR of project excluding inflation and interest on capital

In this section a range of capital invested has been used and the BCR has been calculated on the same range of capital invested, as mentioned earlier. The benefit/cost ratios can be seen in figure 11-4. A BCR of unity or more shows that a project is acceptable. Figure 11-5 clearly shows that this project is not acceptable for all ranges of capital invested.

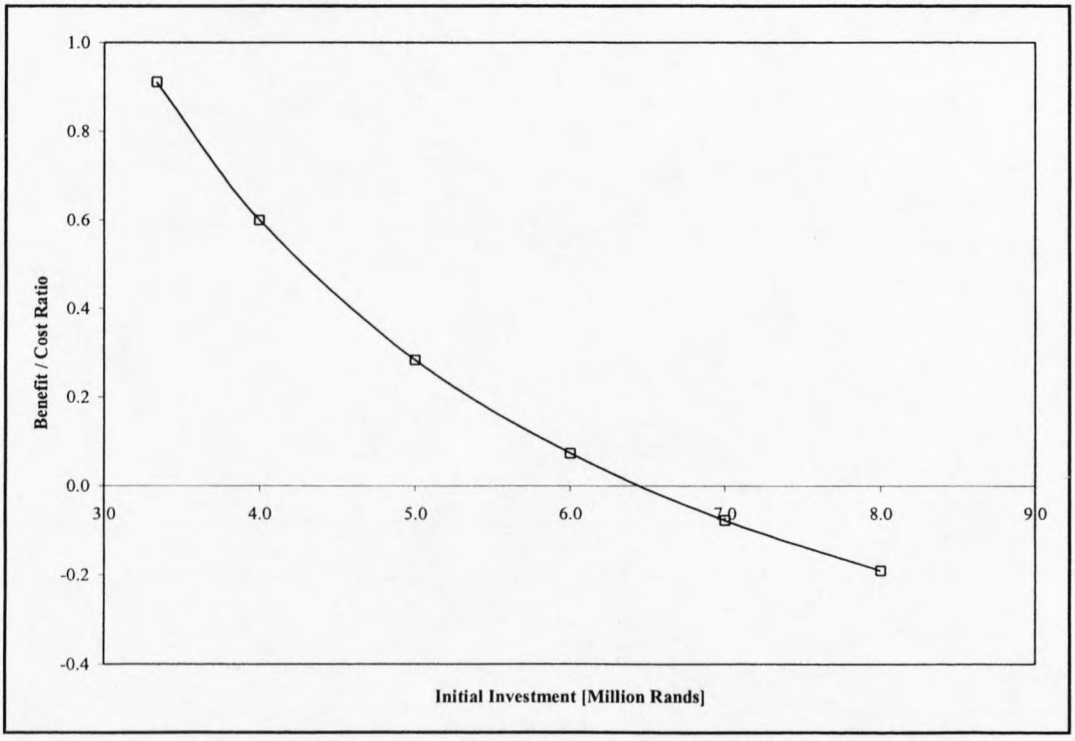

Figure 11-5: BCR for a range of capital invested, excluding inflation.

However, as mentioned earlier, the interest charged on capital can be ignored, since the capital will most probably be financed by a government budget. As the investment is paid at the start of the project in one sum, interest does not apply. Figure 11-4 and figure 11-6 show the BCR, excluding interest on capital invested, but including inflation. The BCR is positive for a capital investment of up about R 6.3million. Thus this project is only acceptable, if there is no need for interest, and then it is only acceptable, if the capital investment is less than R 6.3million.

It is very important to note that the BCR is defined without taking inflation into account, thus not representing the value of the annual savings properly. More sophisticated and detailed analyses like the IRR method have to be applied.

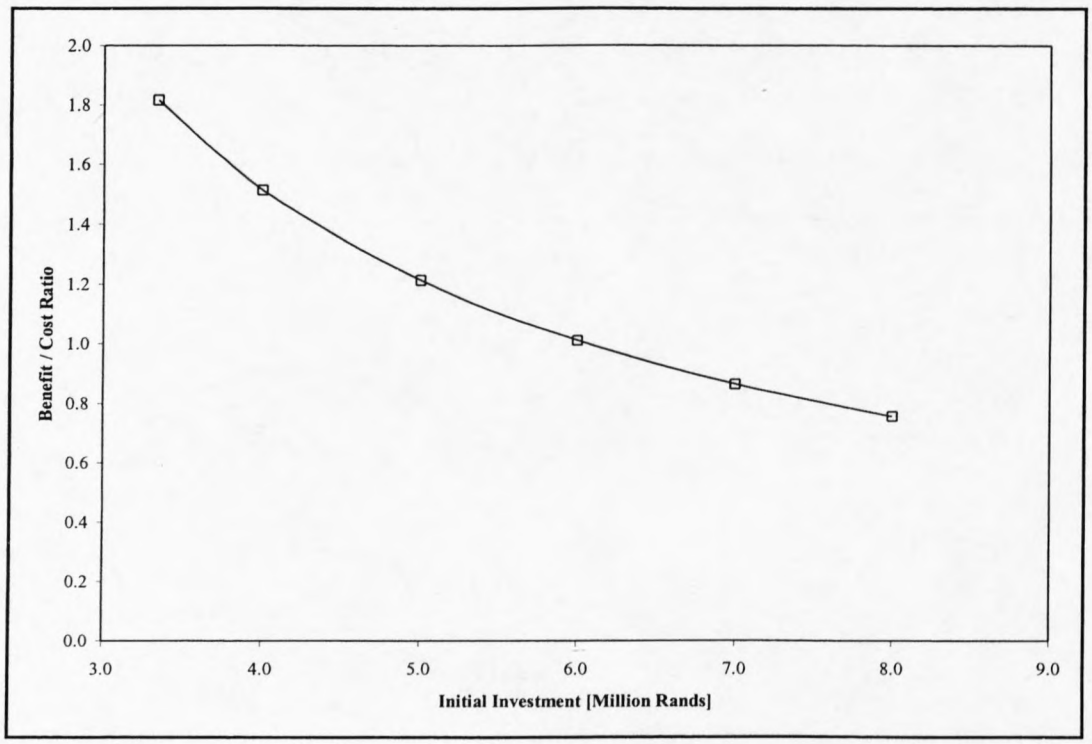

Figure 11-6: BCR excluding interest on capital, but including inflation

11.8.5 Evaluation of internal rate of return

The internal rate of return represents to true interest yield provided by the project over its life. The IRR method includes inflation, unlike the BCR method, which makes it a better method than the BCR method. The IRR is defined as setting the NPV equal to zero and then solving the equation for i, which is called the IRR:

$$NPV := \left(\sum_{j=1}^{N} AS_j \cdot PWF \right) - C_{cap} := 0 \qquad \textbf{(11-12)}$$

Figure 11-7 shows the internal rate of return calculated for a range of capital investments, as mentioned earlier. The IRR value, associated with the amount of capital investment, should be greater than 12% which appears to be the marginal value for accomplishing economic viability of a wind turbine system (Papadopoulos and Dermentzoglou 2001).

Figure 11-7 shows that the IRR is acceptable up to a capital of about R6.0million. With a capital investment of R3.5million, the IRR is about 15%, which is a very favorable rate of return, making the project very attractive.

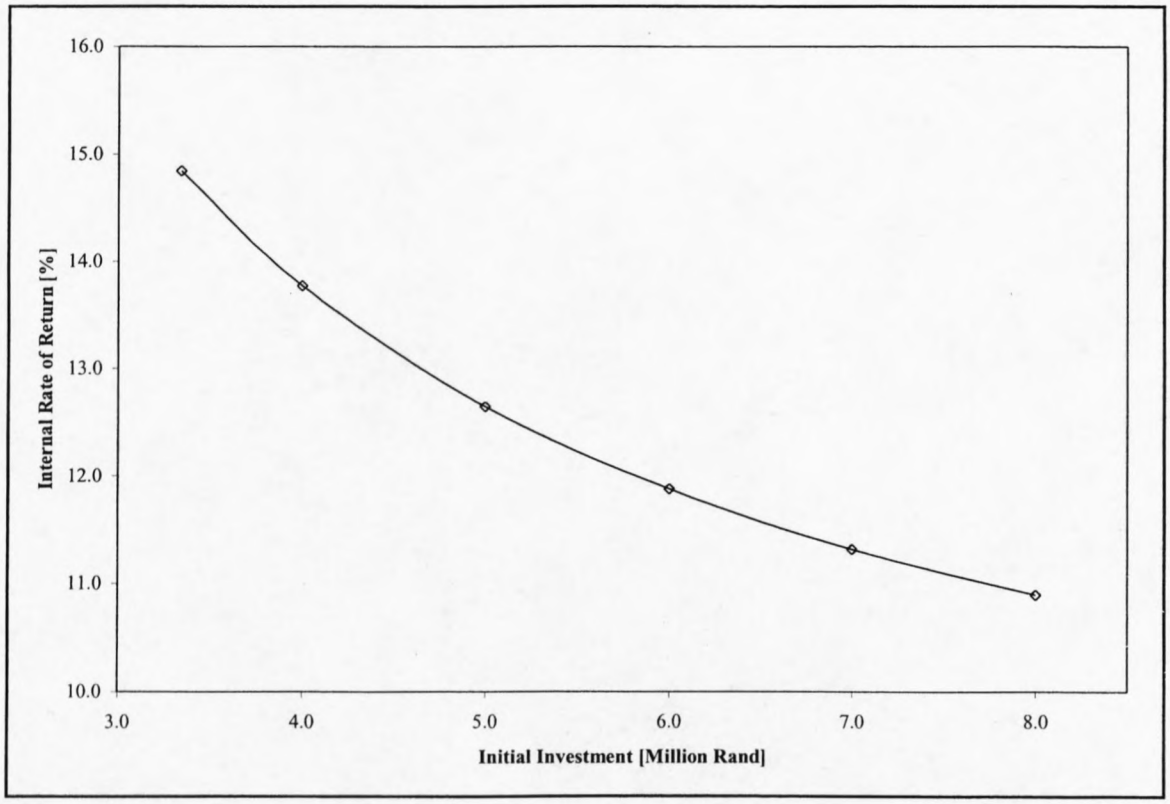

Figure 11-7: IRR for a range of capital investments

11.8.6 Evaluation of payback period

The most familiar economic analysis method is the payback method. The simple payback period ignores the time value of money, thus making it a very crude calculation. However due to its simplicity, the method provide a fairly easy insight to the economic viability of a project. The simple payback period is defined as follows:

$$PBP_s := \left[\sum_{j=1}^{\theta} \left(R_k - E_k \right) \right] - C_{cap} \geq 0 \qquad \textbf{(11-13)}$$

where θ indicates the year of breakeven. Figure 11-8 shows the simple breakeven period.

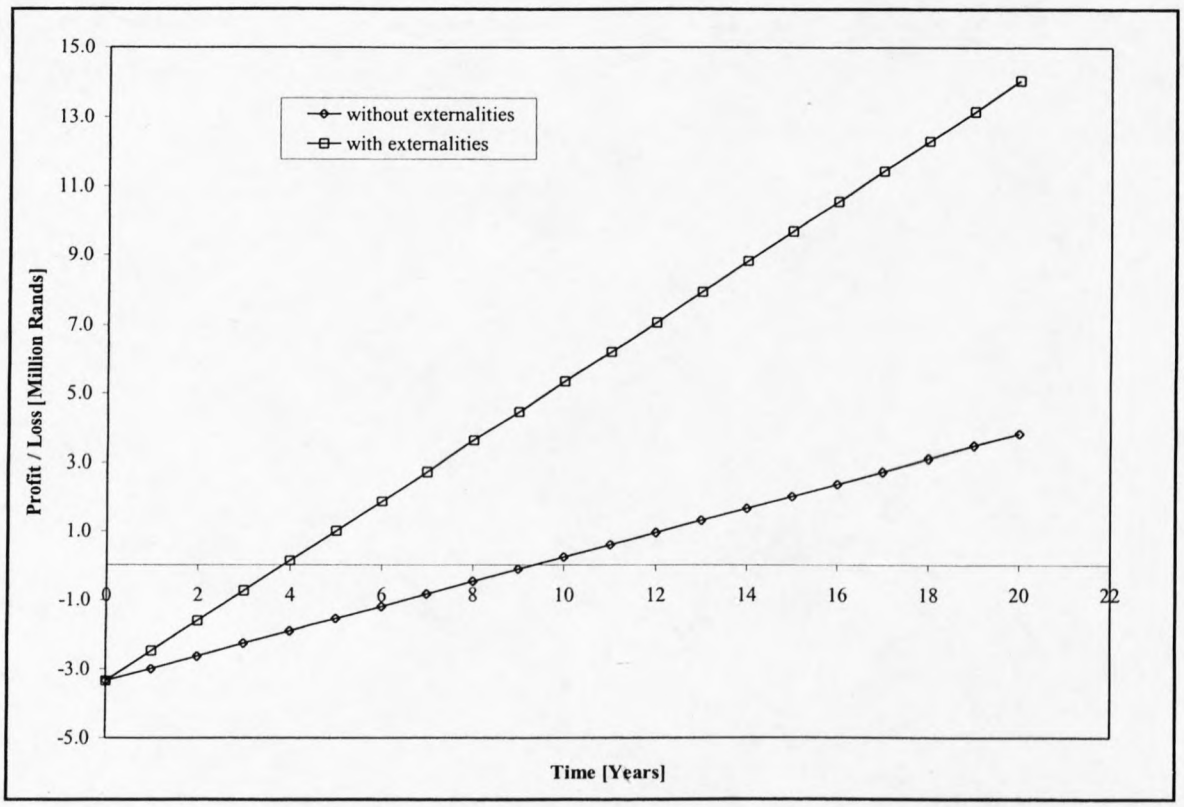

Figure 11-8: Simple breakeven period

When doing a breakeven analysis, it should be noted that only the values in the time before the breakeven point are considered. The values, calculated after the breakeven point, are discarded. Figure 11-8 shows that the breakeven point for this project is about 9 years. When the externalities, calculated in section 11.7, are taken into account, the breakeven period is only about 4 years. This comparison clearly shows the influence of externalities on the economic analysis. Although the externalities saved due to a reduced operating time of the generators are no direct saving for the economic analysis of the project, they do tend to present a figure to the emissions that are occurring at SANAE IV.

A more sophisticated breakeven period analysis is called the discounted breakeven period, which includes interest on capital, escalation costs and inflation in the analysis. The discounted breakeven period is defined as follows:

$$PBP_d := \sum_{j=1}^{\theta} \left(R_k - E_k\right) \cdot PWF - C_{cap} \cdot PWF \geq 0 \qquad \textbf{(11-14)}$$

The basic premise of the PBP is that the more quickly the cost of a project can be recovered, the more desirable is the investment. Figure 11-9 shows the discounted payback period for this project.

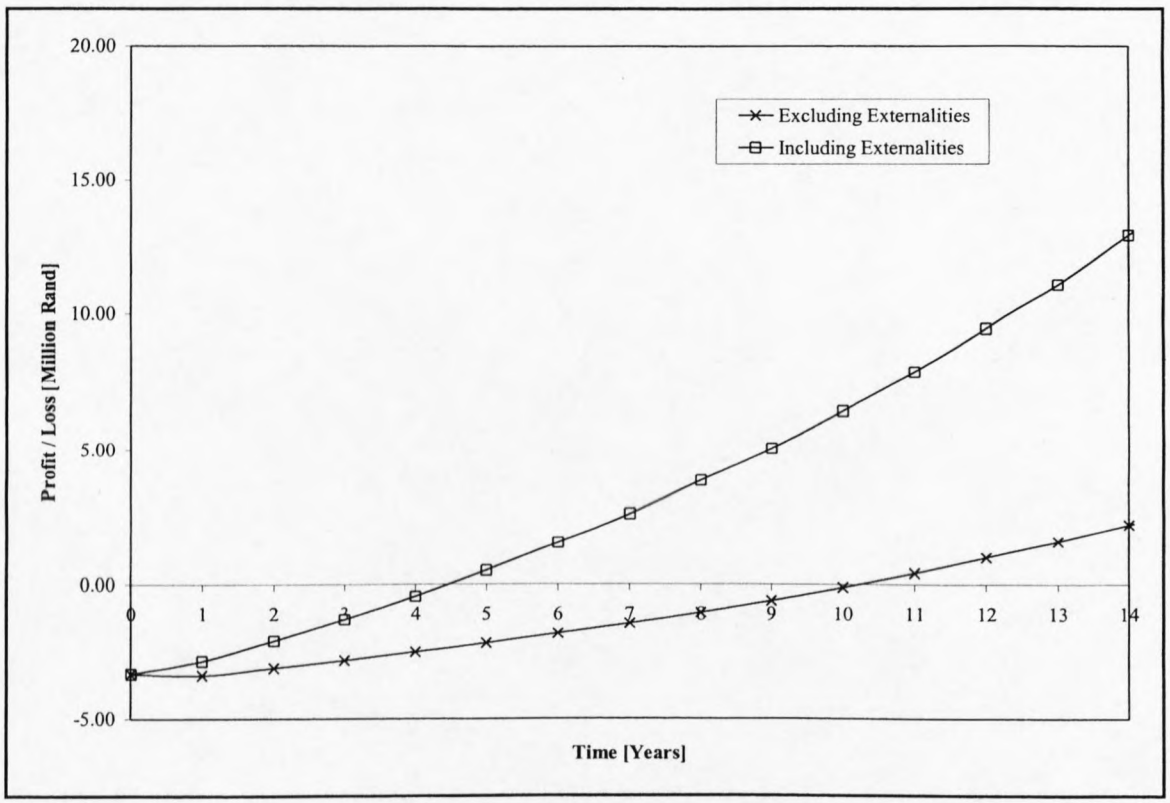

Figure 11-9: Discounted payback period

Figure 11-9 shows that the breakeven point for this project is about 10 years, including interest on capital escalation costs and inflation. Thus the figure provides a true estimation of the payback period. A period of 10 years may seem long for recovering the capital invested, but when the wind turbine design life of 30 years is considered, a payback period of 10 years is acceptable. During 1/3 of the wind turbine's life, it repays the initial investment, after that it provides surplus savings that can be used for other projects.

11.8.7 Evaluation of cost per unit power produced

Another useful economic analysis tool is the cost per unit power produced. In this case, the unit cost is Rand/kWh. The cost of a kWh produced by a wind turbine system may be obtained from the following mathematical relationship:

$$CP := \frac{C_{cap}}{P} \cdot \left[\frac{d \cdot (1+d)^N}{\left[(1+d)^N - 1 \right]} \right] + \frac{OM}{P} + \frac{L}{P} + \frac{FC}{P} \qquad \textbf{(11-15)}$$

Where d is the annual inflation rate, OM is the operating and maintenance costs, L is the labor cost, FC is the fuel cost and P is the total power generated in one year. Figure 11-10 shows the cost per kWh for the following systems:

- Baseline generator cost per kWh produced
- Hybrid, wind- diesel system cost per kWh produced
- Wind turbine cost per kWh produced

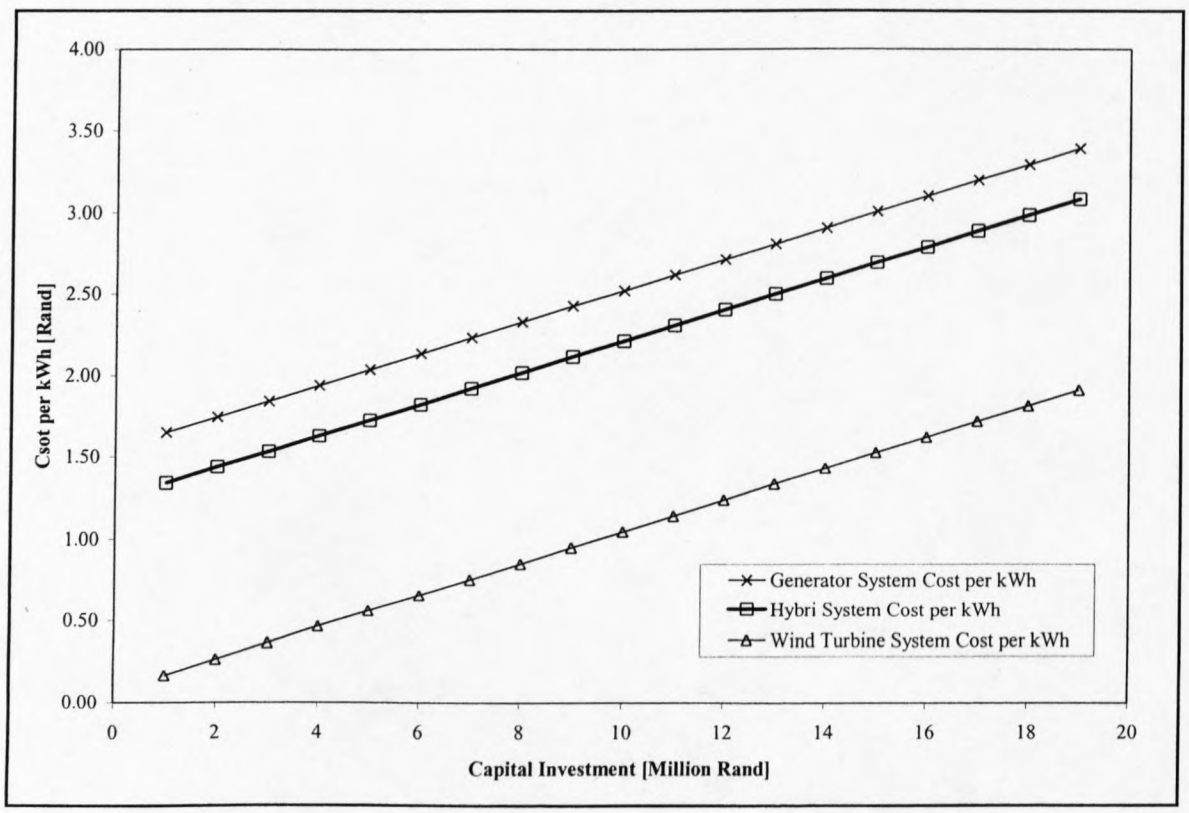

Figure 11-10: Cost per kWh produced for three different systems considered

The figure provides a visual form to see the difference in cost price per kWh produced for the different systems. The fact the fuel cost of the diesel generators system dominates the cost per kWh produced can be seen by a nearly horizontal linear curve. On the other extreme, the cost per kWh produced by the wind turbine system is strongly dependent on the capital invested, resulting in a linear relationship with a moderate gradient. The hybrid system i.e. a combination of wind turbine and diesel generators provides a lower cost per kWh produced than the diesel generator system, but with a small gradient. With a capital investment of R4.0million the cost of the hybrid system is CP = R1.63/kWh, while the cost for the diesel generator system is CP = R1.94/kWh and for the standalone wind turbine system the cost is CP = 0.31/kWh. By performing this analysis it has been shown that the costs of introducing the wind turbine at SANAE IV can reduce the cost per kWh produced by up to 20 %.

The results of the economic analysis clearly show the economic viability of a wind turbine system at SANAE IV, taking certain conditions into account. Some of the economic parameters used are not fixed, like the interest on capital, the US$ to ZAR exchange rate and the general inflation rate. Another variable parameter in the analysis is the purchase price of the wind turbine. As the NW100/19 wind turbine is not in production yet the price of this turbine is not very stable. The economic analysis should thus be refined, once the budget for this project is allocated.

12 ENVIRONMENTAL FACTORS

Wind turbines are always highly visible elements in the landscape, otherwise they are not located properly from a meteorological point of view.

It is interesting to note that the sound emission levels for all new Danish turbine designs tend to cluster around the same values. This seems to indicate that the gains due to new designs of e.g. quieter rotor blade tips, are achieved by slightly increasing the tip speed (the wind speed measured at the tip of the rotor blade), and thus increasing the energy output from the machines. It thus appears that noise is not a major problem for the industry, given the distance to the closest neighbors (usually a minimum distance of about 7 rotor diameters or 300m is observed). Since storms occur frequently and winds are blowing most of the time at the base, the sounds emitted by the wind turbine can be ignored, since they will most probably not be heard.

Birds often collide with high voltage overhead lines, masts, poles, and windows of buildings. Cars in the traffic also kill them. Birds are seldom bothered by wind turbines. Radar studies from Tjaereborg in the western part of Denmark, where a 2 MW wind turbine with 60 m rotor diameter is installed, show that birds - by day or night - tend to change their flight route some 100-200 m before the turbine and pass above the turbine at a safe distance (DWEA, 2001). A wind turbine would not cause a risk for birds at SANAE IV, since no bird colonies exist at the area surrounding SANAE IV.

In Denmark there are several examples of birds (falcons) nesting in cages mounted on wind turbine towers. The only known site with bird collision problems is located in the Altamont Pass in California. Even there, collisions are not common, but they are of extra concern because law protects the species involved (DWEA, 2001).

A study from the Danish Ministry of the Environment shows that power lines, including power lines leading to wind farms, are a much greater danger to birds than the wind

turbines themselves. Some birds get accustomed to wind turbines very quickly; others take a somewhat longer time (DWEA, 2001).

The effect on the environment due to the visual impact of the wind turbine has to be investigated during the implementation stage, when the exact position of the wind turbine is known. The visual impact is the only effect that a wind turbine could have on the environment. However, considering the reduction in emission, caused by the diesel electric generator sets and the reduction in oil spill risks, the visual impact is a small price to pay for a lesser impact on the Antarctic environment.

13 CONCLUSION AND RECOMMENDATIONS

During the course of this project, a feasibility analysis regarding the installation, operation and maintenance of a wind turbine system, based on technical and economic criteria has been performed. In order to do this, an extensive literature research was done at the beginning of the project. The bulk of information gathered aided in the understanding of the subject.

The second step was to obtain information regarding the SANAE IV base. Very useful information regarding the base was obtained from the internet, and thermal energy information was taken from the final year project by Teetz (2000). In order to get all the information necessary, a trip to the SANAE IV was undertaken. The main objective of this trip was to measure wind speed and direction, but ground surveys, data on the energy distribution of the base, generator fuel consumption data and base power demand data were obtained.

The analysis of the energy demand for SANAE IV included assessing the current energy system, the fuel consumption of the diesel electric generators, the energy demand of the base, the electrical and thermal energy distribution, the energy demand variations and the assessment of possible energy dump locations. About 300000 L of SAB diesel fuel is used each year at the base to supply about 1150 MWh of energy, with an electrical efficiency of the diesel electric generators of about 36 %. The main result of the demand variation analysis is that a substantial increase in energy demand is experienced during the winter months, as compared to the summer period. Also there exist daily demand variations, forming between three and four peaks during the day, mainly due to kitchen use and snowsmelter use. The biggest energy consuming equipment at the base, which is frequently used, is the snowsmelter with a power capacity of 94 kW. The snowsmelter has been identified as the best energy dump location, due to the enormous energy demand.

Having done the energy demand study, the wind data had to be analyzed. Three methods to capture wind data were used, namely the 6 m wind mast, the 10 m weather station and the

handheld anemometer. The 6 m wind mast was used to measure wind data for 2 positions with different surfaces around the base, and wind speed profiles for the 2 surfaces are derived from this data. From the 10 m weather station wind speed and direction data was obtained for the year 2001 and the handheld anemometer was used to measure wind speed at 16 different positions around the base.

The average wind speed at the base for the year 2001 was 10.84 m/s, with an hourly averaged maximum wind speed of 38.9 m/s, at 10 m height. The analysis of the wind direction data clearly shows that the winds are highly directional, coming from an eastern and southeastern direction. The data from the handheld device was used to create a wind speed map of the area around the base, in order to select the most suited wind turbine position. The effect of Catabatic winds and maximum wind gusts should be measured and analyzed before the budget is allocated for this project.

The wind characteristics were then analyzed using Weibull distribution functions. These functions are integrated to calculate the power density of the wind. The most frequent wind speed and the wind speed carrying the maximum energy are derived. In order to calculate the power that can theoretically be extracted from the wind, using the Betz Law, has also been derived. Once all the derivations were completed, 5 different wind turbines were selected, ranging in size from 10 kW to 100 kW, and their performance was analyzed. Included in the evaluation is obtaining: regression models for the power curves, the real power output, the power coefficient, the annual energy output, the annual operating time and operating percentage of the wind turbine, and the capacity factor. Based on this evaluation, the most suited wind turbine is the North Wind NW100/19 wind turbine, which has an annual energy production of 430 MWh, an annual operating percentage of 6942 h and a capacity factor of 49 % based on the 2001 wind data.

The site survey was based on the 16 positions where wind speeds were measured, using the hand-held anemometer. The survey included the creation of contour maps from GPS data, assessment of the accessibility to and operation area at the sites and anchoring of wind turbines. The result of the survey is that the NW100/19 wind turbine is much better suited

for use at the recommended sites than the other four wind turbines, since it features a self-erecting mechanism. The final position of the wind turbine can only be chosen during the implementation stages, which is beyond the scope of this project. The sites that are mentioned are only recommendations.

Ice accretion on wind turbines operating in cold weather is a common problem. However, since the precipitation at SANAE IV is almost zero during a year, there is no direct problem with ice build up. Also, since the design of the NW100/19 wind turbine is based on predecessors, which have operated successfully at Antarctica, indicates that there should be no problem with low temperatures and icing. It is recommended that the wind turbine should be fitted with deflectors in its ventilation apertures, so that snow buildup inside the nacelle is prevented. Other options to reduce snow ingress were discussed in section 9.3.

The next step in the study was to investigate the connection of the wind turbine to the existing electricity grid. The output of the diesel generators is 3-phase 380 VAC at 50 Hz. The wind turbine connection to the grid is very simple, since its generator can be purchased with an output line of 380 VAC at 50 Hz. Thus the connection to the grid should be no problem. The different modes of operation of the hybrid wind diesel system were analyzed and the control system for the wind turbine was investigated. It is recommended that the control system manufactured by the wind turbine manufacturers should be used, in order to avoid compatibility problems. The use of an energy storage facility is not recommended, as it is a costly procedure and should be analyzed separately.

The economic viability analysis of utilizing wind energy at SANAE IV was done using the specifications of the NW100/19 wind turbine, because it was shown in the technical analysis that the NW100/19 wind turbine is the best suited wind turbine, from the 5 different wind turbines mentioned, for operation at SANAE IV, Antarctica. With a yearly energy output of 430 MWh, a saving of about 60400 L of SAB diesel fuel is possible. The discounted payback period of the initial capital invested, taking annual expenses and savings in account, is estimated to be 10 years. The payback calculation includes interest

on capital, fuel, labor and maintenance escalation rates and general inflation. The internal rate of return for a capital investment of R3.5million, which is the capital needed to purchase, install and operate the wind turbine, is 15 %. The economic analysis was extended to calculate the cost per unit energy produced. The hybrid wind-diesel system features a cost per kWh of R1.63/kWh, therefore reducing the current cost per kWh of the base by nearly 20 %. The result of the economic analysis is that the proposed system is economically viable, although it has a payback period of 10 years.

The environmental analysis shows that the only effect that the wind turbine has on the Antarctic environment is the visual impact. However there is ample justification for the visual impact, if one considers a reduction in emissions by nearly 20 %, due to energy supply sharing by the wind turbine. Therefore it can be concluded that all the aims of the thesis were achieved and the results clearly show that the proposed hybrid system is technically feasible as well as economically viable for utilizing wind energy at SANAE IV, Antarctica.

The economic analysis should be refined, if a budget is allocated for this project and a wind turbine installation is made possible. New quotations should be obtained for the purchase of a wind turbine. A suitable wind turbine site should be chosen, when all the details regarding the wind turbine installation process have been verified. Another important fact, mentioned in section 7.3.11, is that the design life of the wind turbine has to be taken into account when the economic analysis is refined. The turbine supplier should provide a design life estimate of the turbine, given a higher than usual annual operating percentage of 80 %.

In order to accurately predict the technical feasibility of operating a wind turbine at the station, the energy demand of the base should be measured for at least one year, preferably logging hourly measurements, using the existing logging equipment at the base. The data should be compared to the results obtained in section 4.4, before the budget for the project is being allocated.

14 REFERENCES

Ahmed H and Abouzeid M (2001), Utilization of wind energy in Egypt at remote areas, College of Engineering and Technology, Arab Academy for Science and Technology, Egypt.

Ahmed N and Archer R (2001), Testing of highly loaded horizontal axis wind turbine designed for optimum performance, Aerospace Engineering, University of New South Wales, Australia, http://www.elsevier.com/locate/energy.

Ackermann T and Söder L (2002), An overview of wind energy-status 2002, Royal Institute of Technology, Department of Electric Power Engineering Electric Power Systems, Sweden.

Arnold K (2001), Icing of wind turbines, LIM-Institute für Meteorologie, Universität Leipzig, Germany.

Bakos G and Tsagas N (2002), Techno economic assessment of a hybrid solar/wind installation for electrical energy saving, Laboratory of Energy Economy, Department of Electrical Engineering and Electronics, Democritus University of Thrace, Greece.

Balouktsis A, Chassapis D and Karapantsios T (2001), A nomogram method for estimating the energy produced by wind turbine generators, Department of Mechanical Engineering, Technological Educational Institution of Serres, Greece.

Bazeos N, Hatzigeorgiou G, Karamaneas H, Karabalis D and Beskos D (2002), Static, seismic and stability analyses of a prototype wind turbine steel tower, Department of Civil Engineering, University of Patras, Greece.

Blackadar A (1998), Turbulence and diffusion in the atmosphere, Lectures in environmental sciences, second edition, Springer-Verlag Berlin Heidelberg New York, ISBN 3-540-61406-0, USA.

Brahhimi M, Chocron D and Paraschivoiu I (1998), Prediction of ice accretion and performance degradation of hawt in cold climates, 36th AIAA Aerospace Sciences Meeting and Exhibit.

Beyers J (2003), Numerical analysis of snowdrift surrounding SANAE IV, Antarctica, PhD thesis in progress, Department of Mechanical Engineering, University of Stellenbosch, South Africa.

Beyers J and Harms T (2002), Modeling snowdrift at SANAE IV research station Antarctica, Department of Mechanical Engineering, University of Stellenbosch, South Africa.

Bowen A, Cowie M, Zakay N (2001), The performance of a remote wind-diesel power system, Department of Mechanical Engineering, University of Canterbury, New Zealand, Renewable Energy 22.

Bowen A, Zakay N and Ives R (2002), The field performance of a remote 10kW wind turbine, Mechanical Engineering Department, University of Canterbury, New Zealand.

Brown C, Guichard A, Lyons D (1996), Analysis of the potential for wind and solar energy systems in Antarctica, Institute of Antarctic and Southern Ocean Studies, University of Tasmania, Australia.

Brown C (1997), Renewable energy systems for the Australian Antarctic stations, Degree of Master of Science thesis, Institute of Antarctic and Southern Ocean Studies, University of Tasmania.

Cavall A (1995), Wind turbine cost of electricity and capacity factor, 17th British Wind Energy Association Conference, Mechanical Engineering Publications Limited, London.

Cencelli N (2002), Energy audit of SANAE IV with emphasis on the heating and ventilation system, Project report, Department of Mechanical Engineering, University of Stellenbosch, South Africa.

Cheng C (1999), Characteristics of sea breezes at Chek Lap Kok, Hong Kong Observatory, Technical Note No. 96, Hong Kong.

Craig K and van Reenen A (1996), Unstructured and structured surface grid generation using GPS data, Department of Mechanical and Aeronautical Engineering, University of Pretoria, 1st South African conference on applied mechanics '96.

Drouilhet S (1999), Power flow management in a high penetration wind-diesel hybrid power system with short-term energy storage, National Wind Technology Center, National Renewable Energy Laboratory, USA.

DWEA (2001), Read about Wind Energy, Internet site: http://www.windpower.org, Danish Wind Energy Association, 11/11/2001.

El-Kordy M, Badr M, Abed K and Ibrahim S (2001), Economical evaluation of electricity generation considering externalities, Mechanical Engineering Department, National Research Center, http://www.elsevier.com/locate/energy.

Elhadidy M (2001), Performance evaluation of hybrid (wind/solar/diesel) power systems, Center for Engineering Research, Research Institute, King Fahd University of Petroleum and Minerals, http://www.elsevier.com/locate/energy.

Elhadidy M and Shaahid S (1998), Optimal sizing of battery storage for hybrid (wind + diesel) power systems, Energy Resources Division, Research Institute, King Fahd University of Petroleum and Minerals, http://www.elsevier.com/locate/energy.

Eskander M (2001), Neural network controller for a permanent magnet generator applied in a wind energy conversion system, Electronics Research Institute, Egypt, http://www.elsevier.com/locate/energy.

EWEA (2002), The economics of wind energy, Internet site: http://www.ewea.org, Publications, European Wind Energy Association, 28/08/2002.

Frakovic B and Vrsalovic I (2001), New high profitable wind turbines, Faculty of Engineering, University of Rijeka, Croatia, http://www.elsevier.com/locate/energy.

Fuglsang P and Thomsen K (1998), Site specific design optimization of wind turbines, Wind Energy and Atmospheric Physics Department, Riso National Laboratory, The American Institute of Aeronautics and Astronautics Inc., 36th AIAA Aerospace Sciences Meeting and Exhibit, Publication no. AIAA-98-0059.

Garcia A, Torres J, Prieto E and De Francisco A (1997), Fitting wind speed distributions: A case study, Dpto de Proyectos e Ingenieria Rural, Universidad Publica de Navarra, Spain.

Gevorgian V, Corbus D, Drouilhet S and Holz R (1998), Modeling, testing and economic analysis of a wind-electric battery charging station, National Wind Technology Center, National Renewable Energy Laboratory, USA.

Guichard A, Magill P, Godon P, Lyons D and Brown C (1995), Exploiting wind power in Antarctica, Institute of Antarctic and Southern Ocean Studies (IASOS), University of Tasmania, Australia, Presented at the 1995 Annual Conference of the Australian and New Zealand Solar Energy Society 'Solar' 95'.

Gupta R (2000), Economic implications of non-utility-generated wind energy on power utility, Department of Electrical and Electronic Engineering, Singapore Polytechnic, Singapore, http://www.elsevier.com/locate/energy.

GTZ (1999), Project studies for wind Parks in Walvis Bay and Lüderitz, Deutsche Gesellschaft Für Technische Zusammenarbeit GmbH, Project No. 97.2019.4-001.2, TERNA-Namibia, VN 81015042.

Habali S, Amr M, Saleh I and Ta'ami R (2000), Wind as an alternative source of energy in Jordan, Mechanical Engineering Department, Faculty of Engineering and Technology, University of Jordan, Jordan, http://www.elsevier.com/locate/energy.

Holley W (1998), A regression model for turbulence with reference to wind turbine classes defined in IEC 1400-1, USA, AIAA Aerospace Sciences Meeting and Exhibit, Publication no. AIAA-98-0056.

Isherwood W, Smith J, Aceves S, Berry G, Clark W, Johnson R, Das D, Goering D and Seifert R (1999), Remote power systems with advanced storage technologies for Alaskan villages, Lawrence Livermore National Laboratory (LLNL), USA.

Jagadeesh A (2001), Wind as a supplementary energy source in India, REFOCUS, May, pages16 – 18.

Jurado F and Saenz J (2001), Neuro-fuzzy control for autonomous wind-diesel systems using biomass, Department of Electrical Engineering, University of Jaen, Spain.

Kaldellis J (2002), An integrated time-dependent analysis model of wind energy applications in Greece, Laboratory of Soft Engineering Applications and Environmental Protection, Mechanical Engineering Department, TEI Piraeus, Greece.

Kaldellis J and Gavras T (1999), The economic viability of commercial wind plants in Greece: A complete sensitivity analysis, Laboratory of Soft Energy Applications & Environmental Protection, Mechanical Engineering Department, TEI Piraeus, Greece.

Lace W (2001), Cape winds to power new R90m project, Engineering News, page 50, 3rd August.

Lacroix A and Manwell J (2000), Wind energy: cold weather issues, University of Massachusetts at Amherst, Renewable Energy Research Laboratory.

Lenzen M and Munksgraad J (2001), Energy and CO_2 life-cycle analyses of wind turbines – review and applications, The University of Sydney, Australia.

Lu L, Yang H and Burnett J (2000), Investigation on wind power potential on Hong Kong islands – an analysis of wind power and wind turbine characteristics, Center for Development of Solar Energy Technology, Department of Building Services Engineering, The Hong Kong Polytechnic University, Hong Kong.

Maalawi K and Badawy M (2000), A direct method for evaluating performance of horizontal axis wind turbines, Mechanical Engineering Depratment, National Research Center, Egypt.

Maalawi K and Badr M (2002), A practical approach for selecting optimum wind rotors, Mechanical Engineering Depratment, National Research Center, Egypt.

Magill P, Guichard A and Paterson C (2000), The use of large commercial wind turbines in Antarctica, Poster paper, Australian Antarctic Division, Australia.

Martinez A and Prats P (1999), Wind technology issues, Ecotecnia S.C.C.L., Spain, Renewable Energy 16.

Mathew S, Pandey K and Kumar A (2001), Analysis of wind regimes for energy estimation, Department of Farm Power Machinery and Energy, Kelappaji College of Agricultural Engineering and Technology, India.

Muljadi E, McNiff B and LaWhite N (1998), Characterizing wind turbine system response to lightning activity: Preliminary results, National Renewable Energy Laboratory, USA, 36th AIAA Aerospace Sciences Meeting and Exhibit, Publication no. AIAA-98-0059.

McKenna E and Olsen T (1999), Performance and economics of a wind-diesel hybrid system, NREL / SR-500-24663, NREL, Tim Olsen Consulting.

NPS1 (2002), Universal wind diesel controller, Product brief, Northern Power Systems, USA, email: Imott@northernpower.com, June 6th.

NPS2 (2002), The north wind NW100/19 – simplicity by design, Product brief, Northern Power Systems, USA, email: Imott@northernpower.com, June 6th.

NPS3 (2002), E-mail received from Northern Power Systems by J Stover, email: Imott@northernpower.com, June 6th.

Papadopoulos D and Dermentzoglou J (2001), Economic viability analysis of planned WEC system installations for electrical power production, Electrical Machines Laboratory, Department of Electrical and Computer Engineering, Democritos, University of Thrace, Greece.

Papathanassiou S and Papadopoulos M (2001), Dynamic characteristic of autonomous wind-diesel systems, National Technical University of Athens, Department of Electrical and Computer Engineering, Electric Power Division, Greece.

Potts J, Pierson S, Mathisen P, Hamel J, and Babau V (2001), Wind energy resource assessment of western and central Massachusetts, Worcester Polytechnic Institute (WPI), Worcester, AIAA-2001-0060.

Pryor S and Barthelmie R (2001), Statistical analysis of flow characteristics in the coastal zone, Atmospheric Science Program, Department of Geography, Indiana University, USA.

Rogers A, Manwell J, McGowan J and Ellis A (2001), Design requirements for medium-sized wind turbines for remote and hybrid power systems, Renewable Energy Research Laboratory, Department of Mechanical and Industrial Engineering, University of Massachusetts at Amherst, USA.

Salmon J and Walmsley J (1998), A two-site correlation model for wind speed, direction and energy estimates, Zephyr North, Canada, http://www.elsevier.com/locate/energy.

SANAE Technical (1999), Technical specifications on SANAE IV, Internet site: http://www.geocities.com/Yosemite/Geyser/3161/tech/tech.html.

SANAE Weather (2000), SANAE IV weather data, Internet site: http://www.geocities.com/sanaeiv/weather/weather.html, South African Weather Bureau.

Scheepers J and van der Linde S (1998), Warmer weather necessitates heating adjustments at SA's Antarctic base, Journal of the South African Institute of Refrigeration and Air Conditioning.

Seguro J and Lambert T (1999), Modern estimation of the parameters of the Weibull wind speed distribution for wind energy analysis, Department of Mechanical Engineering, Colorado State University, USA, http://www.elsevier.com/locate/energy.

Sen Z (1999), Stochastic wind energy calculation formulation, Meteorology Department, Energy Group, Istanbul Technical University, Turkey.

Steel J D (1993), Alternative energy options for Antarctic stations, Swinburne University, Thesis for the Graduate Diploma of Antarctic and Southern Ocean, Institute of Antarctic and Southern Ocean Studies (IASOS), University of Tasmania, Australia.

Stover J (2002), Wind – diesel fundamentals, Northern Power Systems, USA, email: Imott@northernpower.com, June 6th.

Sullaiman M, Akaak A, Wahab M, Zakaria A, Sulaiman Z and Suradi J (2002), Wind characteristics of Oman, Physics Department, Faculty of Science and Environmental Studies, University of Putra Malaysia, Malaysia, Energy 27 (2002) 35–46.

Sullivan W, Bontadelli J and Wicks E (2000), Engineering economy, ISBN 0-13-011570-3, Prentice-Hall Inc., USA.

Tariq M (2002), Modeling and control of a wind fuel cell hybrid energy system, Faculty of Engineering, MUN, Canada.

Taylor P (2001), Wind power today: 2000 wind energy program highlights, Produced for the U.S. Department of Energy, www.sciencedirect.com.

Taylor A, Gunalsevam J and Bester W (2002), Investigation into reducing the impact of diesel engines on the Antarctic environment with associated maintenance benefits, Unit for vehicle propulsion, Institute for Thermodynamics and Mechanics, Department of Mechanical Engineering, University of Stellenbosch, South Africa.

Teetz H (2000), Heating and ventilation system analysis and redesign of the SANAE IV base in Antarctica, Project report, Department of Mechanical Engineering, University of Stellenbosch, South Africa.

Valtchev V, Van den Bossche A, Ghijselen J and Melkebeek J (2000), Autonomous renewable energy conversion system, University of Gent, Department of Electrical Power Engineering, Laboratory for Electrical Machines and Power Electronics, Belgium.

White F (1991), Viscous Fluid Flow, second edition, McGraw-Hill International Editions, Mechanical Engineering Series, ISBN 0-07-100995-7, USA.

Wilke S (2001), BWC XL.1 Tilt.Tower installation manual, Bergey Windpower Co. Inc., USA, http://www.bergey.com, Version 2.

Wilks N (2000), Engineer's Antarctic role, Professional Engineering, Test and Measurement: Special report, pages 42-43.

Winterstetter T and Schmidt H (2002), Stability of circular cylindrical steel shells under combined loading, Department of Civil Engineering, University of Essen, Germany.

Yusof Sulaiman M, Akaak A, Wahab M, Zakaria M, Sulaiman Z and Suradi J (2000), Wind characteristics of Oman, Physics Department, Faculty of Science and Environmental Studies, University Putra Malaysia, Malaysia, http://www.elsevier.com/locate/energy.

Zill D and Cullen M (1996), Advanced Engineering Mathematics, ISBN 0-534-92800-5, PWS Publishing Company, USA.

APPENDIX A: PROGRAMS USED FOR DATA MANIPULATION

The programs listed below were used to convert the year data, used in chapters 5, 6 and 7, into a workable format. Microsoft Visual Basic version 6 was used to write the programs. The data obtained from SAWS provides one value for wind speed and direction for each hour during a month. This value has to be split, so that the wind speed and direction data can be analyzed separately. Program 1 has been used to convert the data, so that it can be used to analyze the data based on hourly measurements. Program 2 has been used to convert the data, so that wind analyses can be done using daily averages. This includes sorting the data in a top-down approach, where all the data is listed in one column, so that the analysis of the data is considerably simplified.

Program 1:

```
Private Sub Start_Click()
Dim nodays As Double, filename As Double
Dim data(1 To 100, 1 To 100) As Double
Dim dataf(1 To 100, 1 To 100) As Double
Dim count As Double
Dim counter As Double
Let prompt = "Enter the name of the file containing the information, including the
fileextension."
'Let filename = InputBox(prompt, "Name of File")
Open App.Path & "\winddata.txt" For Input As #1
Let nodays = Val(Text1)
result.Cls
result.Print "This month has"; nodays; "days."

For i = 1 To nodays
   For j = 1 To 53
      Input #1, data(i, j)
      'result.Print data(i, j);
      Next j
      'result.Print
```

```
    Next i
    Close #1
Open App.Path & "\modwinddata.txt" For Output As #2
Let count = 0
Let counter = 0
For i = 1 To nodays
    counter = counter + 1
    For j = 1 To 24
        count = count + 1
        dataf(1, j) = data(i, j * 2)
        dataf(1, j) = dataf(1, j) * 10
        dataf(2, j) = data(i, j * 2 + 1)
        dataf(2, j) = dataf(2, j) / 10
        result.Print counter,
        result.Print count,
        result.Print dataf(1, j),
        result.Print dataf(2, j)
        Write #2, counter,
        Write #2, count,
        Write #2, dataf(1, j),
        Write #2, dataf(2, j)
        Next j
    Next i
Close #2
End Sub
```

Program 2:

```
Private Sub Start_Click()
Dim nodays As Double, noday As Double, filename As Double
Dim data(1 To 100, 1 To 100) As Double
Dim dataf(1 To 100, 1 To 100) As Double
Dim count As Double
Dim counter As Double

Let prompt = "Enter the name of the file containing the information, including the fileextension."
'Let filename = InputBox(prompt, "Name of File")
Open App.Path & "\winddataapr.txt" For Input As #1

Let nodays = Val(Text1)
result.Cls
result.Print "This month has"; nodays; "days."

For i = 1 To nodays
   For j = 1 To 53
      Input #1, data(i, j)
      'result.Print data(i, j);
      Next j
      'result.Print
   Next i
   Close #1

Open App.Path & "\avewinddataapr.txt" For Output As #2
For i = 1 To nodays
   For j = 1 To 24
      dataf(i, j) = data(i, j * 2 + 1)
      dataf(i, j) = dataf(i, j) / 10
```

```
        result.Print dataf(i, j);
        Write #2, dataf(i, j);
        Next j
    result.Print
    Write #2,
    Next i

noday = nodays * 2 - 1
For i = nodays To noday
    For j = 1 To 24
        dataf(i, j) = data(i + 1 - nodays, j * 2)
        dataf(i, j) = dataf(i, j) * 10
        result.Print dataf(i, j);
        Write #2, dataf(i, j);
        Next j
    result.Print
    Write #2,
    Next i

Close #2
End Sub
```

APPENDIX B: WIND ANALYSIS GRAPHS

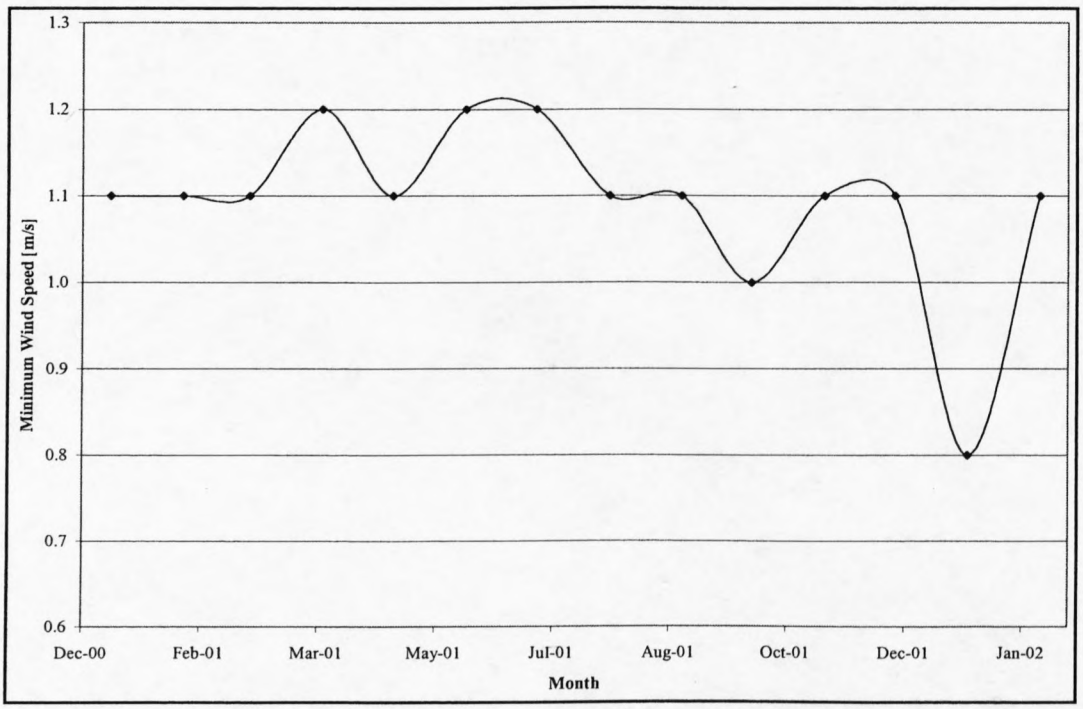

Figure B-1: Minimum wind speed for the period January 2001 to February 2002

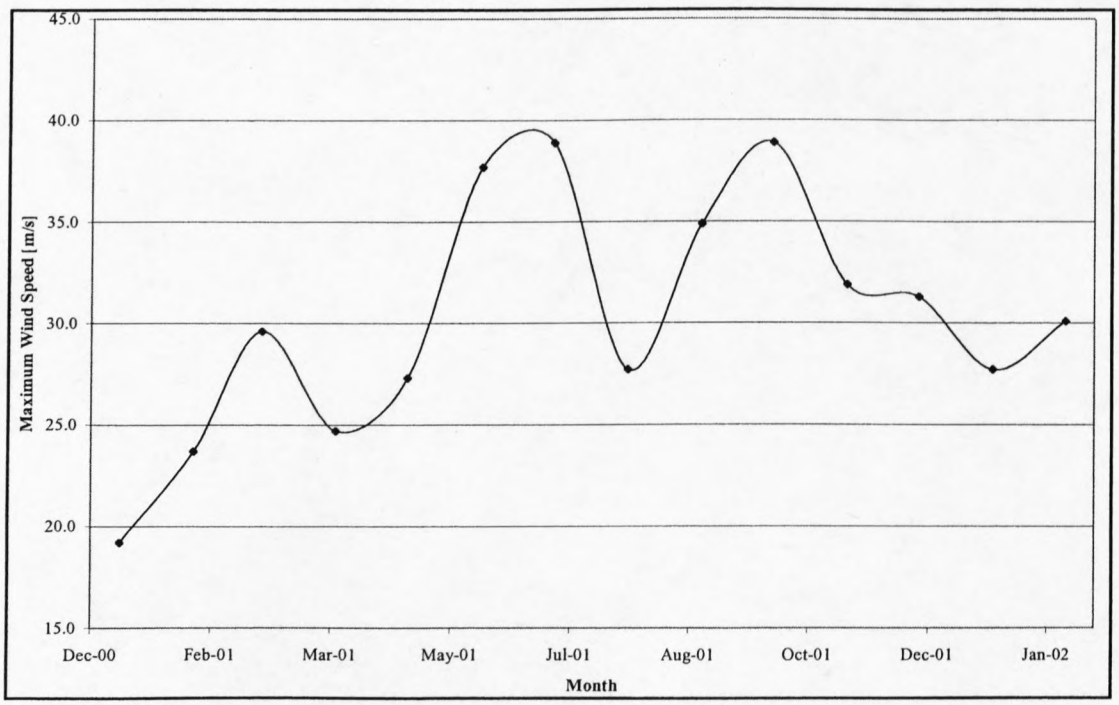

Figure B-2: Maximum wind speed for the period January 2001 to February 2002

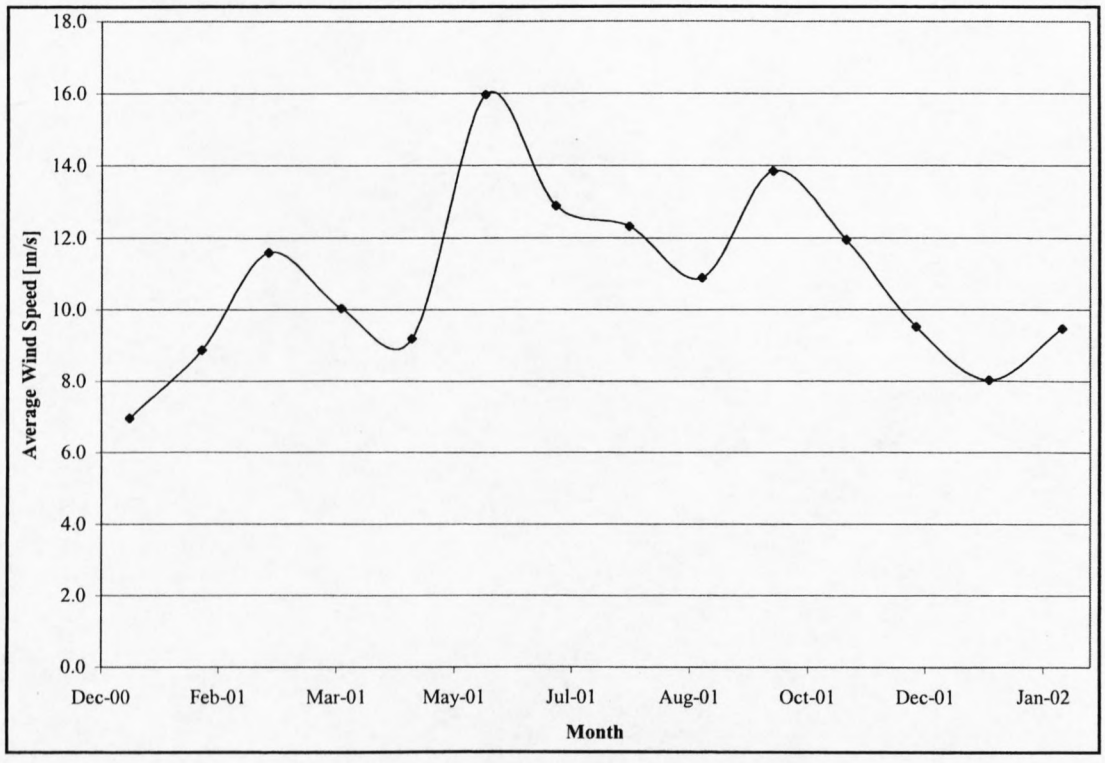

Figure B-3: Average wind speed for the period January 2001 to February 2002

Figure B-1 shows the monthly minimum wind speed, measured at a height of 10 m, at position 4. The values shown in figures B-1 to B-9 are monthly average values.

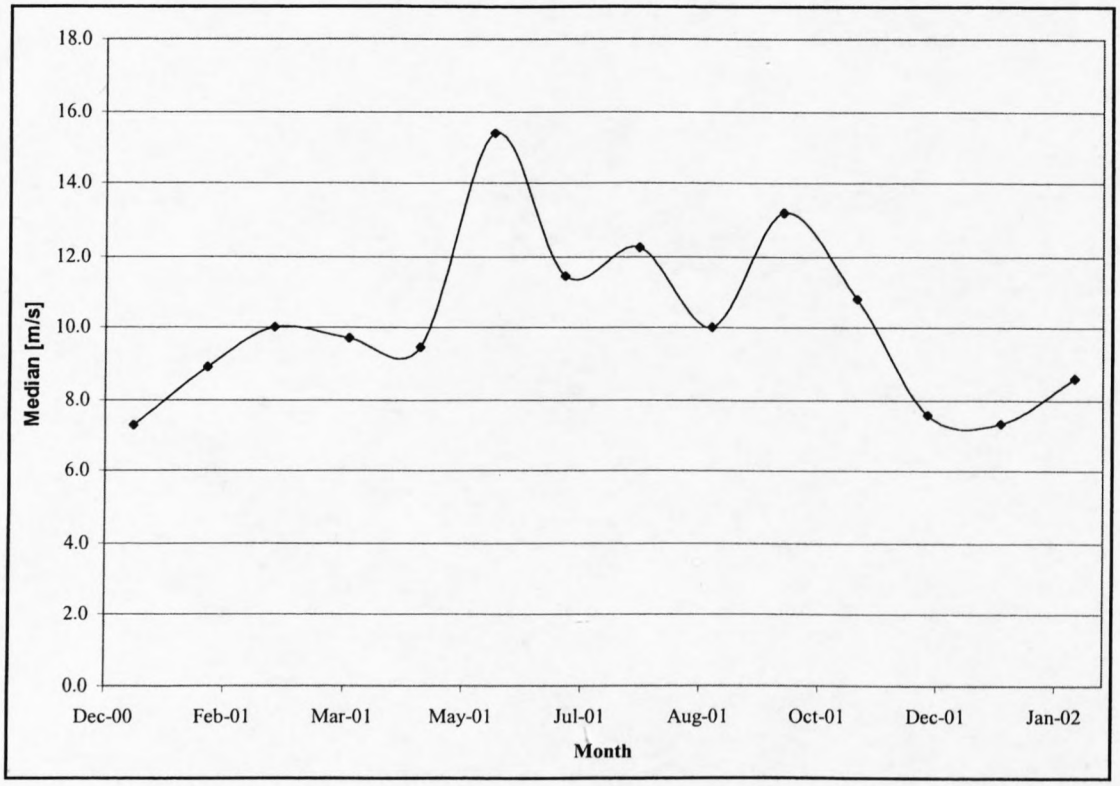

Figure B-4: Median wind speed for the period January 2001 to February 2002

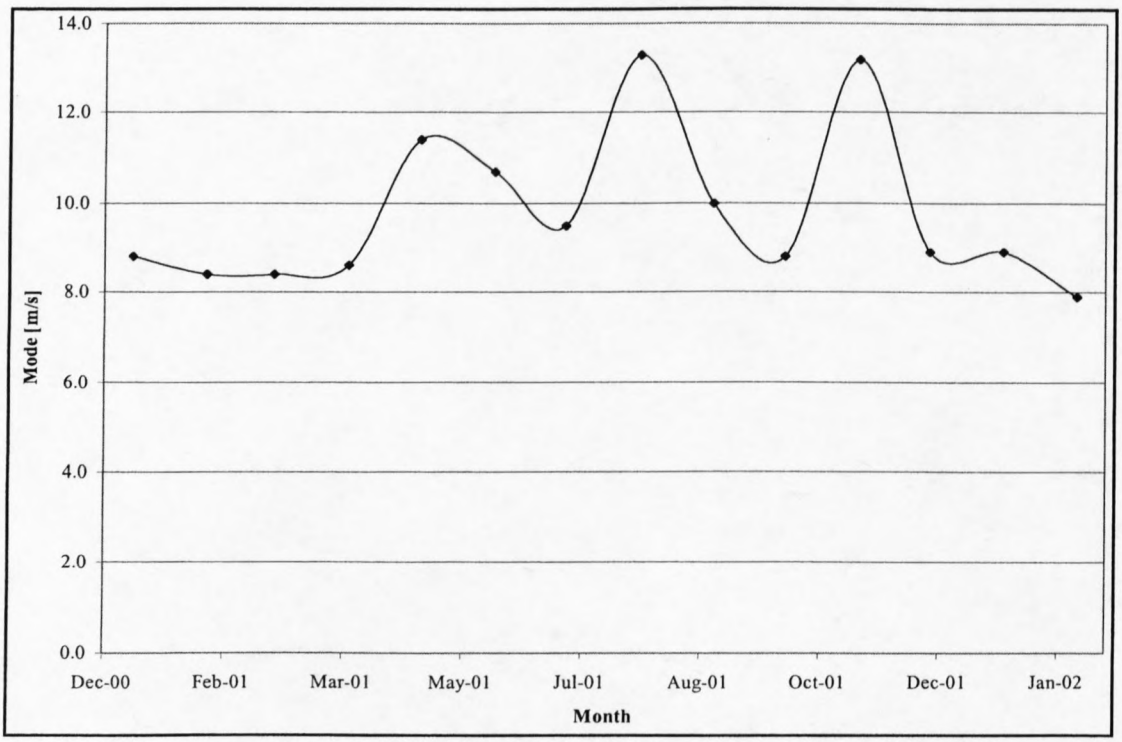

Figure B-5: Mode wind speed for the period January 2001 to February 2002

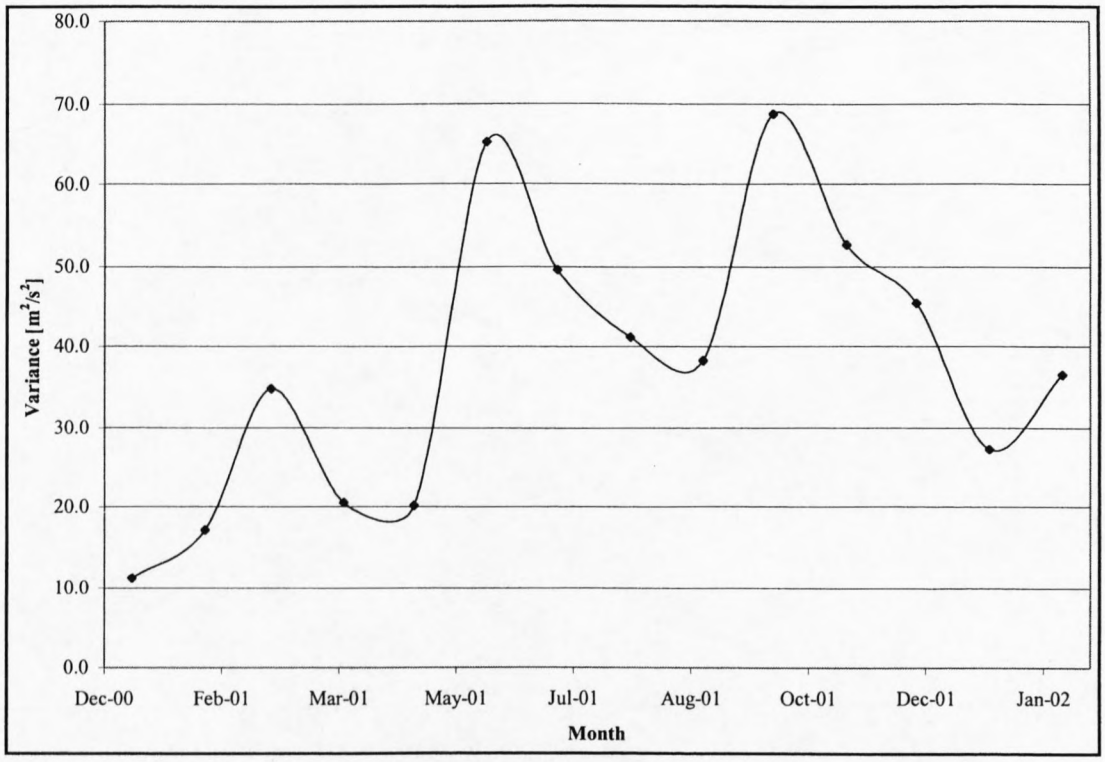

Figure B-6: Variance for the period January 2001 to February 2002

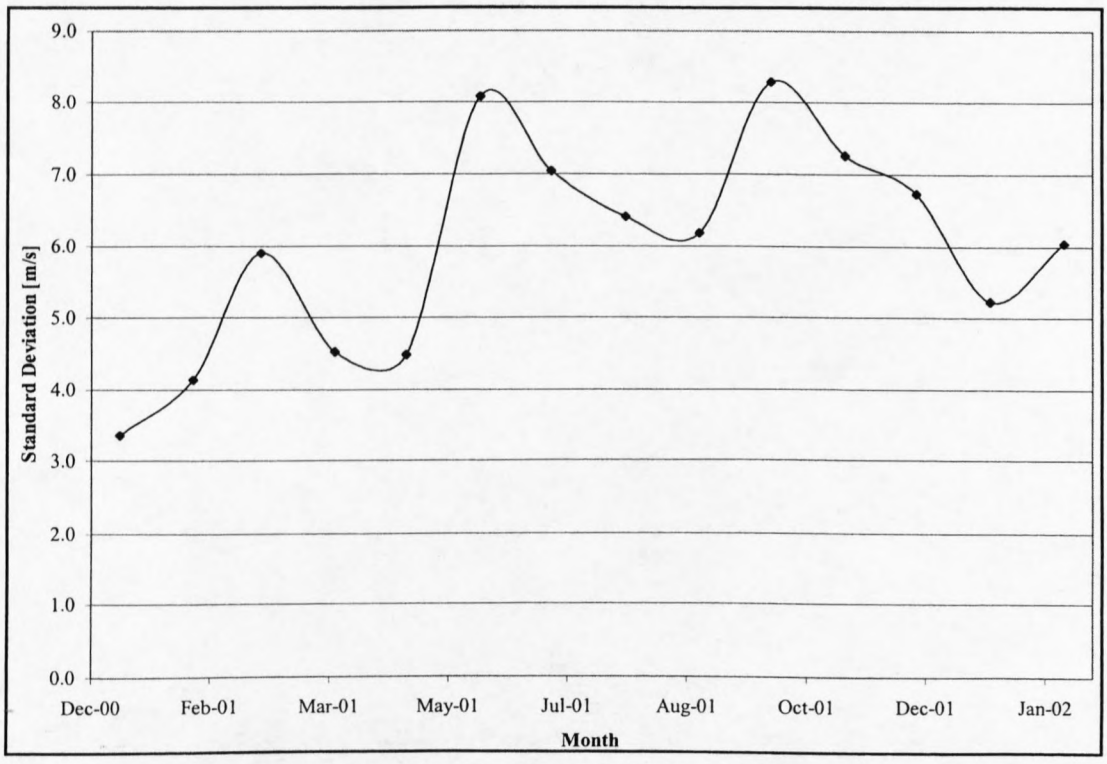

Figure B-7: Standard deviation for the period January 2001 to February 2002

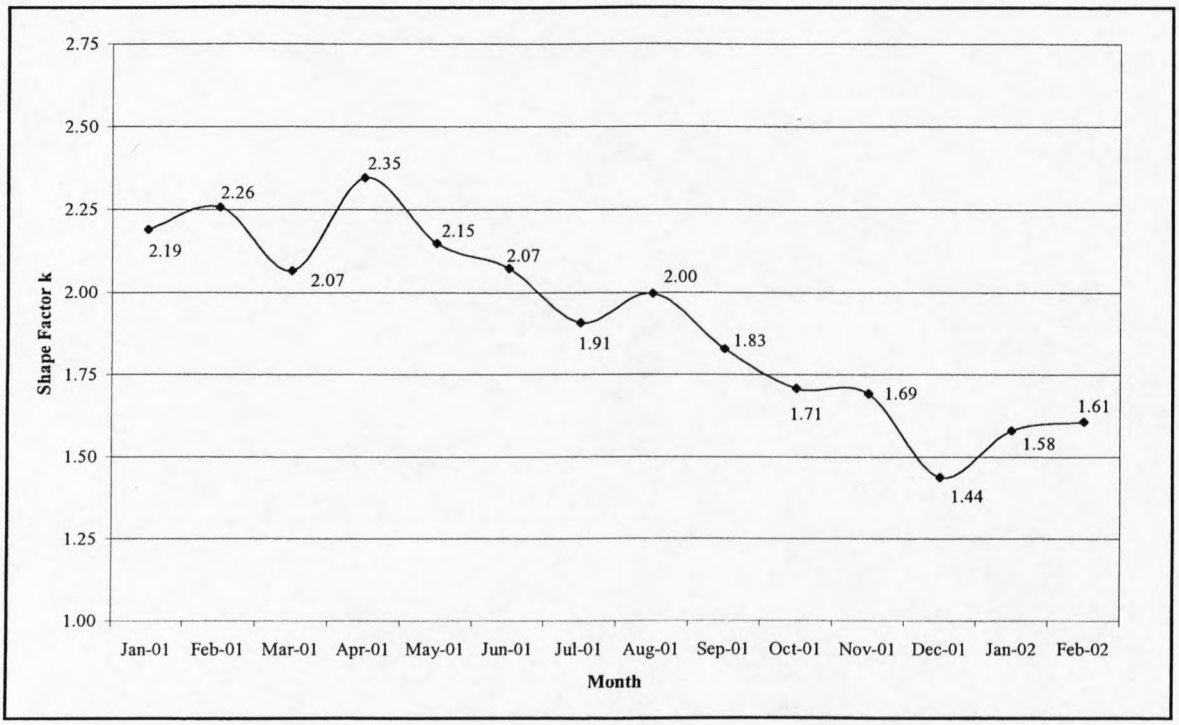

Figure B-8: Weibull shape factor for the period January 2001 to February 2002

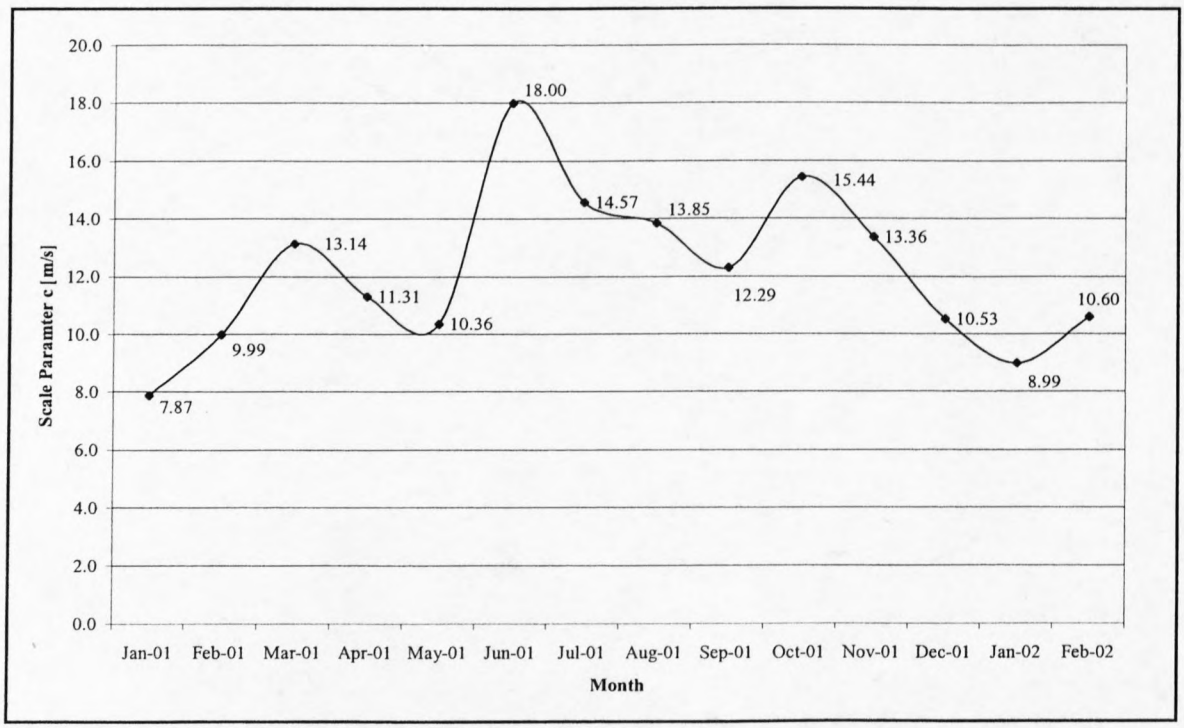

Figure B-9: Weibull scale parameter for the period January 2001 to February 2002

APPENDIX C: WIND SPEED AND FREQUENCY ROSES

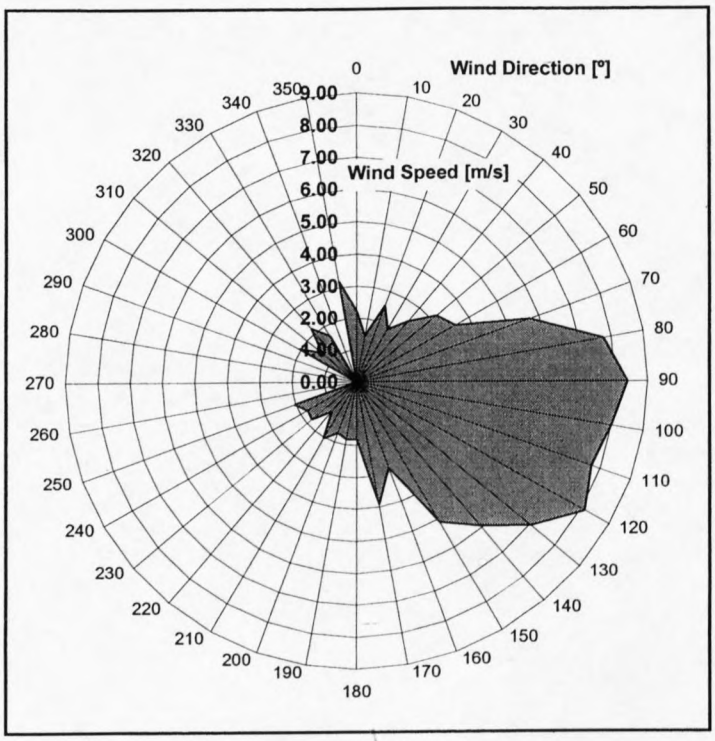

Figure C-1: Wind speed rose for January 2001

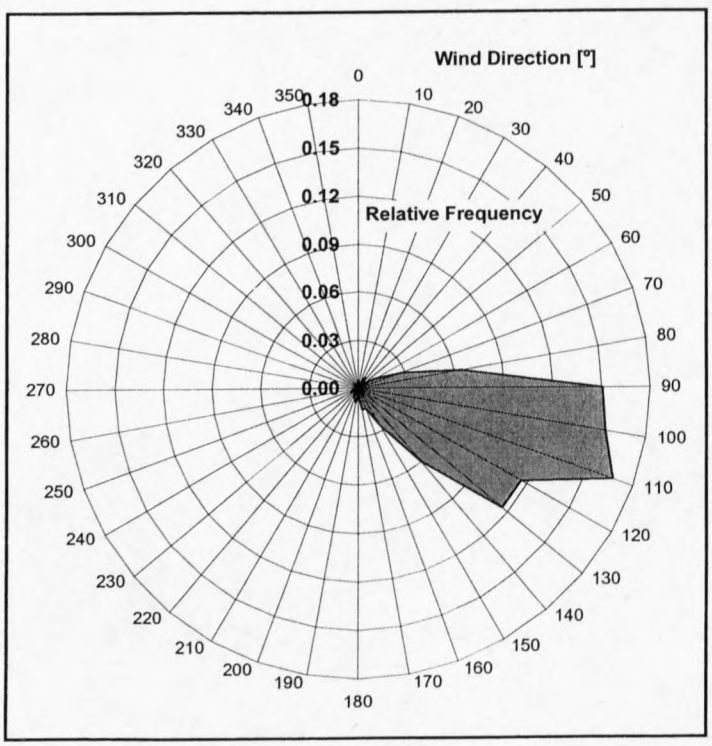

Figure C-2: Wind frequency rose for January 2001

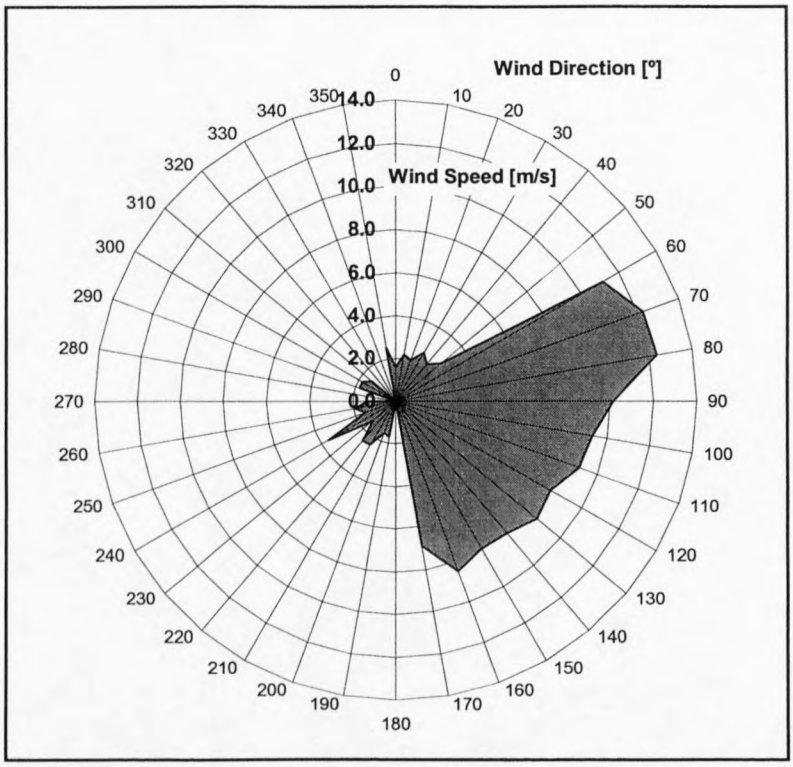

Figure C-3: Wind speed rose for February 2001

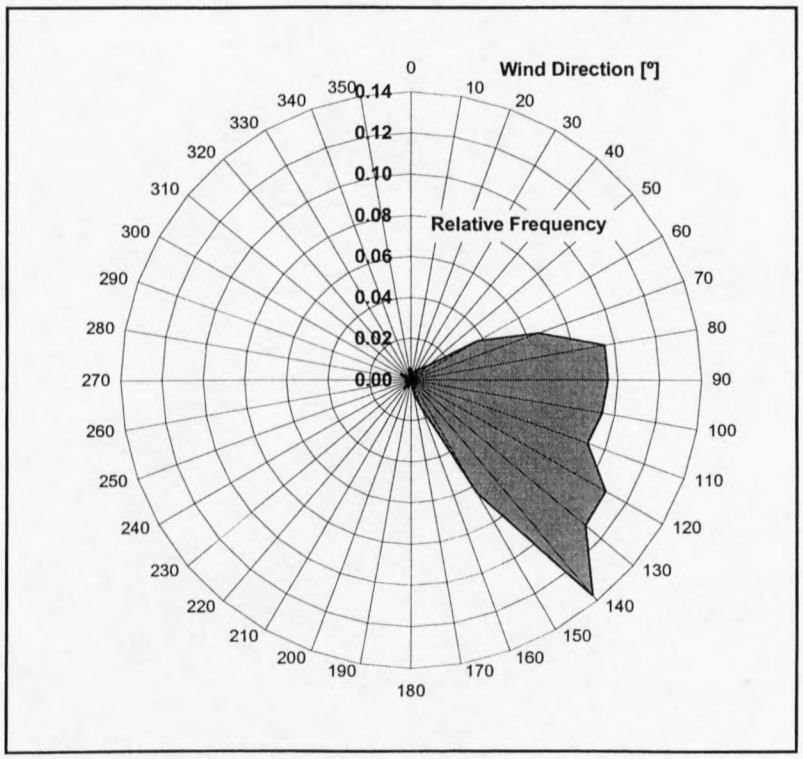

Figure C-4: Wind frequency rose for February 2001

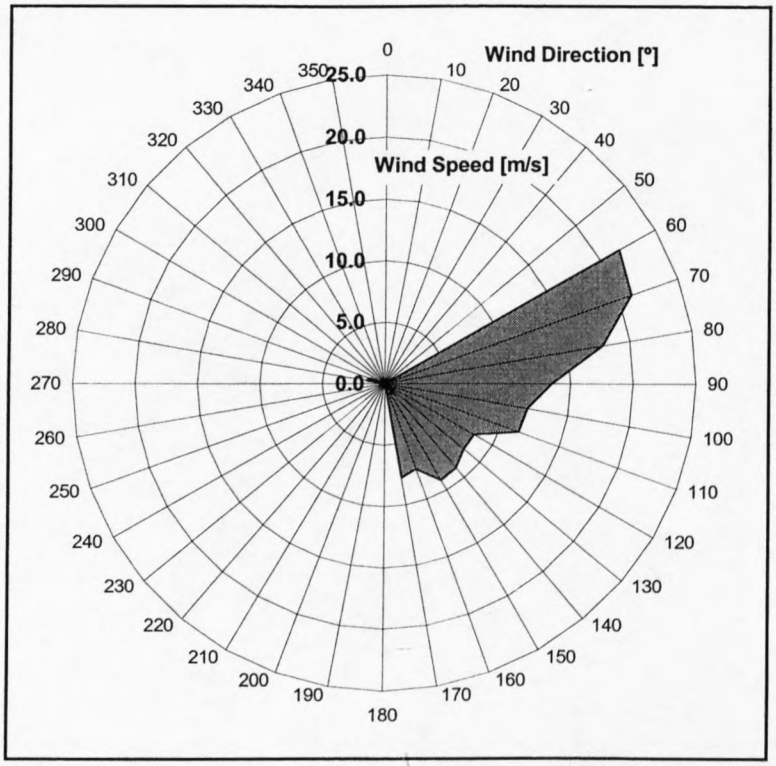

Figure C-5: Wind speed rose for March 2001

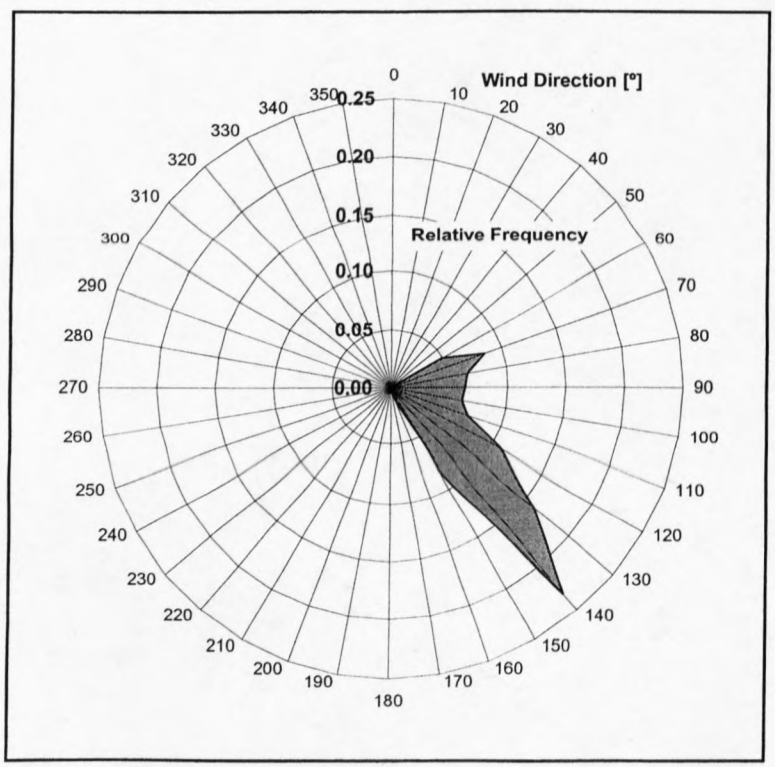

Figure C-6: Wind frequency rose for March 2001

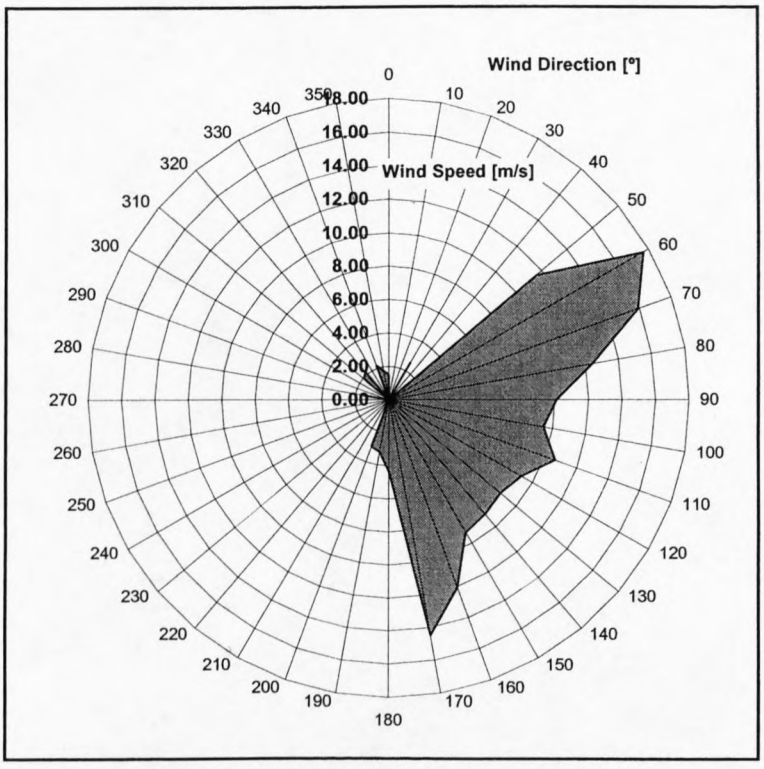

Figure C-7: Wind speed rose for April 2001

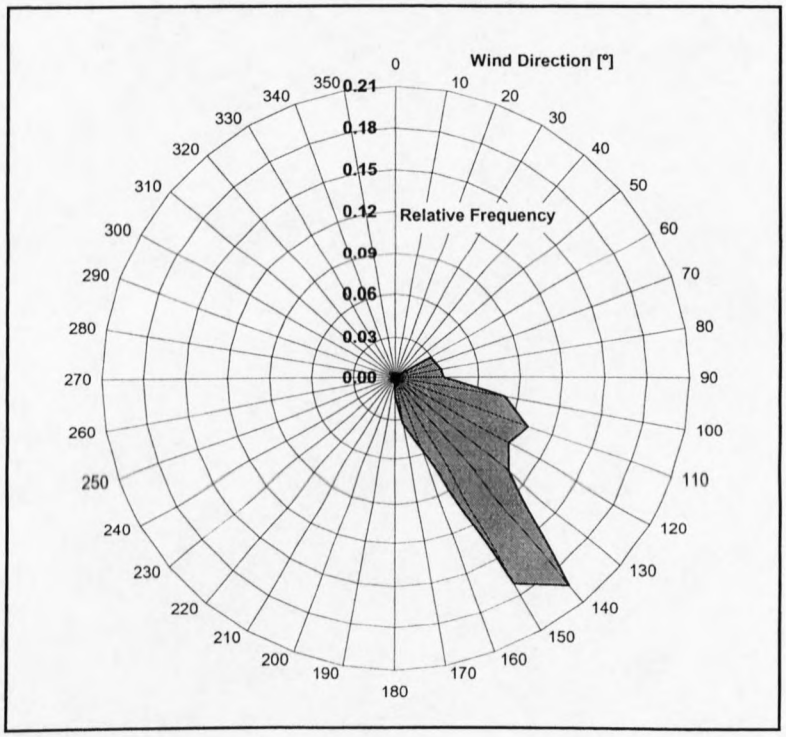

Figure C-8: Wind frequency rose for April 2001

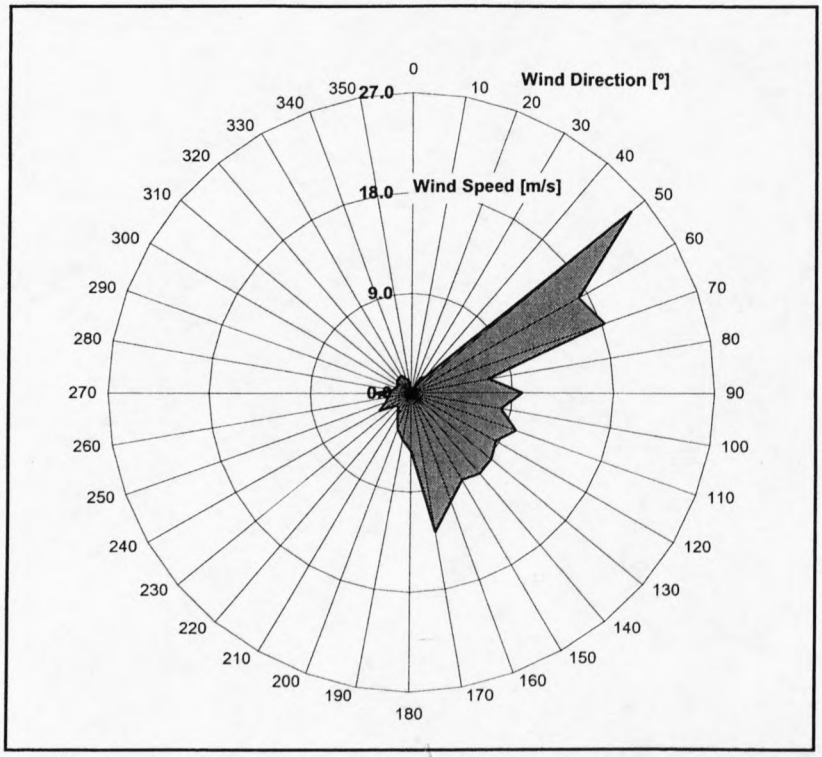

Figure C-9: Wind speed rose for May 2001

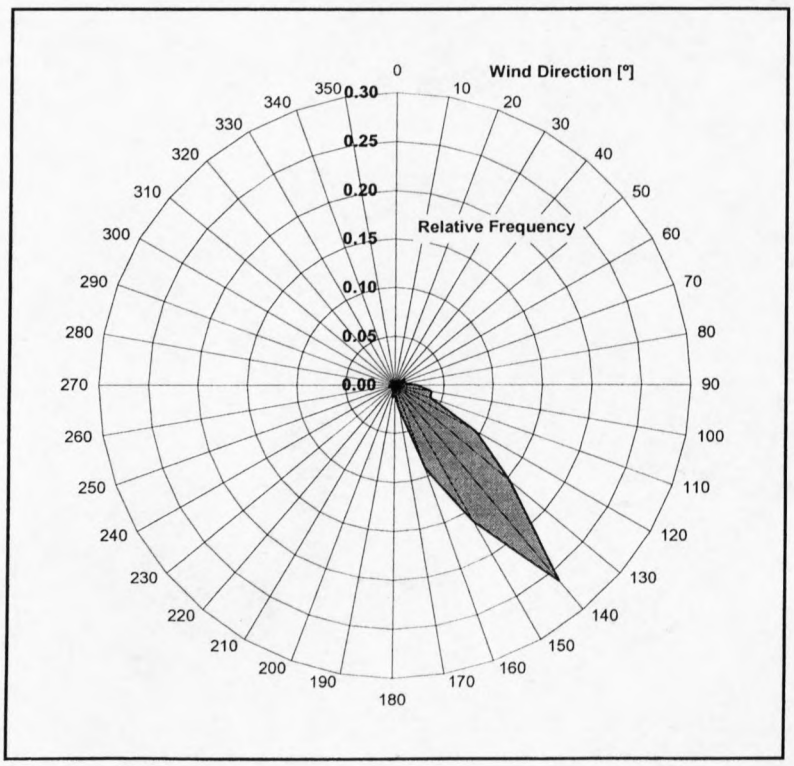

Figure C-10: Wind frequency rose for May 2001

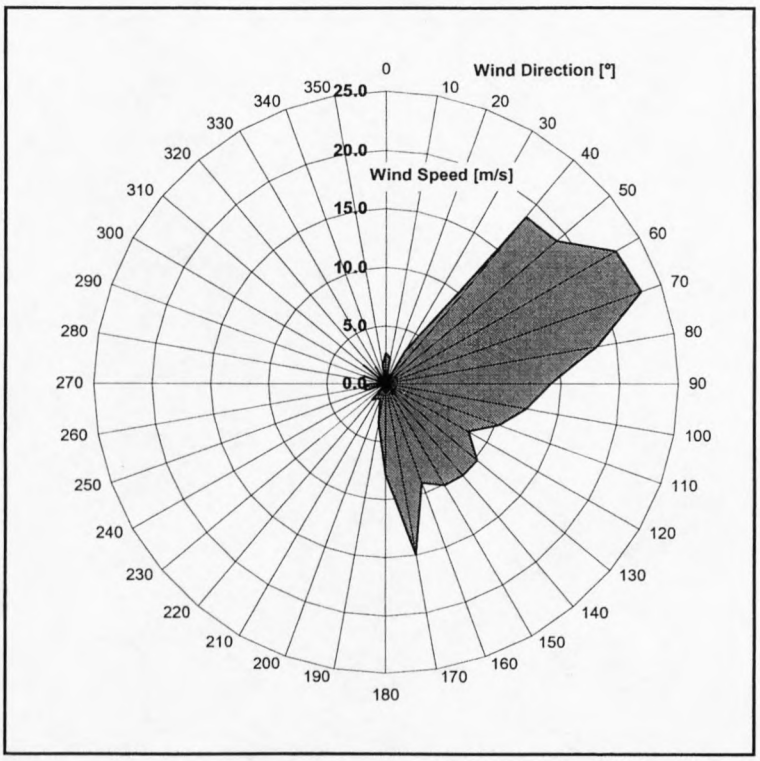

Figure C-11: Wind speed rose for June 2001

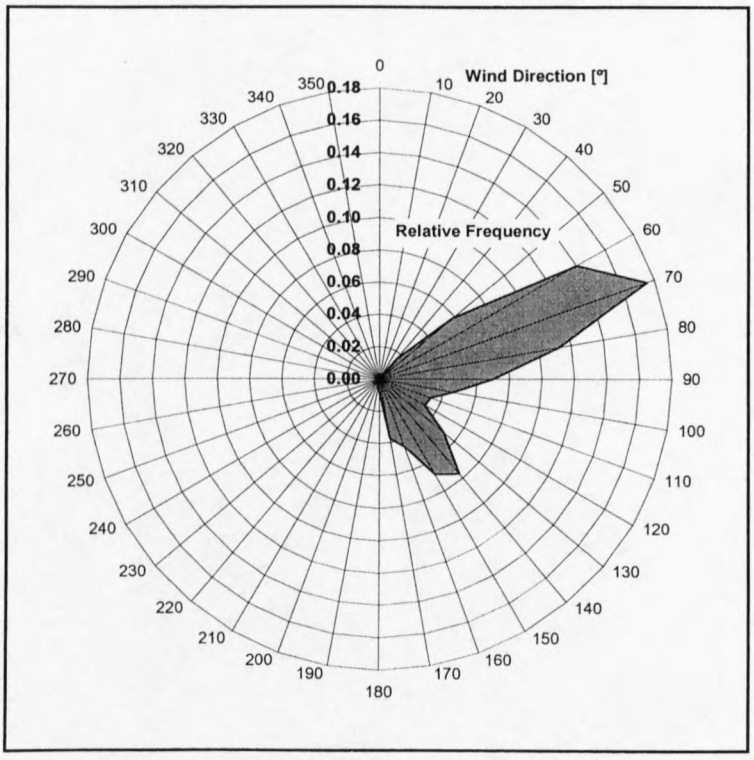

Figure C-12: Wind frequency rose for June 2001

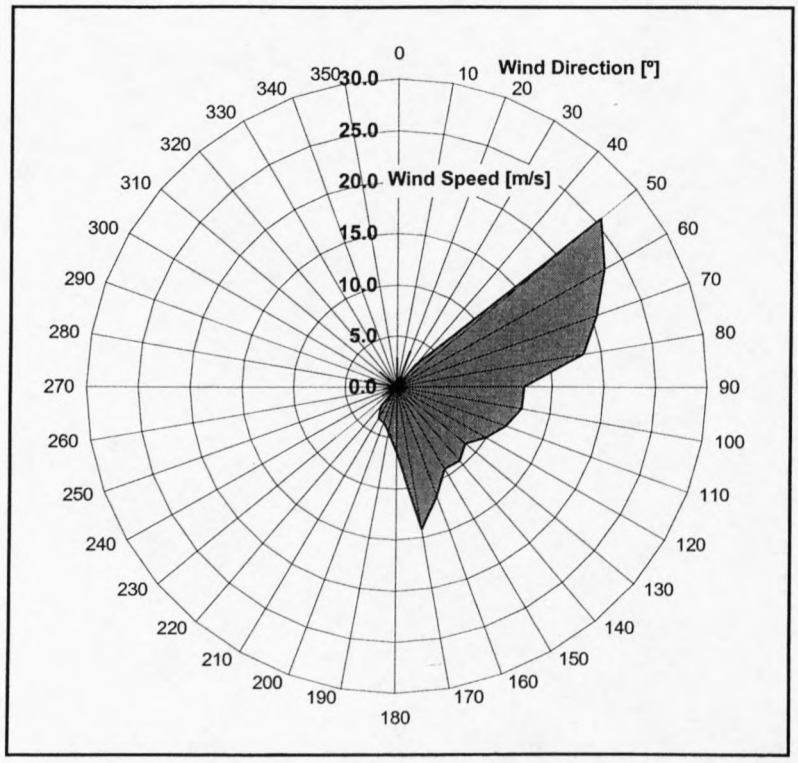

Figure C-13: Wind speed rose for July 2001

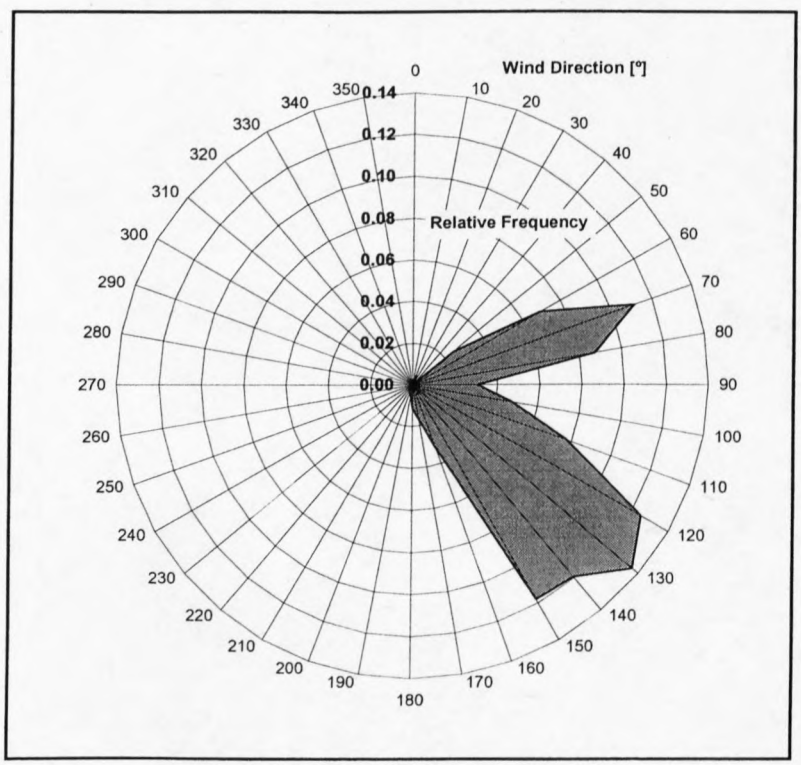

Figure C-14: Wind frequency rose for July 2001

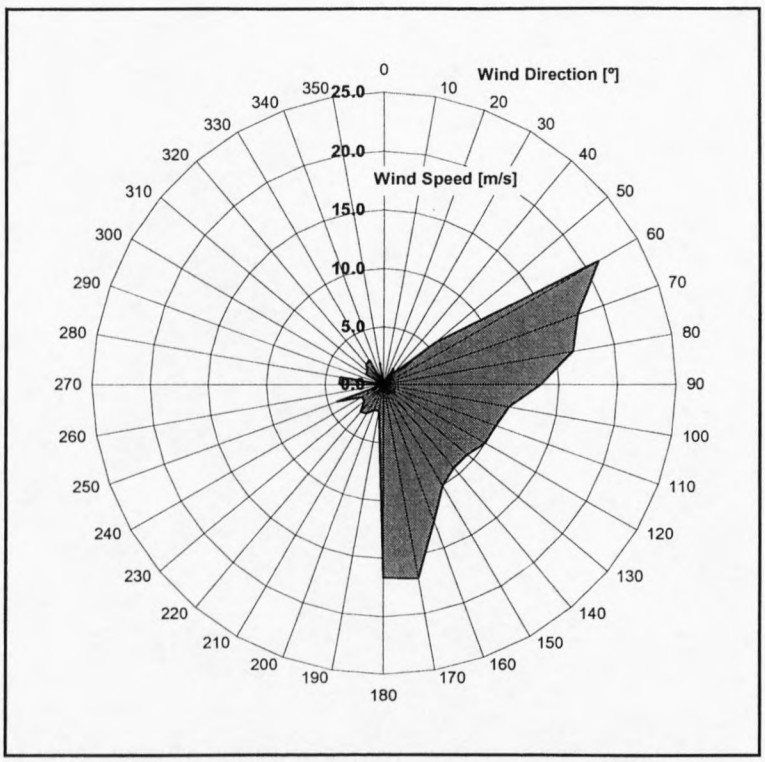

Figure C-15: Wind speed rose for August 2001

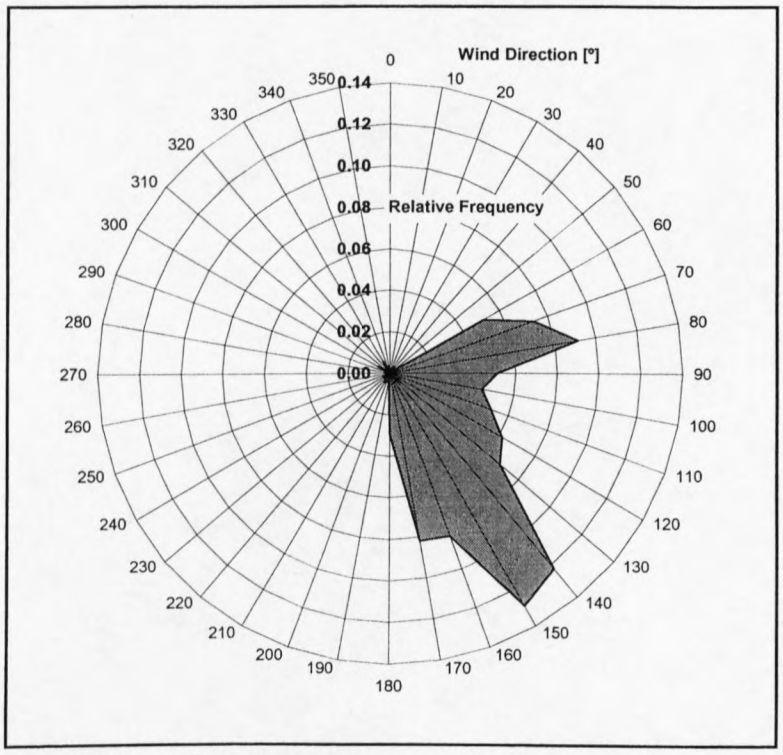

Figure C-16: Wind frequency rose for August 2001

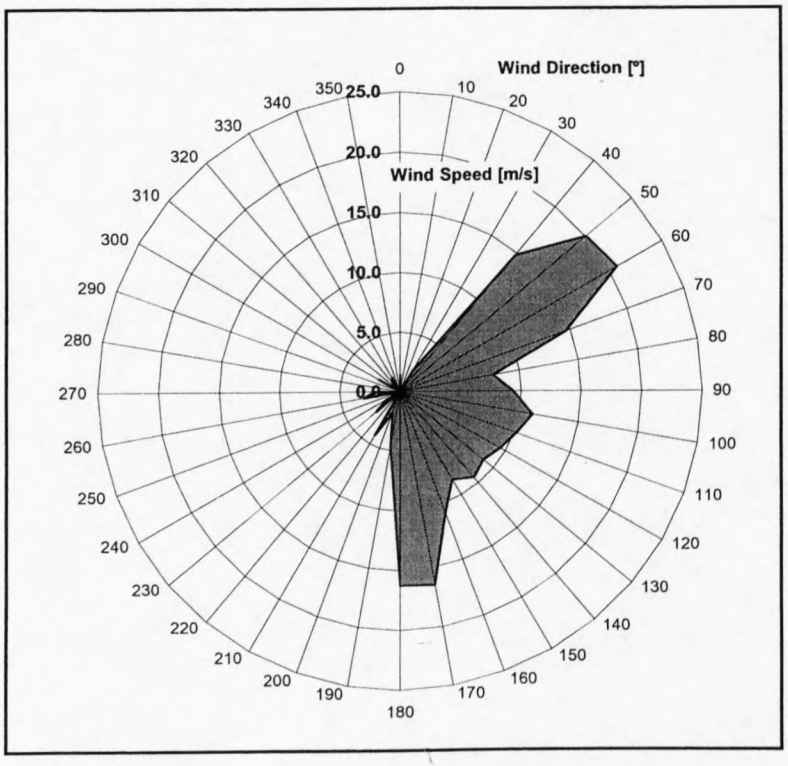

Figure C-17: Wind speed rose for September 2001

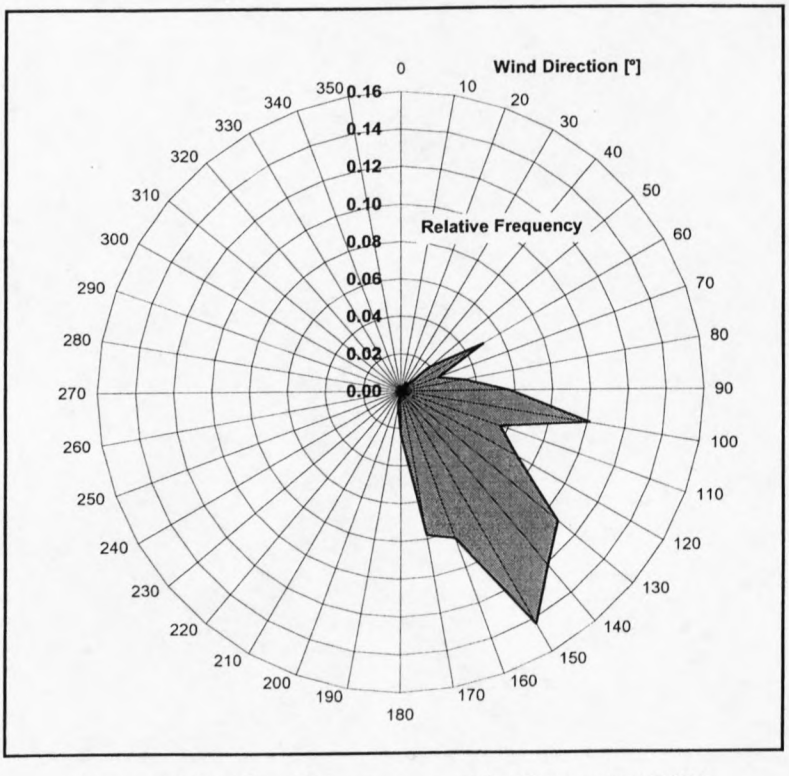

Figure C-18: Wind frequency rose for September 2001

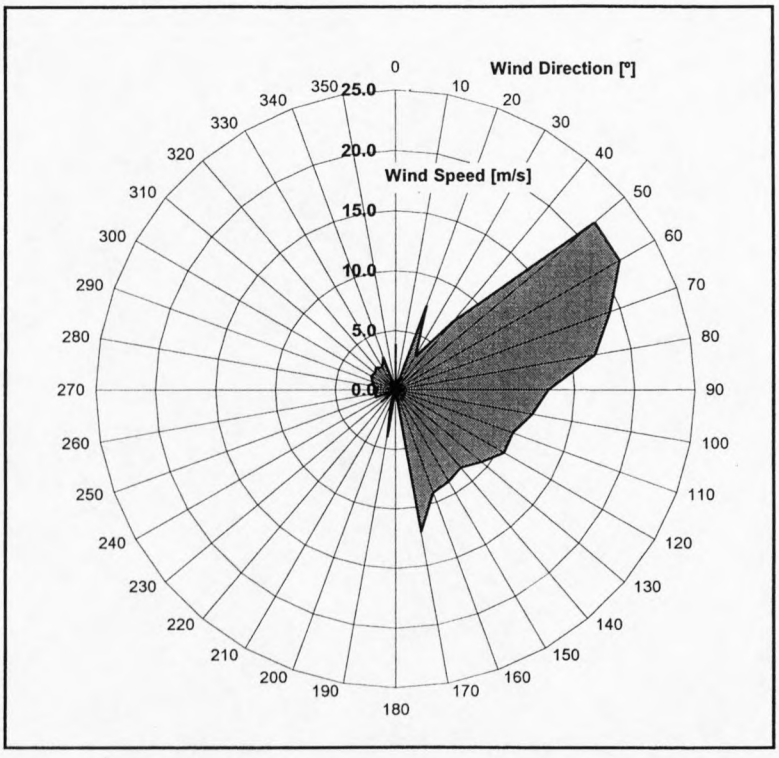

Figure C-19: Wind speed rose for October 2001

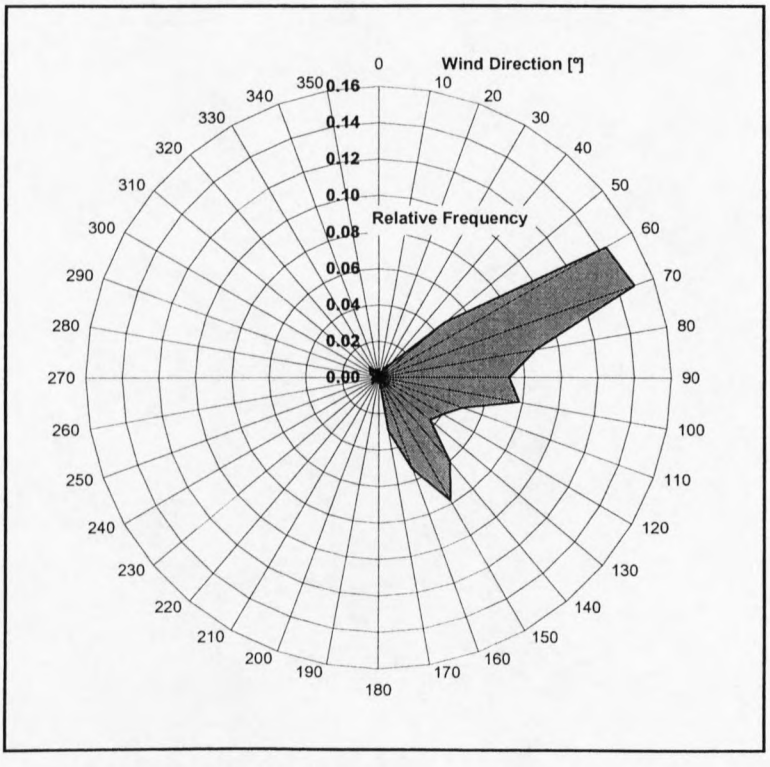

Figure C-20: Wind frequency rose for October 2001

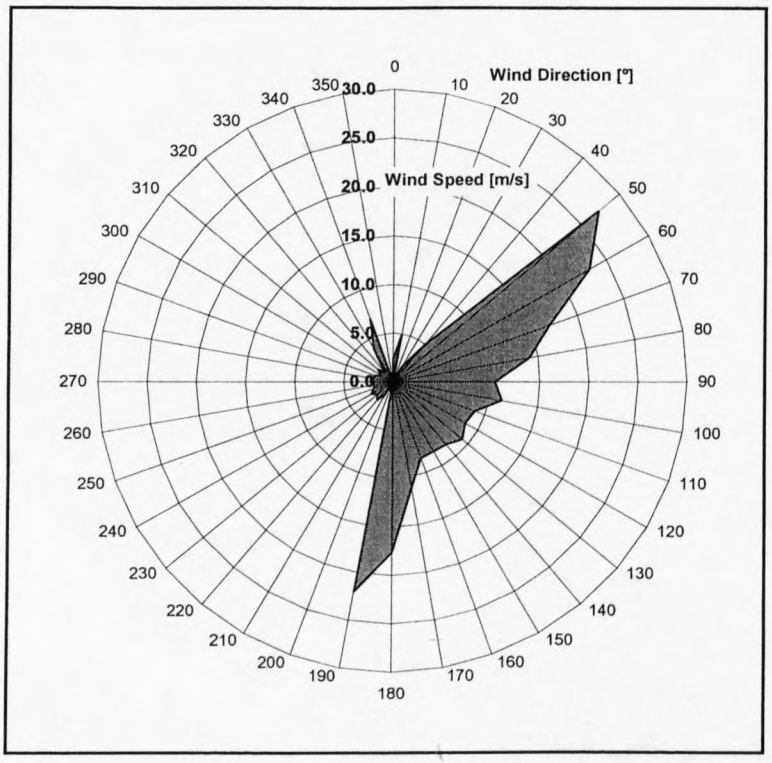

Figure C-21: Wind speed rose for November 2001

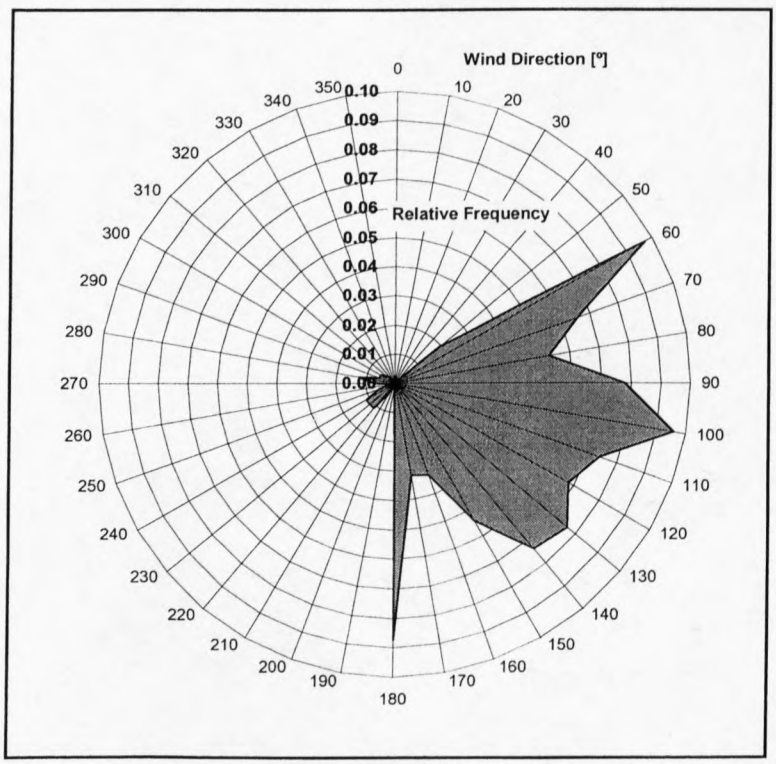

Figure C-22: Wind frequency rose for November 2001

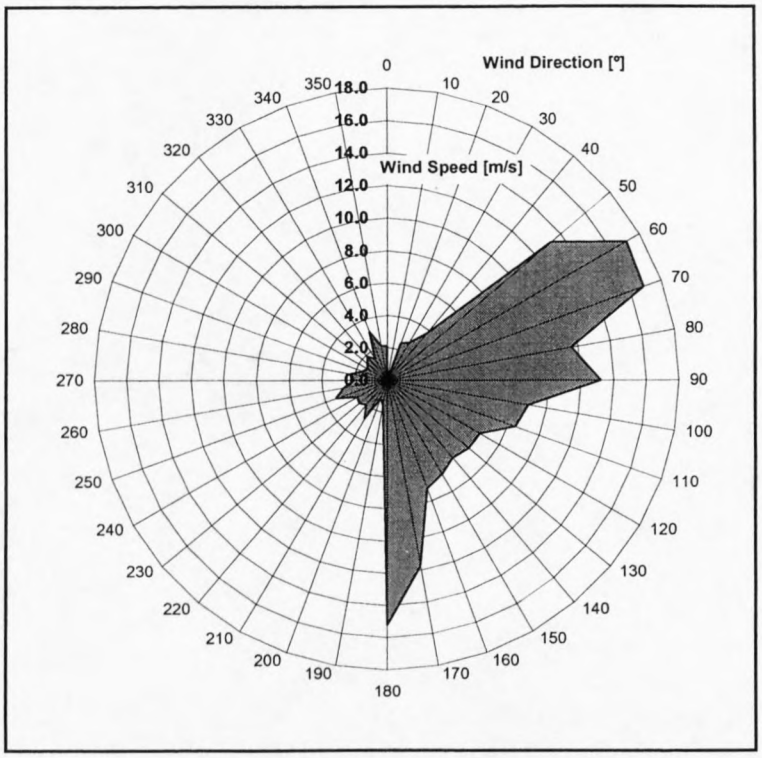

Figure C-23: Wind speed rose for December 2001

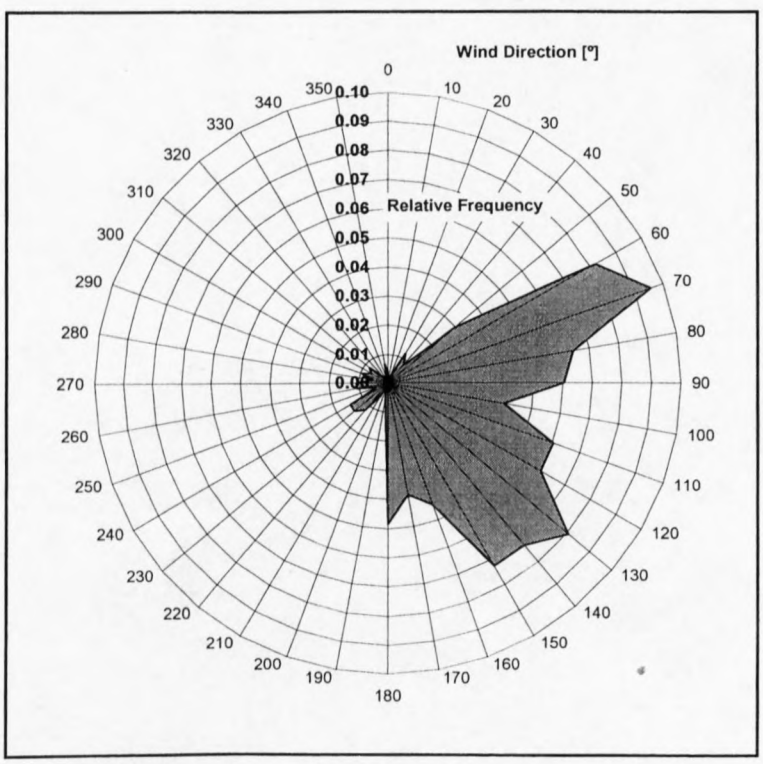

Figure C-24: Wind frequency rose for December 2001

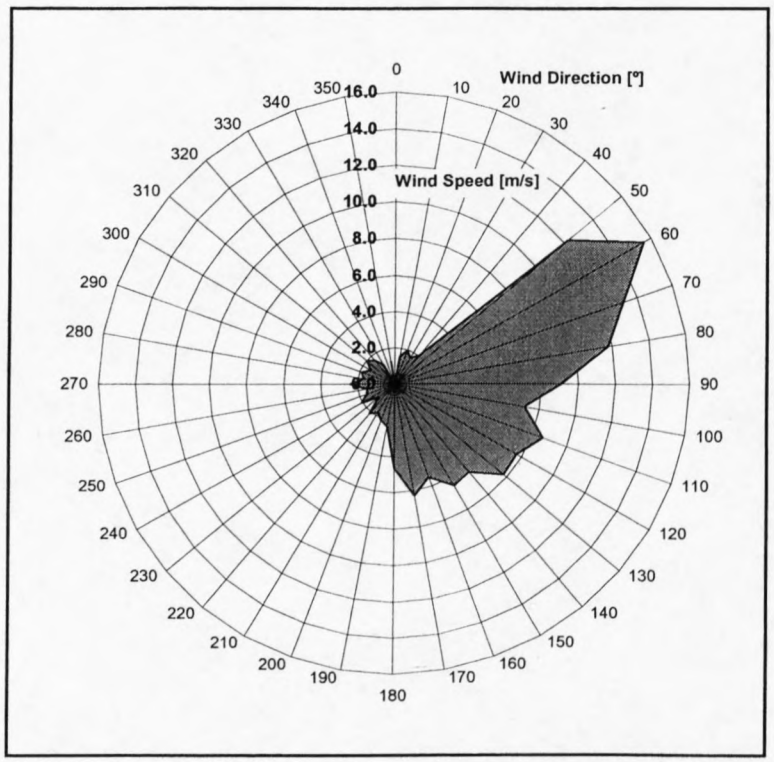

Figure C-25: Wind speed rose for January 2002

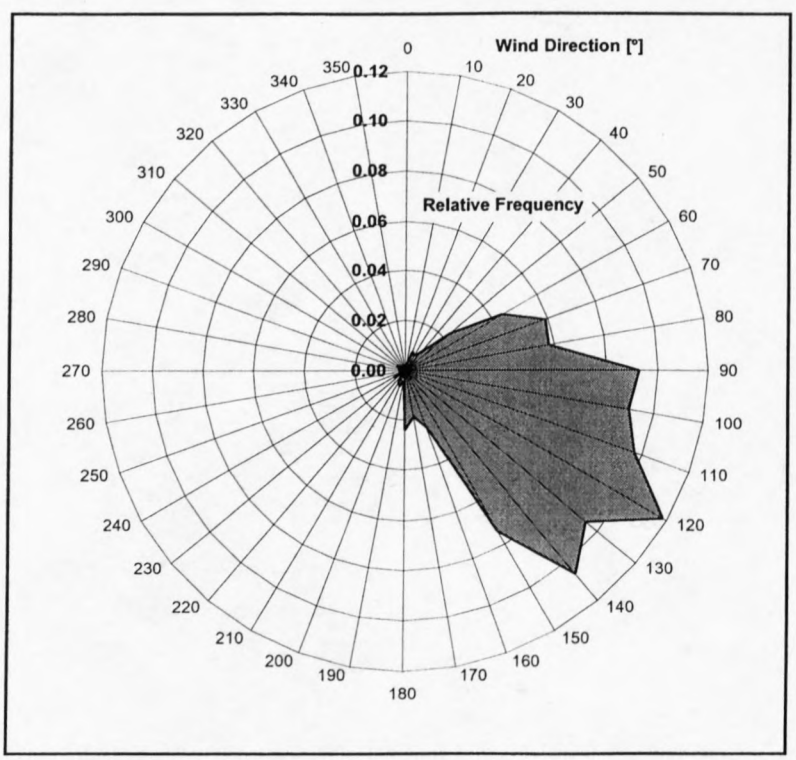

Figure C-26: Wind frequency rose for January 2002

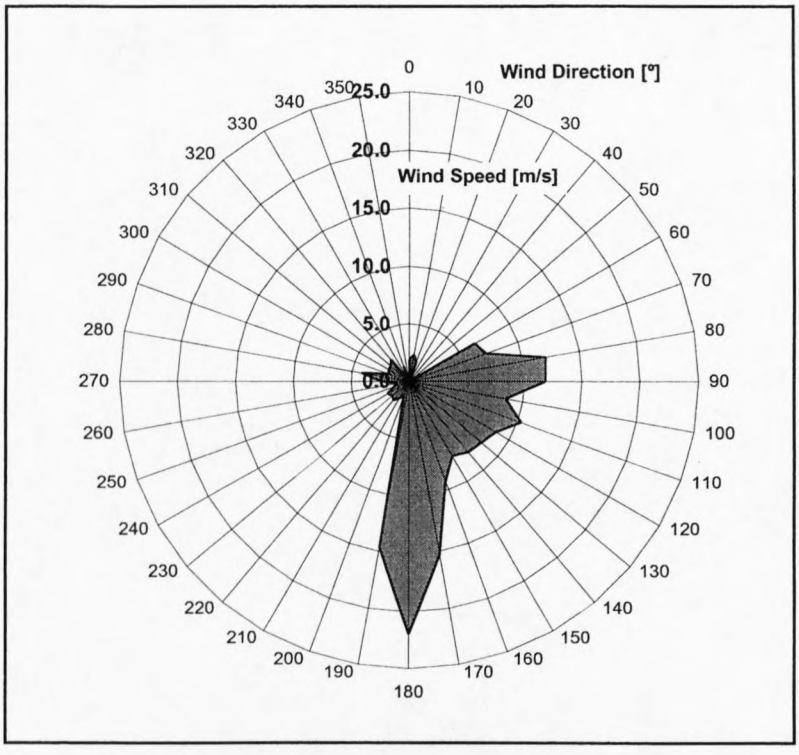

Figure C-27: Wind speed rose for February 2002

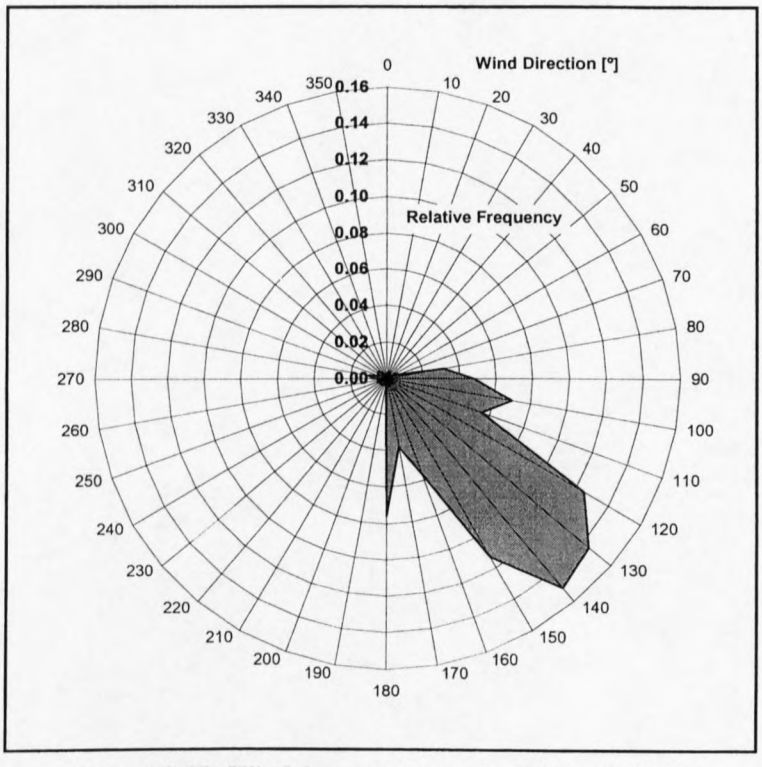

Figure C-28: Wind frequency rose for February 2002

APPENDIX D: ENERGY DEMAND ADDITIONS

The comparison of the fuel consumption and the electrical energy load of the diesel generators can be seen for the mentioned five days during the field trip, in figure D-1.

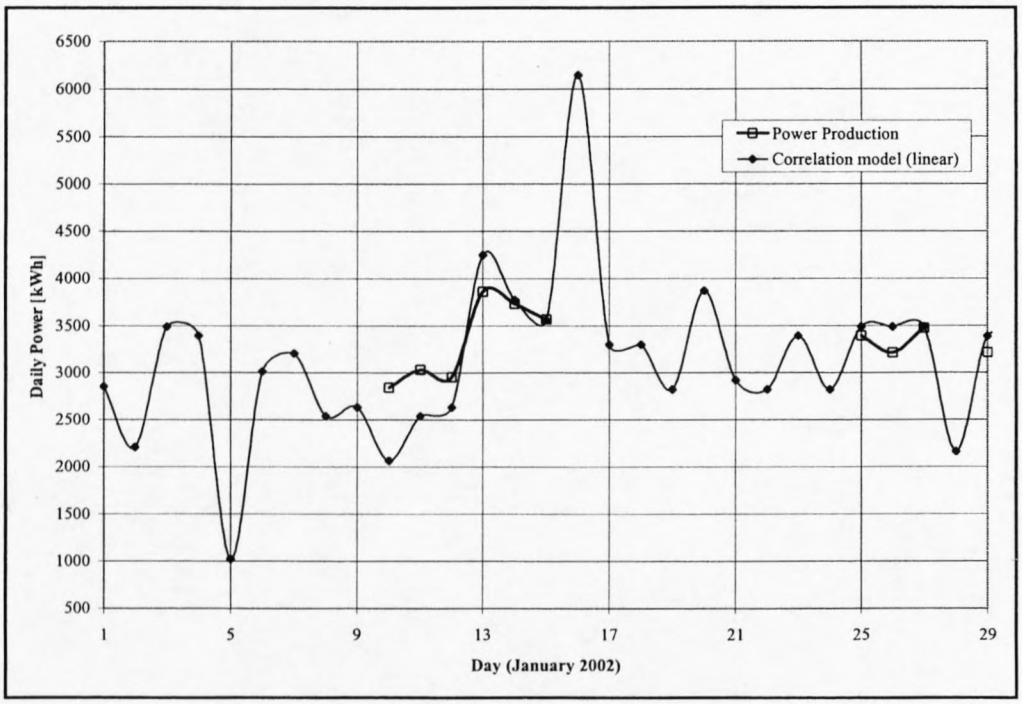

Figure D-1: Daily power production and trend line fit

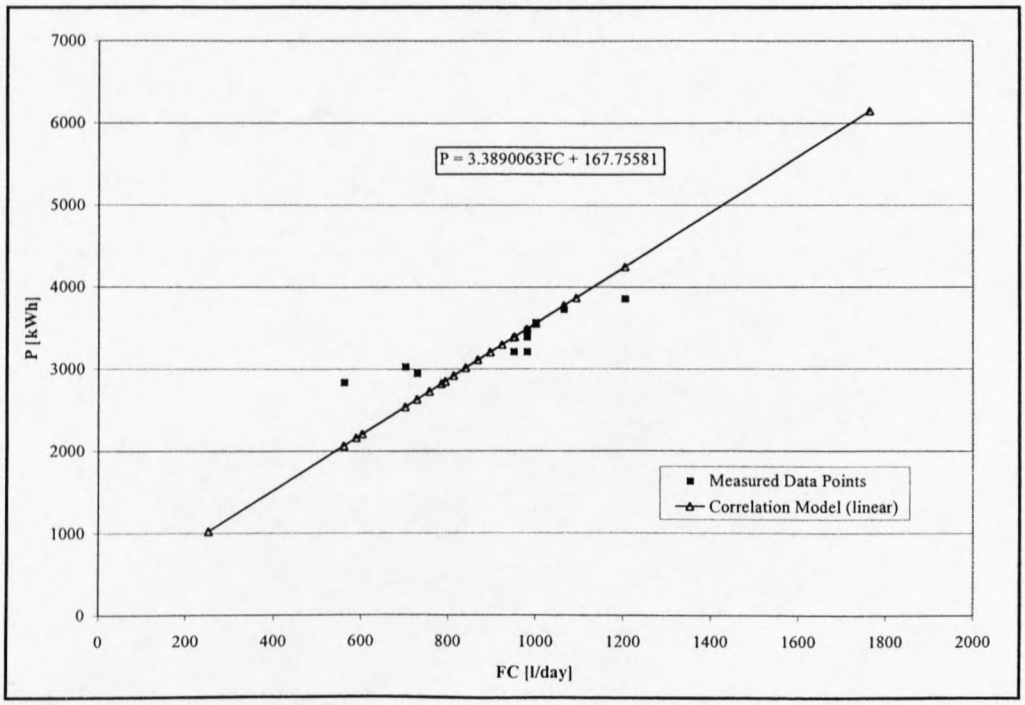

Figure D-2: Regression model between fuel consumption and power demand

Only about 8 days of energy load data is available. The data set from the 10th to the 16th and the data set from the 24th to the 29th can be seen in figure D-3. However only the data set from the 10th to the 16th has been used to evaluate the relationship between the fuel consumption and the power demand. The reason is that the data set from the 24th to the 29th is incomplete and a lot of data is missing in-between.

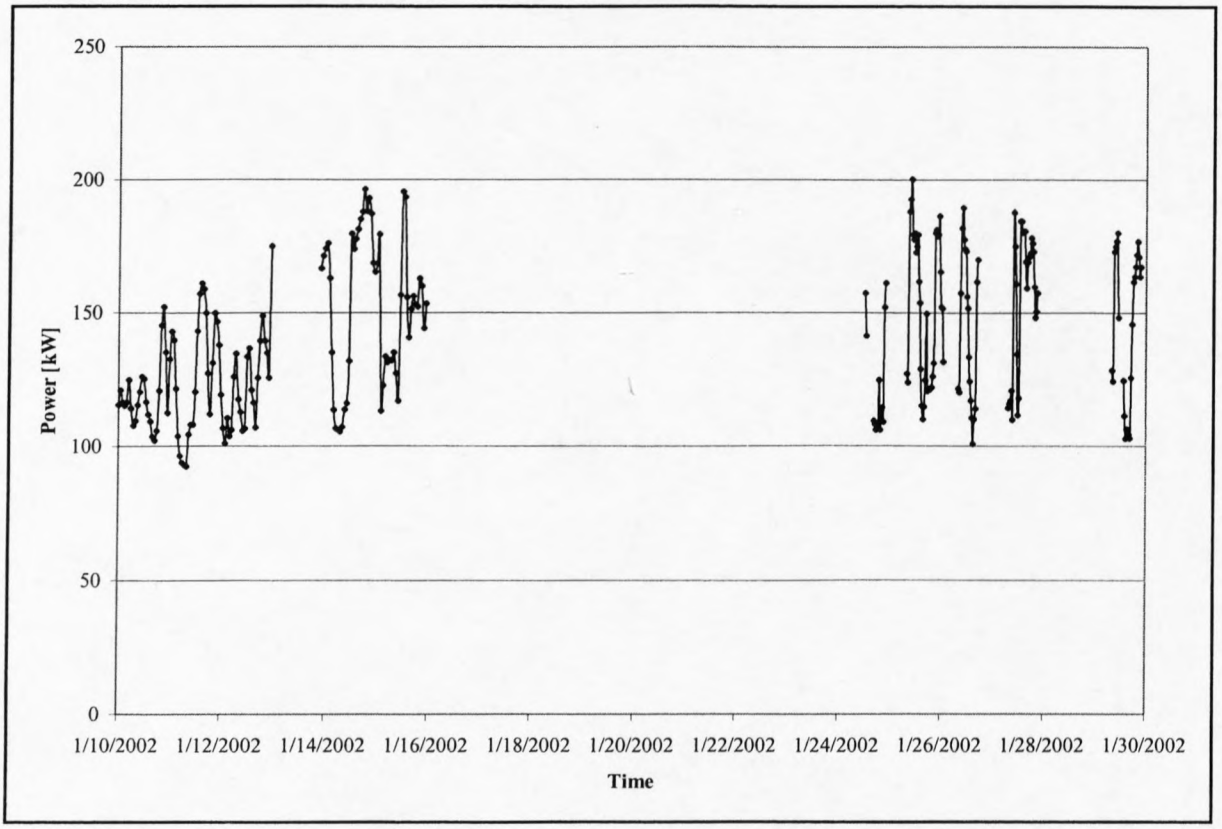

Figure D-3: Power demand data of SANAE IV

The following has been measured during the data logging period:

- Minimum power: 95.5kW
- Maximum power: 200.2kW
- Average power: 146.8kW

APPENDIX E: EQUIPMENT SPECIFICATIONS

As mentioned in chapter 4 there are three Atlantic Diesel Engineering (ADE) diesel electric generators at SANAE IV. The have the following specifications:

Diesel engines:	8 cylinder arranged in v-shape
	2 engines are equipped with turbochargers
	1 engine is equipped with turbocharger and intercooler
Generators:	3 Leroy / Somer synchronous generators
	180kW / 220kVA Power output of each generator (maximum)
Diesel generator controllers:	GENCON II – Standby V1.7h (High Performance Generator-Set Controller)
Controller supplier:	Wexler computer systems developments LTD. P.O.Box: 15108, Rishon Le-Zion 65050, Isreal
Controller hardware:	GENCON II is a computing platform that combines comprehensive, accurate and true RMS set of electrical measurements with control and monitoring functions.
Controller software:	GENCON II with the software STANDBY V1.7h is an extremely powerful gen-set controller system for prime and standby (emergency) power generation. The control system includes all the facilities necessary for paralleling a gen-set with the mains (the electric utility) as well as with other gen-sets.

Table E-1: Diesel engine, generator and controller details

APPENDIX F: ENERGY DEMAND VARIATIONS

In this chapter the second scenario, as described in chapter 4, will be explained. As mentioned before the second scenario assumes an overpopulated base, seen by the current base population. At the moment about 80 people occupy the base during the take over period and about 10 people occupy the base during wintertime.

The assumption that has been made is that the base can be 'overpopulated' by about 50% during the take over period, so that future increases in population won't affect the relevance and outcome of this thesis. Therefore, during the takeover period, the population will be increased to 120 persons. It was estimated that the base can be 'overpopulated' during wintertime by 100%, thus increasing the population to 20 persons.

This increase in population will have the effect that much more energy will be needed. Assuming that the base will stay like it is at the moment, one can assume that not much new power consuming equipment will be taken to the base.

Thus in order to model the theoretical power loading, the correction factors will be left out so that the equipment will be assumed to work at 100% of the capacity. In addition another 5% will be added to the current energy demand, in order to compensate for new power equipment that will be needed for the increased population at the base.

Taking the estimated power demand data from table 5-5 and adding 5%, one gets the estimated power demand data for a 50% overpopulated base, as can be seen in table F-1.

Description	Power [kW]
Estimated average summer day power demand	197.88
Estimated summer day maximum power demand	216.28
Estimated average winter day power demand	237.35

Table F-1: Estimated and measured power demand data (daily averages) for 'overpopulated' base

The estimated power demand data can be seen in the following figures.

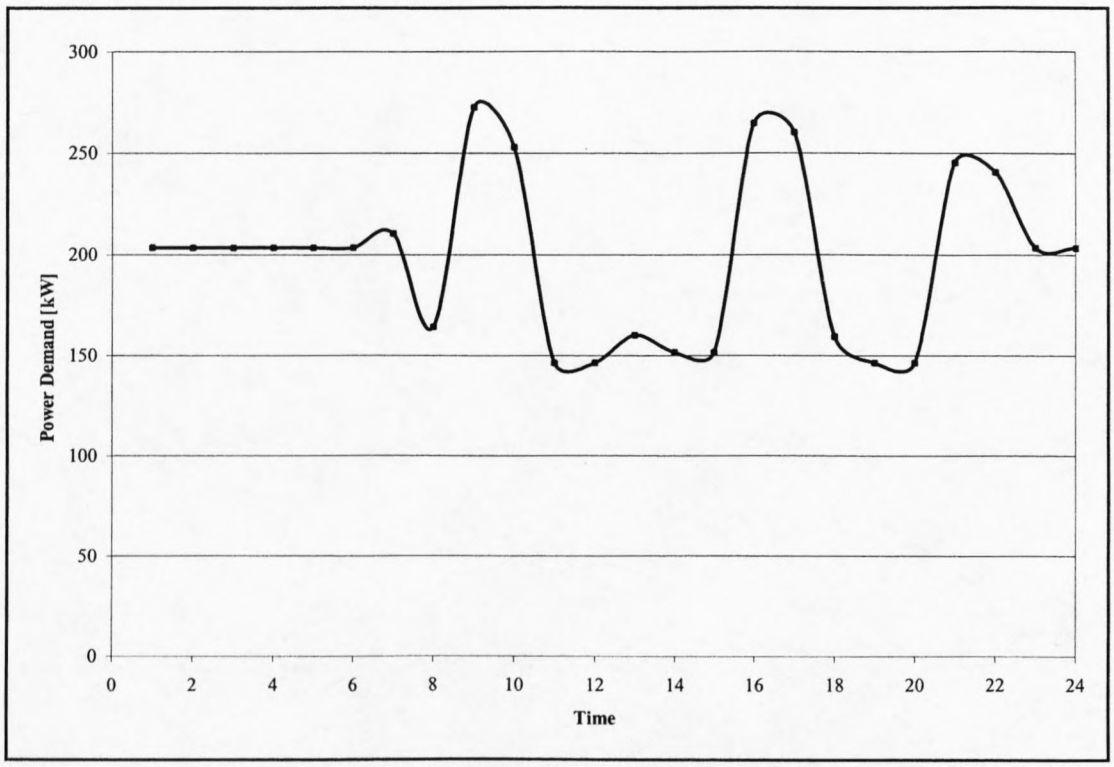

Figure F-1: Estimated daily energy demand for an average summer day (overpopulated base)

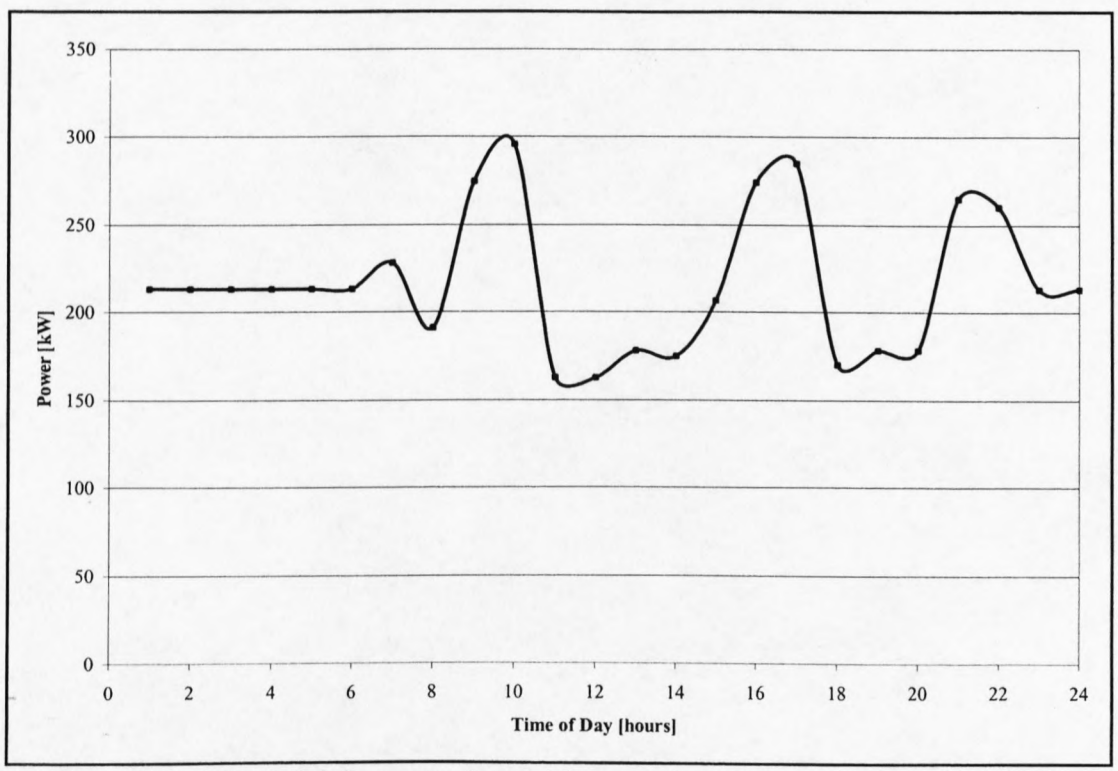

Figure F-2: Estimated daily energy demand for a maximum power demand summer day (overpopulated base)

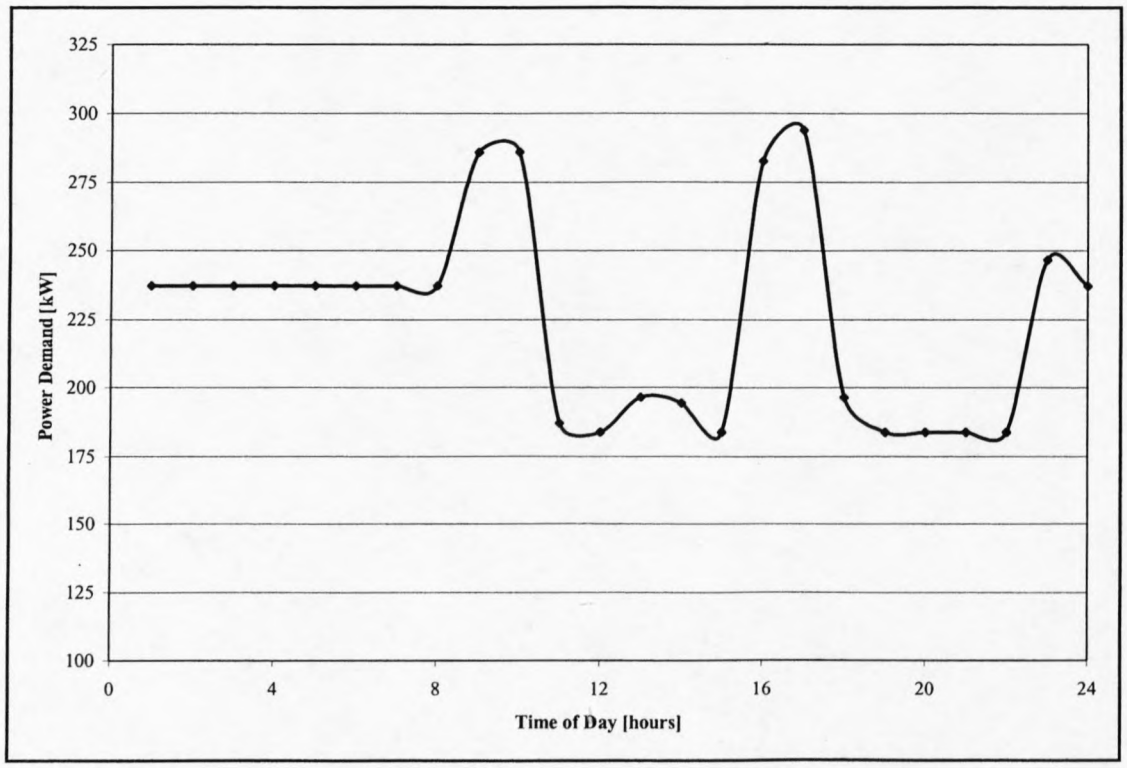

Figure F-3: Estimated daily energy demand for an average winter day

The energy demand variation for all three situations is based on the current scenario, as explained in chapter 4. Figure F-1 shows the average power demand for a summer day. There are also three peaks, which result from using the snowsmelter. During nighttime the power demand is fairly constant, since everybody is asleep and nobody is operating any equipment. Although not entirely true, this assumption is valid for most of time.

During the wintertime it has been assumed again that the snowsmelter will only be operating twice a day. The wintertime daily energy demand variation is similar to the summertime energy demand, since all the equipment has still to be used during wintertime, although not as much. The reason why the wintertime power demand is much higher than the summertime power demand is because the additional heating requirements at the base. The heating is normally achieved by switching on skirting heaters for each room in the base and by switching on the inline heaters for the fan coil units (Cencelli, 2002).

APPENDIX G: WEIBULL PARAMETER CALCULATIONS

The iteration loop in table G-1 calculates the Weibull shape factor k and subsequently the Weibull scale parameter c. The calculation procedure that has to be followed when performing this iteration can be viewed in section 6.1.3. This procedure was used to calculate the Weibull parameters for wind speeds at each height above surface level.

Hour	Wind speed	k	sum(vi^k*ln(vi))	sum(vi^k)	sum(vi^k*ln(vi))/sum(vi^k)	sum(ln(vi))	sum(ln(vi))/n	k	sum(vi^k)	1/n*sum(vi^k)	(1/n*sum(vi^k))^(1/k)
1	3.3	2.93	39.47	33.06	1.19	1.19	1.19	#DIV/0!	33.06	33.06	3.30
2	3.8	2.93	106.18	83.03	1.28	2.53	1.26	69.57	83.03	41.52	3.57
3	4.2	2.93	202.35	150.04	1.35	3.96	1.32	36.66	150.04	50.01	3.80
4	3.3	2.93	241.81	183.09	1.32	5.16	1.29	32.05	183.09	45.77	3.69
5	2.8	2.93	262.84	203.52	1.29	6.19	1.24	18.53	203.52	40.70	3.54
6	3.0	2.93	290.31	228.52	1.27	7.29	1.21	17.85	228.52	38.09	3.46
7	4.0	2.93	370.83	286.60	1.29	8.67	1.24	18.20	286.60	40.94	3.55
8	2.7	2.93	389.06	304.96	1.28	9.67	1.21	14.80	304.96	38.12	3.46
9	5.2	2.93	595.61	430.25	1.38	11.31	1.26	7.86	430.25	47.81	3.74
10	6.7	2.93	1096.38	693.52	1.58	13.22	1.32	3.86	693.52	69.35	4.25
11	6.8	2.93	1623.43	968.46	1.68	15.13	1.38	3.33	968.46	88.04	4.61
12	6.8	2.93	2150.49	1243.41	1.73	17.05	1.42	3.24	1243.41	103.62	4.87
13	5.7	2.93	2435.84	1407.36	1.73	18.79	1.45	3.50	1407.36	108.26	4.95
14	8.5	2.93	3567.26	1936.05	1.84	20.93	1.50	2.88	1936.05	138.29	5.38
15	8.9	2.93	4889.69	2540.99	1.92	23.12	1.54	2.61	2540.99	169.40	5.76
16	9.3	2.93	6424.18	3229.09	1.99	25.35	1.58	2.47	3229.09	201.82	6.12
17	6.5	2.93	6875.09	3469.99	1.98	27.22	1.60	2.63	3469.99	204.12	6.14
18	4.2	2.93	6971.25	3537.00	1.97	28.65	1.59	2.64	3537.00	196.50	6.06
19	4.3	2.93	7075.97	3608.79	1.96	30.11	1.58	2.66	3608.79	189.94	5.99
20	3.7	2.93	7136.44	3655.01	1.95	31.42	1.57	2.62	3655.01	182.75	5.92
21	4.0	2.93	7216.95	3713.09	1.94	32.81	1.56	2.62	3713.09	176.81	5.85
⋮	⋮	⋮	⋮	⋮	⋮	⋮	⋮	⋮	⋮	⋮	⋮
⋮	⋮	⋮	⋮	⋮	⋮	⋮	⋮	⋮	⋮	⋮	⋮
53	2.7	2.93	11635.16	6457.77	1.80	77.86	1.47	3.01	6457.77	121.84	5.15
54	4.3	2.93	11739.87	6529.56	1.80	79.31	1.47	3.04	6529.56	120.92	5.14
55	4.3	2.93	11844.58	6601.35	1.79	80.77	1.47	3.07	6601.35	120.02	5.12
56	4.5	2.93	11967.95	6683.36	1.79	82.28	1.47	3.11	6683.36	119.35	5.11
57	4.5	2.93	12091.31	6765.38	1.79	83.78	1.47	3.15	6765.38	118.69	5.10
58	6.0	2.93	12432.71	6955.92	1.79	85.57	1.48	3.21	6955.92	119.93	5.12
59	10.4	2.93	14668.64	7910.71	1.85	87.91	1.49	2.75	7910.71	134.08	5.32
60	6.7	2.93	15169.40	8173.98	1.86	89.82	1.50	2.79	8173.98	136.23	5.35
61	6.3	2.93	15573.99	8393.80	1.86	91.66	1.50	2.83	8393.80	137.60	5.37
62	9.4	2.93	17164.92	9103.81	1.89	93.90	1.51	2.70	9103.81	146.84	5.49
63	7.7	2.93	17972.73	9499.56	1.89	95.94	1.52	2.71	9499.56	150.79	5.54
64	6.0	2.93	18314.13	9690.10	1.89	97.73	1.53	2.76	9690.10	151.41	5.55
65	8.9	2.93	19636.56	10295.04	1.91	99.92	1.54	2.70	10295.04	158.39	5.63
66	7.7	2.93	20444.37	10690.78	1.91	101.96	1.54	2.72	10690.78	161.98	5.68
67	6.2	2.93	20827.07	10900.54	1.91	103.78	1.55	2.77	10900.54	162.69	5.69
68	5.7	2.93	21112.42	11064.49	1.91	105.52	1.55	2.81	11064.49	162.71	5.69
69	5.7	2.93	21397.77	11228.44	1.91	107.26	1.55	2.85	11228.44	162.73	5.69
70	7.5	2.93	22135.99	11594.82	1.91	109.28	1.56	2.87	11594.82	165.64	5.72
71	7.5	2.93	22874.20	11961.19	1.91	111.29	1.57	2.90	11961.19	168.47	5.75
72	5.3	2.93	23095.13	12093.67	1.91	112.96	1.57	2.93	12093.67	167.97	5.75
		Shape Factor k						Shape Factor k			Scale factor c

The equations have been solved by changing the left hand value until it matches the right hand value.

Table G-1: Iteration loop to calculate the Weibull shape factor and the scale factor

APPENDIX H: HAND-HELD ANEMOMETER WIND SPEED ANALYSIS

The analysis of the hand meter data has been dealt with in chapter 6. The functions describing the relationship between the wind mast and the hand meter can be seen in table H-1.

Position	Function	Regression Coefficient	No.
2	$v_{hand} := 9.5038 \cdot \ln(v_{mast}) - 8.6346$	$R^2 = 0.9355$	(H8-1)
3	$v_{hand} := 1.3619 \cdot v_{mast} - 1.4434$	$R^2 = 0.9476$	(H8-2)
4	$v_{hand} := 1.2154 \cdot v_{mast} - 0.5697$	$R^2 = 0.9417$	(H8-3)
5	$v_{hand} := 1.1873 \cdot v_{mast} - 0.7667$	$R^2 = 0.9689$	(H8-4)
6	$v_{hand} := 1.1834 \cdot v_{mast} - 0.1434$	$R^2 = 0.9791$	(H8-5)
7	$v_{hand} := 1.3112 \cdot v_{mast} - 0.7769$	$R^2 = 0.9609$	(H8-6)
8	$v_{hand} := 1.2809 \cdot v_{mast} - 0.9837$	$R^2 = 0.9980$	(H8-7)
9	$v_{hand} := 1.1336 \cdot v_{mast} + 0.719$	$R^2 = 0.9426$	(H8-8)
10	$v_{hand} := 1.3657 \cdot v_{mast} - 1.1379$	$R^2 = 0.9726$	(H8-9)
11	$v_{hand} := 1.1651 \cdot v_{mast} + 0.2038$	$R^2 = 0.9537$	(H8-10)
13	$v_{hand} := 1.3038 \cdot v_{mast} + 0.7315$	$R^2 = 0.9691$	(H8-11)
14	$v_{hand} := 1.2321 \cdot v_{mast} + 1.0653$	$R^2 = 0.9155$	(H8-12)
15	$v_{hand} := 1.1797 \cdot v_{mast} - 0.3484$	$R^2 = 0.9415$	(H8-13)
16	$v_{hand} := 1.3395 \cdot v_{mast} + 1.4211$	$R^2 = 0.9923$	(H8-14)

Table H-1: Wind speed functions of the 16 positions

As can be seen from table H-1, position 1 has no equation as it matches directly the wind mast data, since the wind mast has been located at position 1. The only position that does not feature a linear relationship is position 2. It has a logarithmic function, as this function yields a better regression coefficient. The graphs for these functions can be seen next.

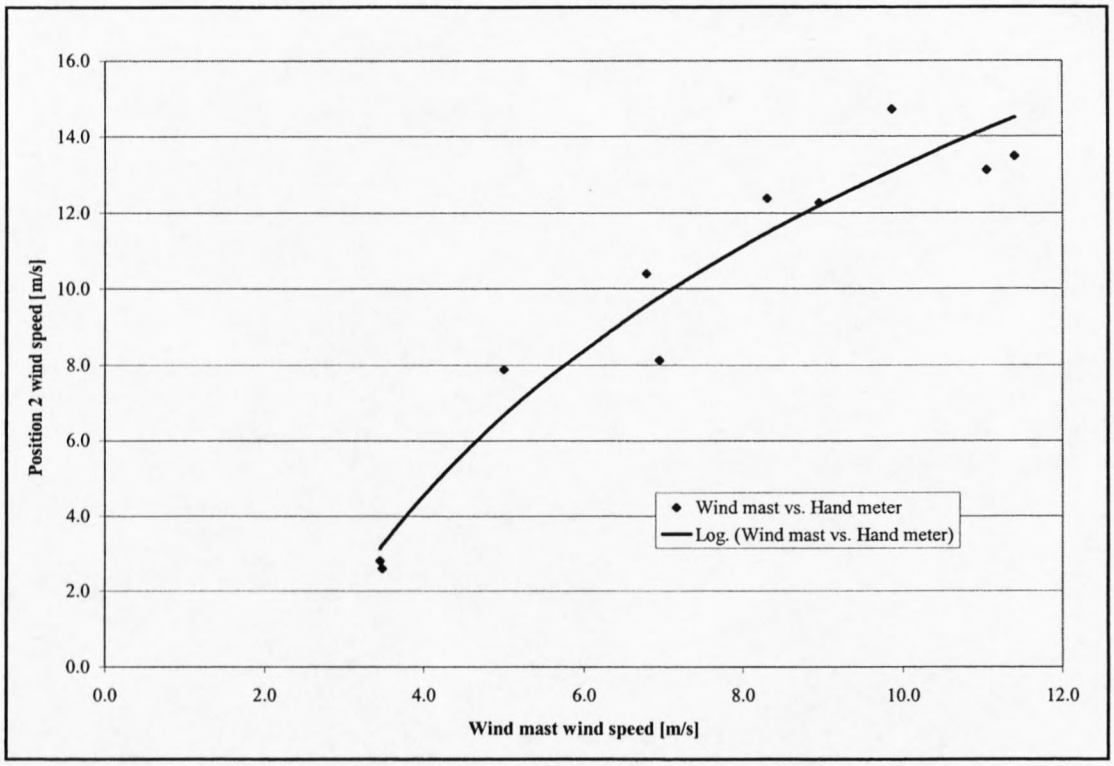

Figure H-1: Linear relationship between wind mast and position 2 wind speeds

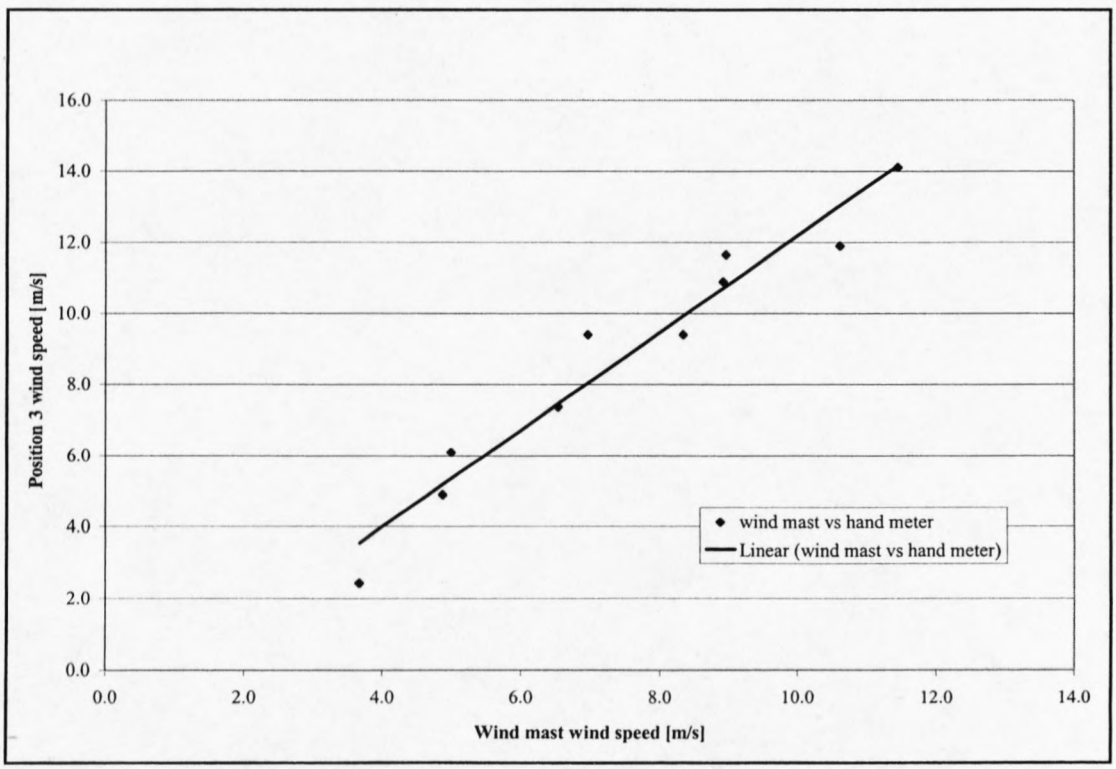

Figure H-2: Linear relationship between wind mast and position 3 wind speeds

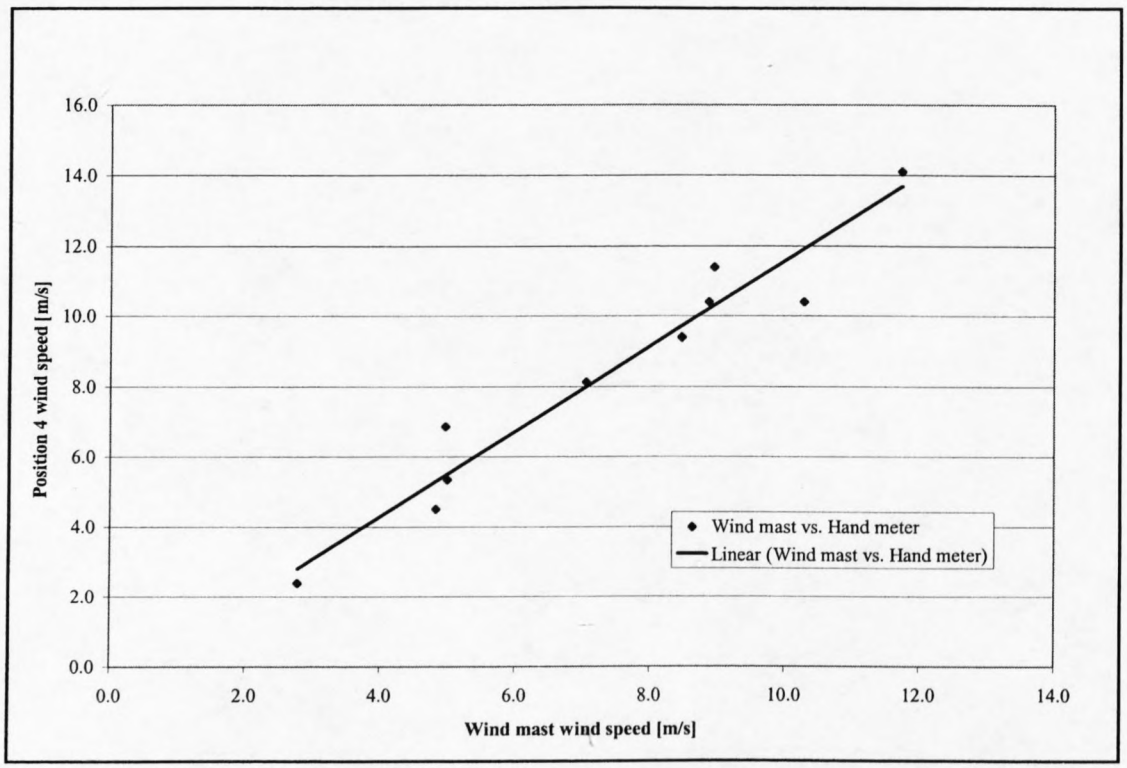

Figure H-3: Linear relationship between wind mast and position 4 wind speeds

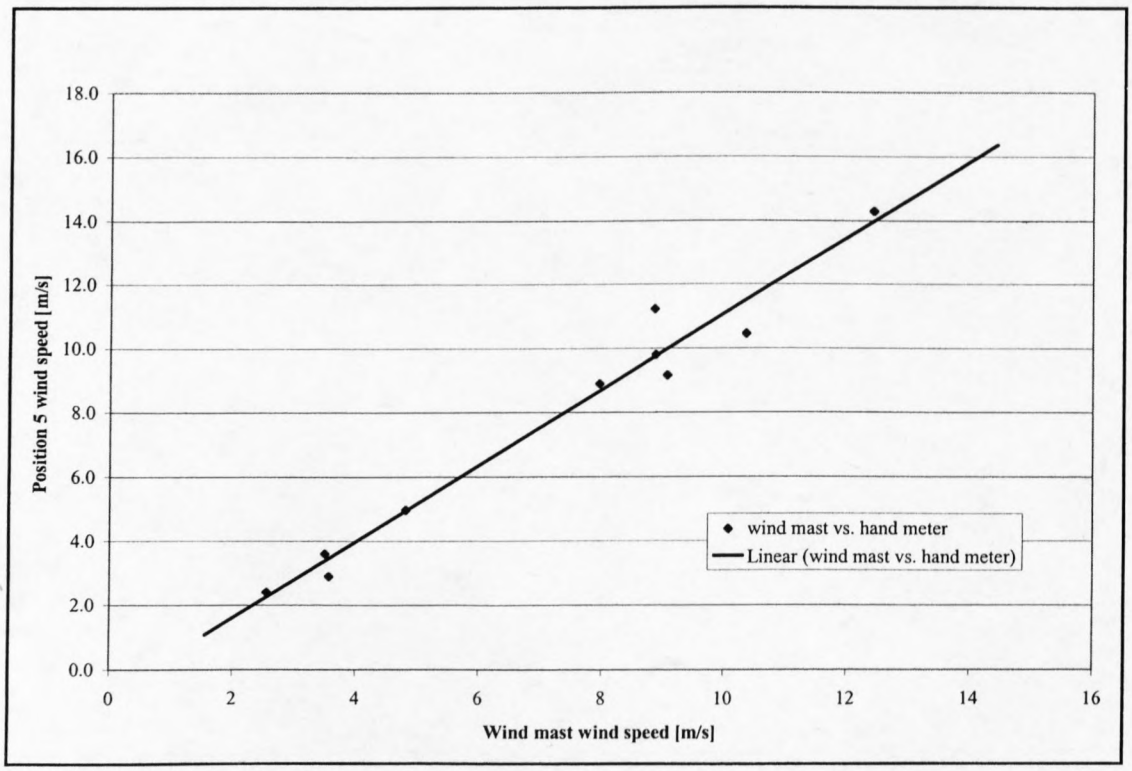

Figure H-4: Linear relationship between wind mast and position 5 wind speeds

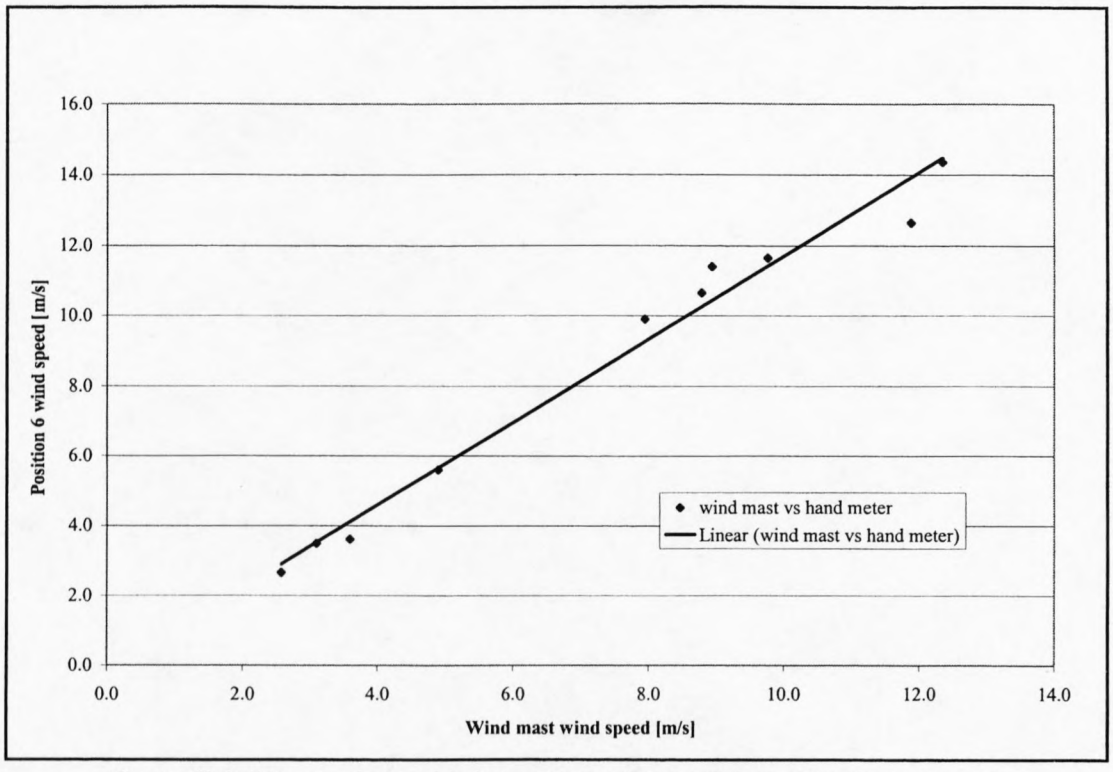

Figure H-5: Linear relationship between wind mast and position 6 wind speeds

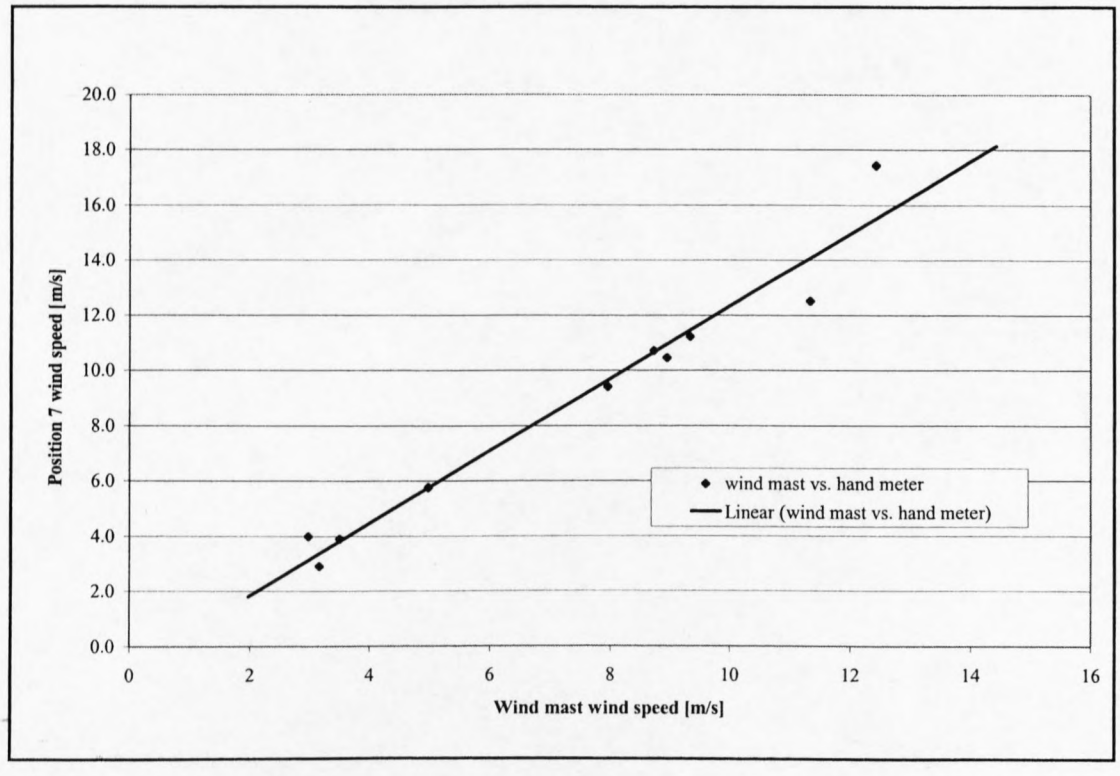

Figure H-6: Linear relationship between wind mast and position 7 wind speeds

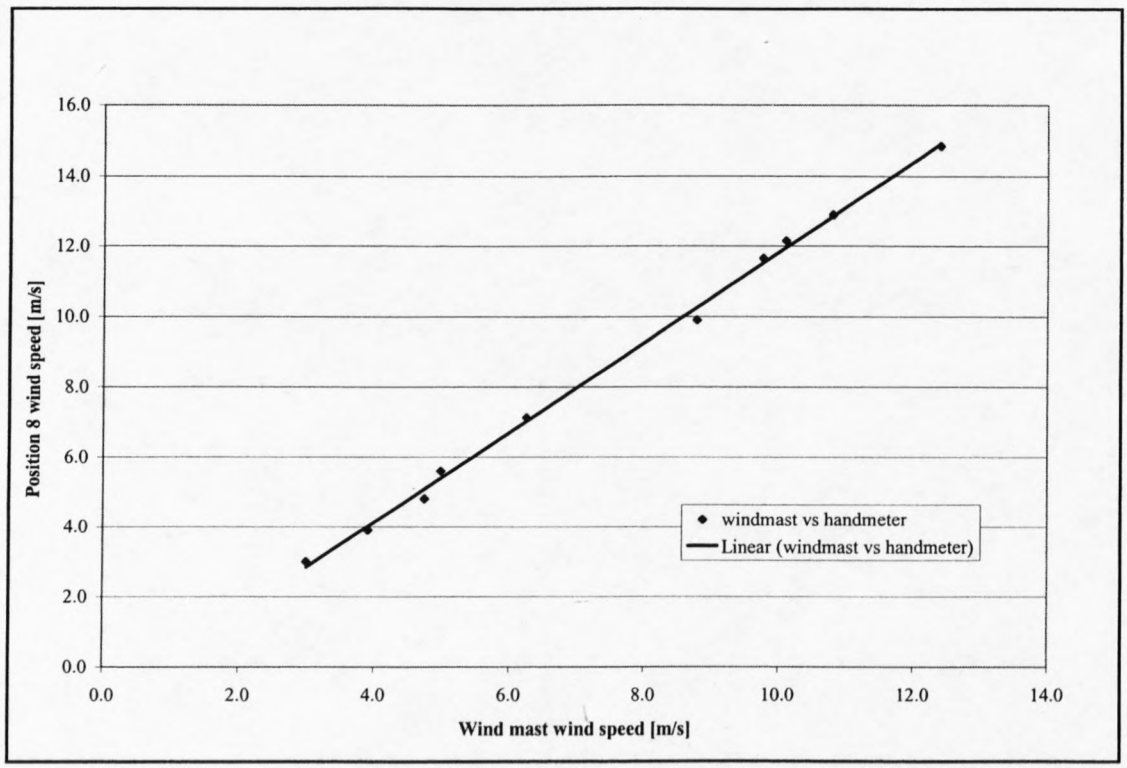

Figure H-7: Linear relationship between wind mast and position 8 wind speeds

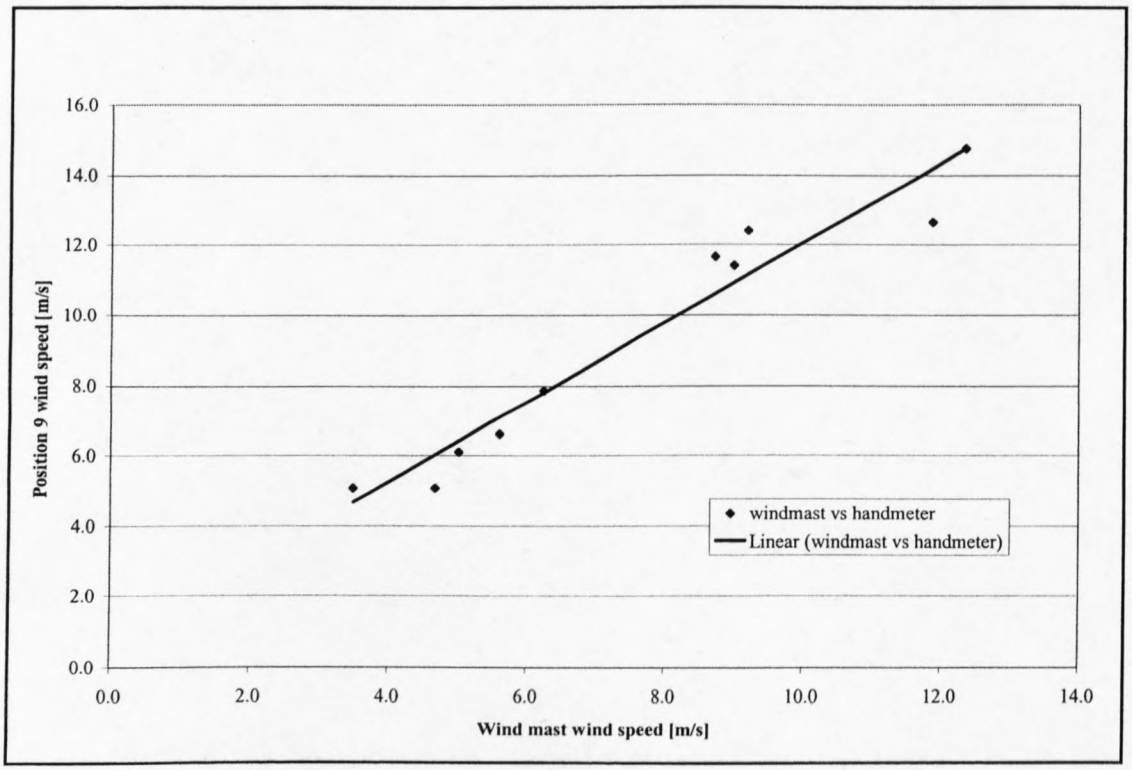

Figure H-8: Linear relationship between wind mast and position 9 wind speeds

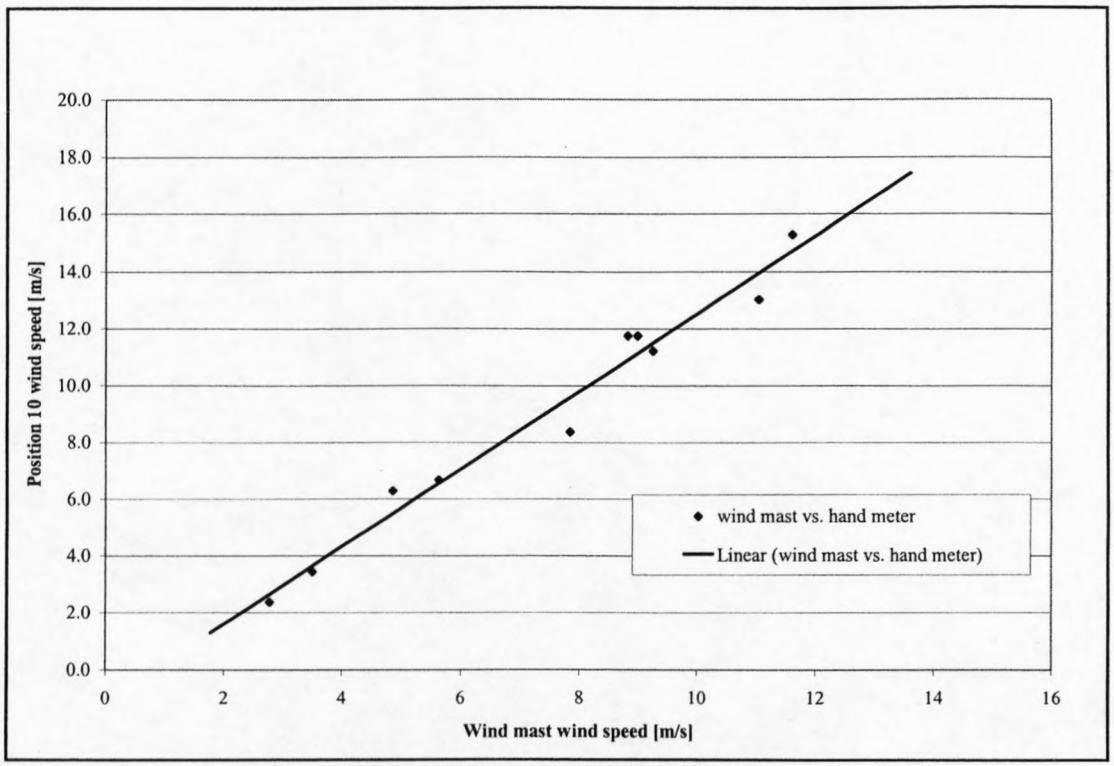

Figure H-9: Linear relationship between wind mast and position 10 wind speeds

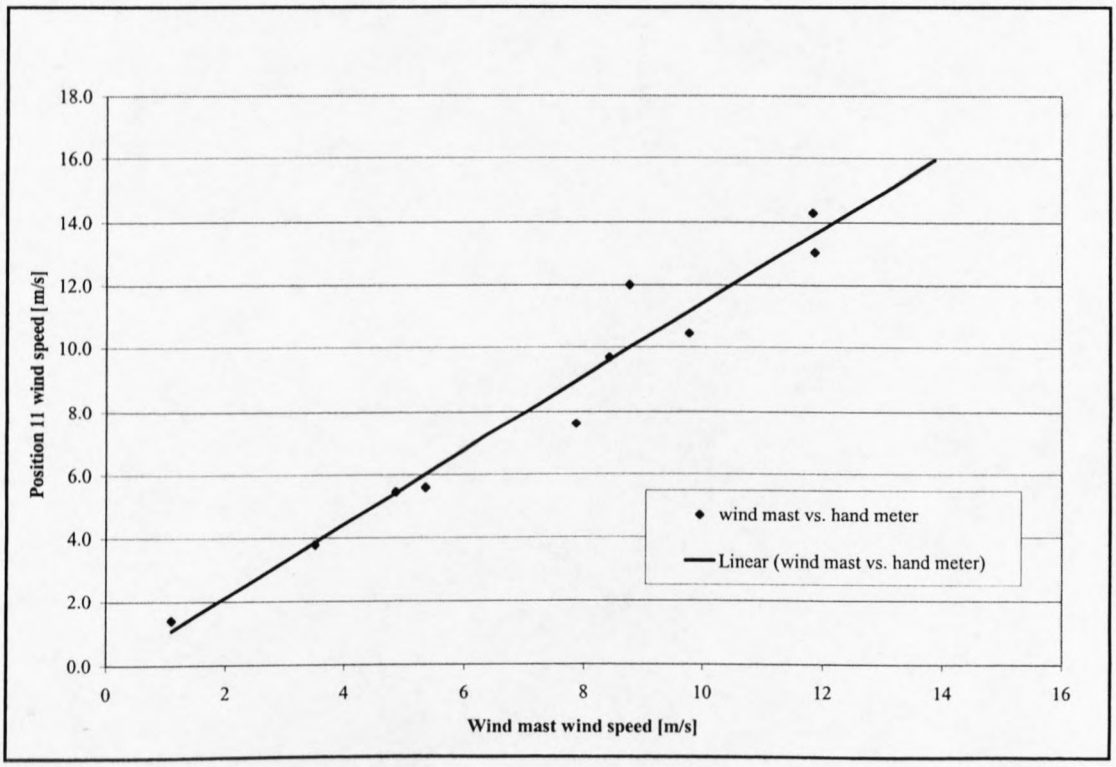

Figure H-10: Linear relationship between wind mast and position 11 wind speeds

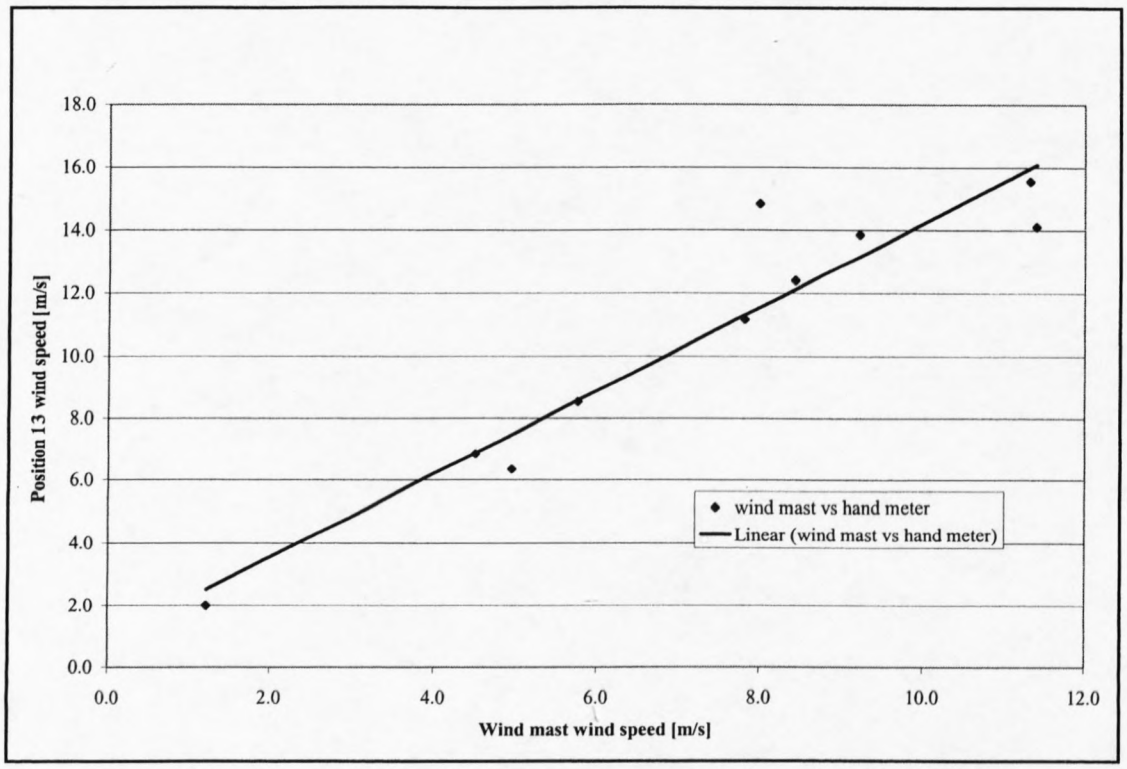

Figure H-11: Linear relationship between wind mast and position 13 wind speeds

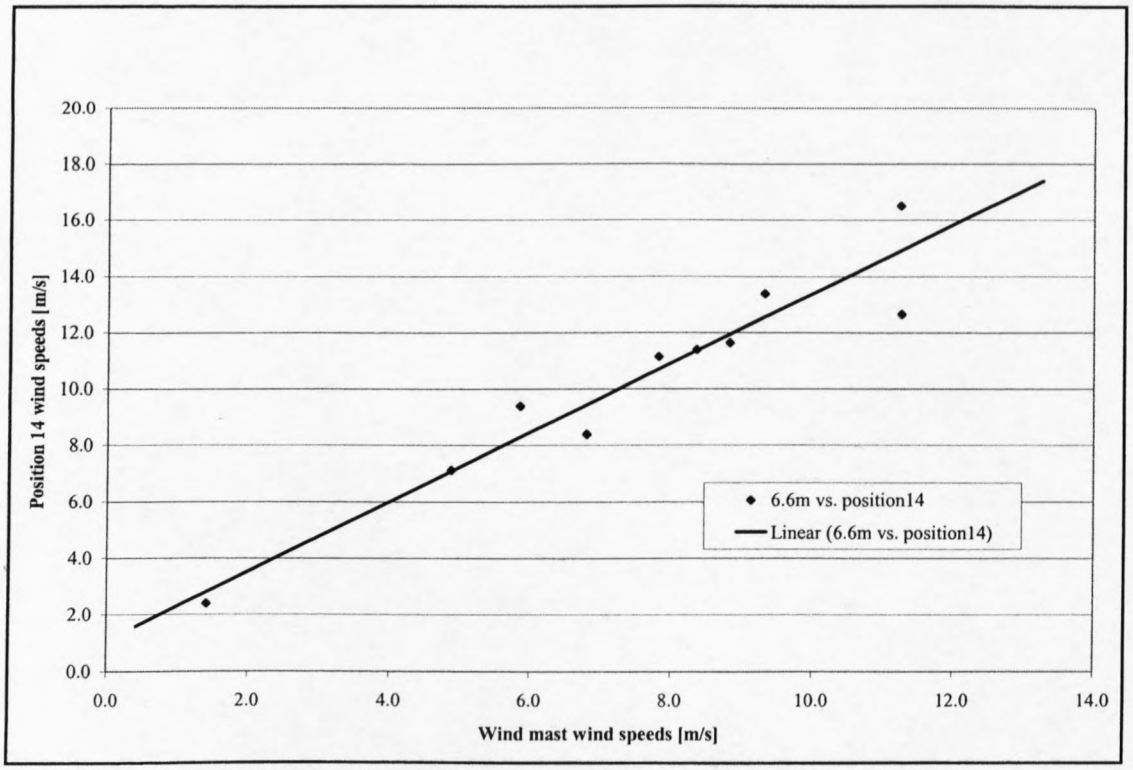

Figure H-12: Linear relationship between wind mast and position 14 wind speeds

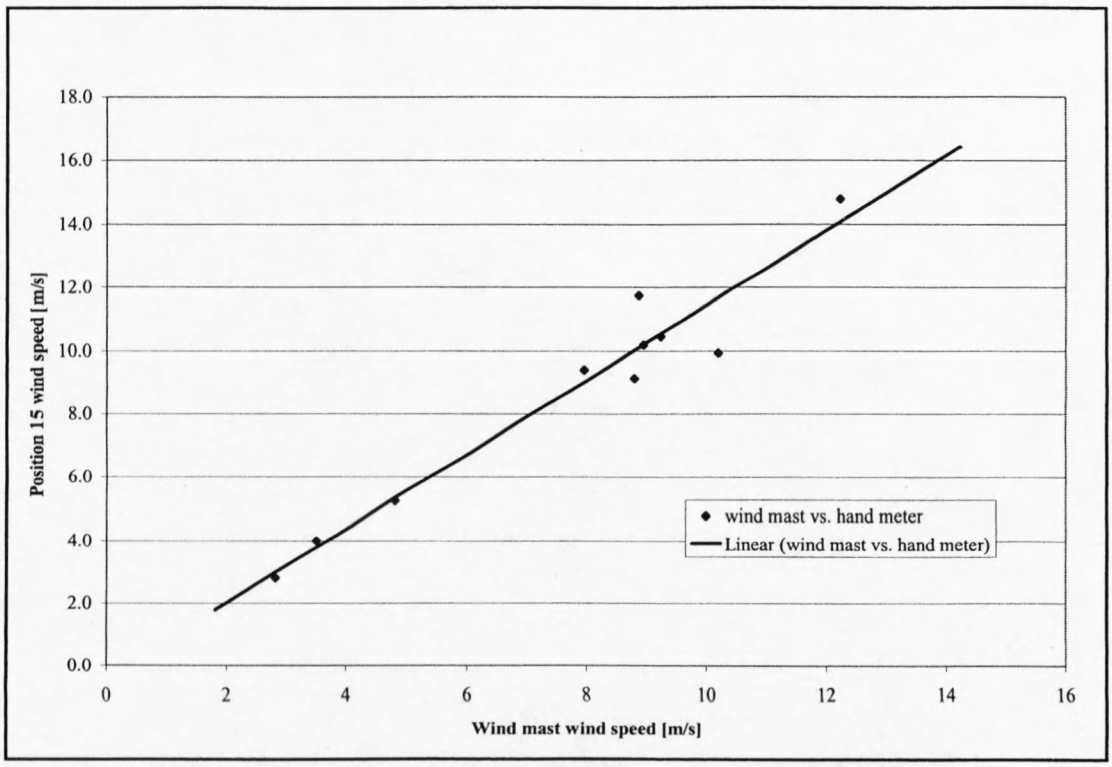

Figure H-13: Linear relationship between wind mast and position 15 wind speeds

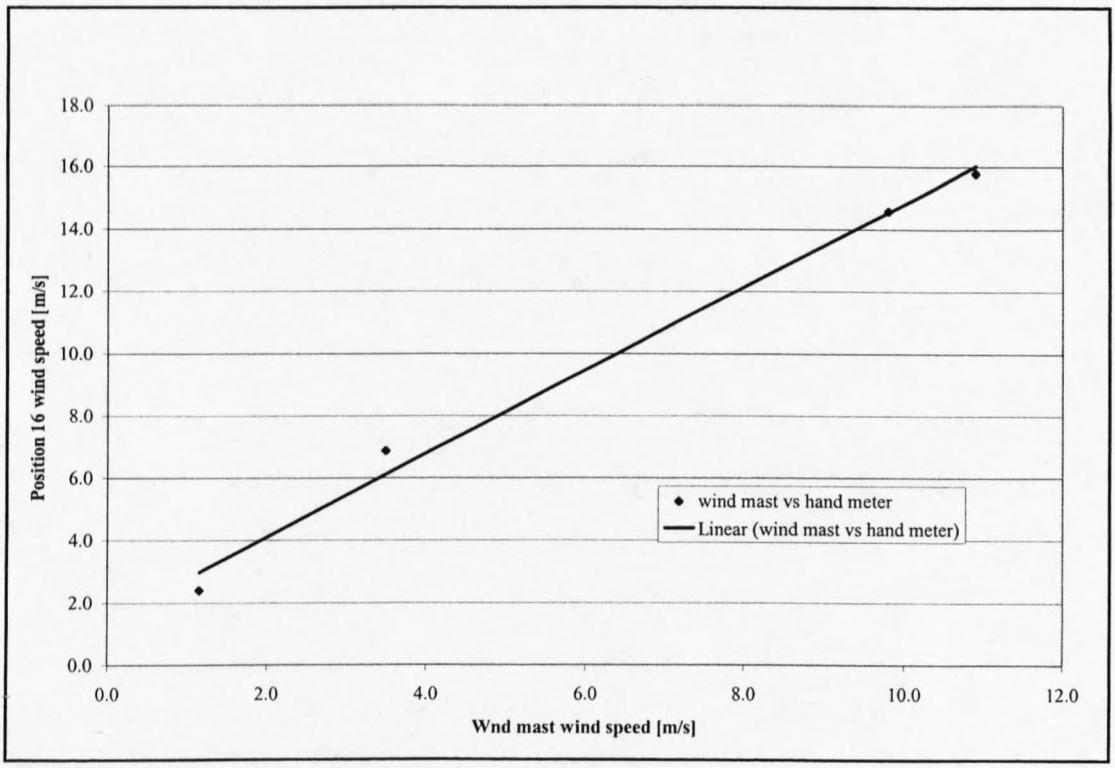

Figure H-14: Linear relationship between wind mast and position 16 wind speeds

From these graphs, the average wind speed at each position was calculated at 10 m height. They are given in table H-2.

Position	X [m]	Y [m]	Average Wind Speed [m/s]
1	1773.2	801.1	**7.87**
2	129.5	310.0	**9.59**
3	236.0	222.2	**9.28**
4	322.8	290.4	**9.00**
5	442.8	68.9	**8.58**
6	776.7	40.0	**9.17**
7	916.8	64.2	**9.55**
8	711.9	519.0	**9.10**
9	343.0	536.2	**9.64**
10	517.4	616.7	**9.61**
11	549.8	818.0	**8.97**
12	375.4	726.4	**9.85**
13	264.4	702.5	**11.38**
14	100.0	733.7	**10.77**
15	476.4	180.9	**8.94**
16	810.3	1435.4	**11.97**

Table H-2: Average wind speeds at each position at 10 m height

As explained in chapter 6, there are some errors, when extrapolating data sets. In the next figures, some comparisons of different wind speed data sets can be seen. In each figure there is always one data set that has been kept as it has been measured. The other data set is an extrapolated or interpolated data set.

Figure H-15 shows the wind speed data taken from the hand-held anemometer data set at 2.5 m height and the 6 m wind mast data set, being interpolated to 2.5 m height. This graph proves the accuracy of the wind data, since the two curves nearly lie on top of each other, thus making it a near perfect interpolation.

Figure H-16 shows the accuracy of the wind profiles for the snow-covered surface. The 2.5 m wind speed data is the hand-held anemometer data, while the 2.7 m wind data is from the wind mast data set, measured by sensor number 3. The 10 m wind speed curve is the extrapolated 10 m wind speed data set.

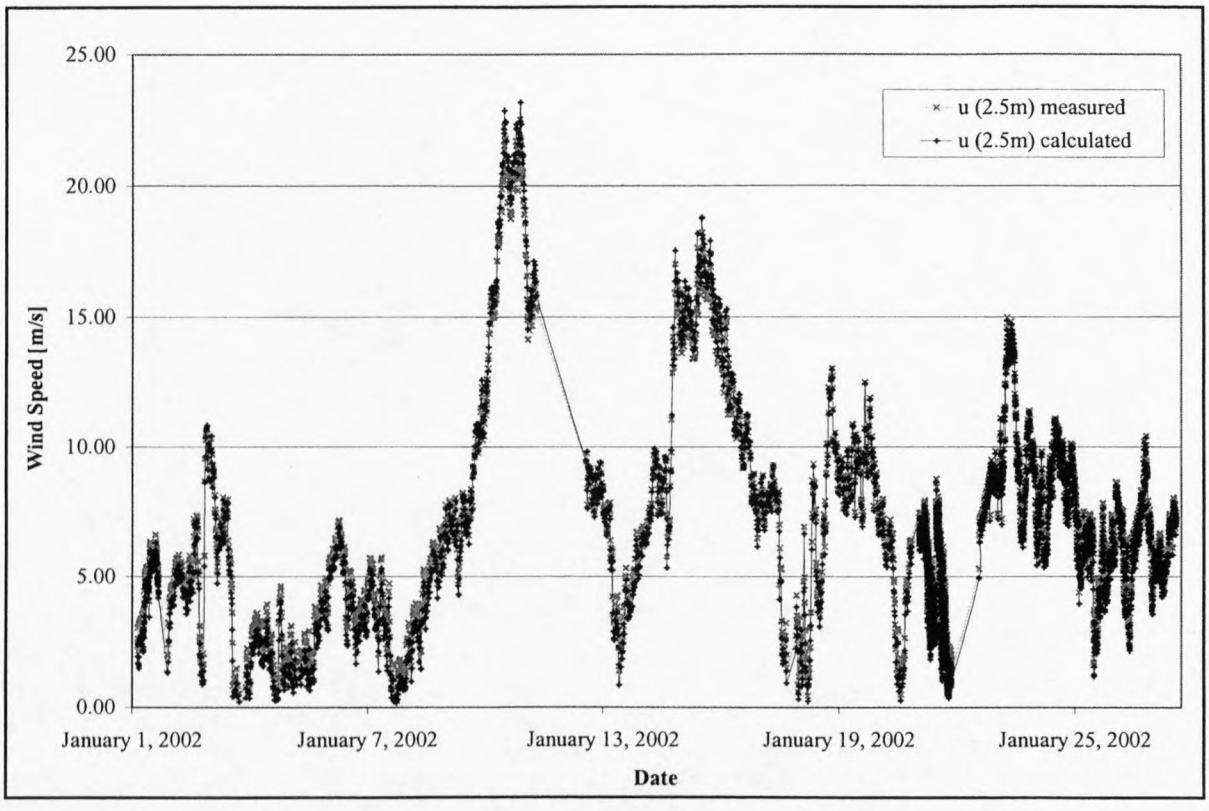

Figure H-15: Comparison of measured 2.5 m wind speed and interpolated 2.5 m wind speed

Figure H-17 show the comparison of different wind speed for a snow-covered surface with protruding rocks. The 10 m height wind speed curve is again the extrapolated wind speed from the 6 m wind mast data set. The 2.5 m height wind speed curve is the hand meter measured data set and the other two curves with measuring heights of 1.9 m and 3.4 m are data curves from the 6 m wind mast data set. The curves originate from wind sensors 2 and 3.

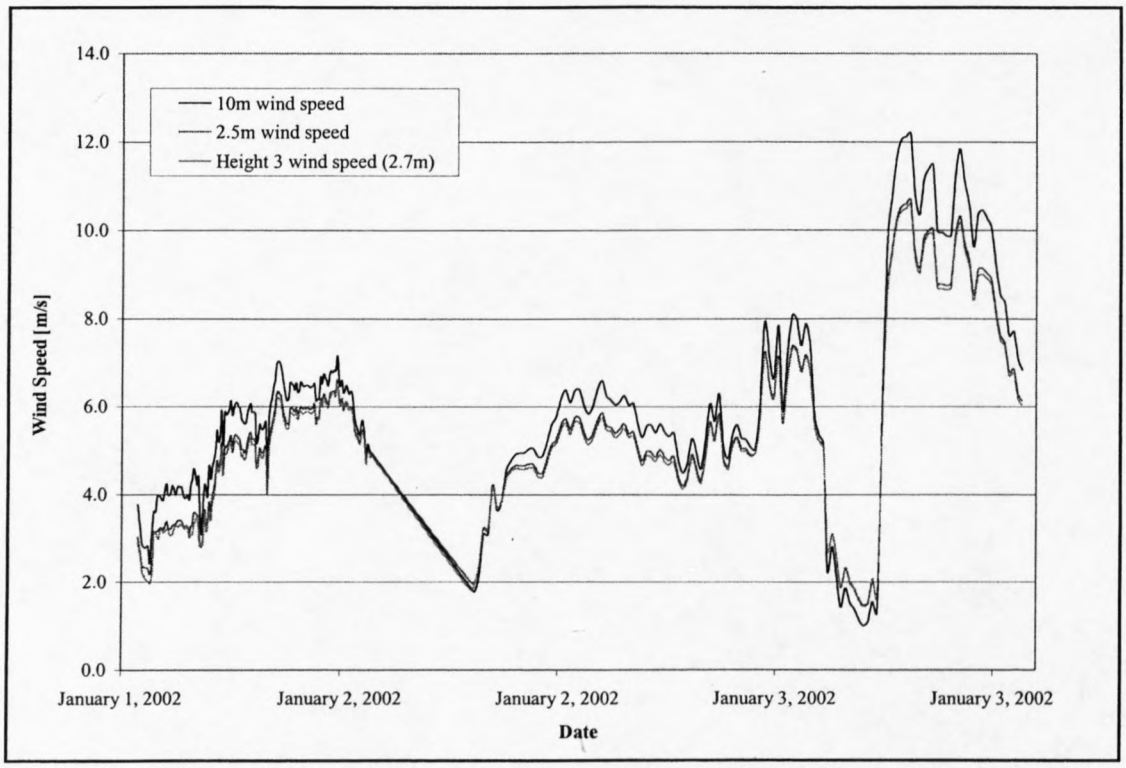

Figure H-16: Comparison of measured 2.5 m and 2.7 m wind speeds and extrapolated 10 m wind speed

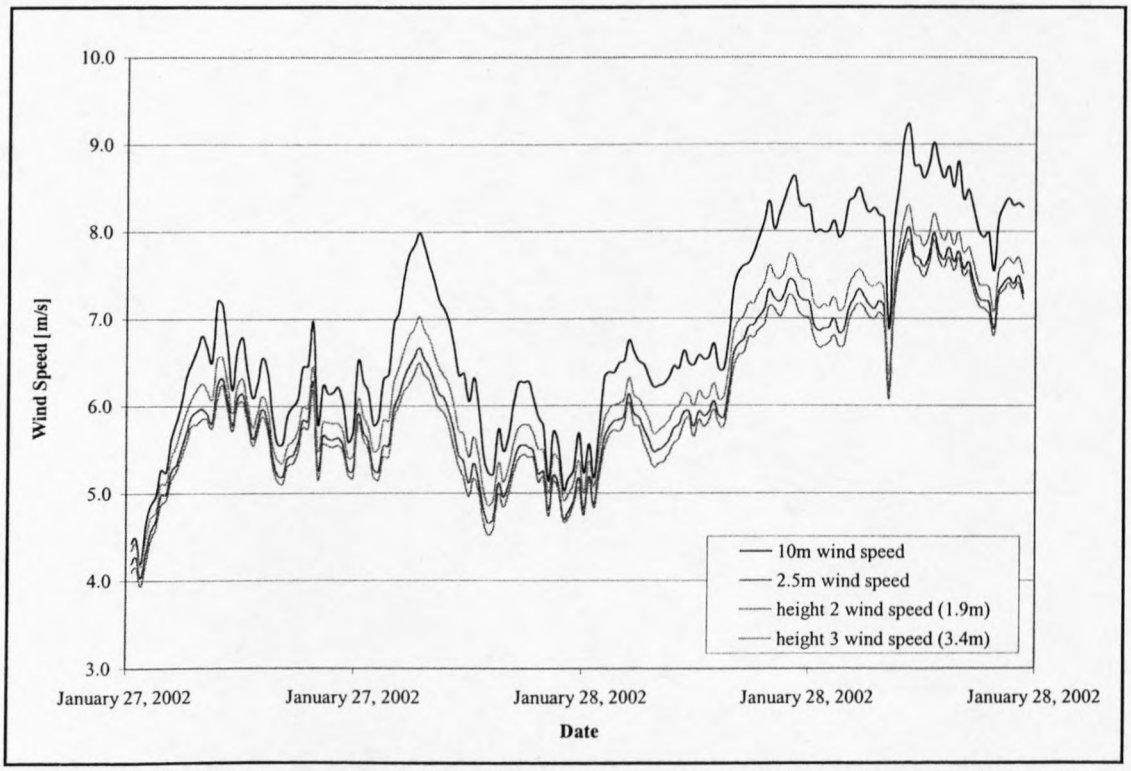

Figure H-17: Comparison of wind speeds for a snow-covered surface with protruding rocks

APPENDIX I: POSITION 2-16 PHOTOGRAPHS

In order to visualize the area surrounding the base and to the see surfaces at each of the 16 positions, photographs have been taken during the field trip and are shown in this chapter. From the photos the elevations at the positions can be seen. There are three photos for each position. One photo is taken from the position looking east, one is taken looking towards the position from the east and the last one is taken looking at the position from the side, either facing towards north or south. Photographs for position 1 are not shown, since this position is the same as the first position of the 6 m wind mast, as can be seen in chapter 6.

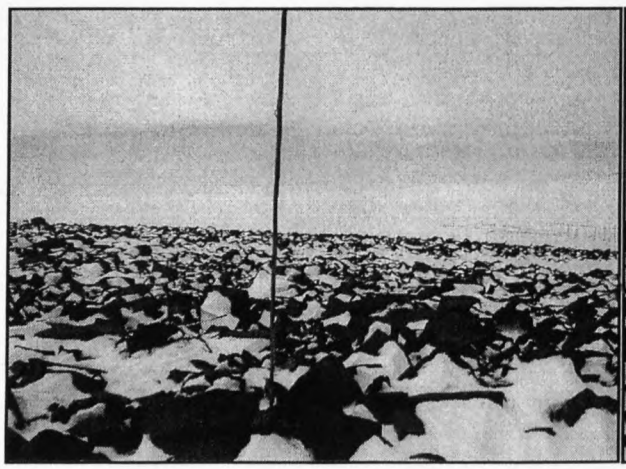

Figure I-1: From position 2 facing east

Figure I-2: From east towards position 2

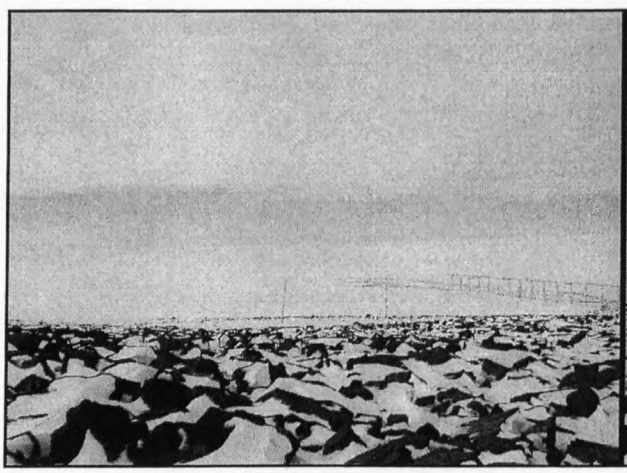

Figure I-3: From position 3 facing east

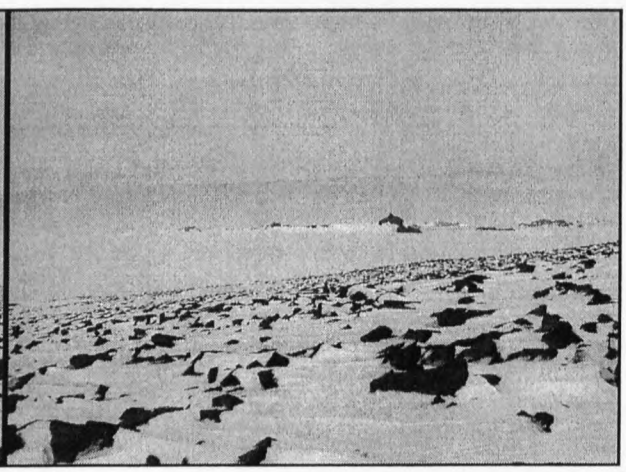

Figure I-4: From side towards south

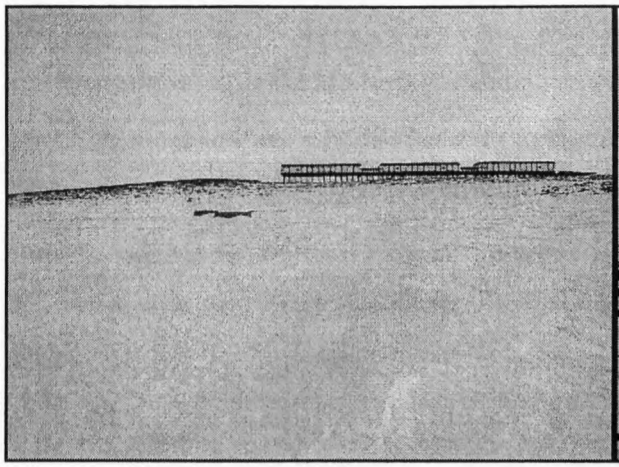

Figure I-5: From east towards position 4

Figure I-6: From side looking towards north

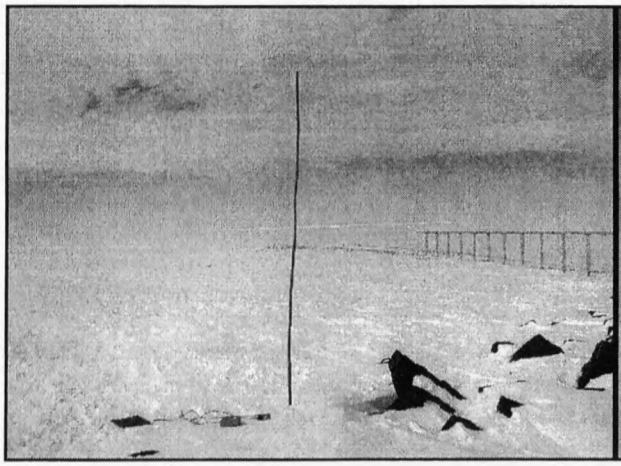

Figure I-7: From position 5 towards east

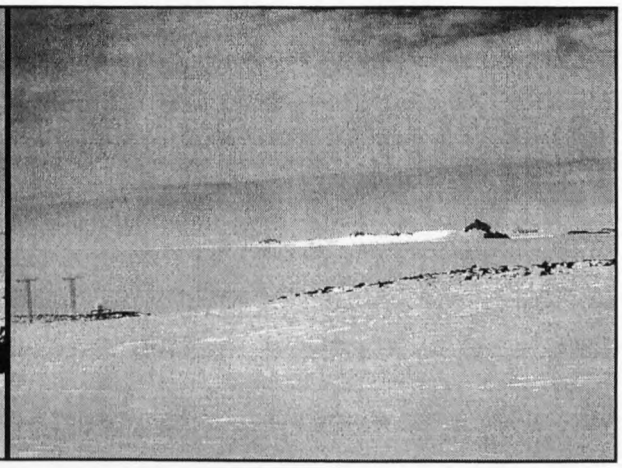

Figure I-8: From side looking towards south

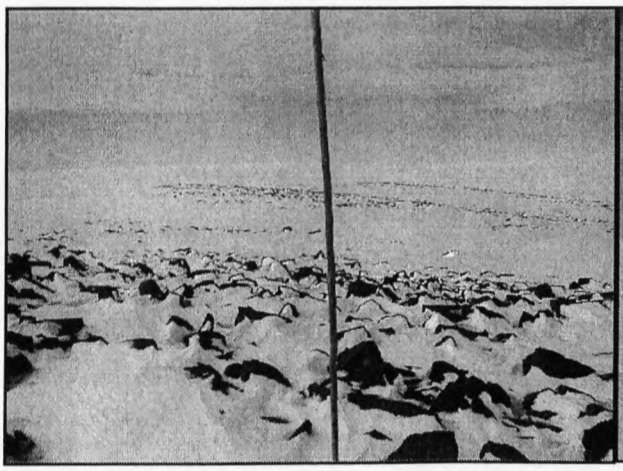

Figure I-9: From position 6 towards east

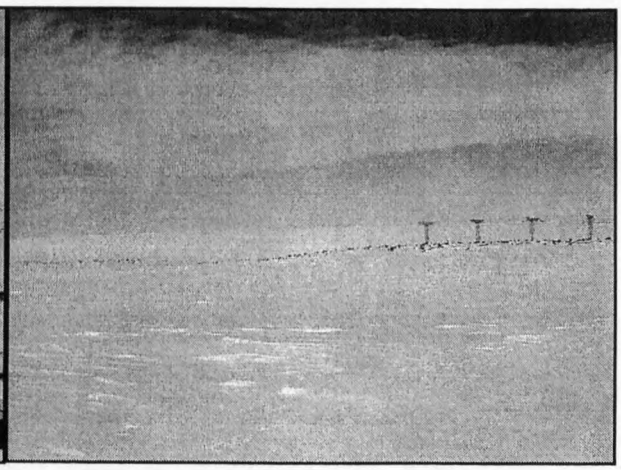

Figure I-10: From side looking towards south

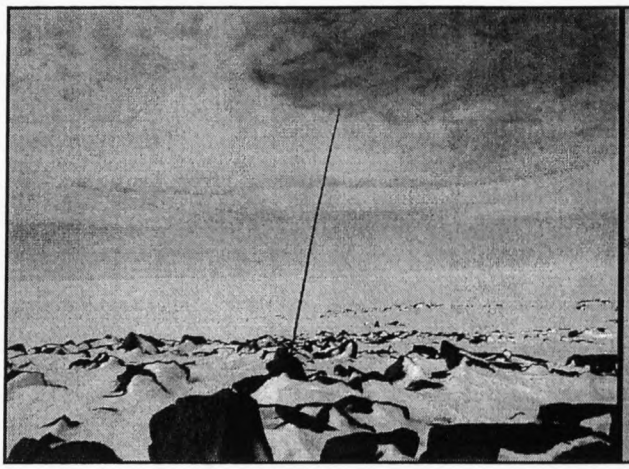

Figure I-11: From position 7 towards east

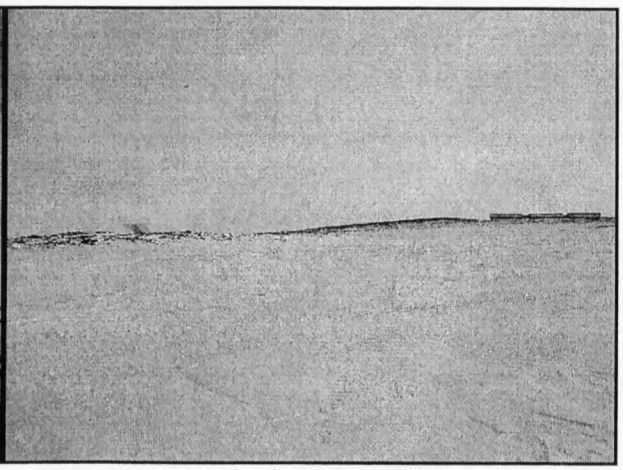

Figure I-12: From east towards position 7

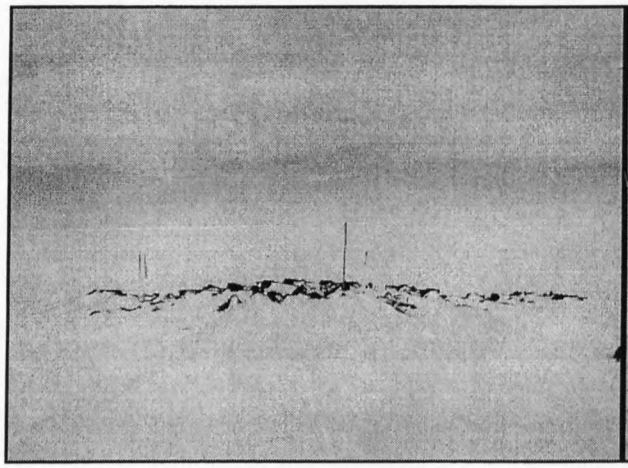

Figure I-13: From position 8 towards east

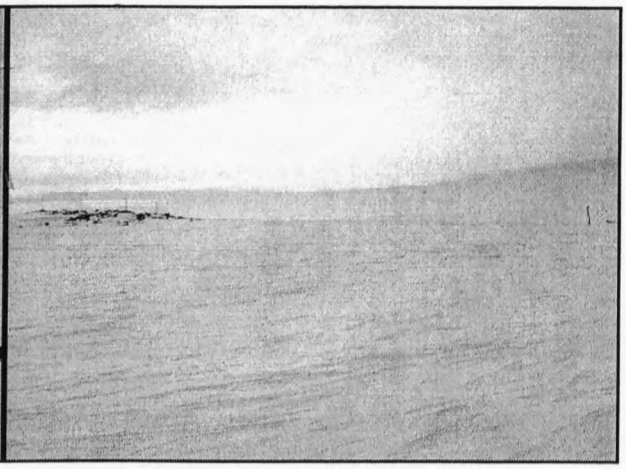

Figure I-14: From side looking towards north

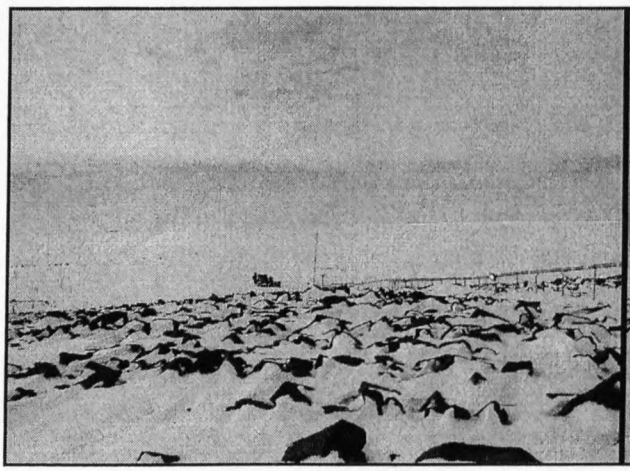

Figure I-15: From position 9 towards east

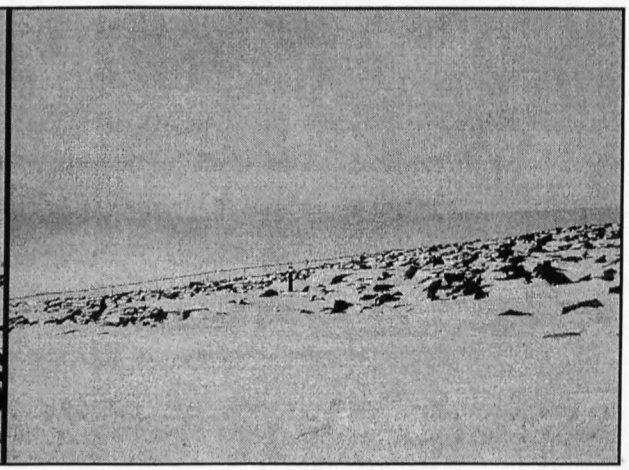

Figure I-16: From side looking towards south

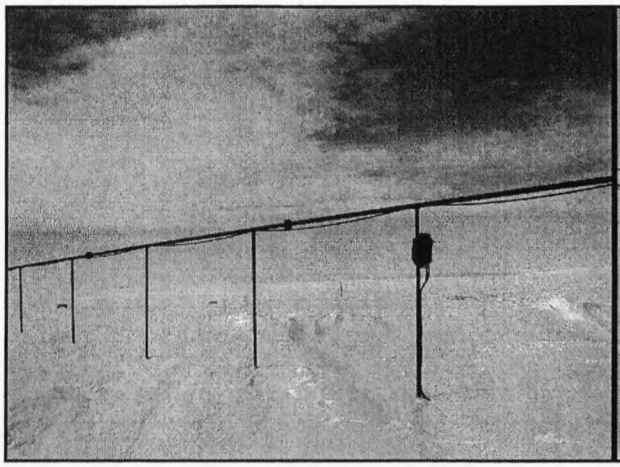

Figure I-17: From position 10 towards east

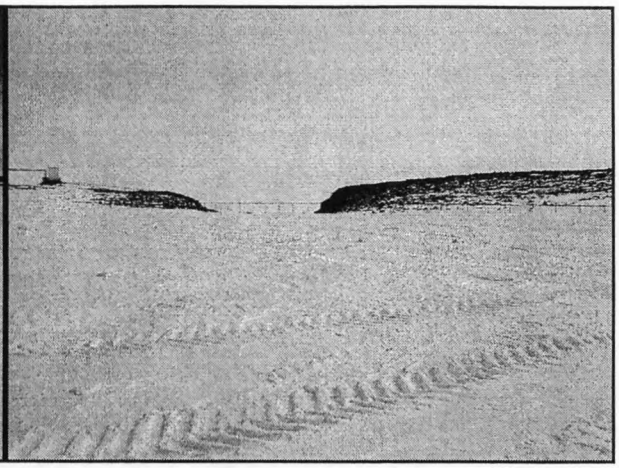

Figure I-18: From east towards position 10

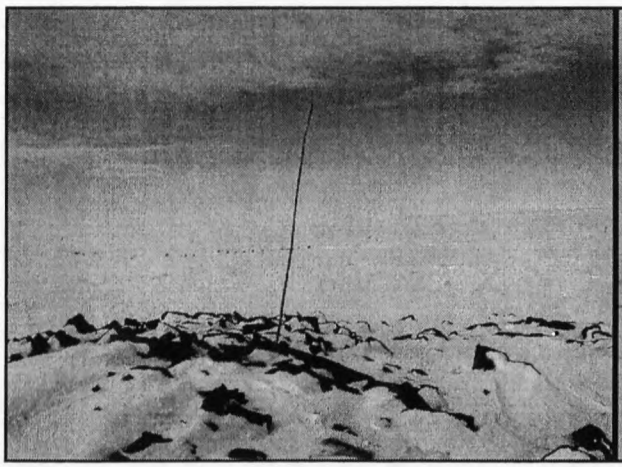

Figure I-19: From position 11 towards east

Figure I-20: From side looking towards north

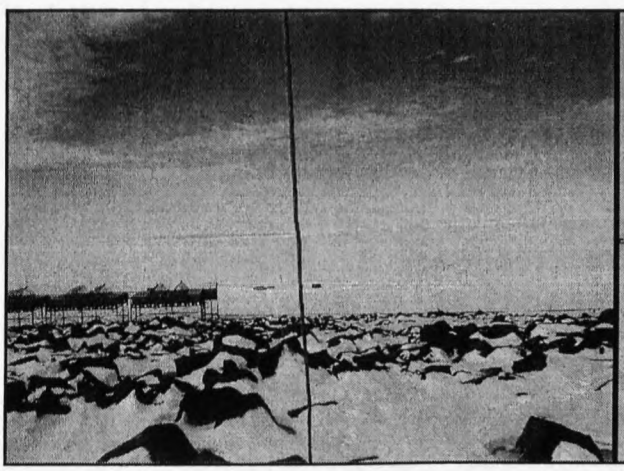

Figure I-21: From position 12 towards east

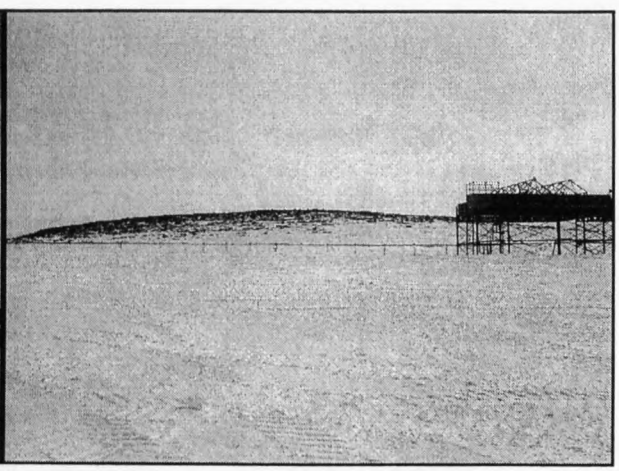

Figure I-22: From east towards position 12

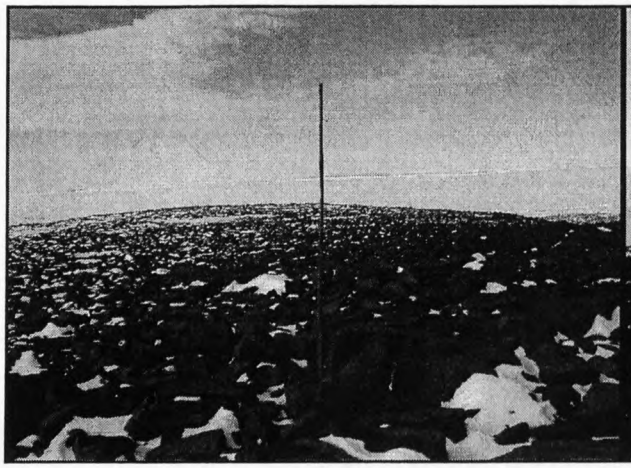

Figure I-23: From position 13 towards east

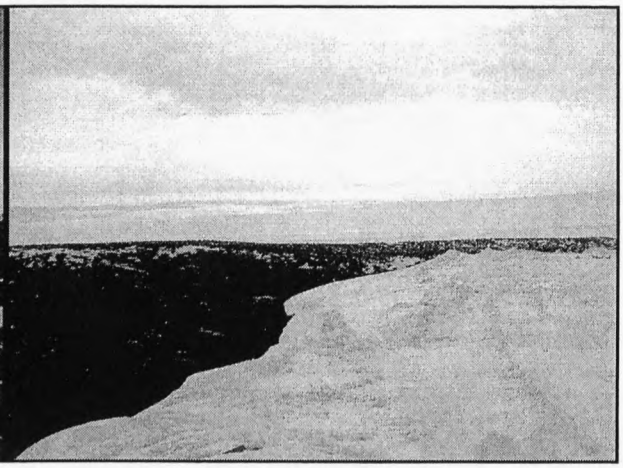

Figure I-24: From side looking towards north

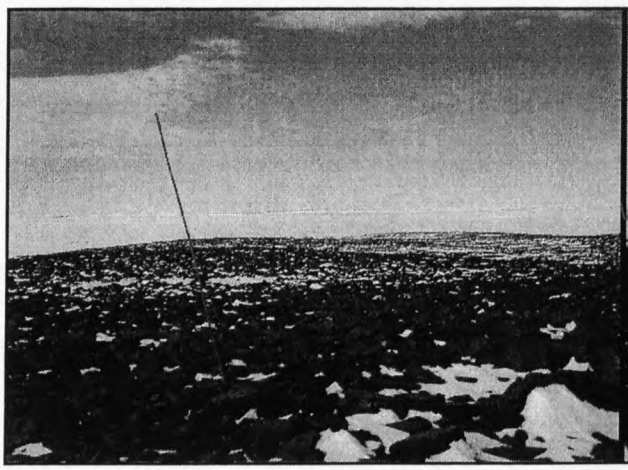

Figure I-25: From position 14 towards east

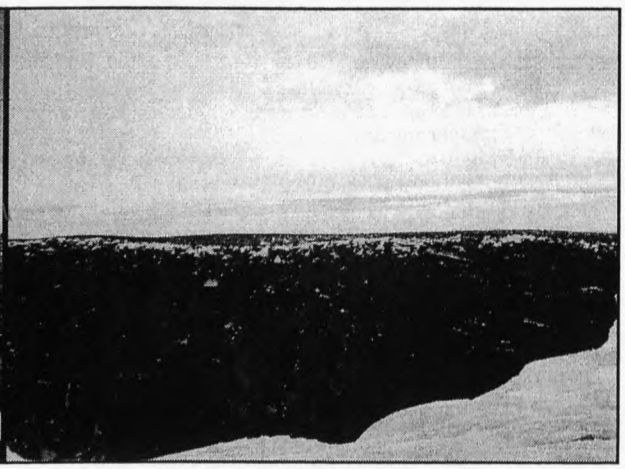

Figure I-26: From side looking towards north

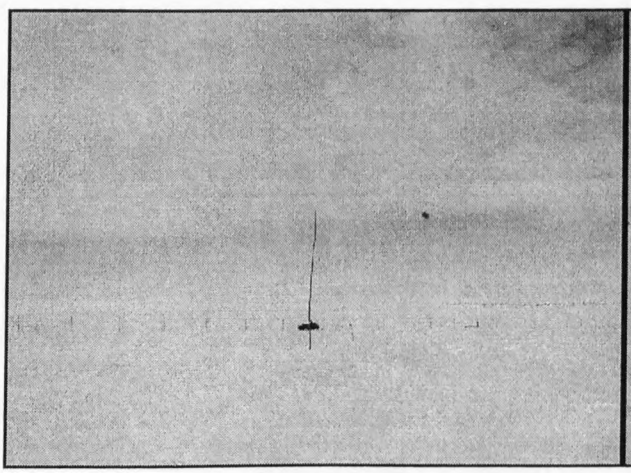

Figure I-27: From position 15 towards east

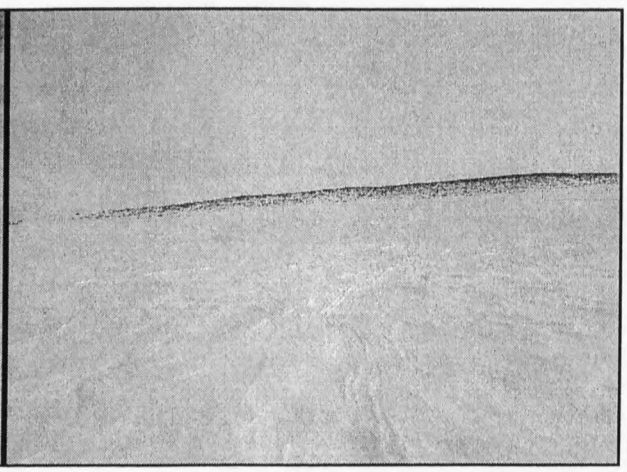

Figure I-28: From east towards position 15

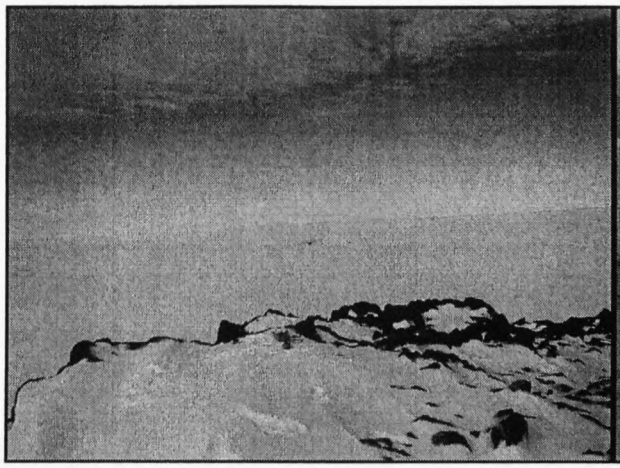

Figure I-29: From position 16 towards east

Figure I-30: From side looking towards north

APPENDIX J: BETZ LAW AND ADDITIONAL TURBINE ENERGY DATA

Betz Law

The more kinetic energy a wind turbine extracts out of the wind, the more the wind will be slowed down as it leaves the left side of the turbine in figure 7-2. Trying to extract all the energy from the wind, results that the air would move away with the zero speed, i.e. the air could not leave the turbine. In that case no energy is extracted at all, since all of the air would obviously also be prevented from entering the rotor of the turbine. In the other extreme case, the wind could pass though our tube without being hindered at all. In this case also, no energy will be extracted from the wind.

One can therefore assume that there must be some way of braking the wind which is in between these two extremes, and is more efficient in converting the energy in the wind to useful mechanical energy. It turns out that there is a surprisingly simple answer to this: An ideal wind turbine would slow down the wind by 2/3 of its original speed (DWEA, 2001). This is given by Betz's law. The following assumptions have been made for this derivation:

- The air flow is assumed frictionless.
- Therefore there is no change in internal energy from the inlet of the turbine to the outlet.
- There is no down stream whirl.

Making the reasonable assumption that the average wind speed through the rotor area is the average of the undisturbed wind speed before the wind turbine, v_1, and the wind speed after the passage through the rotor plane, v_2, i.e. $(v_1+v_2)/2$. The mass of the air streaming through the rotor during one second is

$$m := \rho \cdot F \cdot \frac{(v_1 + v_2)}{2} \qquad \textbf{(J-1)}$$

where m is the kg/s, ρ is the density of air, F is the swept rotor area and $[(v_1+v_2)/2]$ is the average wind speed through the rotor area. The power extracted from the wind by the rotor

is equal to the mass times the drop in the wind speed squared (according to Newton's second law):

$$P := \frac{1}{2}\cdot m\cdot\left(v_1^2 - v_2^2\right) \qquad \textbf{(J-2)}$$

Substituting m into this expression from the first equation we get the following expression for the power extracted from the wind:

$$P := \frac{\rho}{4}\cdot\left(v_1^2 - v_2^2\right)\cdot\left(v_1 + v_2\right)\cdot F \qquad \textbf{(J-3)}$$

Comparing this result with the total power in the undisturbed wind streaming through exactly the same area F, with no rotor blocking the wind. This power is called P_0:

$$P_0 := \frac{\rho}{2}\cdot v_1^3\cdot F \qquad \textbf{(J-4)}$$

The ratio between the powers that is extracted from the wind and the power in the undisturbed wind is then:

$$\left(\frac{P}{P_0}\right) := \frac{1}{2}\cdot\left[1 - \left(\frac{v_2}{v_1}\right)^2\right]\cdot\left[1 + \left(\frac{v_2}{v_1}\right)\right] \qquad \textbf{(J-5)}$$

The ratio between the powers P/P_0, as a function of v_2/v_1 is plotted in figure J-1. It can be seen that the function reaches its maximum for $v_2/v_1 = 1/3$, and that the maximum value for the power extracted from the wind is 0,59 or 16/27 of the total power in the wind.

Thus multiplying equations (7-13) and (7-14) with 0.59 or 16/27 the energy in the wind that can be extracted theoretically by a wind turbine was obtained. Table 7-2 shows the results.

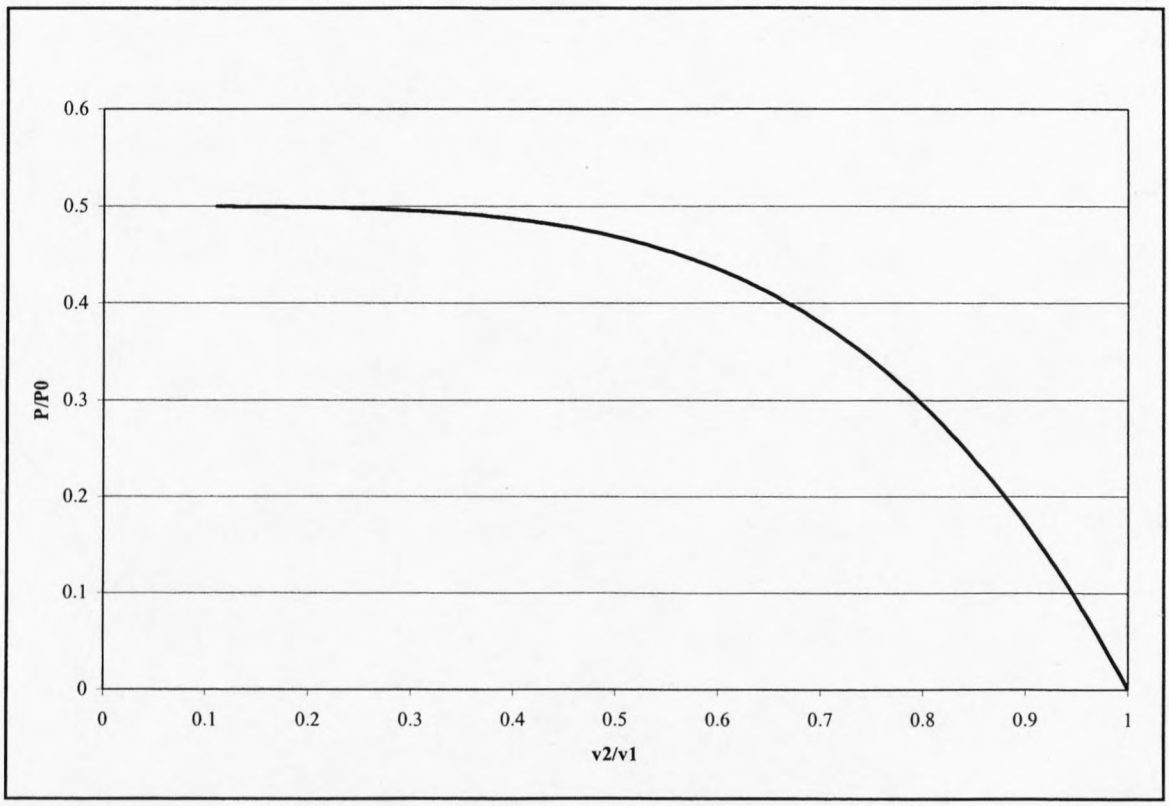

Figure J-1: Plot of power ratio versus velocity ratio

Wind Turbine Energy Output Continued

As mentioned in section 7.3.4, 5 different wind turbines have been selected, which potentially meet the requirements for installation, operation and maintenance at SANAE IV. The different wind turbines and the rated power output are given in table J-1.

Wind Turbine Manufacturer	Wind Turbine Description	Nominal Power Rating
Bergey Windpower Co., Inc.	Bergey BWC Excel	10 kW
Fuhrländer	Fuhrländer FL 30	30 kW
Atlantic Orient	Atlantic Orient 15/50	50 kW
Fuhrländer	Fuhrländer FL 100	100 kW
Northern Power Systems	North Wind NW100/19	100 kW

Table J-1: Wind turbines used for energy calculations and nominal power ratings

In this section the power output of each wind turbine, mentioned above, except for the North Wind NW100/19 wind turbine, will be presented. To do this, the Weibull parameters for the different hub heights are calculated and are shown in table J-2.

This section of the appendix was set up as follows. The performance of the wind turbines was compared. This information was used in section 7.2.12 to do a recommendation regarding the turbine that is most likely the best-suited wind turbine for application at SANAE IV, based on the wind and the power output analysis.

It is very important to note that no calculations will be shown in the following subsections, since the sample calculations are done in section 7.3, and are applicable to these wind turbine configurations as well.

	Weibul Parameters							
	Height: 9m		Height: 10m		Height: 13m		Height: 18m	
Month	**c[m/s]**	**k**	**c[m/s]**	**k**	**c[m/s]**	**k**	**c[m/s]**	**k**
January	1.91	7.42	2.19	7.87	1.90	7.70	1.90	7.95
February	2.04	9.67	2.26	9.99	2.03	10.04	2.02	10.38
March	1.96	12.87	2.07	13.14	1.95	13.40	1.94	13.87
April	2.18	11.04	2.35	11.31	2.16	11.49	2.15	11.88
May	1.96	10.03	2.15	10.36	1.95	10.43	1.94	10.78
June	2.02	17.73	2.07	18.00	2.00	18.51	1.99	19.21
July	1.85	14.29	1.91	14.57	1.83	14.90	1.82	15.43
August	1.86	13.59	2.00	13.85	1.85	14.16	1.84	14.66
September	1.73	11.95	1.83	12.29	1.72	12.44	1.71	12.88
October	1.61	15.09	1.71	15.44	1.60	15.74	1.59	16.32
November	1.58	13.00	1.69	13.36	1.57	13.55	1.56	14.04
December	1.31	10.00	1.44	10.53	1.31	10.40	1.30	10.76
January	1.43	8.48	1.58	8.99	1.42	8.82	1.42	9.12
February	1.47	10.15	1.61	10.60	1.47	10.56	1.46	10.92
Complete Period	1.60	11.80	1.71	12.17	1.59	12.28	1.58	12.71

	Height:25m		Height: 27m		Height: 30m		Height: 35m	
Month	**c[m/s]**	**k**	**c[m/s]**	**k**	**c[m/s]**	**k**	**c[m/s]**	**k**
January	1.90	8.21	1.90	8.26	1.89	8.35	1.89	8.46
February	2.02	10.72	2.01	10.80	2.01	10.91	2.01	11.07
March	1.93	14.35	1.93	14.46	1.93	14.61	1.92	14.83
April	2.15	12.27	2.14	12.37	2.14	12.49	2.14	12.68
May	1.93	11.14	1.93	11.22	1.93	11.34	1.93	11.50
June	1.97	19.91	1.97	20.07	1.97	20.30	1.96	20.63
July	1.81	15.98	1.81	16.11	1.80	16.28	1.80	16.53
August	1.83	15.17	1.83	15.30	1.83	15.45	1.83	15.69
September	1.70	13.32	1.70	13.42	1.69	13.57	1.69	13.77
October	1.58	16.91	1.58	17.04	1.58	17.22	1.57	17.50
November	1.56	14.52	1.55	14.63	1.55	14.78	1.55	15.03
December	1.30	11.13	1.30	11.22	1.29	11.34	1.29	11.51
January	1.41	9.41	1.41	9.50	1.41	9.57	1.41	9.72
February	1.45	11.29	1.45	11.38	1.45	11.49	1.45	11.67
Complete Period	1.57	13.15	1.57	13.24	1.57	13.38	1.57	13.58

Table J-2: Weibull shape and scale parameters for different heights

Energy Output of Different Wind Turbines

The power curve of a wind turbine is a graph that indicates how large the electrical power output will be for the turbine at different wind speeds. Figure J-2 shows the power curves for the four different wind turbines.

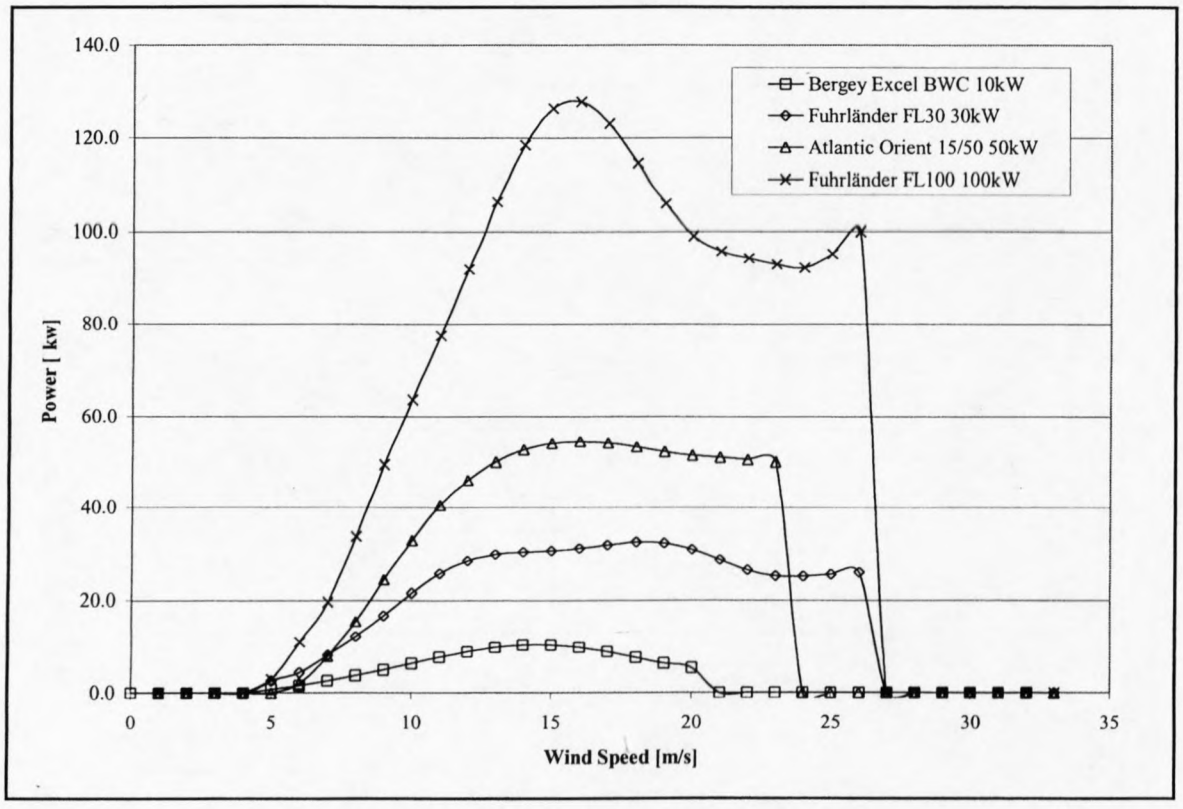

Figure J-2: Power curves of the four different wind turbines

The curves in figure J-2 are curve fits of the power curve data. The functions were found by doing a regression analysis. For the Bergey Excel BWC 10kW wind turbine, the function is a 7-degree polynomial:

$$y := -2.0191 \cdot \exp^{-6} \cdot x^7 + 0.0001805 \cdot x^6 - 0.006549 \cdot x^5 + 0.1122501 \cdot x^4 - 1.37007 \cdot x^3 + 8.753371 \cdot x^2 - 29.511469 \cdot x + 40.467941 \quad \textbf{(J-6)}$$

For the Fuhrländer FL30 30kW wind turbine, the function is a 10-degree polynomial:

$$y := 1.26464 \cdot \exp^{-8} \cdot x^{10} - 1.83743 \cdot \exp^{-6} \cdot x^9 + 0.000116 \cdot x^8 - 0.004180 \cdot x^7 + 0.094758 \cdot x^6 - 1.40809 \cdot x^5 + 13.85503 \cdot x^4 - 89.08065 \cdot x^3 + 358.84595 \cdot x^2 - 817.21105 \cdot x + 799.20876 \quad \textbf{(J-7)}$$

For the Atlantic Orient 15/50 50kW wind turbine, the function is a 10-degree polynomial:

$$y := 9.36632 \cdot \exp^{-9} \cdot x^{10} - 1.12476 \cdot \exp^{-6} \cdot x^9 + 5.7673 \exp^{-5} \cdot x^8 - 0.001637 \cdot x^7 + 0.027723 \cdot x^6 - 0.27624 \cdot x^5 + 1.38513 \cdot x^4 - 0.36615 \cdot x^3 - 31.11134 \cdot x^2 + 141.03734 \cdot x - 207.82464 \quad \textbf{(J-8)}$$

For the Fuhrländer FL100 100kW wind turbine, the function is a 10-degree polynomial:

$$y := -5.2572 \cdot \exp^{-8} \cdot x^{10} + 7.6724 \cdot \exp^{-6} \cdot x^{9} - 4.8768 \exp^{-4} \cdot x^{8} + 0.01772 \cdot x^{7} - 0.40629 \cdot x^{6} + 6.1211 \cdot x^{5} - 61.1860 \cdot x^{4} + 399.5046 \cdot x^{3} - 1625.2544 \cdot x^{2} + 3718.6183 \cdot x - 3636.4059 \quad \textbf{(J-9)}$$

The reason for creating such high degree polynomials is that the power curves will be used to calculate the true power output of the wind turbines and therefore functions for these power curves were found, which are as accurate as possible. The regression coefficients of equations (J-6), (J-7), (J-8) and (J-9) are R^2 = 0.9998, 0.9986, 0.9996 and 0.9988, respectively.

Power density function

Although these are fairly small wind turbines, they could be used to cover part of the energy demand of the base. The application of these wind turbines at SANAE IV range from being test turbines to energy demand covering wind turbines. Some of the important technical specifications for the energy analysis are given in table J-3. The wind data is based on a height of 10 m only. As mentioned before the wind speed data, captured between January 2001 and February 2002, has been extrapolated to the relevant heights. The energy potential per second (the power) varies in proportion to the cube of the wind speed, and in proportion to the density of the air.

Therefore, if the power of each wind speed is multiplied with the probability of each wind speed from the Weibull graph, then the distribution of wind energy at different wind speeds = the power density has been calculated.

$$P_D := \sum_{i=1}^{n} P_i \cdot f(v_i) \quad \textbf{(J-10)}$$

Bergey BWC Excel 10kW wind turbine			
Rotor:		**Performance:**	
Diameter	7.0 m	Nominal power rating	10 kW
Swept area	38.5 m^2	Rated wind speed	13 m/s
Power regulation	Powerflex blade pitch control	Cut-in wind speed	3.1 m/s
Tower:		Cut-out wind speed	20 m/s
Type	Tubular with guides	Survival wind speed	53.6 m/s
Height	13 m		
Fuhrländer FL30 30kW wind turbine			
Rotor:		**Performance:**	
Diameter	13 m	Nominal power rating	30 kW
Swept area	133 m^2	Rated wind speed	12 m/s
Power regulation	Stall regulated	Cut-in wind speed	2.5 m/s
Tower:		Cut-out wind speed	25 m/s
Type	Lattice tower	Survival wind speed	67 m/s
Height	18 m		
Atlantic Orient 15/50 50kW wind turbine			
Rotor:		**Performance:**	
Diameter	15.0 m	Nominal power rating	50 kW
Swept area	177 m^2	Rated wind speed	12.0 m/s
Power regulation	Fixed pitch, blade tip brake	Cut-in wind speed	4.6 m/s
Tower:		Cut-out wind speed	22.4 m/s
Type	3 legged lattice tower	Survival wind speed	59.5 m/s
Height	25 m		
Fuhrländer Fl100 100kW wind turbine			
Rotor:		**Performance:**	
Diameter	21.0 m	Nominal power rating	100 kW
Swept area	346 m^2	Rated wind speed	13 m/s
Power regulation	Stall controlled	Cut-in wind speed	2.5 m/s
Tower:		Cut-out wind speed	25 m/s
Type	Tubular	Survival wind speed	67.0 m/s
Height	35 m		

Table J-3: Technical specifications of the four wind turbines

Power coefficient

The power coefficient indicates how efficiently a turbine converts the energy in the wind to electricity. Very simply, the electrical power output is divided by the wind energy input to measure how technically efficient a wind turbine is. In other words, take the power curve, and dividing it by the area of the rotor to obtain the power output per square meter of rotor area. For each wind speed, divide the result by the amount of power in the wind per square meter.

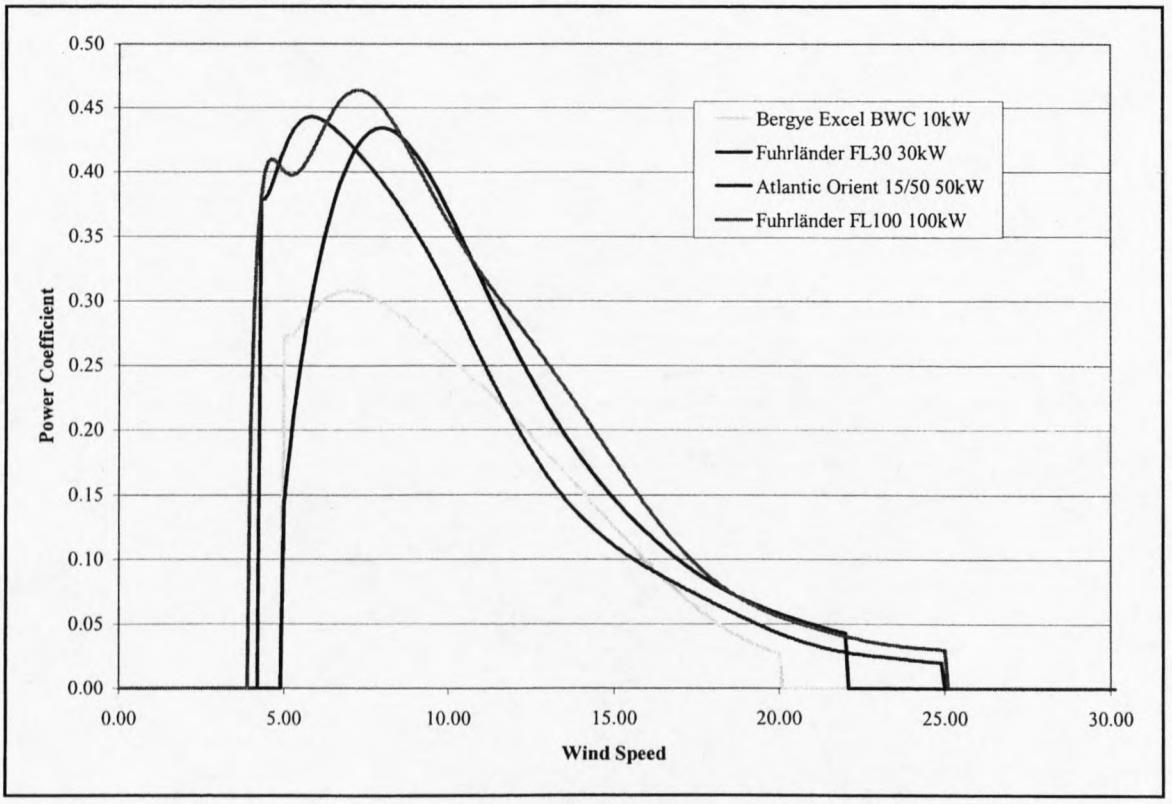

Figure J-3: Power coefficient curve for the four wind turbines

Figure J-3 shows a power coefficient curve for the four wind turbines. Although the average efficiency for these turbines is somewhat above 20%, the efficiency varies very much with the wind speed. At low wind speeds efficiency is not so important, because there is not much energy to harvest. At high wind speeds the turbine must waste any excess energy above what the generator was designed for. Efficiency therefore matters most in the region of wind speeds where most of the energy is to be found.

Annual energy output from a wind turbine

Taking the previous sections into account, it is now possible to calculate the relationship between average wind speeds and annual energy output from a wind turbine.

With the weather data from SANAE IV, the Weibull shape parameter is k = 1.57 at a height of 25 m, as mentioned previously. A smaller k corresponds to a more variable wind, while a bigger k, in the region of 2.5, corresponds to a more even wind speed distribution. A shape parameter of k = 1.57 corresponds to a wind speed distribution that is relatively variable and gusty. The results for the monthly and annual energy output from the four wind turbines can be seen in table J-4.

	Bergey Excel BWC	Fuhrländer FL30	Atlantic Orient 10/50	Fuhrländer FL100
	Yearly / Monthly Turbine Power Output			
	[MWh/Year]			
Complete Year:	35.80	155.17	234.47	536.38
Month:	[MWh/Month]			
Jan-01	2.13	9.26	14.34	32.36
Feb-01	3.13	12.89	20.53	45.74
Mar-01	3.53	14.99	23.08	51.99
Apr-01	3.62	14.71	23.48	52.14
May-01	3.18	13.14	20.84	46.43
Jun-01	3.15	14.45	20.81	48.19
Jul-01	3.33	14.54	21.81	49.68
Aug-01	3.38	14.64	22.22	50.39
Sep-01	3.18	13.61	20.89	47.16
Oct-01	2.94	13.18	19.44	44.60
Nov-01	2.98	13.10	19.64	44.94
Dec-01	2.45	10.73	16.22	37.07
Jan-02	2.35	10.12	15.55	35.22
Feb-02	2.69	11.59	17.73	40.19

Table J-4: Annual and monthly wind turbine energy output

Wind Turbine Operating Percentages

To analyze the effect of the wind turbine's height on the wind power generation, the power density for the four different wind turbines was calculated using different turbine hub heights for the analysis. The results are given in table J-5 and figure J-4. The power density for the different turbines is obviously the same.

Hub height [m]	Average wind speed [m/s]	Shape parameter k	Scale parameter c [m/s]	Average power density [W/m^2]
9	10.85	1.60	11.80	1821.11
13	11.02	1.59	12.28	2073.78
18	11.41	1.58	12.71	2323.63
25	11.81	1.57	13.15	2601.07
30	12.02	1.57	13.38	2739.95
35	12.20	1.57	13.58	2864.67

Table J-5: Power density for different hub heights

The values of average wind speed and average power density increase with height. Obviously, to obtain more wind power, the higher the hub height of the wind turbine should be.

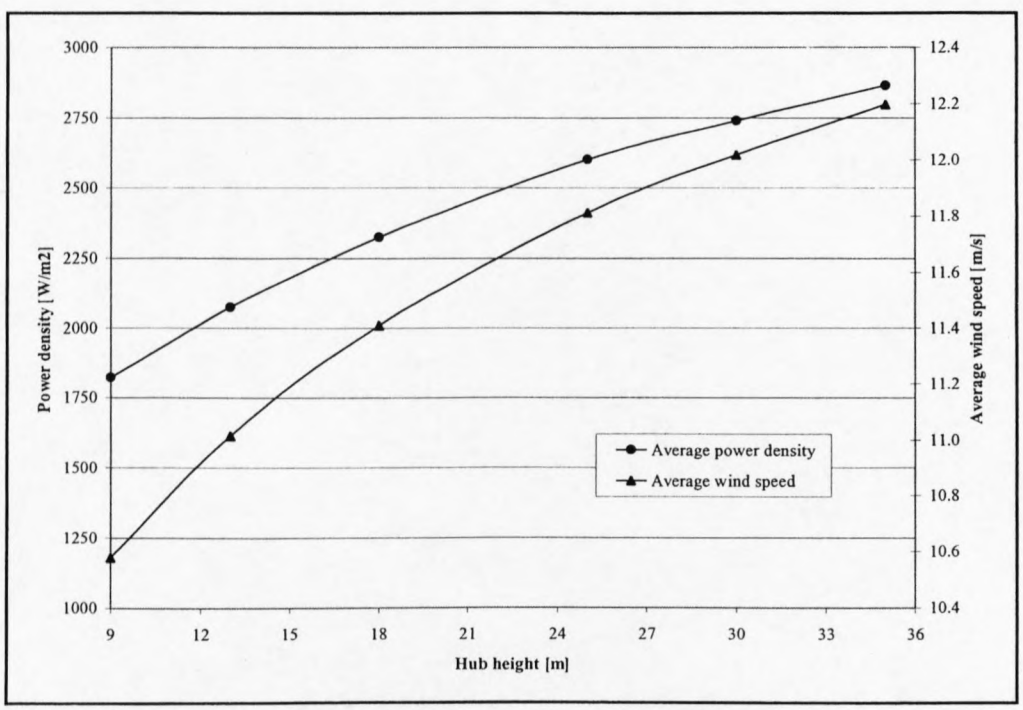

Figure J-4: Annual power density versus average wind speed for different hub heights

For different hub heights, the average wind speed and power density are different. In assessing the wind power potential, or choosing the suitable type of wind turbine, not only

the wind data but also the site circumstances (terrain, different referred height, surface roughness) should be considered.

Operating hours of wind turbine

For the Bergey BWC Excel wind turbine, the cut-in speed is 3.1 m/s and the cut-off wind speed is 20 m/s. For the four tower heights and other heights for comparison, the operating hours of the wind turbine in a year can be calculated, as shown in figures J-5 to J-8. From the operating percentage, the operating time per annum can be simply calculated by multiplying the operating fraction with the amount of hours in a year, which is 8760 h. Thus the operating time for the given example at 25 m hub height is OT = 0.7568 8760 h = 6630 h.

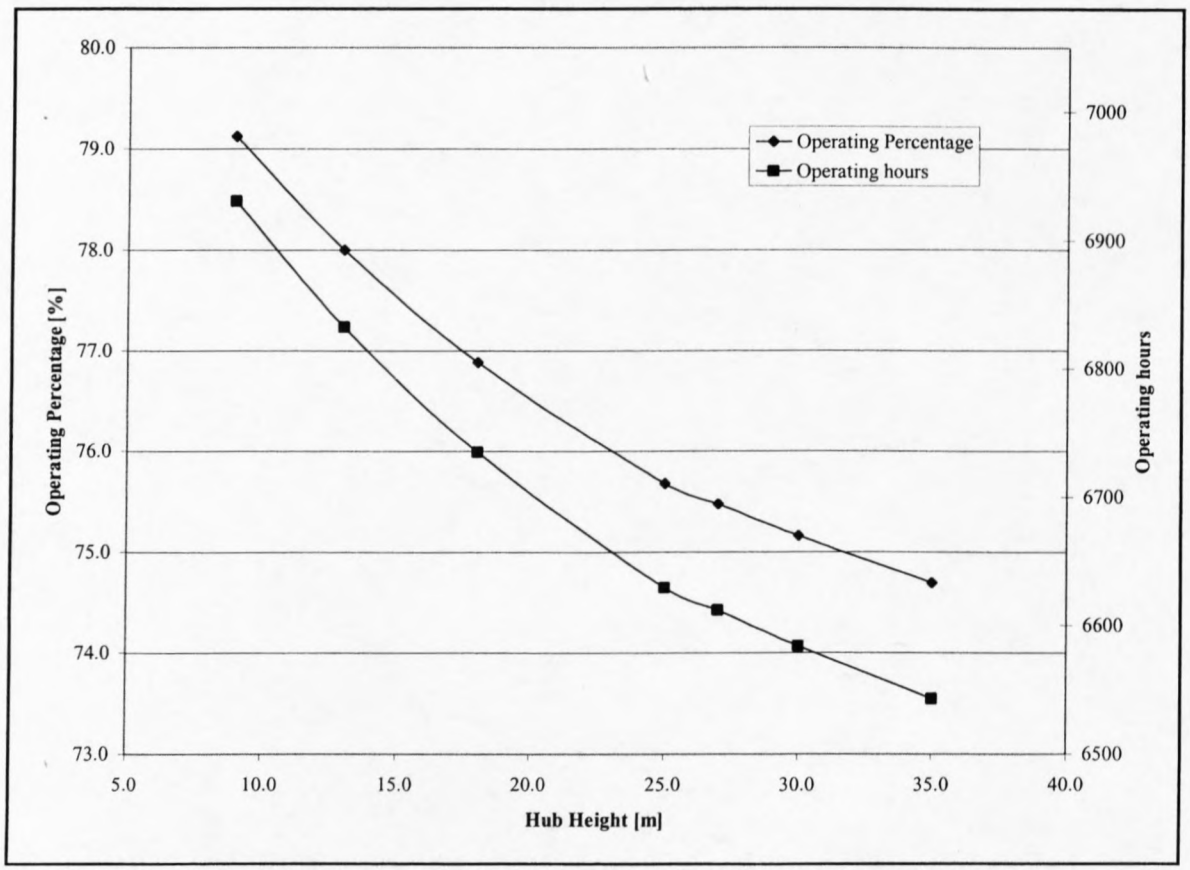

Figure J-5: Operating percentage versus wind turbine hub height (BWC)

For the Fuhrländer FL30 wind turbine the operating hours of the wind turbine in a year are shown in figure J-6.

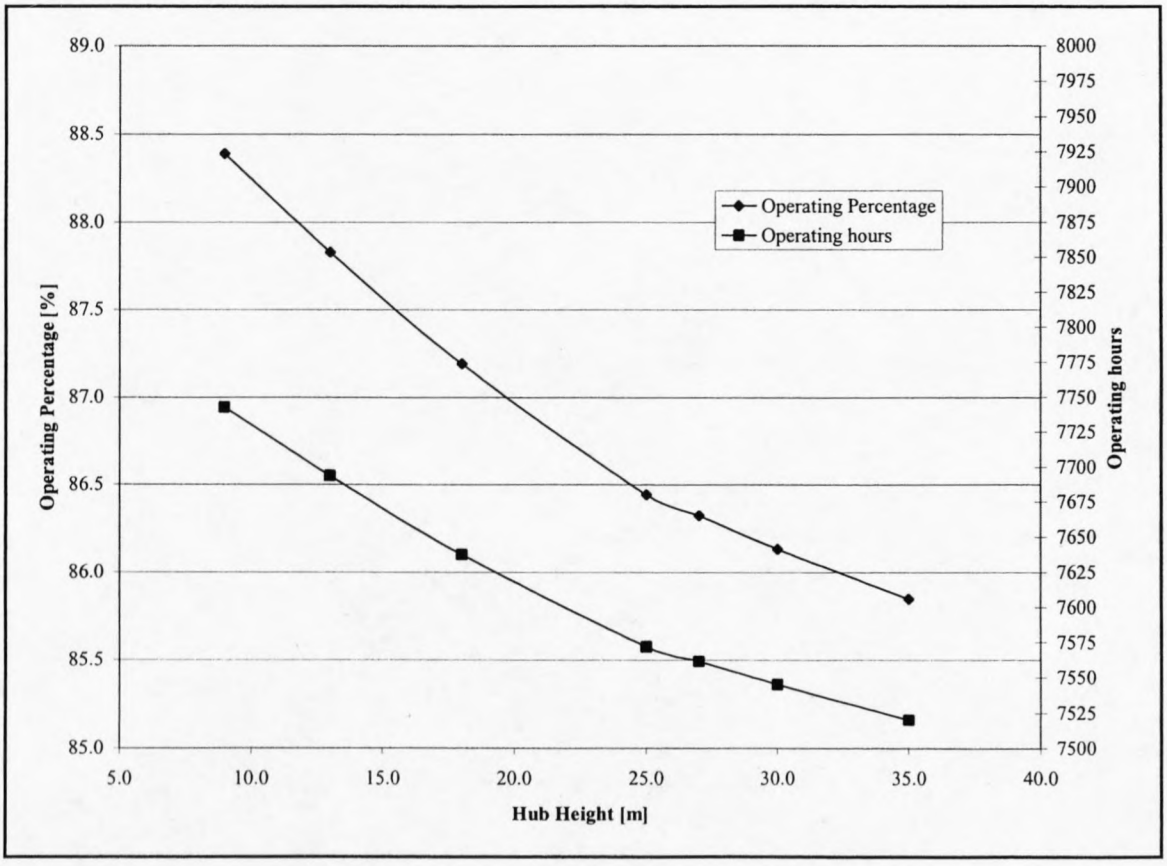

Figure J-6: Operating percentage versus wind turbine hub height (FL30)

Figure J-6 shows that, for different tower heights, the operating hours of the wind turbine are also different. For an 18-m-high tower, the total operating hours are 7638 h (87.19 %) in a year, but 7520 h (85.85 %) for a 35-m-high tower, a difference of 118 h. Normally, the higher the tower is, the bigger is the operating time. The reason why this is not the case for our example is, that the cut-out wind speed is 25 m/s and at higher tower heights, the wind speeds more often exceed the cut-out speed, the wind turbine has to be shut down and thus the operating time is decreased.

For the Atlantic Orient 50/15 wind turbine the operating hours of the wind turbine in a year are shown in figure J-7.

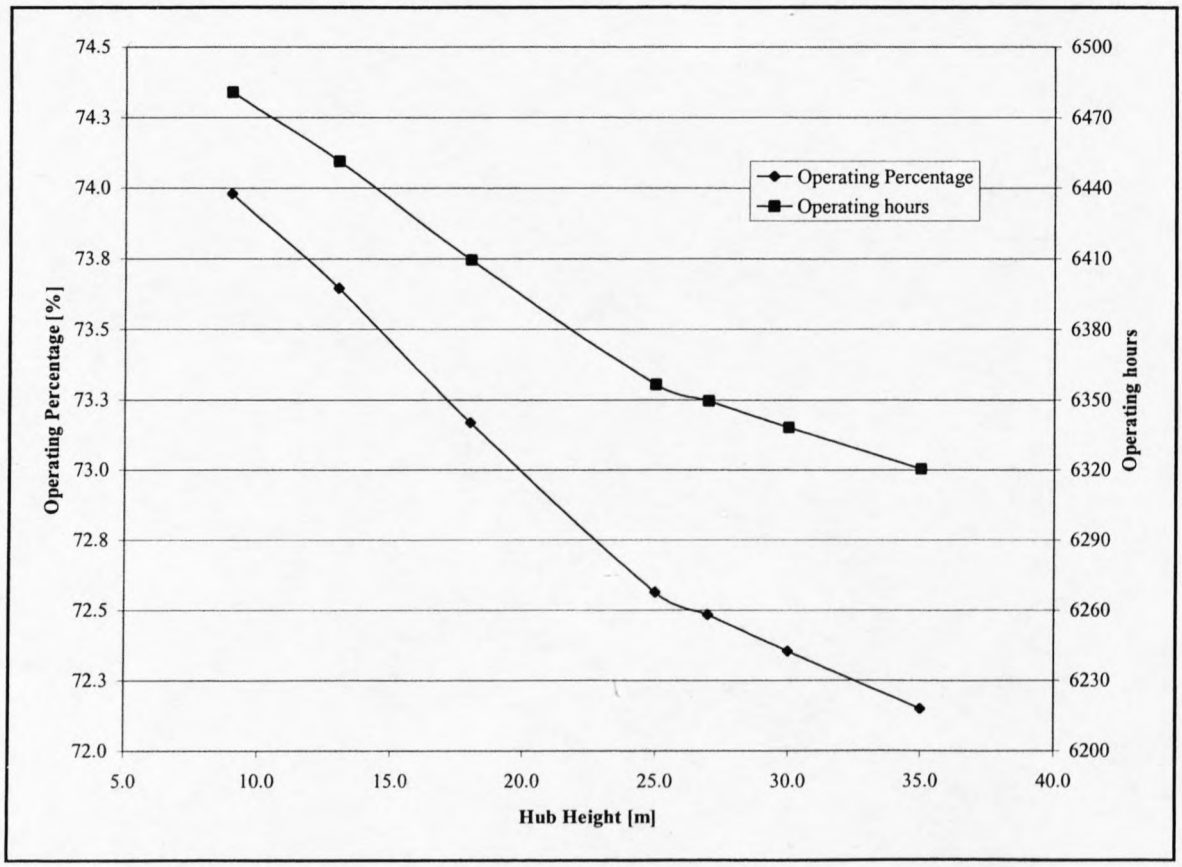

Figure J-7: Operating percentage versus wind turbine hub height (15/50)

Again figure J-7 shows that, for different tower heights, the operating hours of the wind turbine are also different. For an 18-m-high tower, the total operating hours are 6410 h (73.17 %) in a year, but 6320 h (72.15 %) for a 35-m-high tower, a difference of 90 h. Normally, the higher the tower is, the bigger is the operating time. The reason why this is not the case for our example is, that the cut-out wind speed is 22.4 m/s and at higher tower heights, the wind speeds more often exceed the cut-out speed, the wind turbine has to be shut down and thus the operating time is decreased.

For the Fuhrländer FL100 wind turbine the operating hours of the wind turbine in a year are shown in figure J-8.

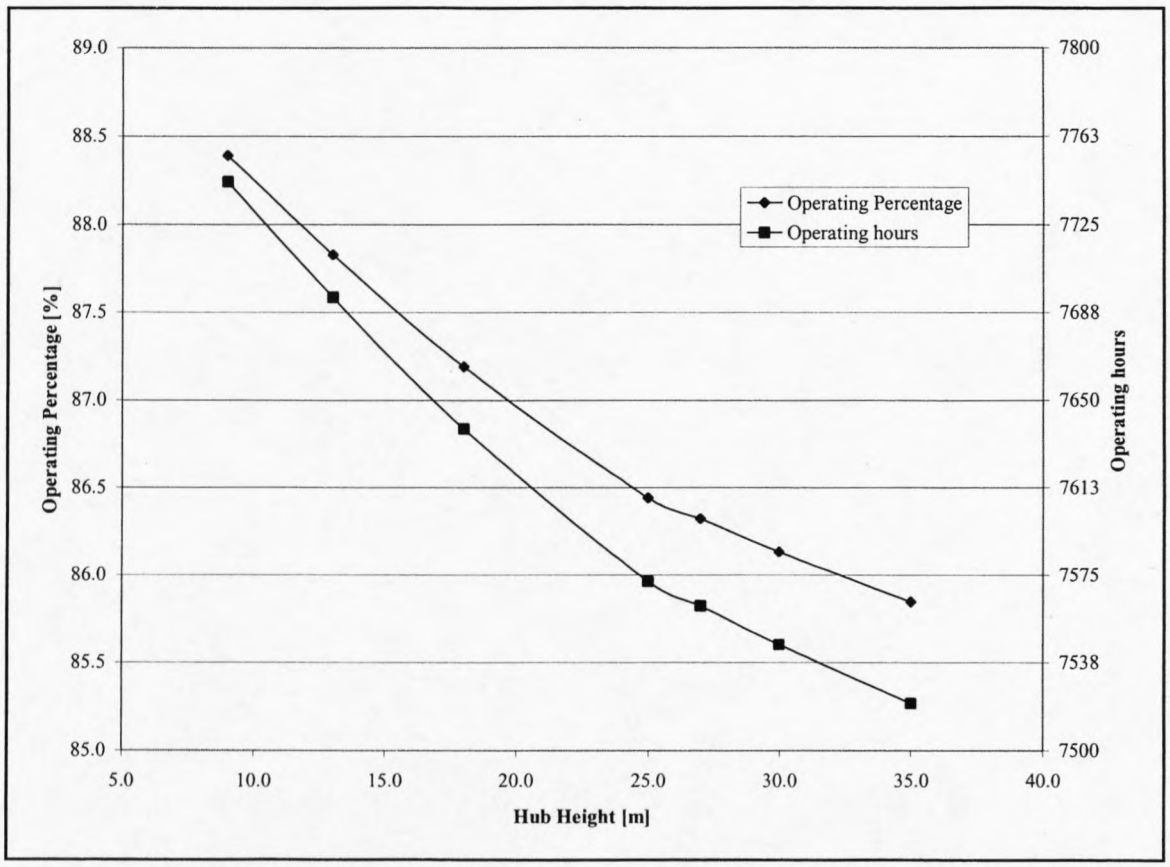

Figure J-8: Operating percentage versus wind turbine hub height (FL100)

Figure J-8 shows that, for different tower heights, the operating hours of the wind turbine are also different. For an 18-m-high tower, the total operating hours are 7638 h (87.19 %) in a year, but 7520 h (85.85 %) for a 35-m-high tower, a difference of 118 h. Normally, the higher the tower is, the bigger is the operating time. The reason why this is not the case for our example is, that the cut-out wind speed is 25 m/s and at higher tower heights, the wind speeds more often exceed the cut-out speed, the wind turbine has to be shut down and thus the operating time is decreased.

Figures J-9 to J-12 show that the operating percentage changes for different months during the year. For the Fuhrländer FL100 wind turbine the highest of 95.52 % occurs in April, while the lowest is 75.16 % in June. The trend is not in accordance with the monthly wind power density, because the operating percentage is not only determined by the wind data distribution, but also by the performance of the wind turbine and specifically the cut-in and cut-out speeds of the wind turbine.

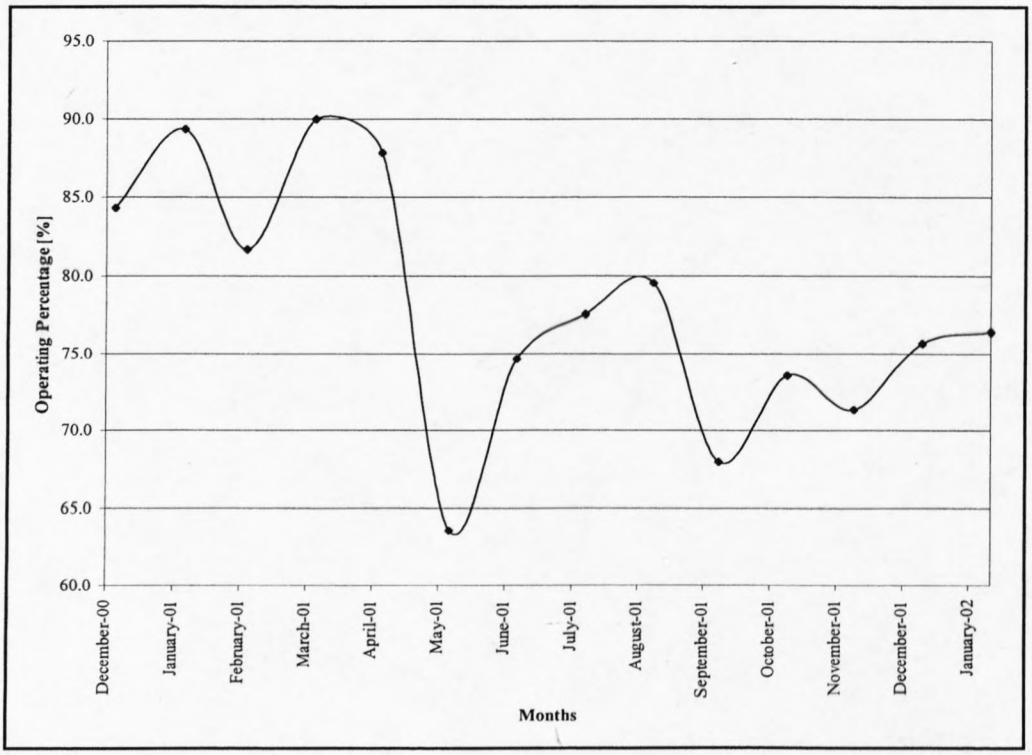

Figure J-9: Monthly operating percentage of the Bergey BWC Excel wind turbine (13 m high tower)

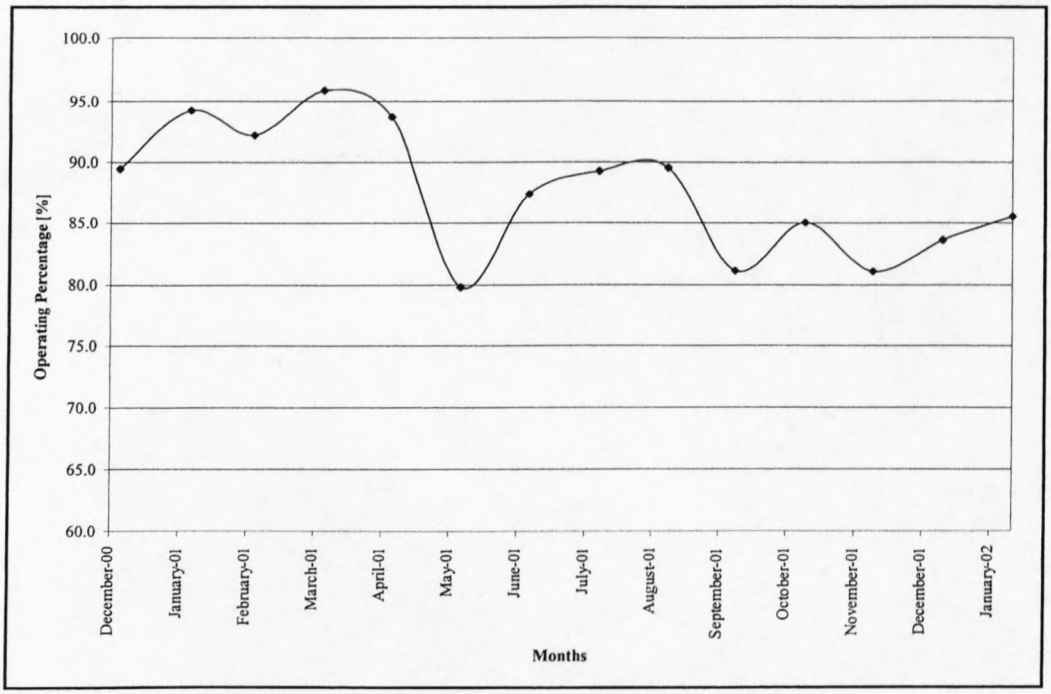

Figure J-10: Monthly operating percentage of the Fuhrländer FL30 wind turbine (18 m high tower)

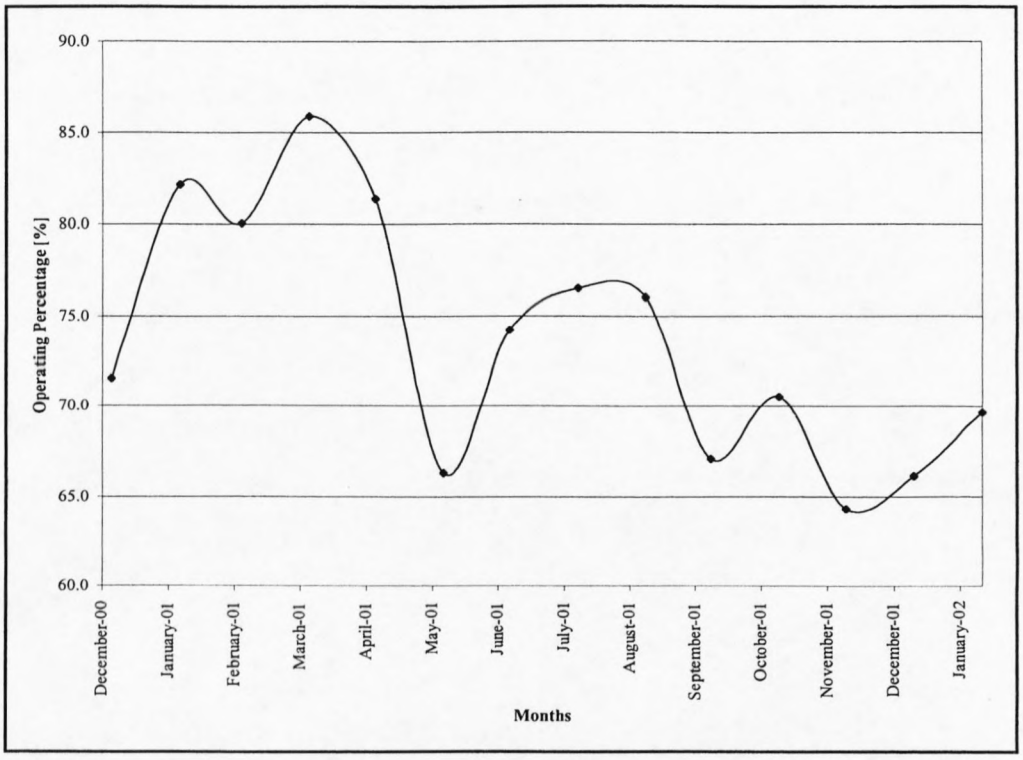

Figure J-11: Monthly operating percentage of the Atlantic Orient 50/15 (25 m high tower)

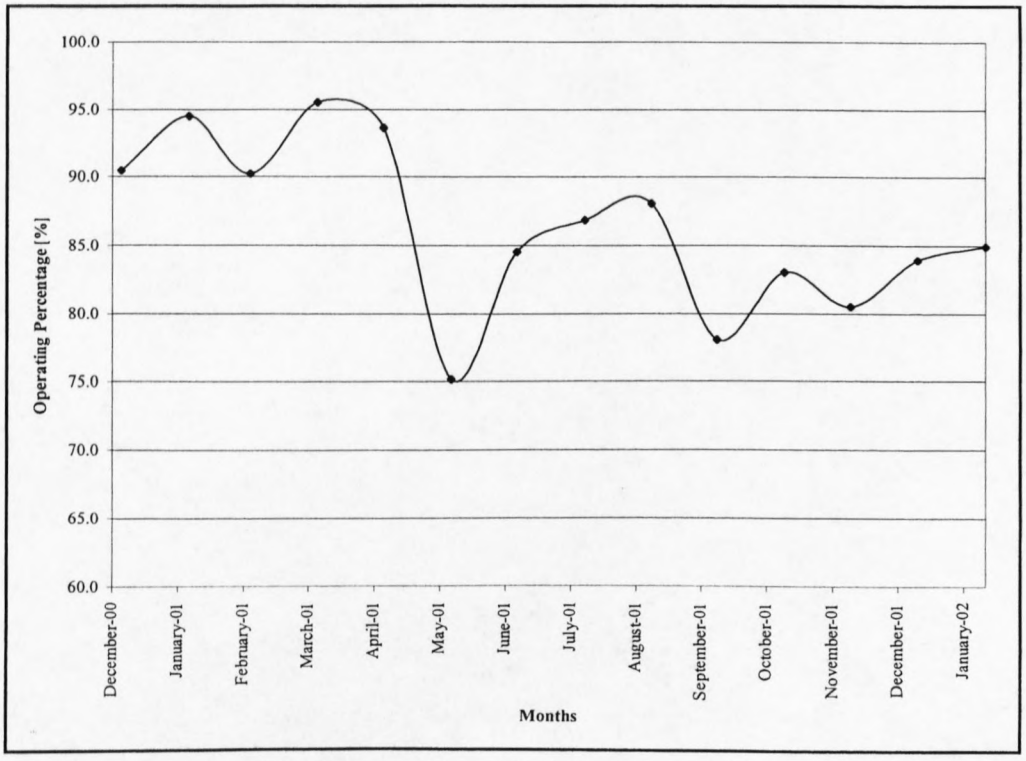

Figure J-12: Monthly operating percentage of the Fuhrländer FL100 wind turbine (35 m high tower)

Power output of wind turbine

Using the Weibull function and the polynomial regression functions, from equation (J-6) to (J-9), the average annual power generated by the wind turbines can be estimated. For different hub heights, the yearly power generated was calculated and the results are given in figures J-13 to J-16. For the Bergey Excel BWC wind turbine the power difference between the different hub heights is relatively small since, again, the cut-out speed limits the wind turbine of producing more energy due to higher wind speeds at higher hub heights. Another interesting fact that can be seen from the graph is that the annual power output of the wind turbine does not change significantly, the power output is even smaller at a height of 35 m, than at a height of 18 m. This paradox comes from the cut-out wind speed of the turbine.

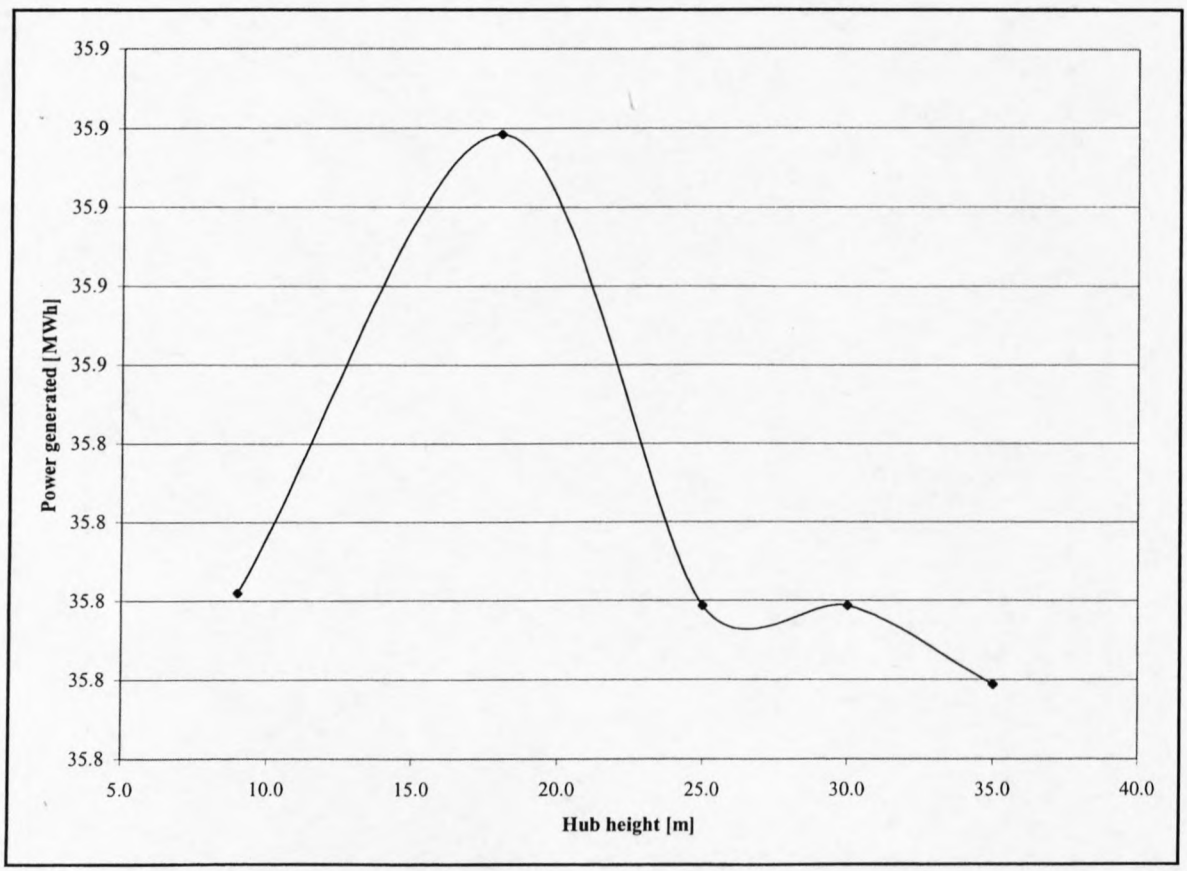

Figure J-13: Annual power output of the wind turbine for different hub heights (Bergey Excel)

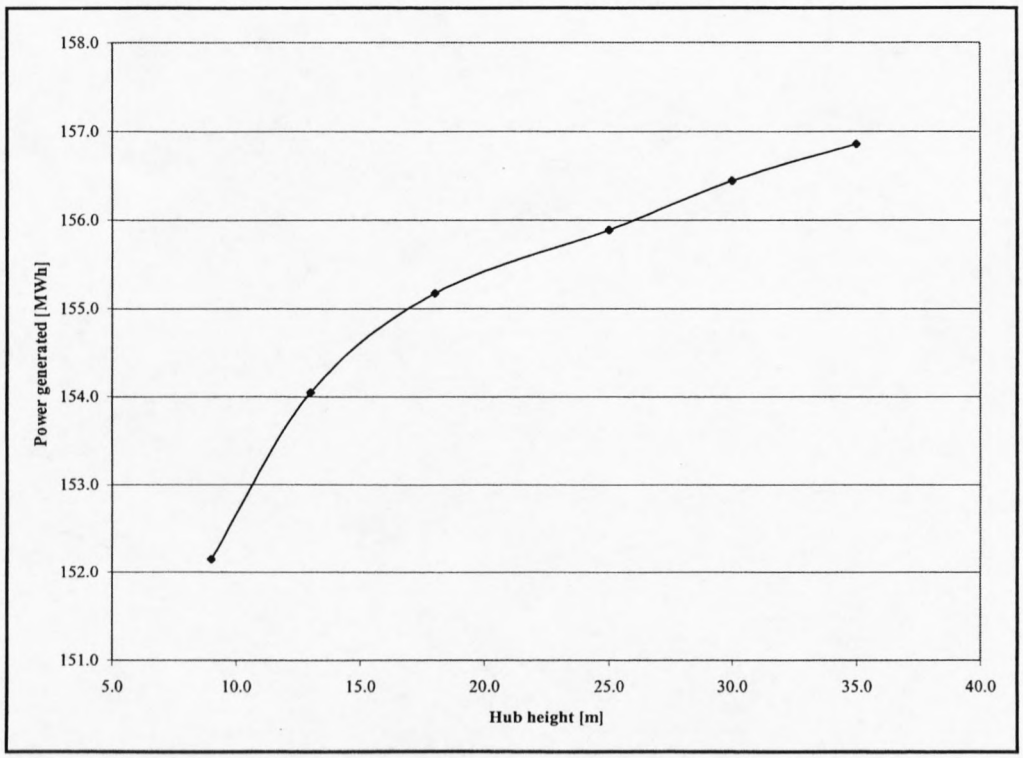

Figure J-14: Annual power output of the wind turbine for different hub heights (Fuhrländer FL30)

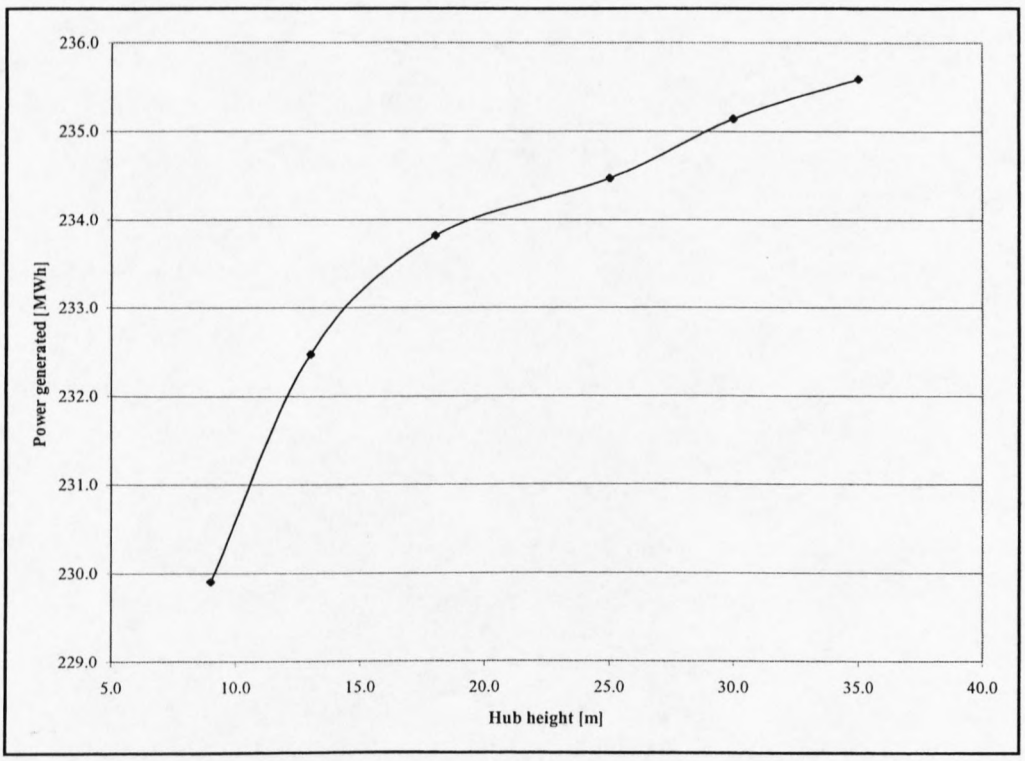

Figure J-15: Annual power output of the wind turbine for different hub heights (Atlantic Orient)

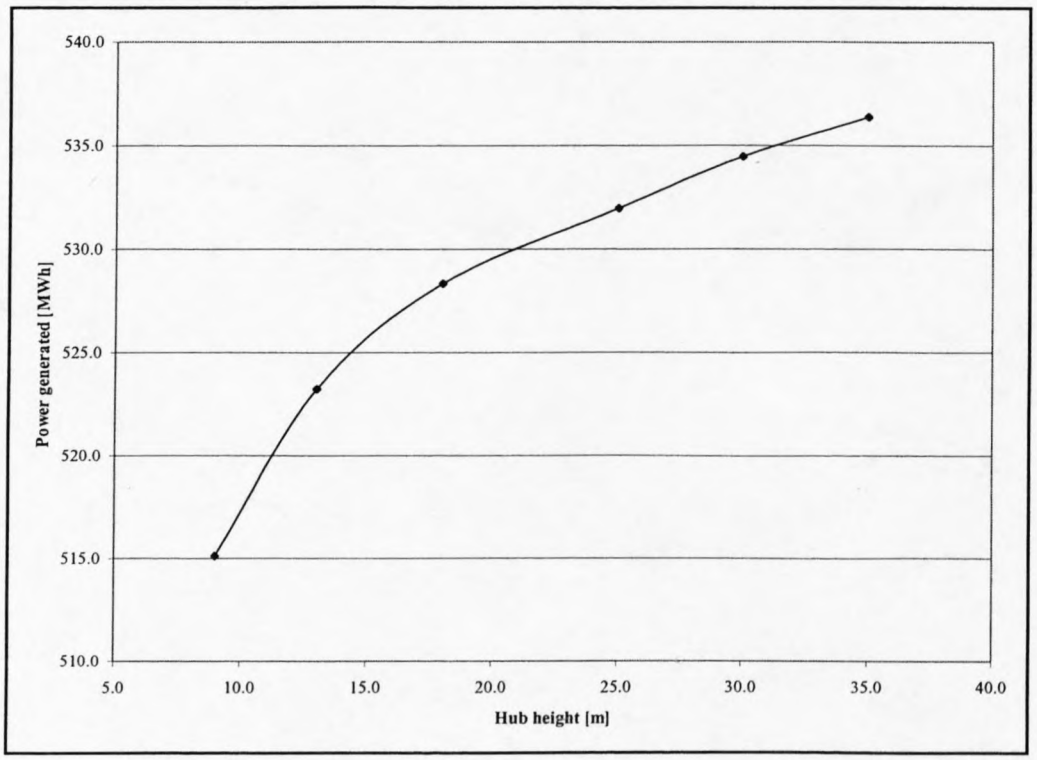

Figure J-16: Annual power output of the wind turbine for different hub heights (Fuhrländer FL100)

For the Fuhrländer FL100 an interesting fact that can be seen from figure J-16 is that the annual power output of the wind turbine changes significantly, unlike with the other wind turbines, the power output ranges from 515 MWh per year to 536 MWh per year.

Similarly, taking the 13-m-high tower as an example, the monthly power output for the Bergey Excel BWC wind turbine is calculated and is shown in figure J-17. For ease of comparison 30 days are chosen for each month. The result shows that for each month the power generated is different, varying from 2.13 MWh to 3.62 MWh. The highest power output is generated in April, which is 1.49 times the lowest, which is in January. From the graph, one can see that the months of highest power production are from February to November and the lowest are from December to January. The peak at March and April is due to the higher wind speeds than in January, but are not high enough to make the cut-out wind speeds critical factor.

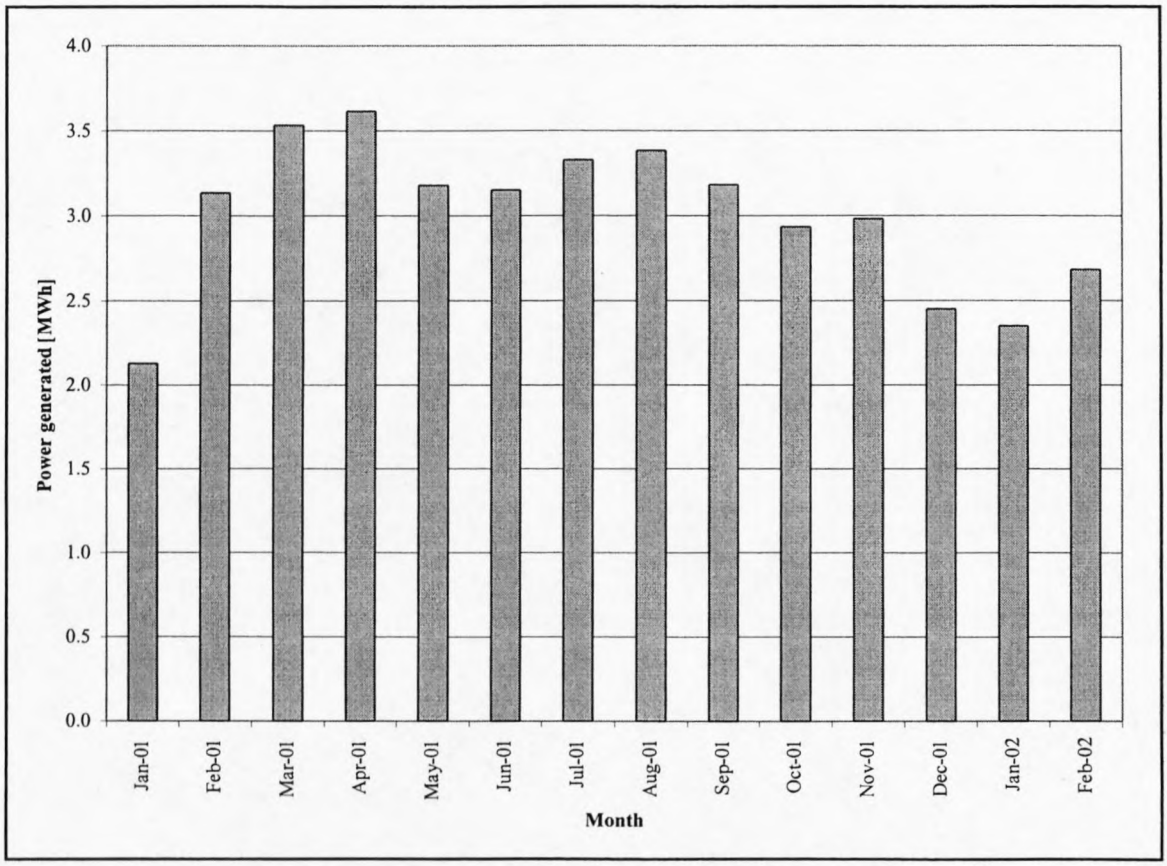

Figure J-17: Monthly power output distribution (13 m high tower)

Similarly, taking the 18-m-high tower as an example, the monthly power output for the Fuhrländer FL30 wind turbine was calculated and is shown in figure J-18. Again for ease of comparison 30 days are chosen for each month. The result shows that for each month the power generated is different, varying from 9.26 MWh to 14.99 MWh. The highest power output is generated in April, which is 1.62 times the lowest, which is in January. From the graph, one can see that the months of highest power production are from February to November and the lowest are from December to January. The peak at March and April is due to the higher wind speeds than in January, but are not high enough to make the cut-out wind speeds critical factor.

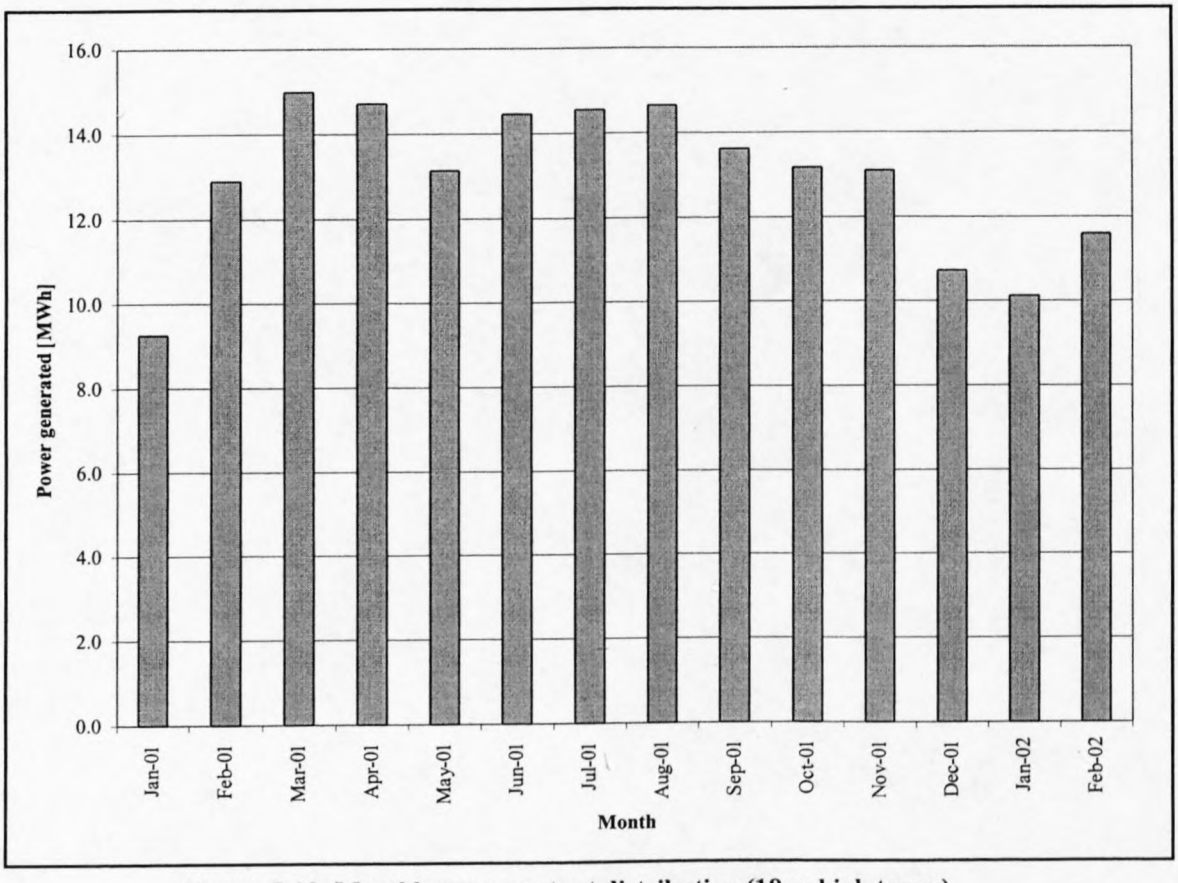

Figure J-18: Monthly power output distribution (18 m high tower)

Similarly, taking the 25-m-high tower as an example, the monthly power output for the Atlantic Orient 15/50 wind turbine is calculated and is shown in figure J-19. The result show that for each month the power generated is different, varying from 14.34 MWh to 23.48 MWh. The highest power output is generated in April, which is 1.64 times the lowest, which is in January. From the graph, one can see that the months of highest power production are from February to November and the lowest are from December to January. The peak at March and April is due to the higher wind speeds than in January, but are not high enough to make the cut-out wind speeds critical factor.

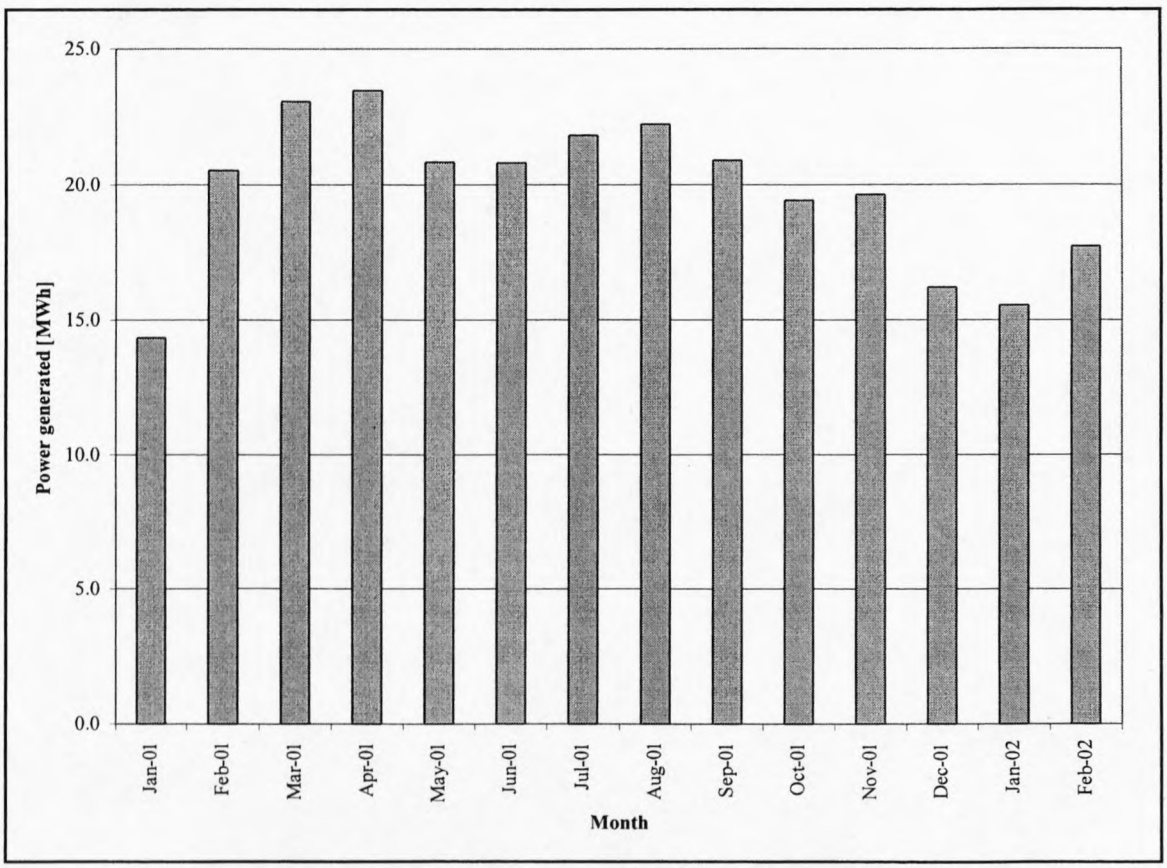

Figure J-19: Monthly power output distribution (25 m high tower)

Similarly, taking the 35-m-high tower as an example, the monthly power output for the Fuhrländer FL100 wind turbine is calculated and is shown in figure J-20. The result shows that for each month the power generated is different, varying from 32.36 MWh to 52.14 MWh. The highest power output is generated in April, which is 1.61 times the lowest, which is in January. From the graph, one can see that the months of highest power production are from February to November and the lowest are from December to January. The peak at March and April is due to the higher wind speeds than in January, but are not high enough to make the cut-out wind speeds critical factor.

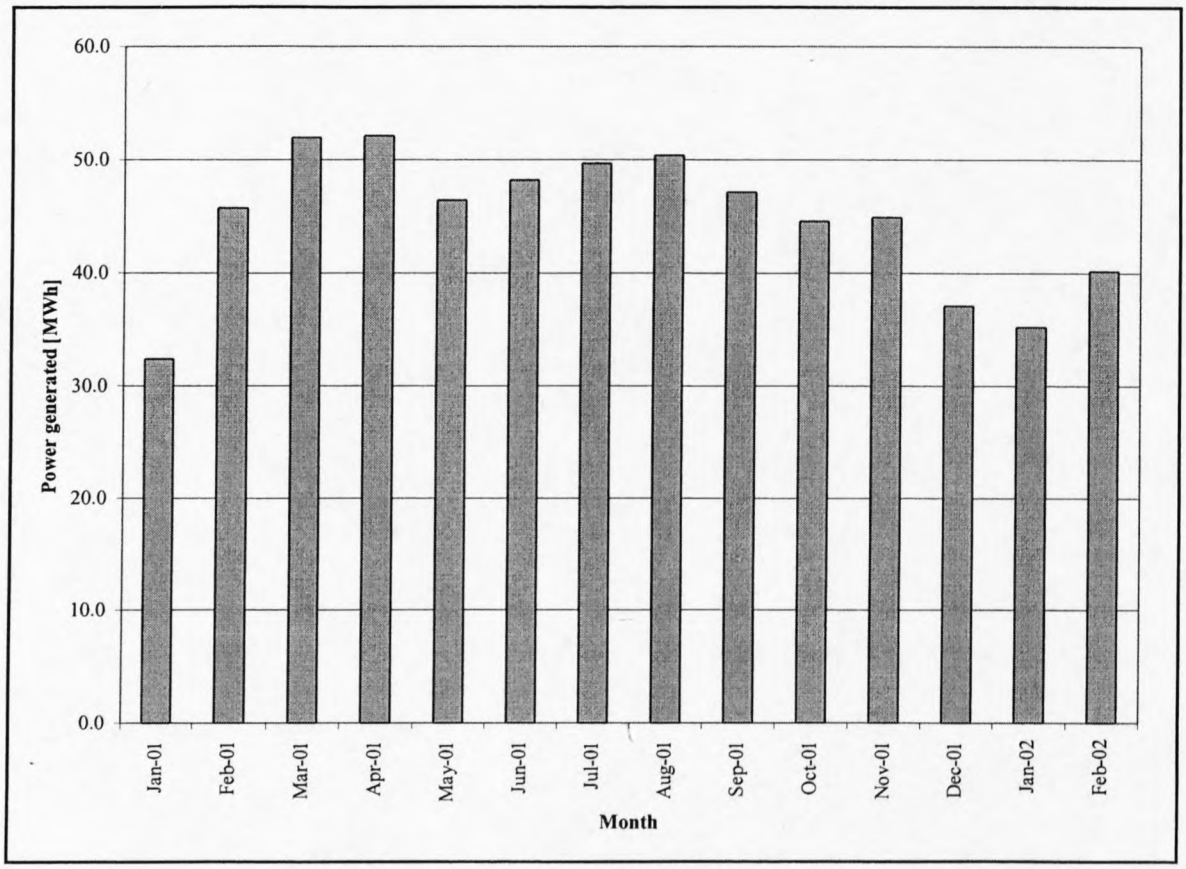

Figure J-20: Monthly power output distribution (35 m high tower)

The capacity factor

Another way of stating the annual energy output from a wind turbine is to look at the capacity factor for the turbine in its particular location. By capacity, the actual annual energy output divided by the theoretical maximum output is meant, if the machine were running at its rated (maximum) power during all of the 8760 h of the year.

Capacity factors may theoretically vary from 0% to 100%, but in practice they will usually range from 20% to 70%, and mostly be around 25-30%. For the four different wind turbines, the capacity factors for each month can be seen in table J-6.

	Bergey Excel BWC	Fuhrländer FL30	Atlantic Orient 10/50	Fuhrländer FL100
	Capacity Factor			
Complete Year:	0.41	0.59	0.53	0.61
Month:				
Jan-01	0.29	0.42	0.39	0.43
Feb-01	0.42	0.58	0.55	0.61
Mar-01	0.47	0.67	0.62	0.70
Apr-01	0.49	0.66	0.63	0.70
May-01	0.43	0.59	0.56	0.62
Jun-01	0.42	0.65	0.56	0.65
Jul-01	0.45	0.65	0.59	0.67
Aug-01	0.45	0.66	0.60	0.68
Sep-01	0.43	0.61	0.56	0.63
Oct-01	0.39	0.59	0.52	0.60
Nov-01	0.40	0.59	0.53	0.60
Dec-01	0.33	0.48	0.44	0.50
Jan-02	0.32	0.45	0.42	0.47
Feb-02	0.36	0.52	0.48	0.54

Table J-6: Annual and monthly capacity factors

Although one would generally prefer to have a large capacity factor, it may not always be an economic advantage. In a very windy location, for instance, it may be an advantage to use a larger generator with the same rotor diameter (or a smaller rotor diameter for a given generator size). This would tend to lower the capacity factor (using less of the capacity of a relatively larger generator), but it may mean a substantially larger annual production. Whether it is worthwhile to go for a lower capacity factor with a relatively larger generator, depends both on wind conditions, and on the price of the different turbine models.

APPENDIX K: WIND TURBINES AND CONTROLLER SPECIFICATIONS

Design Specifications for the Atlantic Orient 15/50 50Hz 50kW Wind Turbine

SYSTEM

Type	Grid Connected
Configuration	Horizontal Axis
Rotor Diameter	15 m (49.2 ft)
Centerline Hub Height	25 m (82 ft)

PERFORMANCE PARAMETERS

Rated Electrical Power	50 kW @12.0 m/s (26.8 mph)
Wind Speed	@hub height 25 m (82 ft)
cut-in	4.6 m/s (10.2 mph)
shut-down (high wind)	22.4 m/s (50 mph)
peak (survival)	59.5 m/s (133 mph)
Calculated Annual Output	
@ 100 % availability	5.4 m/s (12 mph) 85,000 kWh
	6.7 m/s (15 mph) 145,000 kWh
	8.0 m/s (18 mph) 199,000 kWh

ROTOR

Type of Hub	Fixed Pitch
Rotor Diameter	15 m (49.2 ft)
Swept Area	177 m ²(1902 ft²)
Number of Blades	3
Rotor Solidity	0.077
Rotor Speed @ rated wind speed	62 rpm
Location Relative to Tower	Downwind
Cone Angle	6°
Tilt Angle	0°
Rotor Tip Speed	48.6 m/s (109 mph) @ 50 Hz
Design Tip Speed	6.1

BLADE

Length	7.2 m (23.7 ft)
Material	Wood/epoxy laminate
Airfoil (type)	NREL, Thick Series, modified
Twist	7° outer blade
Root Chord	457 mm (18 in) @ 4% 279 mm (11in)
Max Chord	749 mm (29.5 in) @ 39% 2925 mm (115 in)
Tip Chord	406 mm (16 in) @ 100 % 7500 mm (295 in)
Chord Taper Ratio	± 2:1
Overspeed Device	Electro-magnetic tip brake
Hub Attachment	Embedded female bolt receptors
Blade Weight	150 kg (330 lbs) approximate

GENERATOR

Type	3 phase/4 pole asynchronous
Rated Temperature	-25°c
Frequency (Hz)	50 Hz
Voltage (V)	400, 3 phase @ 50 Hz
kW @ Rated Wind Speed	50 kW
kW @ Peak Continuous	55 kW
Speed RPM (nominal)	1500 @ 50 Hz
Winding Configuration	Ungrounded WYE
Insulation	Class F
Enclosure	Totally Enclosed Air Over (TEAO)
Frame Size	365 TC
Mounting	Direct mount to transmission
Options	Aretic low temp. shafting (-40°c)

TRANSMISSION

Type	Planetary
Housing	Ductile iron-integrated casting
Ratio (rotor to gen. speed)	1 to 24.57 (50 Hz)
Rating, output horse power	88
Lubrication	Synthetic gear oil/non toxic
Filtration	Service filtration cartridge @ scheduled maintenance.
Heater (option)	Arctic version, electric

YAW SYSTEM

Normal	Free, rotates 360 degrees
Optional	Yaw damping-required when known conditions frequently exceed 50° yaw rate per second.

DRIVE TRAIN TOWER INTERFACE

Structural	Yaw bearing mounted on tower top casting
Electrical	Twist Cable

TOWER

Type	Galvanized 3 legged, bolted lattice , self-supporting
Tower Height	24.4 m (80 ft)
Options	18.3 m (60 ft), 30.5 m (100 ft), 36.6 m (120 ft)
	Tilt down 24.4 m (80 ft)

FOUNDATION

Type	Concrete or special
Anchor Bolts	Certified ASTMA-A-193-Grade B7

CONTROL SYSTEM

Type	PLC based
Control Inputs	Wind speed, generator shaft speed
Control Outputs	Line interconnection, brake deployment
Communications	Serial link to central computer for energy monitor and maintenance dispatch (optional
Enclosures	NEMA 1, NEMA 4 (optional)
Soft Start	Optional

ROTOR SPEED CONTROL

Production	Blade stall increases with increased wind velocity
Normal Start up	Aerodynamic, electrical boost if necessary
Shut-down	Control system simultaneously applies dynamic brake and deploys tip brakes. Parking brake brings rotor to standstill.

Back-up Overspeed Control: Centrifugally activated tip brakes deploy

BRAKE SYSTEM CONTROL

Fail-safe brakes automatically deploy when grid failure occurs.

APPROXIMATE SYSTEM DESIGN WEIGHTS

Tower	3,210 kgs	(7,080 lbs)
Rotor & Drivetrain	2,420 kgs	(5,340 lbs)
Weight on Foundation	5,630 kgs	(12,420 lbs)

DESIGN LIFE: 30 Years

DESIGN STANDARDS: Applicable Standards, AWEA, EIA and IEC

DOCUMENTATION:
Installation Guide and Operation & Maintenance Manual

SCHEDULED MAINTENANCE: Semi-annual or after severe events.

NOTE 1:Atlantic Orient Corporation and its affiliates are constantly working to improve their products, therefore, product specifications are subject to change without notice.

NOTE 2: Power curves show typical power available at the controller based on a combination of measured and calculated data. Annual energy is calculated using power curves and a Rayleigh wind speed distribution. Energy production may be greater or lesser dependent upon actual wind resources and site conditions, and will vary with wind turbine maintenance, altitude, temperature, topography and the proximity to other structures including wind turbines.

NOTE 3: For design options to accommodate severe climates or unusual circumstances please contact the corporate office in Norwich, Vermont USA

NOTE 4: For integration into high penetration wind-diesel systems and village electrification schemes contact the corporate office in Norwich, VT USA for technical support and systems design.

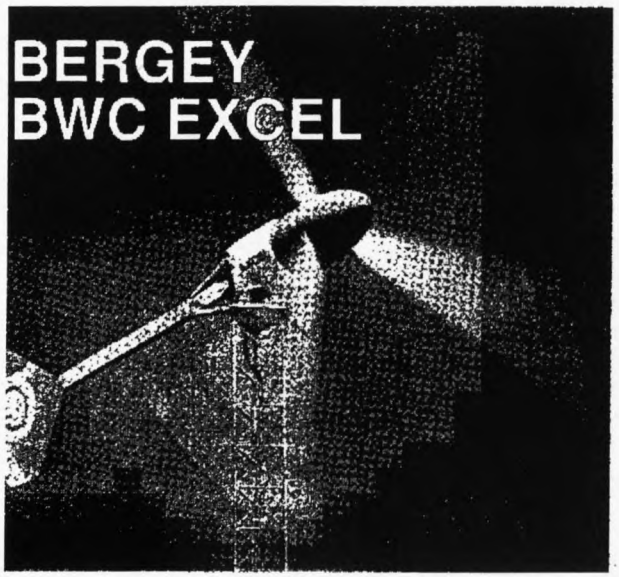

THE BWC EXCEL
WIND TURBINE SYSTEM

The BWC EXCEL is a 10 kilowatt wind turbine designed to supply most of the electricity for an average total electric home in areas with an average wind speed of 12 mph. In remote locations, it can charge batteries for stand-alone applications or pump water electrically without the need for batteries. Simple and rugged, the BWC EXCEL is designed for high reliability, low maintenance, and automatic operation in adverse weather conditions. It is available in three versions.

BWC EXCEL-S: a 240 VAC, 60 Hz (50 Hz optional), 1Ø utility interconnect system. Includes the POWERSYNC® Inverter.

BWC EXCEL-R: a 120 VDC (48 VDC optional) remote battery charging system. Includes the VCS-10 Control System.

BWC EXCEL-PD: a 3Ø AC system that can drive submersible or surface-mounted pumps. Includes the PCU-10 Control System.

BWC EXCEL PERFORMANCE

The performance data shown in the two graphs have been compiled in accordance with industry standards as established by the American Wind Energy Association. The power curve is corrected to standard temperature and pressure. The estimated Annual Energy Output (kilowatt-hours) assumes the AWEA standard distribution of wind speeds.

Multiple units or wind/PV hybrid systems may be used to increase the power available at a given site.

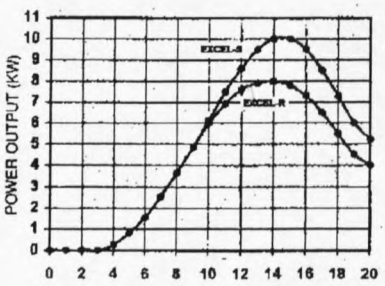

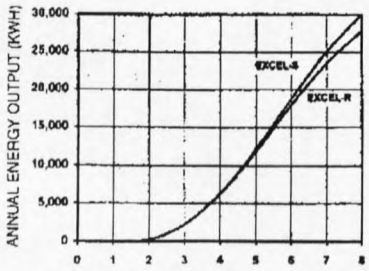

BWC EXCEL SPECIFICATIONS

START-UP WIND SPEED. . . . . 7.5 mph (3.4 m/s)
CUT-IN WIND SPEED . . . . . 7.0 mph (3.1 m/s)
RATED WIND SPEED . . . . . 29.0 mph (13.0 m/s)
RATED POWER . . . . . 10 kilowatts
CUT-OUT WIND SPEED . . . . . None
FURLING WIND SPEED. . . . . 35 mph (15.6 m/s)
MAX DESIGN WIND SPEED. . 120 mph (53.6 m/s)

TYPE . . . . . 3 Blade Upwind
ROTOR DIAMETER . . . . . 23.0 ft (7.0 m)
WEIGHT. . . . . 1050 lbs (477 kg)
BLADE PITCH CONTROL . . . . . POWERFLEX®
OVERSPEED PROTECTION . . . . . AUTOFURL™
GEARBOX/BELTS . . . . . None, Direct Drive
TEMPERATURE RANGE. . . . . –40° to +60° C
–40° to +140° F
GENERATOR . . . . . Permanent Magnet Alternator
OUTPUT FORM . 3 Phase AC, Variable Frequency
WITH VCS-10. . . . . Regulated DC, 48v or 120v
WITH POWERSYNC® INVERTER . . . . Nominal 240 VAC

Authorized Dealer:

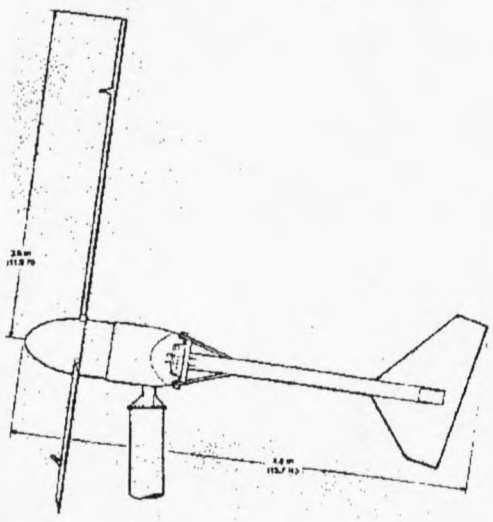

Bergey Windpower Co., Inc. 2001 Priestley Ave., Norman, OK 73069
E-MAIL: sales@bergey.com INTERNET: http://www.bergey.com
Tel: (405) 364-4212 Fax: (405) 364-2078

FL 30

Fuhrländer

30 kW –
seit 15 Jahren zuverlässig am Netz

Völlig unkompliziert läuft die FL 30, die seit Beginn der Windkraftnutzung beweist, dass Fuhrländer-Konzepte stimmen. Technologisch einfach konzipiert erzeugen diese stall-geregelten Anlagen mit Blattspitzenbremse Kilowattstunde um Kilowattstunde - wartungsarm und unauffällig. Eine Weiterentwicklung macht diese Maschine zu einer aktuellen Anlage für entlegene Standorte, ohne Ansprüche an das Stromnetz oder die Infrastruktur – vorwiegend im außereuropäischen Markt.

30 KW -
a 15 year experience

Just from the beginning the FL 30 proved its efficiency. Over the years the stall adjusted machines with tip brake produce kilowatt hour after kilowatt hour. This machine with its improved developments is of immediate interest for problematic sites without any demands on the power supply system or infrastructure and it is used mostly on the non-European market.

ROTOR / *rotor*

Durchmesser / *diameter*	13 m
Fläche / *area*	133 m²
Blattzahl / *nuber of blades*	3
Drehzahl / *speed*	47 / 70 min⁻¹
Leistungsregelung / *power regulation*	stall

GETRIEBE / *gear*

Bauart / *type*	Stirnrad / *spurgear*
Stufen / *stages*	2
Übersetzung / *ratio*	1 : 22

GENERATOR / *generator*

Bauart / *type*	asynchron / *asynchronous*
Drehzahl / *speed*	1.000 - 1.500 min⁻¹
Spannung / *voltage*	400 V AC

LEISTUNG / *power character*

Nennleistung / *rated* output	30 kW (max. 40 kW)
Startwind / *startwind*	2,5 m/s
Nennleistung bei / *rated output at*	12 m/s
Stoppwind / *stopwind*	25 m/s
Überlebensgeschwindigkeit / *survival wind speed*	67 m/s

MAST / *tower*

Nabenhöhe / *hub* height	18 / 27 m
Bauart / *type*	Gitterturm / *lattice tower*

MASSEN / *weight*

Rotor / *rotor*	410 kg
Maschinengondel / *nacelle*	950 kg
Mast / *tower*	2.100 / 3.000 kg

REGELUNG / *control systems*

Drehzahlregelung / *speed regulation*	netzgeführt / *grid connected*
Windnachführung / *yawing control*	Getriebemotor / *yaw motor*
Hauptbremse / *main brake*	Blattspitzenverstellung / *tip brake*
2. Bremssystem / *second brake system*	Scheibenbremse / *disc brake*
Überwachung / *monitoring*	Datenfernüberwachung / *data remote control*

SCHALL / *sound*

Schall-Leistungspegel / *noise level*	93 dB(A)
Tonhaltigkeit / *tonality*	nein / *no*
Impulshaltigkeit / *pulsation*	nein / *no*

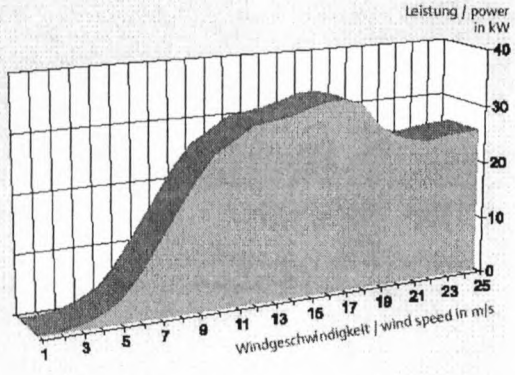

Fuhrländer

FL 100

100 kW –
Grundstein für die Megawatt-Klasse

Ende der 80er Jahre definierte Fuhrländer mit der FL 100 den Begriff „Qualität" neu: Seitdem läuft diese Windkraftanlage selbst unter extremsten Bedingungen mit höchster Zuverlässigkeit. Fuhrländer hat dieses Konzept bis hinauf in die Megawatt-Klasse beibehalten und rechnet mit einer Lebensdauer von gut 25 Jahren. Die Spezialität der FL 100 ist beispielsweise die Versorgung autarker Lebenseinheiten wie ein Kloster in Griechenland oder einer Schule in Südafrika.

ROTOR / *rotor*

Durchmesser / *diameter*	21 m
Fläche / *area*	346 m²
Blattzahl / *number of blades*	3
Drehzahl / *speed*	32 / 48 min⁻¹
Leistungsregelung / *power regulation*	stall

GETRIEBE / *gear*

Bauart / *type*	Stirnrad / *spurgear*
Stufen / *stages*	3
Übersetzung / *ratio*	1 : 31

GENERATOR / *generator*

Bauart / *type*	asynchron / *asynchronous*
Drehzahl / *speed*	1.000 - 1.500 min⁻¹
Spannung / *voltage*	400 V AC

LEISTUNG / *power character*

Nennleistung / *rated output*	100 kW (max. 130 kW)
Startwind / *startwind*	2,5 m/s
Nennleistung bei / *rated output at*	13 / 14 m/s
Stoppwind / *stopwind*	25 m/s
Überlebensgeschwindigkeit / *survival wind speed*	67 m/s

MAST / *tower*

Nabenhöhe / *hub height*	35 m
Bauart / *type*	Rohrturm / *tubular tower*

MASSEN / *weight*

Rotor / *rotor*	2.800 kg
Maschinengondel / *nacelle*	6.200 kg
Mast / *tower*	18.000 kg

REGELUNG / *control systems*

Drehzahlregelung / *speed regulation*	netzgeführt / *grid connected*
Windnachführung / *yawing control*	Getriebemotor / *yaw motor*
Hauptbremse / *main brake*	Blattspitzenverstellung / *tip brake*
2. Bremssystem / *second brake system*	Scheibenbremse / *disc brake*
Überwachung / *monitoring*	Datenfernüberwachung / *data remote control*

SCHALL / *sound*

Schall-Leistungspegel / *noise level*	95 dB(A)
Tonhaltigkeit / *tonality*	nein / *no*
Impulshaltigkeit / *pulsation*	nein / *no*

100 KW -
the basis for series up to 1 MW

The term of quality was newly defined by Fuhrländer at the end of the eighties. Since then this machine that was designed for the most extreme conditions is operating all over the world with highest efficiency as for example on Japanese islands. This wind turbine can be used especially for energy supply of self-supporting institutions such as a monastery in Greece or a school in South Africa.

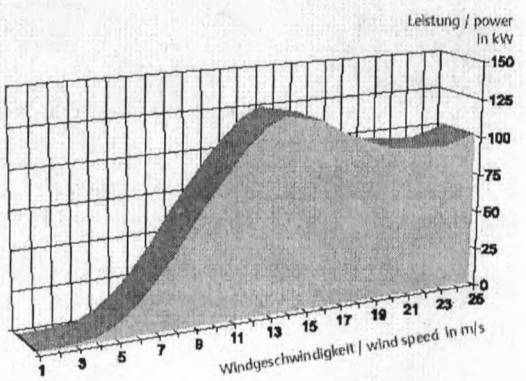

PRODUCT BRIEF

NORTHERN POWER SYSTEMS

Reliable power. Proven worldwide.

*The **North Wind NW100/19**™ Simplicity by Design*

Designed specifically for extreme weather in remote village power and distributed generation applications, the NW100/19 is a state of the art, utility-scale wind turbine. Northern Power Systems has drawn on 25 years of experience to engineer a wind turbine that provides cost-effective, highly reliable renewable energy in demanding environments.

Because we understand the needs of small utilities and independent power producers, the NW100/19 has the following features:

SIMPLICITY

Designed specifically for high reliability and low maintenance. The NW100/19 integrates industry proven robust components with innovative design features to maximize wind energy capture in severe and remote locations. The turbine features a minimum of moving parts and vulnerable subsystems to deliver high system availability. The uncomplicated rotor design allows safe, efficient turbine operation.

- Direct drive generator eliminates the drivetrain gearbox

- Dual fail-safe disk brake and electro-dynamic braking system eliminates blade brakes

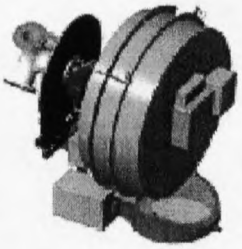

SERVICEABILITY

All service activities can occur within the tubular tower or nacelle housing, providing complete protection from severe weather conditions. Designated work areas provide ample room to perform service activities.

POWER QUALITY

The most common generator utilized in the wind industry is a gear driven asynchronous (induction) generator. Induction generators must be connected to a stable voltage source for excitation and reactive power (VAR) support. While large power grids can easily provide this support, power quality and system stability is compromised in distributed generation and village systems where the power grid is typically "soft and unbalanced."

NPS has solved this issue with the NW100/19. Our synchronous, variable speed direct drive generator and integrated power converter increases energy capture, while eliminating current in-rush during control transitions. This turbine can be connected to large power grids and remote wind-diesel configurations without inducing surges, effectively providing grid support rather than compromising it.

(continued)

P.O. Box 999 | Waitsfield, Vermont 05673 | USA | T 802-496-2955 | F 802-496-2953 | www.northernpower.com | contact@northernpower.com

SYSTEM DESCRIPTION

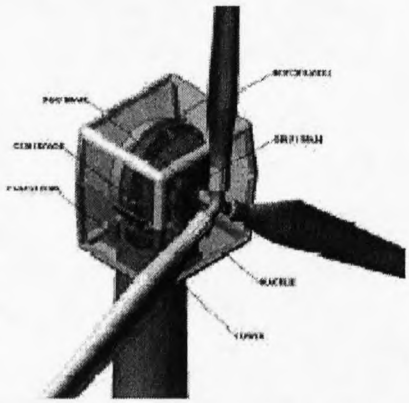

The variable speed, stall controlled turbine rotor assembly consists of three fiberglass reinforced plastic (FRP) blades bolted to a rigid hub, which mounts directly to the generator shaft. This simple, robust design eliminates the need for rotating blade tips, blade pitch systems, and speed increasing gearboxes.

Using a state-of-the-art airfoil design increases the blade's aerodynamic efficiency and renders them insensitive to surface roughness caused by dirt build-up and insects. The advanced FRP-resin infusion molding process ensures a high-quality blade while the root connection guarantees it will meet extreme temperature requirements.

The direct drive generator is a salient pole synchronous machine designed specifically for high reliability applications. Electrical output of the generator is converted to high quality AC power that can be synchronized to conventional or weak isolated grids. The advanced power conversion system also eliminates the inrush currents and poor power factor of conventional wind turbines. The output complies with IEEE 519-1992 power quality specifications.

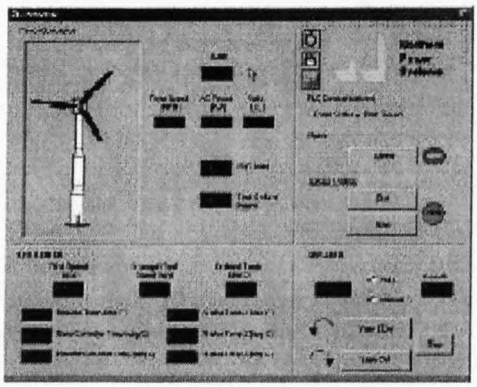

The variable speed direct drive generator / converter system is tuned to operate the rotor at the peak performance coefficient, and also allows stall point rotor control to contend with wide variation in air density found in the target applications.

The safety system consists of a spring applied, pressure released disk brake mounted on the generator shaft for emergency conditions, and an electrodynamic brake system that provides both normal shutdown and emergency braking backup functions.

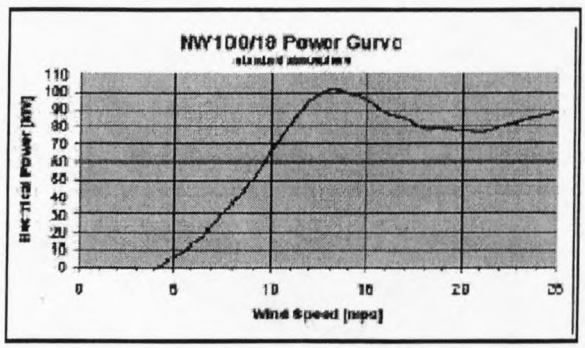

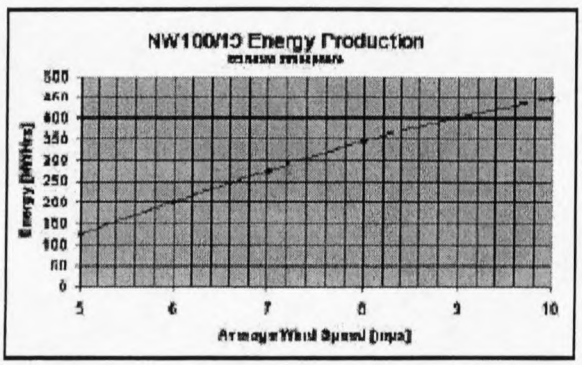

NW100/19 Technical Specifications

Design Specifications

Turbine Class	IEC WTGS Class I
Design Life	30 year
Design Standards	In Accordance with IEC 1400-1

Performance

Nominal Power Rating	100 kW
Rated Wind Speed	13 m/s (29mph)
Cut-In Wind Speed	4 m/s (9mph)
Cut-Out Wind Speed	25 m/s (56mph)
Survival Wind Speed	70 m/s (157mph)

General Configuration

Rotation Axis	Horizontal
Orientation	Upwind
Yaw Control	Active
Number of Blades	3
Hub Type	Rigid
Drive Train	Direct Drive
Power Regulation	Stall

Rotor

Diameter	19.1 m
Swept Area	284 m^2
Speed Range	45-69 RPM
Speed @ rated power	68.5 RPM
Structural Configuration	Flange Mounted Blades, Rigid Hub
Power Regulation	Variable Speed Stall
Rotor Rotation	Clockwise (Viewed from Upwind)
Pitch Angle	-0.75° @ tip, nominal
Coning	0°

Blades

Airfoil	S819, S820, S821 Series
Material	Fiberglass Reinforced Plastic (FRP)
Lightning Protection	Standard Integrated System

Drive Train

Configuration	Variable Speed Direct Drive
Tilt Angle	4°
Generator Type	Salient Pole Synchronous
Insulation Class	NEMA H
Generating Speed	45-69 RPM
Generator Rating	100 kW w/ 1.15 Service Factor
Generator Output	575 VAC
Speed Control	IGBT Controller

Grid Connection

Grid Voltage	480 VAC std: 380-30kV available
Grid Frequencies	50/60 Hz

Braking Systems

Mechanical Brake	Main Shaft Disc Brake w/ Dual Spring Applied Calipers
Electro-Dynamic Brake	Parking and emergency backup

Yaw System

Type	Active Upwind
Damping system	Adjustable Friction
Yaw Drive	Electrically Driven Planetary Gearbox
Yaw Bearing	Slew Ring

Tower

Type	Tubular
Hub Height	25/30/35 m (82/98/115 ft)
Material	Steel
Corrosion Protection	Marine Paint

Service Environment

Tower	Fully Enclosed, Ladder Way
Nacelle	Fully Enclosed

Controller

Type	*Northern WTGS-100 Controller*, Microprocessor-based
Functions	Complete Supervisory Control and Data
Remote Control/Monitoring	Acquisition
Power Electronics	Integrated *RemoteView*™ Access Software
Power Quality	IGBT Pulse Width Modulation (PWM) Converter
	IEEE 519-1992

Environmental Specifications

Temperature Operating Range	-46°C to 50°C (-50°F to 122°F)
Lightning Protection	In Accordance with IEC 61024-1
Icing	Ice cover to 30 mm (1 in)
Seismic Loading	Zone 4

Packages available for specific site condition such as coastal environment.

Masses

Rotor	761 Kg (1 680 lbs)
Nacelle (excluding rotor)	6325 Kg (13 950 lbs)
Tower (25m)	6500 Kg (14 330 lbs)

Northern Power reserves the right to alter turbine specifications at any time.

P.O. Box 999 | Waitsfield, Vermont 05673 | USA | T 802-496-2955 | F 802-496-2953 | www.northernpower.com | contact@northernpower.com

DEVELOPMENT

The NW100/19 turbine was developed by NPS with support from cooperating agencies within the U.S. government, including the National Aeronautics and Space Administration (NASA); the National Science Foundation (NSF); the Department of Energy (DOE); and the DOE-funded National Renewable Energy Laboratory (NREL). Siemens-Westinghouse acted as a subcontractor to NPS in developing the innovative direct drive generator subsystem.

Turbine certification testing is being carried out at the National Renewable Energy Laboratories National Wind Test Site at Rocky Flats, CO. This testing is near completion and will result in a Type Testing Conformity Statement, which validates the turbine safety systems and structural design. Turbine testing also includes Type Characteristic Measurements that prove the performance and acousticsignature of the turbine.

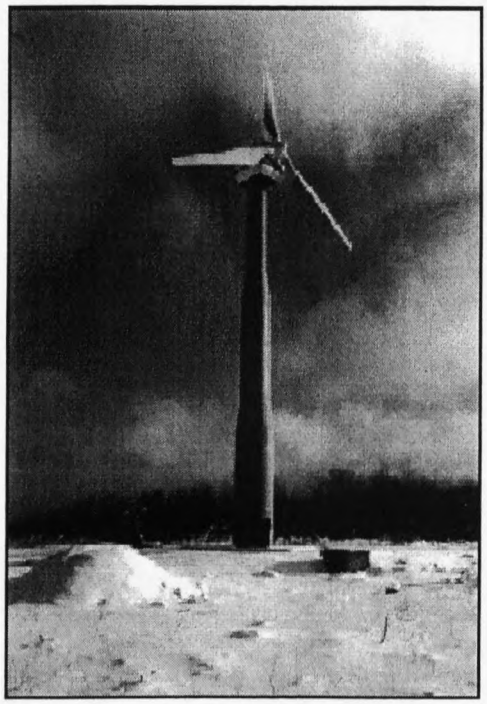

NORTHERN POWER SYSTEMS

Founded in 1974, Northern Power Systems specializes in hybrid design solutions for standalone and grid-tied power system applications. Utilizing the latest in renewable and conventional fuel generation technologies, NPS is recognized as a world leader in the commercial application of proven wind-diesel technology. We have completed over 700 installations on all 7 continents.

NPS wind turbines at the South Pole and the Antarctic coast have operated in more extreme conditions than any other turbines, including winds to 198 mph (88.5 m/s) and temperatures to -112°F (-80°C.) This experience gained in harsh, remote conditions has been incorporated into key NW100/19 design decisions affecting configuration, materials selection, performance characteristics, and deployment procedures.

For further information contact:
Lawrence Mott
Northern Power Systems
Waitsfield, VT 05673
(802) 496-2955x-239
lmott@northernpower.com

Northern Power Systems designs, builds, and installs high reliability electric power systems. Northern has installed over 800 systems worldwide since 1974, earning a reputation for delivering top-quality energy solutions.

PRODUCT BRIEF

NORTHERN POWER SYSTEMS

Reliable power. Proven worldwide.

Northern Power Systems' Universal Wind Diesel Controller

Northern Power Systems™ developed its ***Universal Wind Diesel Controller***™ for stand-alone wind-diesel "village power" applications. This unit provides supervisory control of diesel generators and wind turbines to provide seamless utility-grade power in remote locations. Its modular, pre-integrated design allows it to adapt to a variety of applications without expensive custom engineering.

The ***Universal Wind Diesel Controller*** combines a proven, robust microprocessor control module with Northern's own refined control software. The result of its reliable control and monitoring functions is stable, high quality, utility grade power.

*Northern's **Universal Wind Diesel Controller** provides reliable control and monitoring functions, resulting in stable, high quality, utility grade power.*

CONTROLLER FEATURES

- Proven, mature technology from the generator control industry. The hardware modules are interchangeable and readily available.
- Easy integration of a variety of system elements including synchronous condensers, rotary converters, electrical storage components, and critical/non-critical load controls. Custom hardware design costs are eliminated.
- Automatic generator-only operation in the event of a failure. The loss of the control system will not result in a loss of power.
- Flexible system architecture able to accommodate the range of existing diesel generator and wind turbine control packages.

OPERATION

- The ***Universal Wind Diesel Controller*** will switch a wind/ diesel hybrid system between four states of operation.
- In times of no wind, the system will operate "diesel only," bringing generators on and off line for maximum fuel efficiencies.
- When there is enough wind to produce power, the controller will reduce the output of the diesel generators to match the load.
- If the wind increases just to the point where the wind turbine can match the load by itself, the controller will set one diesel generator to a minimum level and dump excess wind power to a secondary heat load. The addition of battery storage would allow the generator to be shut down in this state.
- When the wind power is ample enough to allow a margin of safety, the controller will switch off the last diesel generator and use the heat load to absorb the excess power production.

The heat load is variable, and acts along with the synchronous condenser or rotary converter to maintain power stability. The controller ensures seamless transitions between operating states and the most efficient use of both diesel fuel and the wind resource.

(continued)

P.O. Box 999 | Waitsfield, Vermont 05673 | USA | T 802-496-2955 | F 802-496-2953 | www.northernpower.com | contact@northernpower.com

COMPONENTS

The WDC consists of a range of digital based control modules especially designed for power control applications. These are:

Universal Wind Diesel Controller

The WDC handles the sequencing (On/Off control) of power units (wind turbines, diesels, storage systems, synchronous condensers, rotary converters and dump loads). The WDC is aware of loading on the diesel generator sets, power output of the wind turbines, and status of the secondary load controller. From this information, the WDC makes state change decisions for the major power system components in the overall system.

The Wind Power Controller, the Energy Storage Controller and the Secondary Load Controller are software modules that will exist in the same hardware module as the WDC.

Wind Power Controller

Normal control of the wind turbine generator is provided by the turbine manufacturer. The WDC sends a "permission to operate" signal to the wind turbine controller to allow it to start, and interfaces with the turbine controls to monitor its operation.

Secondary Load Controller (SLC)

The SLC is designed to switch a set of binary dump loads in order to match the total electrical demand to the power being generated. The SLC will act as the prime bus frequency control during operation at high levels of wind power penetration.

Energy Storage Controller (ESC)

The ESC is a software module to provide overall supervisory and state control to an electrical power storage system such as a battery bank. The ESC will provide load support during wind-only operation.

Engine/Generator Modules

Each engine will have Northern Power's Engine Control System and an electronic governor. These are typical hardware components on all diesel genset units and control basic engine functions. Each generator will have an automatic voltage regulator as part of its standard equipment. Northern's Engine Control System will provide the engine sequencing, synchronizing, and load and reactive power sharing between generators.

Synchronous Condenser Controller (SCC)

The synchronous condenser consists of a synchronous generator with a clutched pony motor for starting, and an automatic voltage regulator. The synchronization and control of the unit will be carried out by a standard power controller with software adaptations. In applications with battery storage the synchronous condenser would be replaced with a rotary converter. The RC would take on the functions of the SC, plus battery charging and inverting.

Communications Processing Module (CPM)

The CPM is a PC based industrial computer platform that will collect data from the various control platforms. It is possible to configure this subsystem with a monitor running a local operator interface. The CPM acts as a data storage and collection device through which operating data can be retrieved via remote link.

By using a PC platform the form of remote communications is transparent. The CPM allows an electric utility or other remote provider to connect in real time to the control system. It is able to communicate using the public switched telephone network (PSTN), internet, radio modem, microwave modem, satellite modem, or cellular phone.

Networked I/O

To enable comprehensive control of ancillary site requirements such as environmental systems, thermal systems, or specific dump load applications such as electric heaters, desalinization or ice making, the system architecture allows additional I/O and processing to be added to either the Modbus or Echelon communications networks. This feature makes the overall control architecture flexible enough to meet a variety of applications without requiring custom parallel control systems, or adversely affecting the cost of individual components.

APPENDIX L: SAMPLE CALCULATIONS OF ECONOMIC ANALYSES

Sample calculations are presented in this appendix for the economic models used in section 11.8. The parameters used in the sample calculations were taken from table 11.5.

Evaluation of cumulative system cost comparison

The cumulative system cost for year n is defined as:

$$C_{cum} := \left[\sum_{j=0}^{N} \left[\frac{C_{cap.j}}{(1+i_{cap})^{j}} + \frac{C_{fuel.j}}{(1+i_{fuel})^{j}} + \frac{C_{maint.j}}{(1+i_{maint})^{j}} + \frac{C_{labor.j}}{(1+i_{labor})^{j}} \right] \right] \quad \text{(L-1)}$$

where $C_{cap,j}$, $C_{fuel,j}$, $C_{maint,j}$ and $C_{labor,j}$ are the capital, fuel maintenance and labor costs during the year j, i_{cap} is the interest rate on capital, and i_{fuel}, i_{maint} and i_{labor} are the cost escalation rates for fuel, maintenance and labor costs. During year 0 there only exist the capital investment. Therefore the cumulative system cost for year 0 is as follows, using the relevant values from table 11.5:

$$C_{cum.0} := \left[\frac{R3342092,50}{(1+0.14)^{0}} \right] := R3342092,50$$

For year one the cumulative costs is as follows:

$$C_{cum.1} := C_{cum.0} + \left[\frac{R1744838,40}{(1+0.04)^{1}} + \frac{R50000,00}{(1+0.02)^{1}} + \frac{R33626,84}{(1+0.02)^{1}} \right] := R4734966,49$$

It has to be noted from the previous equation that there are no capital costs associated during year 1, since there is a complete capital investment during year 0. The cumulative cost obtained above can be verified in figure 11.1.

Evaluation of net present value

In order to accurately determine the NPV, the general inflation rate will be introduced and the present worth factors will change to:

$$PWF := \sum_{j=1}^{N} \frac{(1+d)^{j-1}}{(1+i)^{j}} \quad \text{(L-2)}$$

where d is the general inflation rate. The NPV is defined as follows:

$$NPV := \left(\sum_{j=1}^{N} AS_j \cdot PWF \right) - C_{cap} \qquad \text{(L-3)}$$

where AS_j is the net annual savings, defined as: AS = Annual Savings – Annual Expenses. The annual savings in our case are the fuel costs that are saved because of the power penetration by the wind turbine and therefore the reduced diesel consumption by the diesel generators and the saved labor and maintenance costs due to the reduced running time of the diesel generators. The annual expenses include interest on capital, labor and maintenance expenses. The NPV for year j is

$$NPV(j) := \frac{FCS \cdot (1+d)^{j-1}}{(1+i_{fuel})^{j}} + \frac{(LMS - C_{labor} - C_{maint}) \cdot (1+d)^{j-1}}{(1+i_{labor})^{j}} - IOC - NPV(j-1) \qquad \text{(L-4)}$$

Where FCS is the annual fuel savings, LMS is the annual diesel electric generator labor, maintenance and operation saving and IOC is the yearly interest on capital. The interest on capital is defined as

$$IOC_j := \frac{C_{cap} \cdot (1+d)^{j-2}}{(1+i_{cap})^{j-1}} - \frac{C_{cap} \cdot (1+d)^{j-1}}{(1+i_{cap})^{j}} \qquad \text{(L-5)}$$

The IOC for the fifth year is

$$IOC_5 := \frac{R3342092,50 \cdot (1.1061)^{3}}{(1.14)^{4}} - \frac{R3342092,50 \cdot (1.106)^{4}}{(1.14)^{5}} := R79843,21$$

The NPV for the fifth year is

$$NPV(5) := \frac{R381493,00 \cdot (1.106)^{4}}{(1.04)^{5}} - \frac{R23626,84 \cdot (1.106)^{4}}{(1.02)^{5}} - R79843,21 - R2499172,74$$

$$NPV(5) := -R2141855,26$$

The net present value for the fifth year, as calculated above, can be verified in figure 11.2.

Evaluation of benefit / cost ratio

As the name implies, the benefit/cost ratio method involves the calculation of a ratio of benefits to costs, taking interest, escalation rates and inflation into consideration. The BCR is defined as follows:

$$BCR := \frac{\left(\sum_{j=1}^{N} AS_j \cdot PWF \right)}{C_{cap}} \qquad \textbf{(L-1)}$$

Rearranging the equation, the benefit / cost ration for year j is defined as

$$BCR(j) := \frac{\frac{FCS}{(1 + i_{fuel})^j} + \frac{(LMS - C_{labor} - C_{maint})}{(1 + i_{labor})^j} + BCR(j-1)}{C_{cap}}$$

The BCR for the fifth year is

$$BCR(5) := \frac{\frac{381493.00}{(1 + 0.04)^5} + \frac{(10000 - 13626.84 - 20000)}{(1 + 0.02)^5} + 1294815.38}{3342092.5} := 0.474$$

The benefit / cost ratio for the fifth year, as calculated above, can be verified in figure 11.4. To calculate the BCR for a range of different capital investments, the procedure mentioned above will be applied to the different cases of initial investments and the results are plotted on one graph, as is done in figure 11.6.

Evaluation of internal rate of return

The IRR is defined as setting the NPV equal to zero and then solving the equation for i, which is called the IRR:

$$NPV := \left(\sum_{j=1}^{N} AS_j \cdot PWF \right) - C_{cap} := 0 \qquad \textbf{(L-2)}$$

From equation (L-4), we define the equation for the IRR as

$$\frac{FCS\cdot(1+d)^{j-1}}{(1+i_{fuel})^{j}}+\frac{(LMS-C_{labor}-C_{maint})\cdot(1+d)^{j-1}}{(1+i_{labor})^{j}}-IOC-NPV(j-1):=0 \qquad \textbf{(L-5)}$$

for year j. Adapting equation (L-5) for the interest on capital to evaluate the IRR as follows

$$IOC_{j}:=\frac{C_{cap}\cdot(1+d)^{j-2}}{(1+i)^{j-1}}-\frac{C_{cap}\cdot(1+d)^{j-1}}{(1+i)^{j}}$$

Using the relevant values from table 11.4 and evaluating the internal rate of return for an initial investment of R3342092.50, the following result is obtained, when equation (L-5) is applied for each investment year and the results are added:

$$\frac{R381493,00\cdot(1.106)^{29}}{(1+i)^{30}}-\frac{R23626,84\cdot(1.106)^{29}}{(1+i)^{30}}-IOC-R67099,57:=0$$

where the IOC is calculated as

$$IOC_{30}:=\frac{R3342092,50\cdot(1.1061)^{28}}{(1+i)^{29}}-\frac{R3342092,50\cdot(1.106)^{29}}{(1+i)^{30}}$$

Inserting the equation for the IOC and solving the complete equation, the IRR is obtained. The internal rate of return for the abovementioned calculation is IRR = 14.84%. The equations for the internal rate of return have been solved, using the Program Excel, Version 2000. The internal rate of return for a capital investment of about R3,4 million, as calculated above, can be verified in figure 11.7.

Evaluation of payback period

The simple payback period is defined as follows:

$$PBP_{s}:=\left[\sum_{j=1}^{\theta}(R_{k}-E_{k})\right]\rightarrow C_{cap}\geq 0 \qquad \textbf{(L-6)}$$

where θ indicates the year of breakeven. A more sophisticated breakeven period analysis is called the discounted breakeven period, where interest on capital, escalation costs and inflation are included in the analysis. The discounted breakeven period is defined as follows:

$$PBP_d := \sum_{j=1}^{\theta} \left(R_k - E_k\right)\cdot PWF - C_{cap}\cdot PWF \geq 0 \qquad \textbf{(L-7)}$$

The basic premise of the PBP is that the more quickly the cost of a premise can be recovered, the more desirable is the investment. Rearranging equation (L-7), the discounted payback period for year j is defined as

$$PBP_d(j) := \frac{FCS\cdot(1+d)^{j-1}}{\left(1+i_{fuel}\right)^{j}} + \frac{\left(LMS + ES - C_{labor} - C_{maint}\right)\cdot(1+d)^{j-1}}{\left(1+i_{labor}\right)^{j}}$$

$$- IOC - PBP_d(j-1) \geq 0 \qquad \textbf{(L-8)}$$

Evaluating the PBP_d for the fifth year in operation, excluding externalities, is

$$PBP_d(j) := \frac{R381493,00\cdot(1.106)^4}{(1.04)^5} - \frac{R23626,84\cdot(1.106)^4}{(1.02)^5} - R79843,21 - R2499172,74 \geq 0$$

$$PBP_d(5) := -R2141855,26$$

The discounted payback period for the fifth year, as calculated above, can be verified in figure 11.9.

Evaluation of cost per unit power produced

The cost of a kWh produced by a wind turbine system may be obtained from the following mathematical relationship:

$$CP := \frac{C_{cap}}{P}\cdot\left[\frac{d\cdot(1+d)^N}{\left[(1+d)^N - 1\right]}\right] + \frac{OM}{P} + \frac{L}{P} + \frac{FC}{P} \qquad \textbf{(L-9)}$$

Where d is the annual inflation rate, OM is the operating and maintenance costs, L is the labor cost, FC is the fuel cost and P is the total power generated in one year. Using a capital investment of R 4.00 million the cost per kWh produced for the hybrid, wind diesel system is

$$CP := \frac{R4000000,00}{1153000\ kWh}\cdot\left[\frac{0.106\cdot(1.106)^{30}}{\left[(1.106)^{30}-1\right]}\right] + \frac{R20000,00 + (1-0.2)\cdot R30000,00}{1153000\ kWh}$$

$$+ \frac{R13626,84 + (1-0.2)\cdot R20000,00}{1153000\ kWh} + \frac{(298416\ L - 65246\ L)\cdot\frac{R5,847}{L}}{1153000\ kWh} := \frac{R1,63}{kWh}$$

APPENDIX M: 6 M WIND MAST DRAWINGS

During the field trip, the 6 m wind mast was used to measure wind speed profiles on two different surfaces as mentioned in chapter 5. The data was used for this project and a PhD project by Beyers (2003). Part of Beyers project deals with the outdoors modeling of snowdrift at SANAE IV research station, Antarctica. He designed the 6 m wind mast, which can be seen in figures M-1 and M-2. The author and Beyers shared the installation and setup work of the wind mast at the two positions. The derivation of the equations for the velocity profiles in section 6.1.2 was done in collaboration with Beyers.

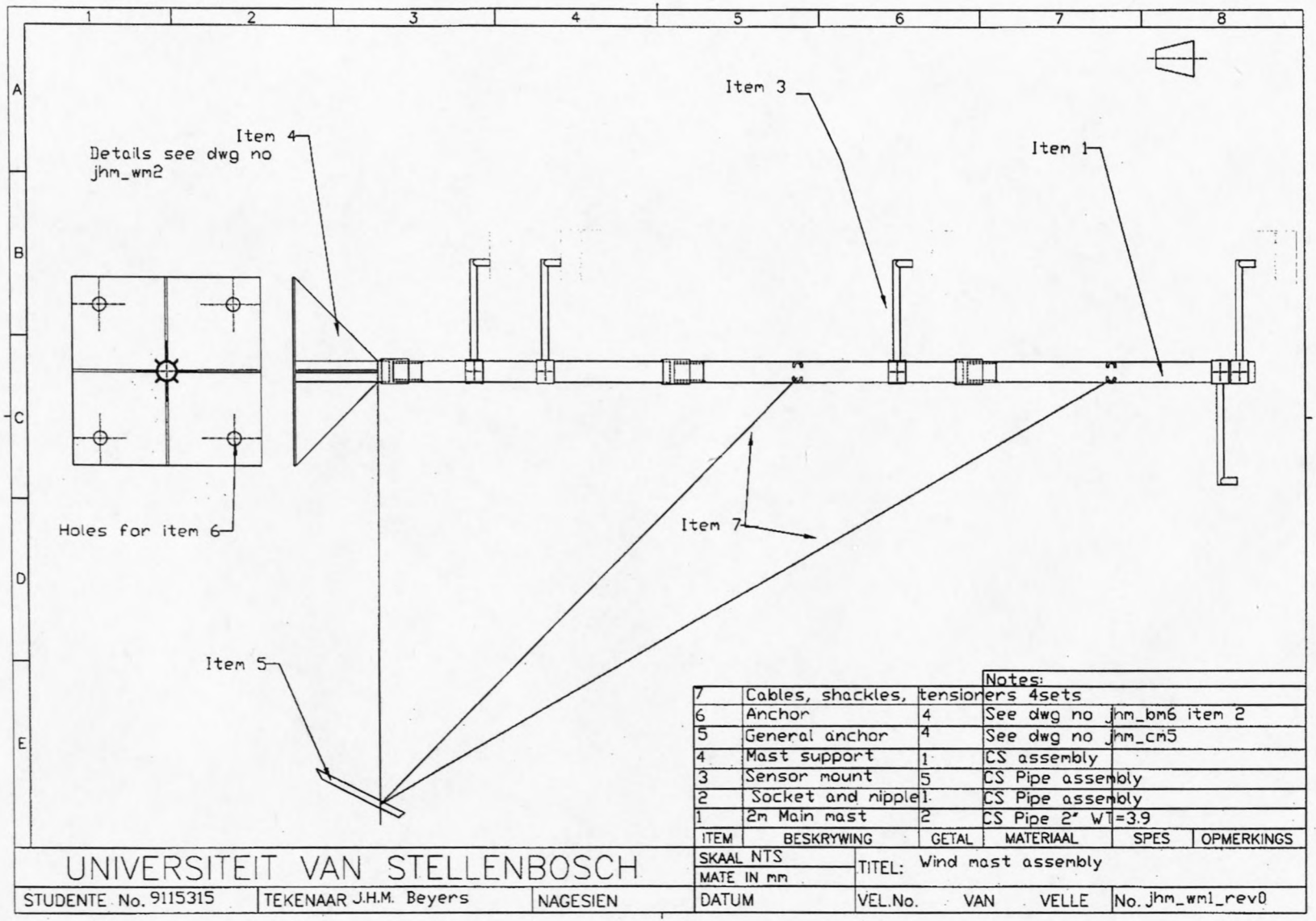

Figure M-1: Wind mast assembly drawing

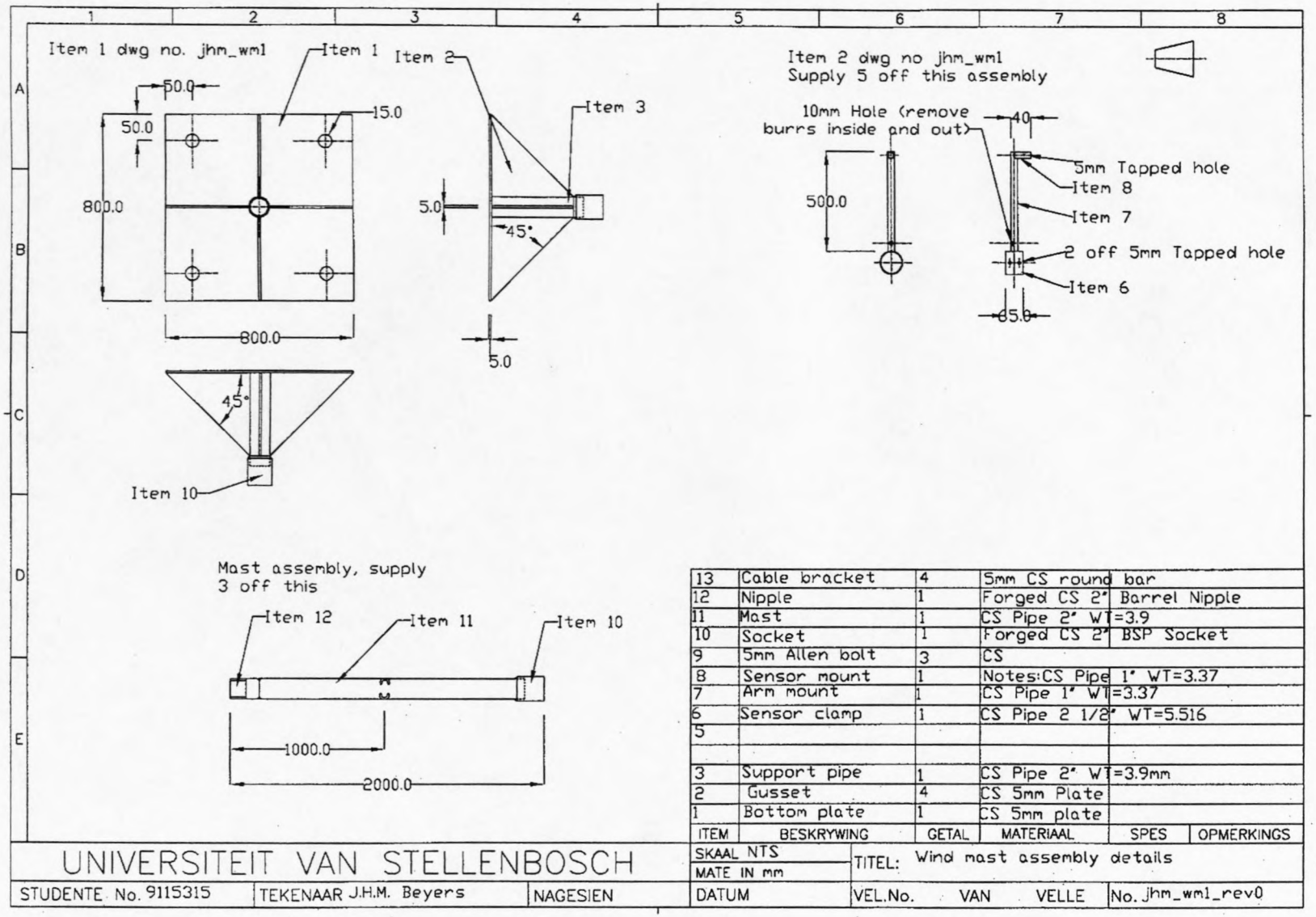

ITEM	BESKRYWING	GETAL	MATERIAAL	SPES	OPMERKINGS
13	Cable bracket	4	5mm CS round bar		
12	Nipple	1	Forged CS 2" Barrel Nipple		
11	Mast	1	CS Pipe 2" WT=3.9		
10	Socket	1	Forged CS 2" BSP Socket		
9	5mm Allen bolt	3	CS		
8	Sensor mount	1	Notes:CS Pipe 1" WT=3.37		
7	Arm mount	1	CS Pipe 1" WT=3.37		
6	Sensor clamp	1	CS Pipe 2 1/2" WT=5.516		
5					
3	Support pipe	1	CS Pipe 2" WT=3.9mm		
2	Gusset	4	CS 5mm Plate		
1	Bottom plate	1	CS 5mm plate		

UNIVERSITEIT VAN STELLENBOSCH

STUDENTE No. 9115315	TEKENAAR J.H.M. Beyers	NAGESIEN

SKAAL NTS	TITEL: Wind mast assembly details		
MATE IN mm			
DATUM	VEL.No.	VAN VELLE	No. jhm_wm1_rev0

Figure M-2: Wind mast detail assembly drawing


teetz_technical_2002